

AD A 039833

(12)
ARPA/NRL X-Ray Laser Program

Final Technical Report on
ARPA Order No. 2694
to Defense Advanced Research Projects Agency

*Interaction Physics Branch
Optical Sciences Division*

April 1977



NAVAL RESEARCH LABORATORY
Washington, D.C.

Approved for public release; distribution unlimited.

ID NO. _____
LDC FILE COPY.

UOC
MAY 25 1977
B
JH

The Interaction Physics Branch of the Optical Sciences Division, Naval Research Laboratory, Washington, D.C., prepared this report on work sponsored jointly by the Defense Advanced Research Projects Agency, DARPA Order 2694, and the Naval Research Laboratory. Co-authors of the report were R. A. Andrews, R. C. Elton, J. Reintjes, R. C. Eckardt, R. H. Dixon, R. Waynant, T. N. Lee, and L. J. Palumbo.

DISCLAIMER NOTICE

THIS DOCUMENT IS THE BEST
QUALITY AVAILABLE.

COPY FURNISHED CONTAINED
A SIGNIFICANT NUMBER OF
PAGES WHICH DO NOT
REPRODUCE LEGIBLY.

(9) Final technical rept.

SECURITY CLASSIFICATION OF THIS PAGE (When Data Entered)

REPORT DOCUMENTATION PAGE		READ INSTRUCTIONS BEFORE COMPLETING FORM
1. REPORT NUMBER NRL Memorandum Report 3482 ✓	2. GOVT ACCESSION NO.	3. RECIPIENT'S CATALOG NUMBER (14) NRL-MR-3482
4. TITLE (and Subtitle) ARPA/NRL X-RAY LASER PROGRAM, FINAL TECHNICAL REPORT ON ARPA ORDER NO. 2694 TO DEFENSE ADVANCED RESEARCH PROJECTS AGENCY ✓		5. TYPE OF REPORT & PERIOD COVERED Final report.
7. AUTHOR(s) Interaction Physics Branch Optical Sciences Division		6. PERFORMING ORG. REPORT NUMBER
9. PERFORMING ORGANIZATION NAME AND ADDRESS Naval Research Laboratory Washington, D.C. 20375		8. CONTRACT OR GRANT NUMBER(s)
11. CONTROLLING OFFICE NAME AND ADDRESS Defense Advanced Research Projects Agency Arlington, Virginia 22209		10. PROGRAM ELEMENT, PROJECT, TASK AREA & WORK UNIT NUMBERS NRL Problem N01-43 (15) ARPA Order-2694 Program Code 4D10
14. MONITORING AGENCY NAME & ADDRESS (if different from Controlling Office)		12. REPORT DATE (11) April 1977 (12) 287p.
		13. NUMBER OF PAGES 287
		15. SECURITY CLASS. (of this report) UNCLASSIFIED
		15a. DECLASSIFICATION/DOWNGRADING SCHEDULE
16. DISTRIBUTION STATEMENT (of this Report) Approved for public release; distribution unlimited.		
17. DISTRIBUTION STATEMENT (of the abstract entered in Block 20, if different from Report)		
18. SUPPLEMENTARY NOTES		
19. KEY WORDS (Continue on reverse side if necessary and identify by block number) X-ray lasers Lasers Ultraviolet lasers Laser-plasma interactions see also A023055		
20. ABSTRACT (Continue on reverse side if necessary and identify by block number) The ARPA/NRL x-ray laser program is concerned with demonstrating gain in the soft x-ray region. The overall program is jointly supported by ARPA and NRL. The approaches include electron-collisional pumping of ions, resonant charge transfer pumping, optical parametric mixing to short wavelengths, traveling wave e-beam and discharge pumping, and analysis and numerical modeling. This report covers the overall program for the ARPA portion as well as the progress made during the second half of FY-76 and FY-76T for both the ARPA portion and the continuing NRL effort.		

DD FORM 1 JAN 73 1473

EDITION OF 1 NOV 65 IS OBSOLETE
S/N 0102-014-6601

i
SECURITY CLASSIFICATION OF THIS PAGE (When Data Entered)

2519509B

CONTENTS

I.	INTRODUCTION	1
II.	COHERENT VACUUM-UV/SOFT X-RAY PULSES BY NONLINEAR MIXING AND AMPLIFICATION	5
	A. Introduction	5
	B. Efficient Second and Fourth Harmonic Conversion	6
	C. Compensation of Self-Phase Modulation	29
	D. Tunable Visible and VUV via Parametric Downconversion and Four-Wave Mixing	30
	E. Coherent Radiation in the XUV via Fifth and Seventh Order Mixing Processes	31
III.	ELECTRON-COLLISIONAL PUMPING VIA PICOSECOND LASER PUMPING OF PLASMAS	38
	A. Modeling of $3p-3s$ Lasing Schemes.	38
	B. Laser Plasma Interaction Experiments	45
	C. Hypocycloidal Pinch Device	69
IV.	RESONANT CHARGE TRANSFER PUMPING	70
V.	TRAVELING WAVE PUMPED VUV LASERS	77
	A. Introduction	77
	B. Molecular and Ion Laser Research	77
	C. Rare Gas Halide Excimer Laser Research	78
VI.	MISCELLANEOUS ANALYSES	84
VII.	SUMMARY	87
VIII.	APPENDICES (Separate Contents)	

ACCESSION	
NTIS	89
DOC	White Section <input checked="" type="checkbox"/>
UNANNOUNCED	Ref Section <input type="checkbox"/>
JUSTIFICATION	<input type="checkbox"/>
BY	
DISTRIBUTION/AVAILABILITY CODES	
Dist.	AVAIL. SEC. OR SPECIAL
A	

FINAL TECHNICAL REPORT
ON ARPA PROJECT

1. DARPA Order	2694
2. Program Code No.	4D10
3. Name of Contractor	Naval Research Laboratory Optical Sciences Division
4. Effective Date of Contract	1 January 1974
5. Contract Expiration Date	12 December 1976
6. Amount of Contract	\$250K (FY 76)
7. Contract No.	N/A
8. Principal Investigator	Dr. R. A. Andrews
9. Telephone No.	202-767-3528
10. Scientific Officer	Capt. H. Winsor, ARPA
11. Title of Work	X-Ray Lasers

Sponsored by

Defense Advanced Research Projects Agency

ARPA ORDER 2694

ARPA/NRL X-RAY LASER PROGRAM
Final Technical Report on ARPA Order No. 2394 to
Defense Advanced Research Projects Agency

I. INTRODUCTION

This is the final technical progress report for the ARPA portion of the ARPA/NRL co-sponsored X-Ray Laser Program. Prior to this report there were four semiannual technical progress reports. Each of these previous reports* was prepared in considerable detail. These reports are referenced frequently in this report, and no attempt has been made to duplicate that material in this report.

The goals of the program have remained the same since the program began in January 1974 — to define and explore at a number of locations the most promising approaches to achieve laser action and coherent radiation in the soft x-ray region. Considerable progress has been made in attaining this goal. Various promising approaches have evolved during the program, and the presently described approaches offer considerable promise for a continuing NRL program. Although significant progress has been made, ARPA has seen fit to terminate the program. Hence the promising results reported here do not represent the completion of a useful x-ray laser but strong evidence that the goal could be attained if the program had continued.

The approaches that have proved most promising and that are being pursued currently are:

Nonlinear optical mixing for producing coherent radiation in the vacuum-UV and soft x-ray regions;

Electron collisional pumping of ions in schemes amenable to isoelectronic extrapolations to short wavelengths;

*Previous semiannual reports on this project are referred to liberally in the present report. These are published as NRL Memorandum Reports N9. 2910 (October 1974), No. 3057 (March 1975), No. 3130 (September 1975), and No. 3241 (March 1976). Copies are available on request.

Note: Manuscript submitted April 6, 1977.

Investigation of resonant charge transfer pumping at a high rate into preferential levels as an advanced soft x-ray amplifier; and

Theory, analysis, and numerical modeling in support of these approaches and continual investigation of new concepts.

The overall theme in this program is to generate a coherent, collimated laser beam at as short a wavelength as possible for materials diagnostic applications. The general approach is to transfer a high degree of coherence from long wavelengths, with amplification through molecular and ionic devices in an eventual chain system as illustrated in Fig. 1. The areas of current NRL activity are bounded by solid lines; those of conceivable future activity by dashed lines. A high peak intensity pulse from a coherent laser at $1\text{ }\mu\text{m}$ is frequency upconverted into the vacuum ultraviolet (VUV), possibly with accurate tuning capability. This step is described in Section II. Electron collisional population inversion at shorter VUV wavelengths appears promising in magnetic pinch-heated plasmas (Section III). At shorter soft x-ray wavelengths, the rapid resonance charge transfer process remains most interesting for achieving significant inversion, and progress on the current definitive experiments is described in Section IV. An alternative to the nonlinear mixing process to achieve short wavelengths in the UV is traveling-wave pumped lasers. These are described in Section V. They suffer from a lack of coherence, however, and therefore are of limited application, i.e., primarily candidates for amplifiers. Some alternatives to these approaches have been studied. The results of the analysis appears in Section VI.

This general scheme as shown in Fig. 1 has changed since the last report. First, the concept of the electron collisional amplifier no longer includes a line focus laser-heated plasma as a possibility. This approach to the amplifier has been ruled out following a careful characterization of the laser-produced plasmas. This work showed that extremely high plasma density gradients make the region of interest for this problem extremely thin and in general not in a linear configuration. The details of this work appear in Section III. Second, the need for a H_2 or Xe amplifier in the region around $1600\text{ }\text{\AA}$ may have been eliminated. A major accomplishment of the last period has been the efficient generation of coherent radiation at 53 and 38 nm. The technique used was resonantly enhanced nonlinear mixing in rare gases. This work represents the shortest wavelength coherent radiation ever generated anywhere. The efficiency of the 53 nm generation is $\geq 10^{-5}$. This work is described in Section II. Finally, the charge transfer amplifier is on firmer ground. Recent work, which is described in Section IV, appears to confirm the existence of this physical process in an interaction region between a neutral gas and an expanding laser-produced plasma.

SOFT X-RAY LASERS
—NONLINEAR MIXING/AMPLIFIER CHAIN—

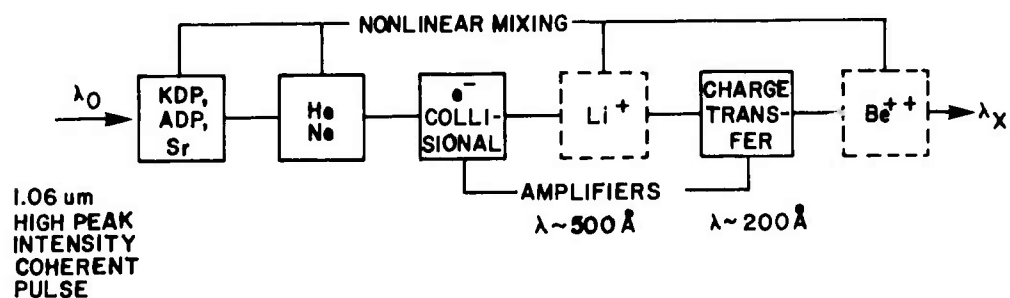


Fig. 1 — Block diagram of coherent amplification scheme

The following sections of this report describe the details of progress made in each of these areas since the last technical report. A summary of the important points is included in the last section. In some instances the work has been prepared for publication or has been published. In these cases the reprint has been included in the appendices and only brief mention of the work is made in the main body of the report. Each section also contains comments about where progress could be expected with continued effort.

Note added in proof (29 April 1977): Word has arrived that scientists at the Institute of Spectroscopy, Moscow under the direction of Prof. Letokhov have achieved a gain coefficient of 10 cm^{-1} at a wavelength of 60 \AA using a plasma produced from KCl and using photon pumping. While further details are not yet available, the resemblance to the scheme (2) described in Appendix A here and proposed to ARPA for an experiment in April 1976 is striking.

II. COHERENT VACUUM UV/SOFT X-RAY PULSES BY NONLINEAR MIXING AND AMPLIFICATION

II. A. INTRODUCTION

Single pass amplified spontaneous emission devices produce radiation of limited coherence. Because of the short lifetimes involved in the short wavelength emission processes, the coherence properties of the radiation is not easily improved by use of cavities. Frequency up-conversion through nonlinear optical processes provides a method of generating coherent light at desired wavelengths in the extreme ultraviolet and soft x-ray regions by transferring the coherence of laser radiation generated at longer wavelengths. In this section, the goals and major results of that part of the program which was directed toward demonstration of frequency upconversion into the XUV are described. This concept is based on a cascaded frequency conversion procedure. The primary attraction of this approach is that it takes advantage of the high quality coherent radiation generated in the mode-locked Nd:YAG laser. Two stages of second harmonic generation are used to generate the fourth harmonic at a wavelength of 266.1 nm. Using this as a primary source of radiation, two separate approaches have been investigated. In the first, the fourth harmonic pulses (266.1 nm) are converted to tunable radiation in the vacuum ultraviolet (VUV), through successive stages of parametric conversion followed by four wave mixing. This radiation can be tuned to match the wavelengths of multi-photon non-allowed transitions in appropriate gaseous media. This makes possible efficient resonantly enhanced conversion to even shorter wavelengths in the extreme UV (XUV). The possibility of amplification with appropriate VUV lasers was also considered.

In the second approach, the 266.1 nm radiation is converted directly to the XUV through higher order nonlinear processes (e.g., fifth or seventh harmonic conversion). Under appropriate conditions the efficiency of such high order conversion processes can be comparable to or exceed that of lower order processes due to resonant enhancement or phase matching considerations. Although such processes have been proposed in the literature for the generation of coherent short wavelength radiation, they have not previously been successfully demonstrated.

Both of these approaches require pulses at 266.1 nm of the highest possible power and beam quality and free of either spatial or temporal substructure. Thus, it is imperative to optimize both the laser performance and the harmonic conversion efficiency at each stage. Several aspects of this part of the program are summarized in what follows: (1) optimization of the second and fourth harmonic generation processes, (2) demonstration of compensation of self phase modulation at 1.06 μm using Cs vapor, (3) generation of tunable visible and VUV radiation using parametric down conversion and four wave mixing and, (4) generation of coherent radiation in the VUV through fifth and seventh order mixing processes.

Work on this approach has resulted in the establishment of two successive world records for the shortest wavelength coherent radiation - first at 53.2 nm by fifth harmonic generation and later at 38 nm by seventh harmonic conversion. In addition, this work is the first application of nonlinear optical processes of order higher than three to the generation of coherent radiation in the XUV. It demonstrates the feasibility of using such processes to extend the range of coherent wavelengths ever closer to the soft x-ray range and doing so with significant conversion efficiency.

II. B. EFFICIENT SECOND AND FOURTH HARMONIC CONVERSION

In this section we describe the optimization of the first two second harmonic generation (SHG) processes, which convert the neodymium laser output to 266 nm. The previously low observed conversion efficiencies of the individual harmonic generation steps has been an argument against cascaded upconversion of laser radiation to obtain coherent radiation at short wavelengths. This would result in severe reduction in energy and limit the process before useful wavelengths were reached. It is apparent from reports in the literature that there has been widespread difficulty in achieving satisfactory results in fourth harmonic generation of the 1.064 μm emission of neodymium lasers. However, there was good motivation to improve this situation. In addition to being a high intensity source for further nonlinear processes, the resulting fourth harmonic of this laser has many other potential applications, such as material studies and photochemistry. High efficiency conversion of Nd laser output to the fourth harmonic would provide a 266 nm source with many desirable characteristics: ease of operation, high power, good optical characteristics, and pulse durations that can be selected in the range from picoseconds to nanoseconds. Through careful control of experimental conditions and expanding theoretical understanding of the second harmonic generation process, greatly improved conversion efficiencies to 266 nm have been achieved and new aspects of the harmonic conversion process which are important to the laser research community have been discovered.

The second frequency doubling from 532 nm to 266 nm is the more difficult step in obtaining the fourth harmonic of the laser emission. At the time this investigation of harmonic generation was begun, 80% conversion had already been reported for the 1.064 μm to 532 nm first step¹. The best reported experimental conversions for doubling from 532 nm to 266 nm were in the range of 30 to 40%, whereas corresponding theoretically predicted conversions were in the range of 70 to 80%. Energy conversions of 80% in the first doubling have been duplicated and 85% conversion efficiency in the second doubling to 266 nm has been obtained. This is the highest value yet reported, and these experimental results are in excellent agreement with theory. In addition, it has been demonstrated that harmonic generation under improper conditions will result in distortion of both pulse shape and spectral distribution, which further limits the usefulness of the harmonic and transmitted

fundamental pulses.

II. A.1. EXPERIMENTAL

a. LASER

The essential experimental tool that allowed these results was the mode-locked Nd:YAG laser system developed early in this program^{2,3}. Briefly, the laser is operated at a single pulse output of 70-mJ energy and 35-psec duration. The spatial distribution is Gaussian-like and propagates nearly diffraction limited with the far field distribution only 10% larger in radius than the diffraction limited value. The spectral distribution is only slightly in excess of the time-bandwidth limited value due to the presence of a $.8\pi$ peak self-phase modulation occurring in the final stages of laser amplification. As is described below, good optical quality of the fundamental laser beam is essential to high level second harmonic generation. Minimum pulse distortion due to self focusing and self-phase modulation as well as good optical quality become critically important to the more difficult cascaded second harmonic generation process used to obtain the fourth harmonic of the laser output.

b. SECOND HARMONIC GENERATION, 1.064 μm TO 532 nm

A 50-mm long crystal of KDP is used for the first doubling step with 00-E phase matching and angle tuning. For both steps of harmonic conversion it is necessary to adjust input intensity to match crystal length. Excessive intensity makes tuning to phase matching extremely critical, and low intensity results in low conversion. The direct output of the laser had a peak intensity of $3 \times 10^9 \text{ W/cm}^2$. At this intensity satisfactory harmonic conversion with the 50 mm crystal was not possible. It was necessary to use a telescope to double the beam diameter and reduce the peak intensity to $8 \times 10^8 \text{ W/cm}^2$. Even at the reduced intensity, angle tuning to phase matching was extremely critical requiring adjustment to 5×10^{-5} radian to obtain optimum harmonic conversion.

c. CASCADED SECOND HARMONIC GENERATION FROM 532 nm TO 266 nm

High efficiency harmonic conversion from 532 nm to 266 nm in phase-matched crystals was more difficult. The discrepancies between observed experimental conversion and theoretically predicted values had been attributed in the literature to such varied processes as linear or non-linear absorption at 266 nm, disturbance of the phase-matching condition due to absorption followed by local heating, group velocity dispersion, and improper or incomplete phase matching^{1,4,5,6}. This process was investigated using crystals of ADP and KD*P of various lengths observing conversion efficiency, total energy transmission, and spectra of incident and transmitted radiation. The results of this investigation

showed it was necessary to use short crystals (~ 4 mm) to obtain satisfactory phase matching in the presence of the self-phase modulation of the fundamental pulse and large group velocity dispersion of the crystals at these wavelengths. With crystals of this length it is necessary to use high intensities ($\sim 10^{10}$ W/cm²) to achieve conversion in the 70 to 80% range.

The experimental setup used to measure conversion is shown in Fig. 2. The 532 nm radiation from the first SHG crystal was isolated with a polarizing prism. Telescopes were used to obtain different intensities at the second doubler crystal. Energy at 532 nm was monitored both before and after the crystal with beam splitters and a calibrated photodiode. Harmonic energy at 266 nm was monitored with a second calibrated photodiode. The crystals were tuned through phase matching either by temperature or angle tuning. A variation from unity of the normalized sum of fundamental and harmonic energies would indicate the presence of nonlinear absorption. No such absorption was observed in the SHG process (Fig. 3). Similar measurements with ADP and KD*P crystals of various lengths tuned to phase matching showed large oscillations of conversion efficiency with crystal length but no evidence of nonlinear absorption (Fig. 4). This indicated that the problem of low conversion in long crystals was caused by improper phase matching.

Conversion efficiency was also measured at different pump energies in 4 mm samples of ADP and KD*P (Fig. 5). The observed conversion for ADP lies between theoretical curves for a plane wave with Gaussian pulse shape and a pulse Gaussian in both time and space. This is expected since the fundamental pulse will have experienced reduced conversion in its low intensity wings in the first doubling process. Conversion efficiencies are slightly higher for ADP than the corresponding values for KD*P due to the larger SHG coefficient of ADP. The greater temperature sensitivity of ADP⁷ and the larger two photon absorption coefficient described below, however, make KD*P the crystal of choice for SHG from 532 nm to 266 nm.

Spectra of the input and transmitted pulses give further insight into the physical processes involved. Simultaneous spectra of the incident fundamental at 532 nm and the transmitted fundamental and harmonic at 266 nm were made by illuminating different portions of the input slit of a grating spectrograph with the three beams. The spectra obtained with short crystals (4 mm) and high conversion show no development of structure (Fig. 6 a). In contrast, the spectra of the transmitted fundamental and harmonic with long crystals (25 mm) show deep modulation even though the incident pump spectrum has little distortion and only slight broadening due to self-phase modulation (Fig. 6 b).

d. NONLINEAR ABSORPTION OF ADP AND KD*P AT 266 nm

An immediate application of the intense, well characterized pulses

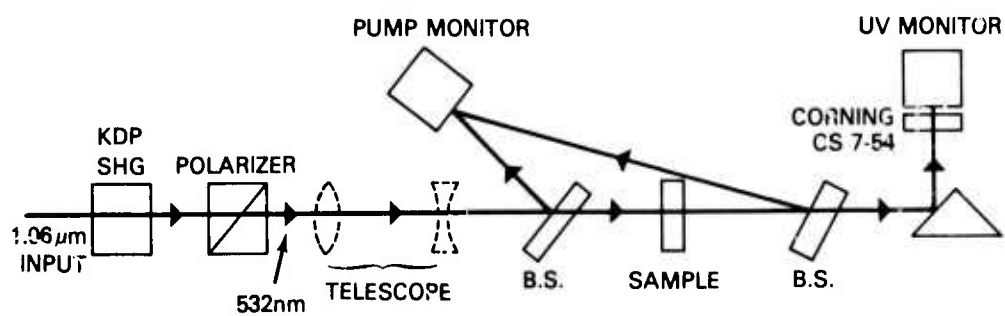


Fig. 2 — Experimental setup used to measure second harmonic conversion from 532 nm to 266 nm

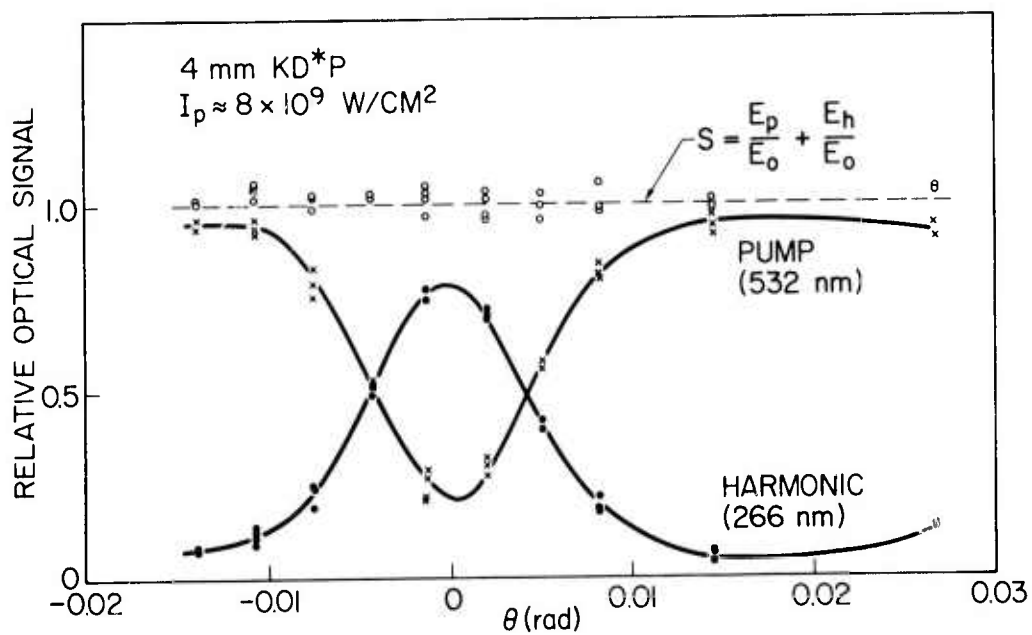


Fig. 3 — Fundamental pump transmission and harmonic conversion efficiency dependence for angle tuned SHG from 532 to 266 nm. The normalized sum of pump and harmonic signals shows no evidence of nonlinear absorption at high harmonic intensities.

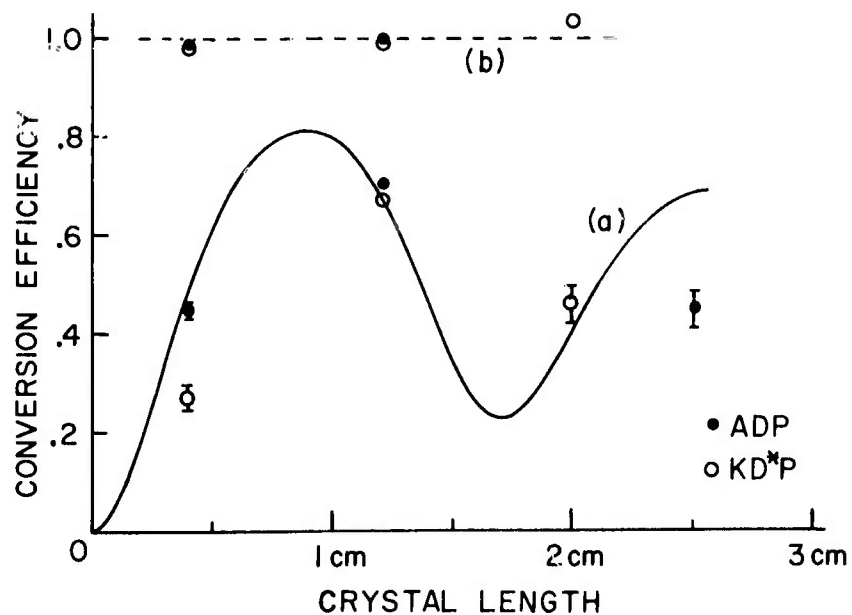


Fig. 4 — SHG conversion efficiency as a function of crystal length. Initial fundamental peak intensity was 10^9W/cm^2 for these measurements. The solid curve (a) is obtained from a time dependent numerical solution. The dashed line (b) is the sum of normalized transmitted fundamental and harmonic signals.

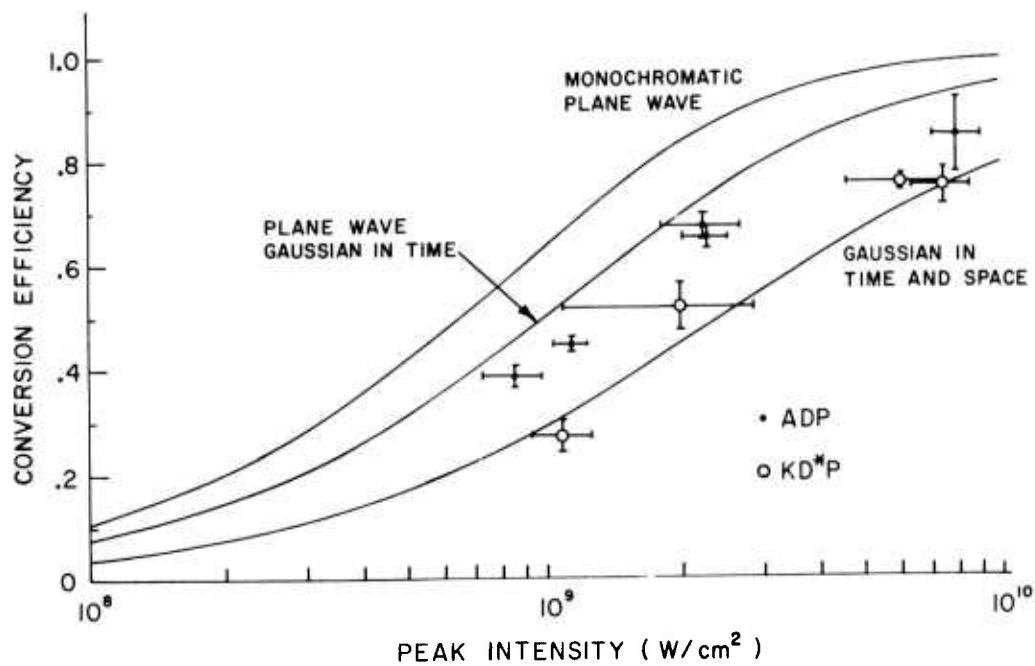


Fig. 5 — Conversion efficiencies for different pump intensities in 4 mm samples of ADP and KD*P (data points). Solid lines are theoretical SHG conversion efficiencies for various spatial and temporal intensity distributions of the incident fundamental.

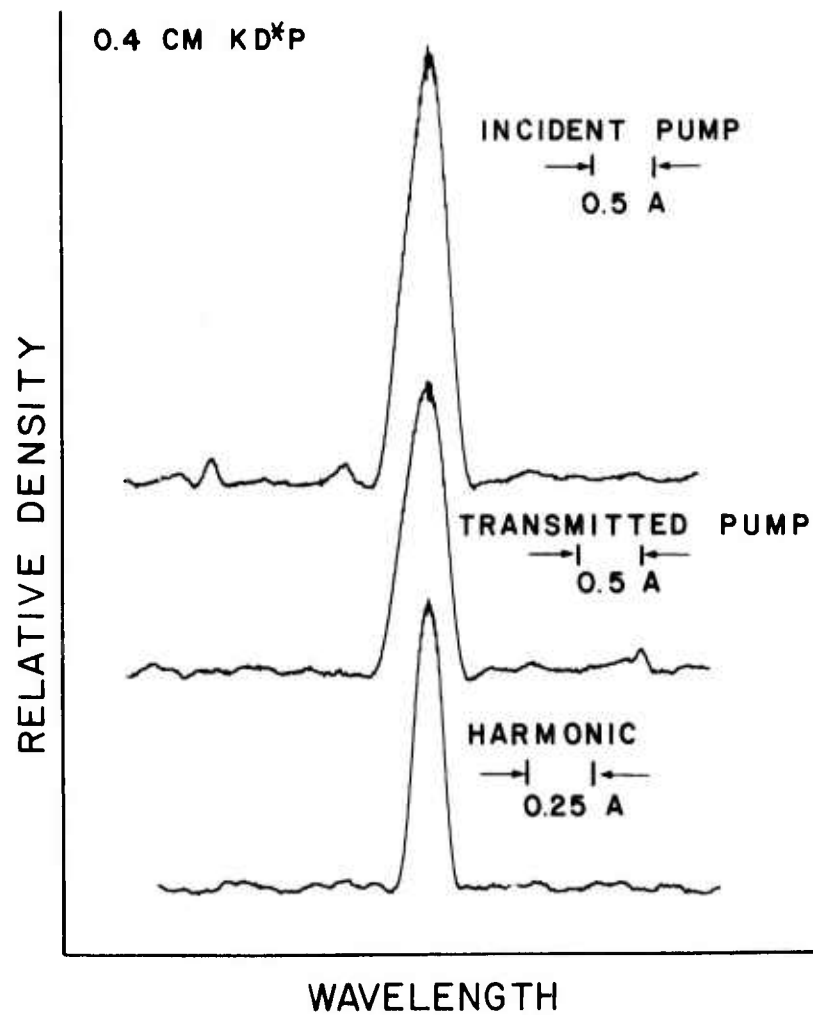


Fig. 6(a) — Spectra of fundamental and harmonic pulses obtained with .4 cm crystal in experimentally observed SHG from 532 nm to 266 nm

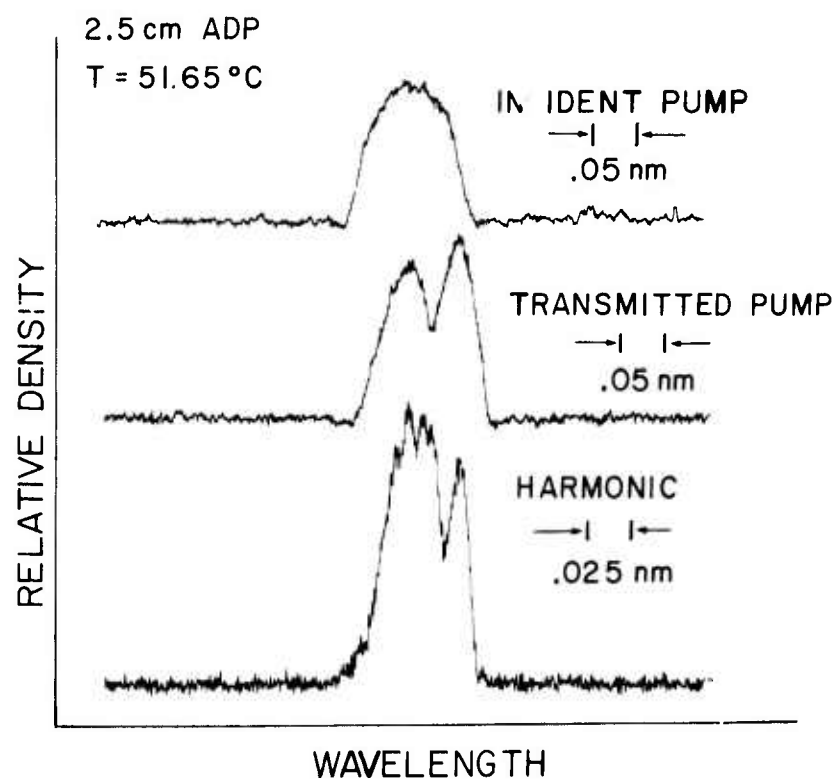


Fig. 6(b) — Spectra obtained with 2.5 cm crystal

at 266 nm was the study of nonlinear absorption in the two crystal materials, which it was not possible to infer indirectly from the previous measurements of the SHG process. After fourth harmonic generation, the 266 nm radiation was isolated with dispersing prisms. The intensity of the radiation was adjusted by telescoping and tuning the cascaded SHG crystal through phase matching. The 266 nm pulse was then transmitted through additional samples of ADP and KD*P with the crystal rotated 90° to prevent the inverse parametric process from depleting the pulse. Incident and transmitted intensities were measured to determine the dependence of transmission on intensity. It was found that the nonlinear transmission coefficients were 11×10^{-11} cm/W and 2.5×10^{-11} cm/W for ADP and KD*P respectively. Linear absorption coefficients were measured on a spectrophotometer and found to be $.035 \text{ cm}^{-1}$ for both materials.

The effect of linear absorption ($\alpha = .035 \text{ cm}^{-1}$) and nonlinear absorption ($\beta = 11 \times 10^{-11} \text{ cm/W}$) on harmonic conversion efficiency for a monochromatic planewave is shown in Fig. 7. A family of curves is given for different input pump intensities with harmonic conversion efficiency plotted as a function of crystal length. The curves indicate that, for input intensities between 10^9 W/cm^2 and 10^{10} W/cm^2 , four mm is a good choice for crystal length. The broad maximum in the envelope near 20 mm indicates the optimum length for conversion of a monochromatic plane wave. This length is reduced by phase matching considerations for short pulses with phase modulation.

II. B.2. THEORETICAL

a. MONOCHROMATIC PLANEWAVE APPROXIMATION

The equations which describe SHG generation of a monochromatic planewave are

$$\frac{dE_2(z)}{dz} = \frac{d\omega}{nc} E_1^2(z) \exp(-i\Delta kz) \quad (1)$$

$$\frac{dE_1(z)}{dz} = -\frac{d\omega}{nc} E_1^*(z) E_2(z) \exp(i\Delta kz). \quad (2)$$

Here MKS units are used, $E_1(z)$ and $E_2(z)$ are the complex amplitudes of the fundamental and harmonic electric fields, d is the effective SHG coefficient, ω the angular frequency of the fundamental, n the index of refraction, c the velocity of light, z the coordinate in the direction of propagation in the crystal and Δk the wavevector mismatch $\Delta k = k_{2\omega} - 2k_\omega$. Simple solutions exist for two cases, first where conversion is small and E_1 can be treated as a constant, and second where phase matching is perfect and $\Delta k = 0$.

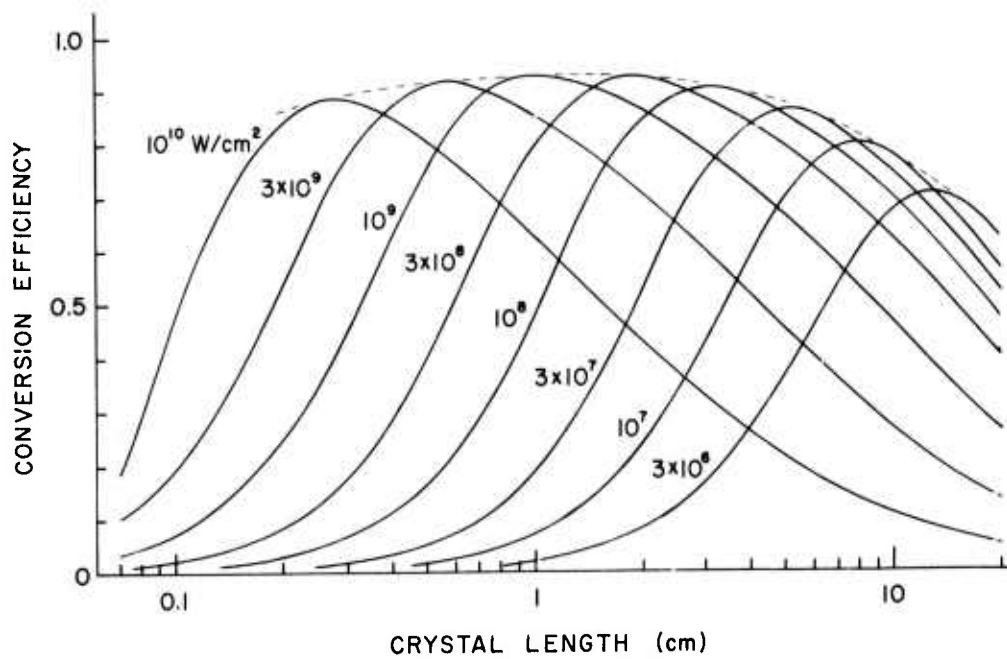


Fig. 7 — Theoretical SHG conversions for monochromatic plane waves with linear and nonlinear absorption at 266 nm. Curves for different initial pump intensities are shown.

$$\text{For } E_1 = \text{const. } E_2(z) = \frac{\omega d}{nc} E_1^2 \frac{\sin\left(\frac{\Delta kz}{2}\right)}{\frac{\Delta k}{2}} \exp\left(-i \frac{\Delta kz}{2}\right) \quad (3)$$

$$\text{For } \Delta k = 0 \quad E_2(z) = E_1(0) \tanh\left(\frac{\omega d}{nc} E_1(0)z\right) \quad (4)$$

Equation (4) is a valid approximation for high level harmonic conversion when $\Delta kz \ll 1$ which is the case for our harmonic conversion experiments with 4 mm crystals. The total conversion efficiency is obtained by integrating over the pulse in space and time,

$$\eta = \frac{\int_{-\infty}^{+\infty} dt \int_0^{\infty} dr 2\pi r E_{in}^2(t,r) \tanh^2\left(\frac{\omega d}{nc} E_{in}(t,r)z\right)}{\int_{-\infty}^{+\infty} dt \int_0^{\infty} dr 2\pi r E_{in}^2(t,r)} \quad (5)$$

The solid curves in Fig. 5 were obtained by numerical integration of Eq. (5) using the specified pulse shapes. Comparison of the three curves in the figure illustrates that very high conversion are required at the peak of the pulse to obtain moderate overall conversions. The table below shows overall and peak conversions for some values using a fundamental pulse Gaussian in time and space.

<u>Overall Conversion</u>	<u>Conversion at Peak</u>
85%	99.9%
75%	99.0%
50%	87.0%
25%	56.0%

The low level tuning curve described by Eq. (3) cannot be arbitrarily extended to any level of conversion. To obtain tuning curves for high level harmonic conversion, it is necessary to solve Eqs. (1) and (2) numerically (Figs. 8 and 9). When this is done we find that the central phase matching peak narrows and the secondary maxima increase in height as conversion increases. It is not possible to obtain perfect phase matching under laboratory conditions, nor is it possible to obtain zero beam divergence. Therefore, attempting conversion at too high a level will make phase matching impossible. At best, tuning to phase matching is extremely sensitive at high conversion levels as has been demonstrated in the 1.064 μm to 532 nm conversion.

The addition of linear and nonlinear absorption to the problem of harmonic generation with a monochromatic planewave requires a simple

SHG PHASE-MATCHING CURVE
50.8mm KDP, $\lambda_r=1064\text{ nm}$

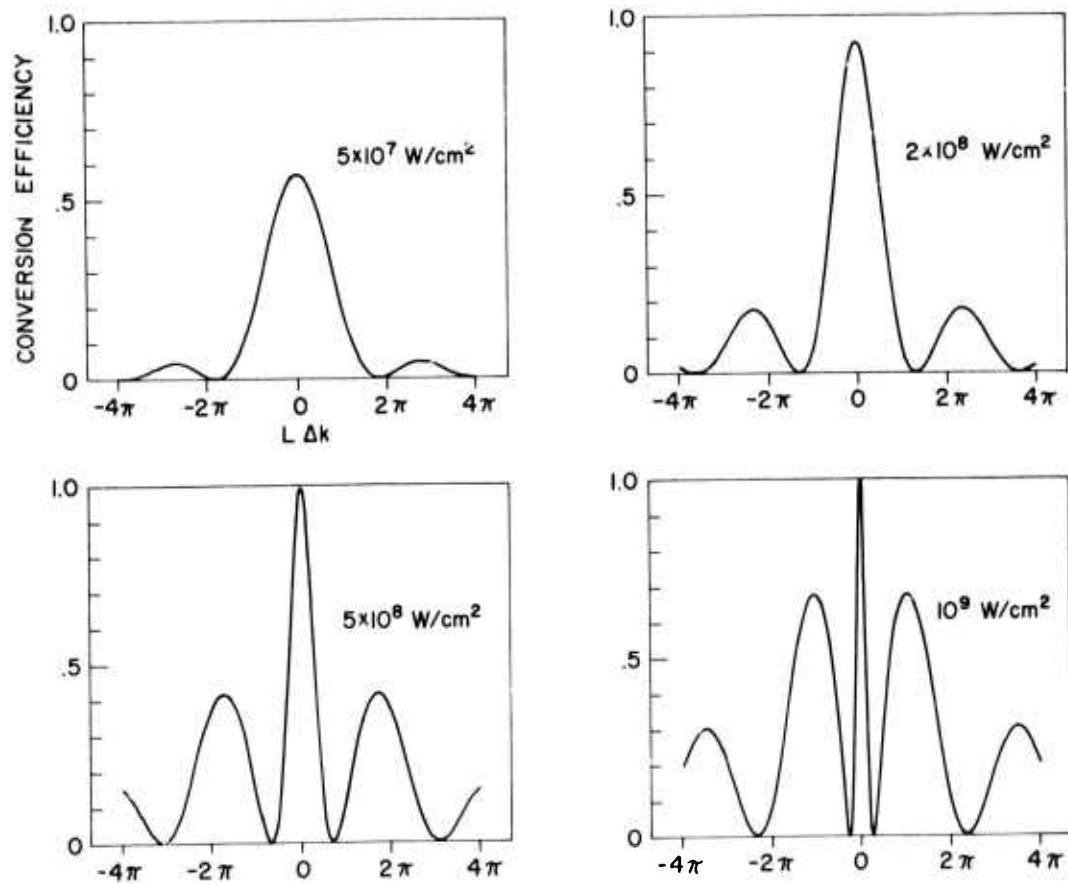


Fig. 8 — Theoretical tuning curves for SHG from 1064 to 532 nm in 50.8 mm long KDP.
Different initial intensities for a monochromatic planewave fundamental are used.

SHG PHASE-MATCHING CURVE
4mm ADP, $\lambda_r = 532$ nm

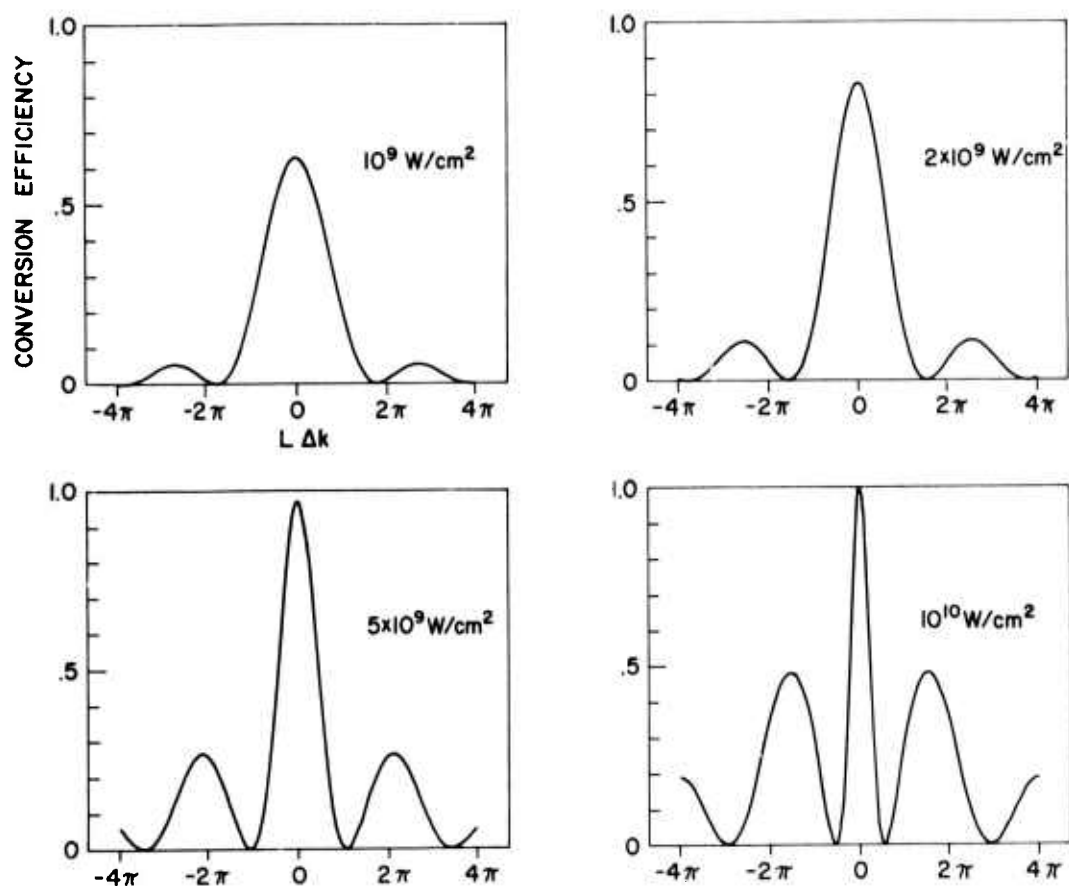


Fig. 9 — Tuning curves for SHG from 532 to 266 nm in 4 mm long ADP. Different initial intensities for a monochromatic planewave fundamental are used.

extension of Eqs. (1) and (2).

$$\begin{aligned} \frac{dE_2(z)}{dz} = & -\frac{\alpha}{2} E_2(z) \\ & -\frac{n}{2} \sqrt{\frac{\epsilon_0}{\mu_0}} \frac{\beta}{2} E_2(z) E_2^*(z) E_2(z) \\ & + \frac{d\omega}{nc} E_1^2(z) \exp(-i\Delta kz) \end{aligned} \quad (6)$$

$$\frac{dE_1(z)}{dz} = -\frac{d\omega}{nc} E_2(z) E_1(z) \exp(i\Delta kz) \quad (7)$$

Here a linear absorption coefficient α and a two photon absorption coefficient β for absorption only at the second harmonic have been included. These equations were solved numerically for the case of $\Delta k = 0$ to obtain the curves shown in Fig. 8.

a. GROUP VELOCITY DISPERSION

The group velocities for room temperature angle tuned ADP obtained from dispersion data⁹ are $v_{g,f} = 1.9177 \times 10^{10}$ cm/sec for the o-ray at $\lambda_f = 532$ nm and $v_{g,h} = 1.8029 \times 10^{10}$ cm/sec for the e-ray at $\lambda_h = 266$ nm. The difference between these two values $v_{g,f} - v_{g,h} = 1.48 \times 10^9$ cm/sec is about ten times as large as the corresponding value in KDP for harmonic generation from $1.064 \mu\text{m}$ to 532 nm. This is the reason shorter crystals are required for the 532 nm to 266 nm process. Dispersion in group velocity will cause the harmonic pulse to propagate slower and "walk off" the fundamental. The rate of this walk off is $(v_{g,f} - v_{g,h})/(v_{g,f} v_{g,h}) = 3.3$ psec/cm of crystal length. The group velocity dispersion will reduce harmonic conversion over the case of no group velocity dispersion, but conversion efficiency remains a monotonically increasing function of crystal length for time bandwidth limited pulses⁹. Only when the fundamental pulse has some excess bandwidth due to modulation, will the conversion efficiency oscillate with crystal length.

The presence of phase modulation on the input pulse disturbs the phase relationship between harmonic and fundamental as the more slowly propagating harmonic walks through the fundamental pulse. The harmonic pulse can then drive the fundamental through the inverse parametric process, resulting in a limitation of the conversion efficiency, generation of new frequencies, and distortion of both pulses.

c. TIME DEPENDENT SOLUTION

It is necessary to express the equations for harmonic generation in

time dependent form to include the effects of dispersion and self-phase modulation:

$$\frac{\partial}{\partial z} \mathcal{E}_{2\omega}(z, \Delta\omega) = i \frac{\omega d}{nc} \exp \left\{ -i \left(\Delta k + \frac{\Delta\omega}{v_{g,h}} \right) z \right\} \times \frac{1}{\pi} \int_{-\infty}^{+\infty} E_{\omega}^2(z, t) \exp(i\Delta\omega t) dt \quad (8)$$

$$\frac{\partial}{\partial z} \mathcal{E}_{\omega}(z, \Delta\omega) = i \frac{\omega d}{nc} \exp \left\{ i \left(\Delta k - \frac{\Delta\omega}{v_{g,f}} \right) z \right\} \times \frac{1}{\pi} \int_{-\infty}^{+\infty} E_{2\omega}(z, t) E_{\omega}^*(z, t) \exp(i\Delta\omega t) dt. \quad (9)$$

Here \mathcal{E}_{ω} and $\mathcal{E}_{2\omega}$ are complex spectral amplitudes and E_{ω} and $E_{2\omega}$ are complex electric field amplitudes. The electric field amplitude and spectral amplitudes are related by the Fourier transform pair

$$\left. \begin{aligned} E(z, t) &= \frac{1}{2} \int_{-\infty}^{+\infty} \mathcal{E}(z, \Delta\omega) \exp(-i\Delta\omega t) dt \\ \mathcal{E}(z, \Delta\omega) &= \frac{1}{\pi} \int_{-\infty}^{+\infty} E(z, t) \exp(i\Delta\omega t) d\Delta\omega. \end{aligned} \right\} \quad (10)$$

The time dependent equations (Eqs. 8 and 9) were solved numerically for different conditions of interest for comparison with the experimental investigations. An input pump pulse with intensity dependent phase modulation was used

$$E_{\omega}(0, t) = E_0 \exp(i\phi e^{-t^2/a^2}) \exp(-t^2/2a^2). \quad (11)$$

Parameters used were appropriate for 532 nm to 266 nm conversion in ADP. Peak input intensity was chosen to be 10^9 W/cm², and pulse width, $2a$, was set equal to 27 psec. Different values of peak intensity-dependent phase modulation ϕ and central frequency wavevector mismatch Δk were used (Fig. 10). Even a slight amount of phase modulation, $\phi = .1\pi$, which would be difficult to detect experimentally, drastically reduces harmonic conversion in a 25 mm crystal. The solution for $\phi = .8\pi$ has a fortuitous fit with the experimental data.

The distortion of harmonic and transmitted fundamental pulses is illustrated by following the calculation for $\phi = .4\pi$ in more detail. Pulse shapes obtained from the numerical calculation are shown for 4 mm

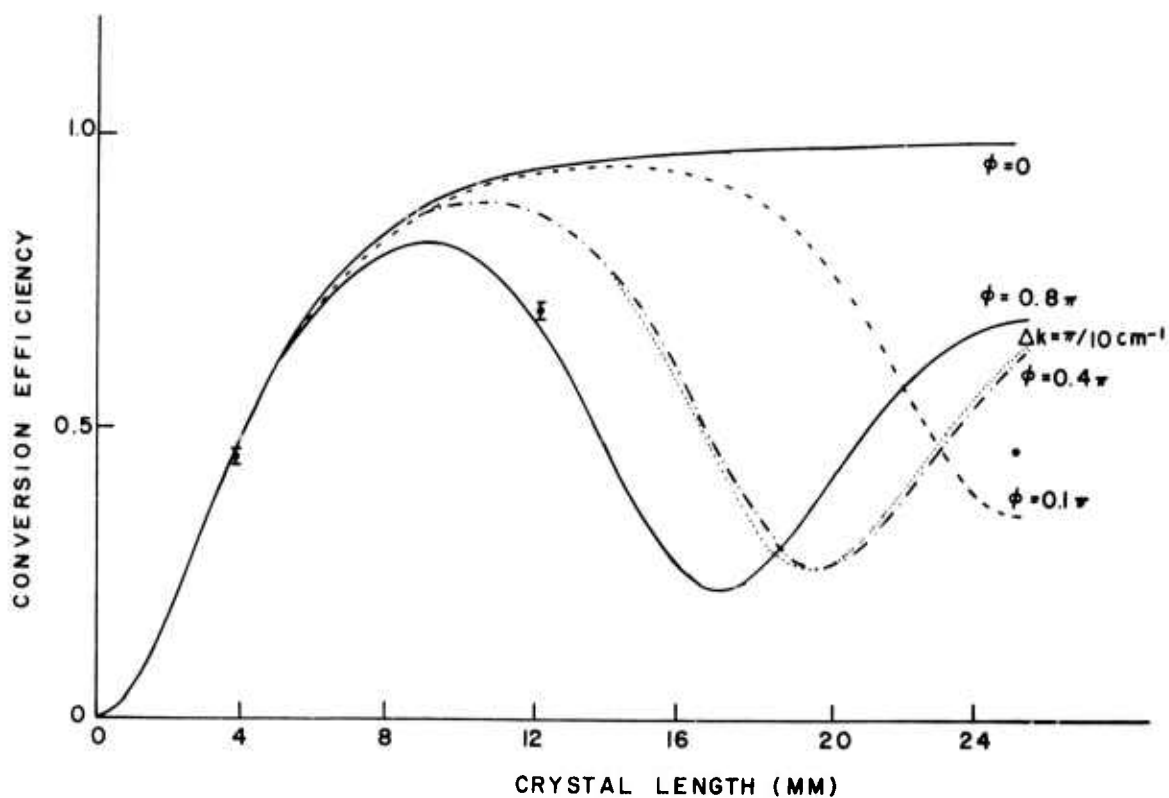


Fig. 10 — Theoretical conversion efficiencies as a function of crystal length for different amounts of shelf-phase modulation or central frequency wavevector mismatch. Curves are numerical solutions to time dependent equations.

increments of crystal length (Figs. 11a and 11b). The corresponding spectra for the fundamental and harmonic are also given (Figs. 12a and 12b). For crystal lengths up to 8 mm, harmonic generation shows no anomalies, and the structure that develops in the fundamental pulse is due to depletion of the central region. At 12-mm crystal length, harmonic conversion has peaked, and the harmonic pulse is starting to drive the fundamental through the inverse parametric process. As the two pulses propagate through greater crystal lengths, energy is exchanged between fundamental and harmonic and the distortion increases. Finally, at 25.5 mm crystal length the pulses are reduced to bursts of fluctuations. This type of distortion severely limits the applications of these pulses. There is a marked similarity between the calculated spectra at $L=20$ mm (Fig. 12b) and the experimentally measured spectra (Fig. 6b).

It is possible to define an effective wavenumber mismatch Δk_{eff} resulting from the intensity dependent phase modulation and group velocity dispersion. This effective mismatch is obtained from the equation

$$\Delta k_{\text{eff}} = \frac{1}{L} \frac{\int \{\phi_{2\omega}(t) - 2\phi_{\omega}(t)\} e^{-t^2/2a^2} e^{-(t-\Delta t)^2/2a^2} dt}{\int e^{-t^2/2a^2} e^{-(t-\Delta t)^2/2a^2} dt} \quad (12)$$

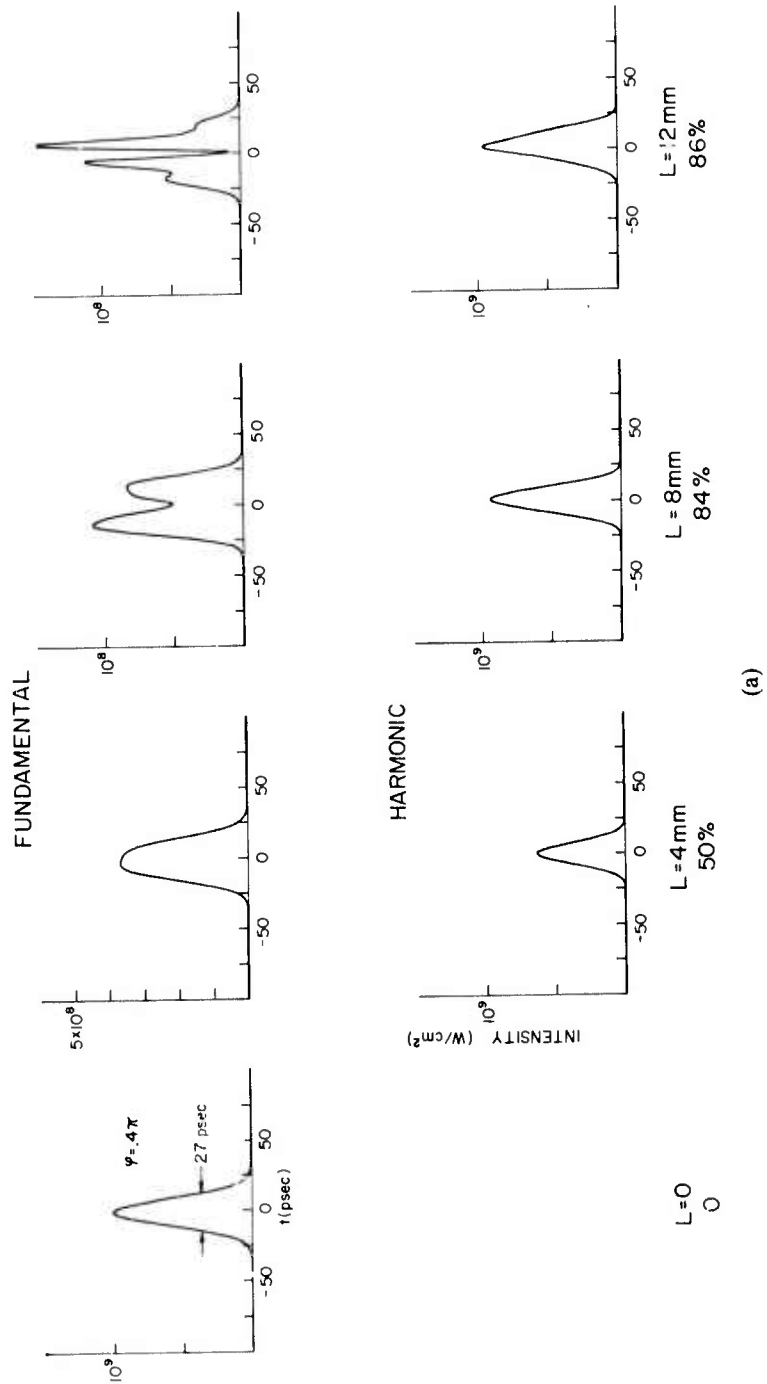
with $\phi_{2\omega}(t) = 2\phi e^{-(t-\Delta t)^2/a^2}$, $\phi_{\omega}(t) = \phi e^{-t^2/a^2}$ and $\Delta t = \ell(\nu_{g,f} - \nu_{g,h})/(\nu_{g,f} \nu_{g,h})$. For small Δt , i.e., $\Delta t \ll a$ Eq. 12 can be integrated to yield

$$\Delta k_{\text{eff}} \approx \frac{\phi}{a} \left(\frac{\nu_{g,f} - \nu_{g,h}}{\nu_{g,f} \nu_{g,h}} \right). \quad (13)$$

With $\phi = .4\pi$ and $a = 13.5$ psec, $\Delta k_{\text{eff}} \approx .31$. Numerical solutions for $\phi = .4\pi$, and $\Delta k = 0$ yield similar results for conversion efficiency as a function of crystal length (Fig. 10). With knowledge of the amount of phase modulation on the input pump pulse and group velocity dispersion it is now possible to set additional criteria for crystal length and input intensity. The maximum value of $\Delta k_{\text{eff}} L$ can be determined from tuning curves such as those shown in Figs. 8 and 9. Knowledge of Δk_{eff} and the desired peak conversion efficiency determine the maximum crystal length that can be tolerated. Solution of Eq. 4 then determines the peak input intensity required for the desired conversion. This value must be below the damage threshold, which is observed to be $\sim 2 \times 10^{10}$ W/cm² for the crystals used in this work.

It has been demonstrated that greatly improved efficiency can be obtained in the conversion of neodymium laser radiation to its fourth harmonic if high optical quality is maintained in the fundamental laser

CALCULATED SHG IN ADP, $\lambda_f = 532 \text{ nm}$
(PULSE SHAPES)



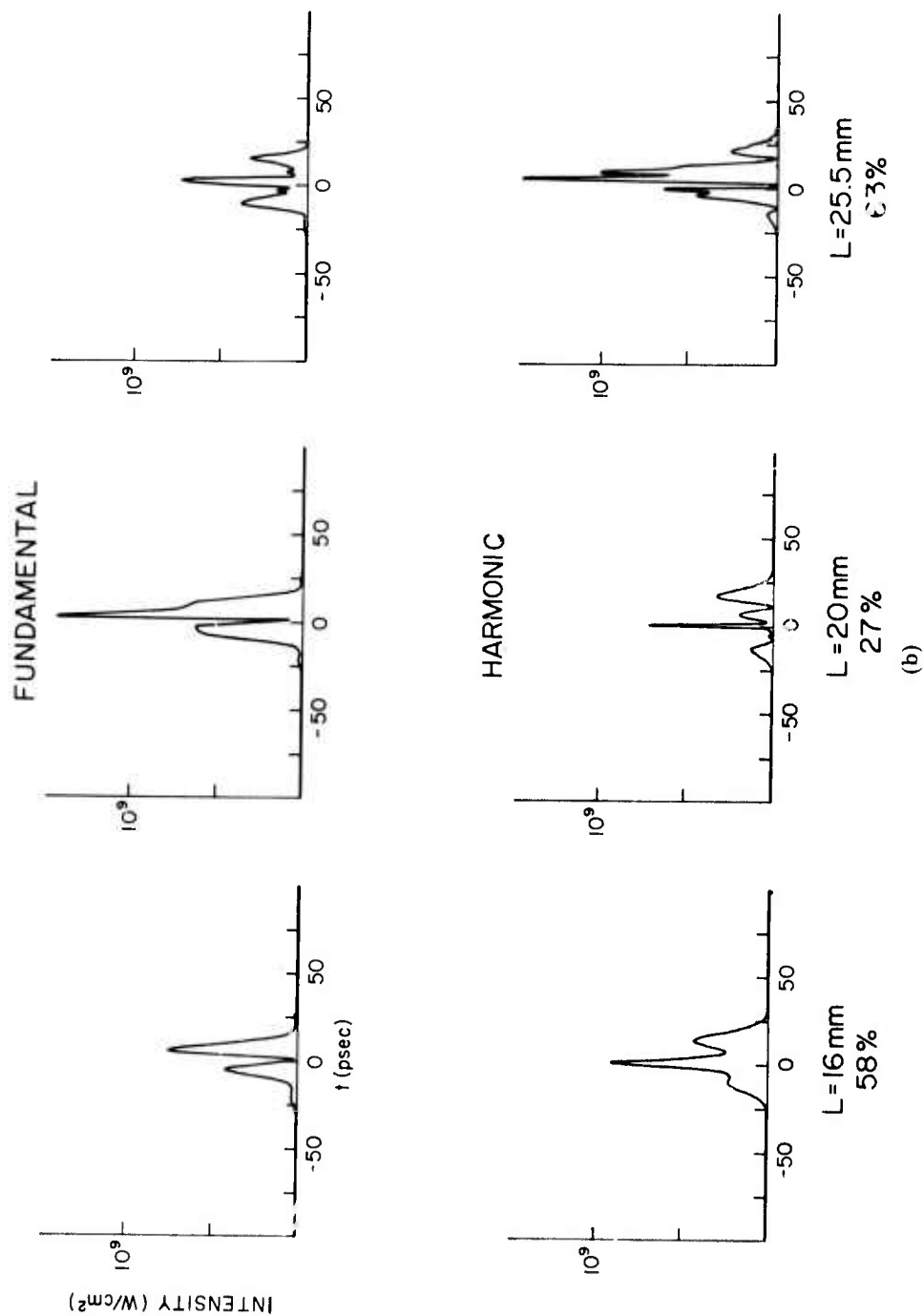
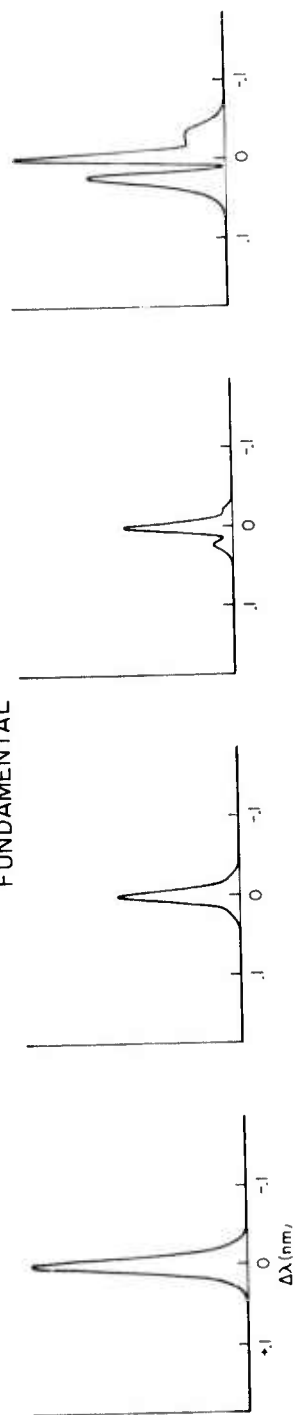


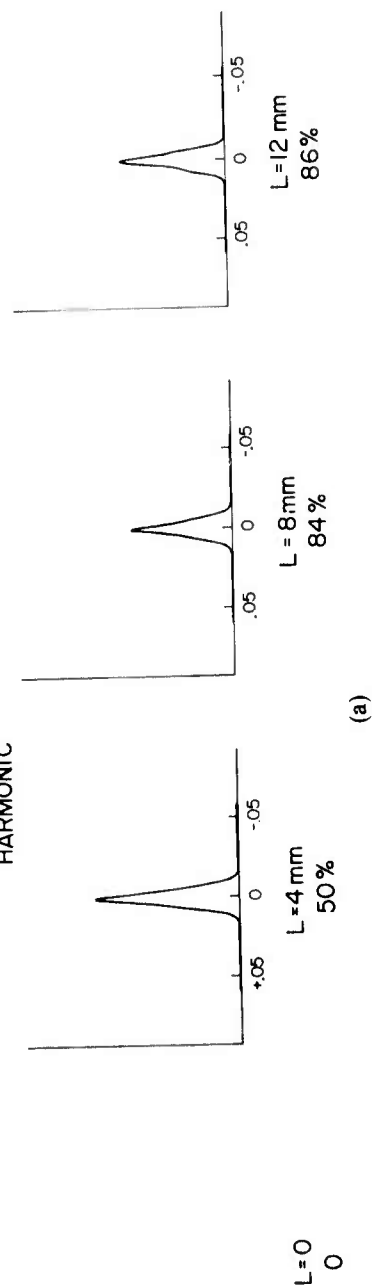
Fig. 11 — Theoretical development of pulse shape for SHG from 532 to 266 nm in ADP

CALCULATED SHG IN ADP, $\lambda_f = 532$ nm
(SPECTRA)

FUNDAMENTAL

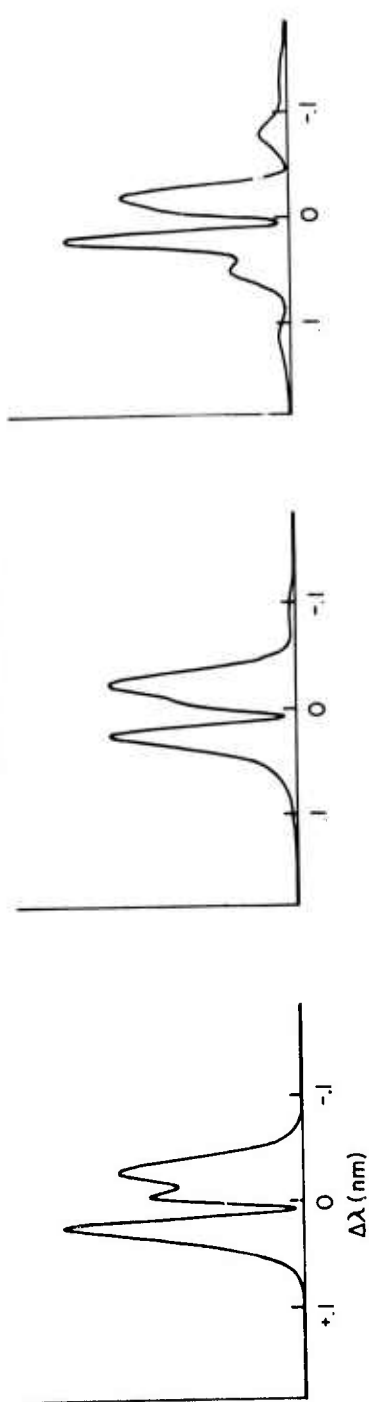


HARMONIC



(a)

FUNDAMENTAL



HARMONIC

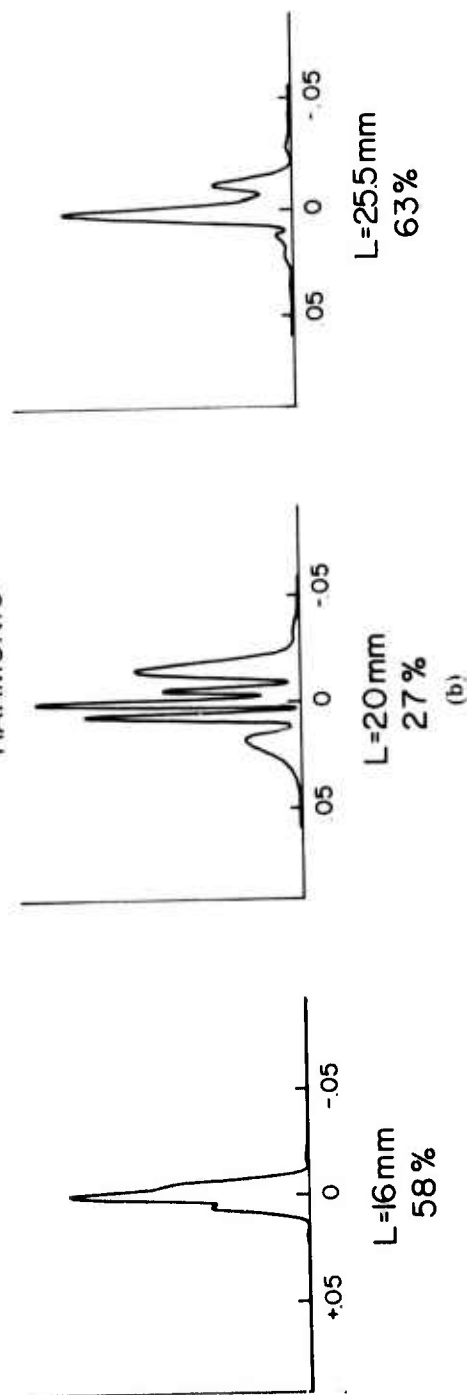


Fig. 12 — Calculated spectra; development for SHG from 532 to 266 nm in ADP

pulse and intensities and crystal lengths are properly chosen for optimum harmonic generation. In work performed on this contract, the highest second harmonic conversion efficiencies reported in the literature have been obtained. It has been demonstrated that problems caused by group velocity dispersion and self-phase modulation, which have limited the 532 nm to 266 nm harmonic generation in the past, can be avoided. The first reported measurement of two photon absorption coefficients of ADP and KD*P at 266 nm have been made. Finally, the theoretical understanding of high conversion efficiency second harmonic generation has been expanded. With these advances, the fourth harmonic of the neodymium laser provides distinct advantages as an ultraviolet source compared to lasers that generate output directly in the ultraviolet. Most importantly, the resultant fourth harmonic provides a more useful source for further coherent upconversion to the vacuum ultraviolet.

REFERENCES

1. V. D. Volosov, V. N. Krylov, V. A. Serebryakov, and D. V. Sokolov "Highly Effective Generation of the Second and Fourth Harmonics of High-Power Picosecond Pulses," *ZhETF Pis. Red.* 19, 38-41 (1974).
2. Interaction Physics Branch, Optical Sciences Division, "ARPA/NRL X-Ray Laser Program Semiannual Technical Report — 1 Jan 1974 - 30 Jun 1974," *NRL Memorandum Report 2910* (Oct 1974).
3. Interaction Physics Branch, Optical Sciences Division, "ARPA/NRL X-Ray Laser Program Semiannual Technical Report — 1 Jul 1974 - 31 Dec 1974," *NRL Memorandum Report 3057* (May 1975).
4. W. H. Glenn, "Second-Harmonic Generation by Picosecond Optical Pulses," *IEEE J. Quant. Electron.* QE-5, 284-290 (1969).
5. K. Kato, "Conversion of High-Power Nd:YAG Laser Radiation to the UV at 2661 Å," *Opt. Commun.* 13, 361-362 (1975).
6. Y. S. Lin, W. B. Jones, and J. P. Chernoch, "High-Efficiency High-Power Coherent UV Generation at 266 nm in 90° Phase-Matched Deuterated KDP," *Appl. Phys. Lett.* 29, 32-34 (1976).
7. R. A. Phillips, "Temperature Variation of the Index of Refraction of ADP, KDP and Deuterated KD*P," *J. Opt. Soc. Am.* 56, 629-632 (1966).
8. Frits Zernike, Jr., "Refractive Indices of Ammonium Dihydrogen Phosphate and Potassium Dihydrogen Phosphate between 2000 Å and 1.5 μ," *J. Opt. Soc. Am.* 54, 1215-1220 (1964).
Frits Zernike, Jr., *Errata, J.O.S.A.* 55, 210 (1965).

9. Yu N. Karamzin and A. P. Sukhorukov, "Limitation on the Efficiency of Frequency Doublers of Picosecond Light Pulses," Sov. J. Quant. Electron. 5, 496-500 (1975).

II. C. COMPENSATION OF SELF-PHASE MODULATION

As part of the development of a mode-locked Nd:YAG laser system for these experiments, investigations were made to check the feasibility of reducing the phase modulation introduced by the Nd:YAG amplifiers by using Cs vapor as a nonlinear compensating element. Atomic Cs has a negative nonlinear coefficient of refractive index which at number densities of around 10^{17} cm^{-3} can be made equal in magnitude to the positive coefficient of common Nd amplifier host materials. Use of such a material for nonlinear phase compensation can in principle provide compensation at all times during the pulse and at all points on the spatial profile, making it superior to passive correction optics which can provide compensation for only a single pulse intensity.

A series of experiments to determine the feasibility of such a process have been performed. In the first experiments, the self defocusing which results from the negative value of n_2 was observed, and the value of n_2 was measured and compared with theory. Agreement was found to within a factor of 2 between our absolute measurements of n_2 and our first principle calculations. Also, excellent agreement was found between observed and predicted differences for linear and circular polarizations. The details of these experiments are given in previous reports (NRL Memo Report 3057).

In more recent experiments actual compensation of phase modulation on a pulse from a Nd laser has been observed. Phase modulation in a positive sense was introduced on a pulse in a cell of CS_2 . The pulse was then propagated through a 1 m long Cs vapor cell. The degree of phase modulation was determined by measuring the spectral distribution of the pulses. Comparison of the spectrum of pulses entering and leaving the Cs cell was made as the Cs number density was varied. The spectral distribution of the input pulses had a double peaked structure, which is characteristic of phase modulation. As the Cs number density was increased, the spectrum of the output pulses decreased in width until they reached their time bandwidth limit. Further increase in Cs number density resulted in increased width as the initial phase modulation was overcompensated. Complete compensation of phase modulation depths up to 3π , the maximum which could be generated in the present system was observed. Although this experiment was designed to introduce a controlled amount of phase modulation on a pulse and then compensate for it, some of the initial positive phase modulation was determined to have originated in the amplifier chain. These results demonstrate that phase modulation which arises in the amplifier chains of large Nd lasers can be effectively compensated with Cs vapor.

This work has recently been submitted to Physical Review Letters. A copy of the paper entitled, "Complete Compensation of Self-Phase Modulation in Cesium Vapor at $1.06\ \mu$," appears in the Appendix of this report.

II. D. TUNABLE VISIBLE AND VUV VIA PARAMETRIC DOWNCONVERSION AND FOUR-WAVE MIXING

The experimental setup used for generation of coherent radiation in the XUV through resonantly enhanced frequency conversion has been described previously in a semiannual technical report (NRL Memo Report 3057). In this arrangement pulses at 266.1 nm are downconverted through a parametric generation process to produce light which is tunable throughout the visible. This radiation is then upconverted to the VUV by four-wave mixing in a suitable medium. A second third order mixing process is then used for conversion to the XUV. This approach has the advantage that the VUV pump radiation can be tuned to multiphoton resonances in the final mixing stage, improving the efficiency of the conversion process. It is anticipated that some degree of resonant enhancement will be necessary because of the low available power resulting from inefficiencies in each of the cascade steps. Amplification of the VUV pulses by appropriate VUV laser amplifiers was considered in order to make up for the inefficiencies in the cascade process. This approach has several advantages over use of a VUV laser directly for a pump source.

First many of the VUV lasers are single pass, traveling wave devices of limited coherence. The limited coherence means that the conversion efficiency of the parametric process is expected to be low. However, if the same device is used as an amplifier the coherence of the incoming pulse is maintained. In addition, the VUV laser amplifiers operate in an inversion depletion mode in which the laser pulse sweeps out the available gain in most of the amplifier volume. Extraction of this amount of energy in a picosecond duration pulse would result in a considerable increase of power, accompanied by significant improvement in the efficiency of intensity dependent parametric conversion processes. For some of the higher order processes considered, such an increased intensity could make the difference between a successful and an unsuccessful experiment. Finally, since these processes are intensity dependent, highest efficiency will be achieved at the highest possible intensities. One of the limitations on ultimate intensity will be optically induced breakdown.

Since the breakdown strength of a material increases with decreasing pulse duration, the use of picosecond pulses for the pump radiation in the VUV would allow higher intensities to be reached. Thus even higher conversion efficiencies could conceivably be achieved by using the short amplified pulses rather than the longer pulses generated in the VUV lasers directly. With the variety of existing VUV lasers currently in existence, amplification in a large part of the spectrum

between 100 and 200 nm can be covered in this manner.

Initial development of this system was carried out. Parametric conversion of the 266.1 nm pulses was accomplished with about 10% efficiency, giving pulses of 10 mW which could be tuned throughout the visible. This radiation was then mixed in Mg vapor to give pulses at 153.2 and 168.4 nm.

Several schemes were considered for further mixing to achieve even shorter wavelengths. These are shown in Table 1, reproduced from NRL Memo Report 3057. The cascaded approach outlined above has shown indications of being a practical one for generation of short wavelength radiation by frequency mixing. The improvement in conversion efficiency in the second harmonic stages serves as an indication that cascaded schemes are not inherently inefficient. With further work, similar improvements in the downconversion and four-wave mixing efficiencies are also to be expected. As a result, this approach can provide intense radiation in the VUV for pumping third or higher order processes which can be tuned to a multiphoton resonance of the nonlinear medium. Amplification with a VUV laser holds the promise of providing power levels of 10^9 W in the VUV. However, some question exists as to the availability of the stored energy in the rare gas lasers for amplifying single narrow lines. Sufficient information on the rate kinetics of the amplifying medium does not exist to determine the extent of this limitation. Further study on this aspect of the problem is certainly warranted in view of the potential for high power tunable coherent VUV radiation which exists.

Work on this particular approach to coherent short wavelength radiation has terminated at this point with the end of the program. Further work was confined to higher order mixing from 266 nm directly to the XUV. This work is described in the next section.

II. E. COHERENT RADIATION IN THE XUV VIA FIFTH AND SEVENTH ORDER MIXING PROCESSES

As an alternative to successive cascading, the use of higher order nonlinear processes to convert the 266.1 nm pulses to the VUV directly has been considered. At the high intensities available in our VUV pulses, such processes can be expected to produce usable radiation at the output wavelength. A study of fifth and seventh order conversion of 266.1 nm pulses in the rare gases has been made. Such conversion schemes can be optimized either by optimizing possible resonant enhancements or by optimizing phase matching properties. The experiments reported here utilized each of these techniques. Fifth harmonic conversion in neon was observed with the aid of a near four-photon resonance between the pump radiation and the $3P[1\frac{1}{2}]J=2$ level, where the detuning was 12 cm^{-1} (see Fig. 13). In helium, there are no useful resonances. However, calculations show that helium is negatively dispersive for this process, i.e., fifth harmonic generation. Thus

TABLE 1
INITIAL EXPERIMENTS INVOLVING GENERATION OF SHORT WAVE
RADIATION THROUGH NONLINEAR MIXING

ACTIVE MEDIUM	PROCESS	GENERATION OF VUV	λ_{out} Å	$\omega_{2\omega-1}$ cm ⁻¹	$\omega_{3\omega}$	UV AMPLIFIER
He	3 x 1512 Å	3 x 4536 Å	504	34,000	c	NO
He	3 x 1202 Å	2 x 4385 Å + 2660 Å	400	0	c	NO
He	3 x 1610 Å	2 x 4779 Å + 4935 Å	537	42,000	16.7	YES
He	3 x 1230 Å	2 x 4575 Å + 2660 Å	410	3,700	c	YES
Li ⁺	9 x 1608.4 Å	2 x 4779 Å + 4920 Å	178.7	7,309	2,186	YES
Li ⁺	7 x 1230	2 x 4575 Å + 2660 Å	175	2,270	7,400	YES

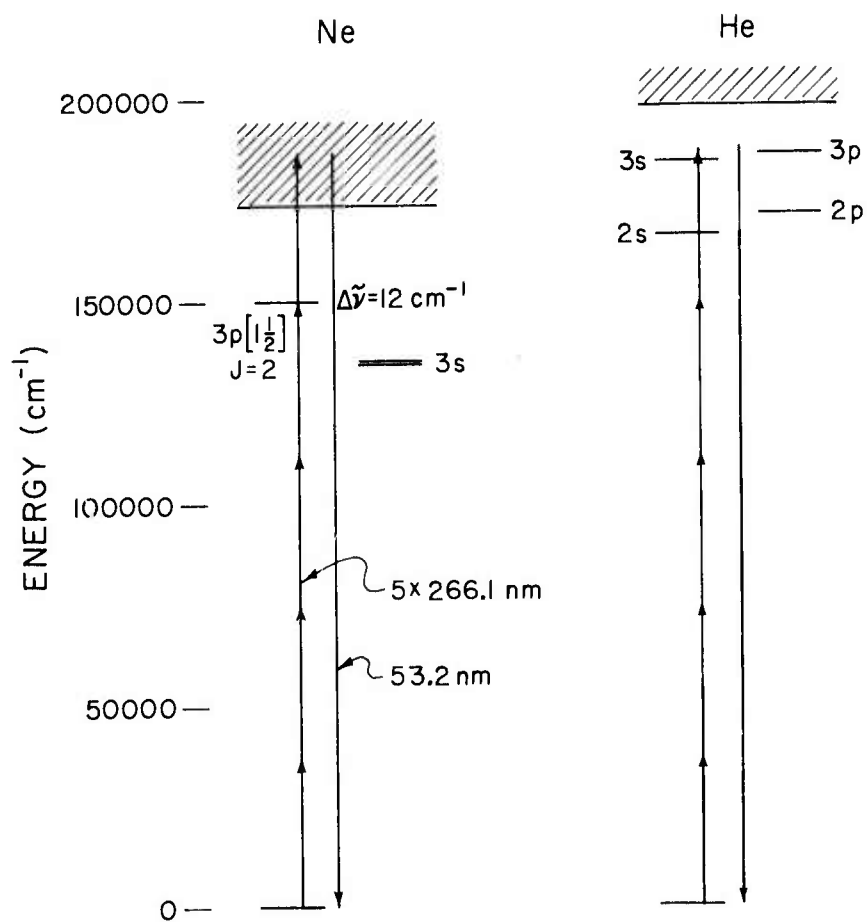


Fig. 13 — Partial energy level diagram of Ne and He showing levels involved in fifth harmonic conversion from 266.1 nm to 53.2 nm

optimization by tight focusing should be possible. In Ne, the generated radiation lies in the ionizing continuum and absorption will limit achievable conversion efficiency. In He, the radiation lies in a transparent region of the spectrum, and as a result, higher conversion efficiencies would be expected in helium, despite the lack of resonant enhancement of the nonlinearity.

The generation of radiation at 53.2 nm by fifth harmonic conversion was observed in both He and Ne. Details of these results are given in a paper entitled, "Generation of Coherent Radiation at 53.2 nm by Fifth Harmonic Generation," which is included in the Appendix. Briefly, the 266.1 nm pump radiation was focused into a cell (Fig. 14) containing the rare gas under study. The focus was at a gas-vacuum interface maintained by differential pumping. The output radiation was analyzed with a vacuum monochromator for intensity (using a photomultiplier) and wavelength (using Kodak 101-01 film). The spectrum showed a single narrow spectral line at a wavelength of 53.2 nm, in good agreement with the expected value of 53.225 nm (Fig. 15). The dependence of the intensity of the generated radiation on the power level of the pump radiation agreed with the expected fifth power law within experimental accuracy (Fig. 16). Two different focusing lenses were used, a 10 cm lens, giving a spot size of 10 μm , a confocal parameter of 2 mm and a peak intensity of $3 \times 10^{14} \text{ W/cm}^2$; and a 5 cm lens giving a spot size of 5 μm , a confocal parameter of 0.5 mm and a peak intensity of about 10^{15} W/cm^2 . With the weaker focus, conversion levels in Ne were higher than those in He even though the depth of the focus was greater than the absorption length in Ne (0.7 mm at a pressure of 40 torr). With the tighter focus conversion increased in both gases, but the increase in He was considerably greater, resulting in a 10-fold increase in signal level over that observed with Ne with the 10 cm lens. The highest conversion efficiency was estimated to be in the range of 10^{-8} to 10^{-5} , giving pulse powers in the range of 1 kW.

Conversion levels seem to be limited in Ne since breakdown is evident at pressures below 40 torr for the 5 cm focus. No similar limitation has yet been observed in He and further improvement should be possible by matching the phase slippage due to the focus to an initial offset in the dispersion of the gas. Calculations indicate that in the absence of limiting effects such as breakdown, conversion levels as high as 1% should be achievable, with pulse powers at 53.2 nm of 10^8 W being possible. Fifth harmonic conversion has also been seen in Ar at a conversion level similar to that in Ne.

In addition to odd harmonic generation, six-wave mixing processes involving combinations of other laser harmonics can be used to generate radiation at other wavelengths in the XUV. As a demonstration of this technique, four photons at 266.1 nm were combined with one at 532. nm to generate radiation at the 4th harmonic of the original laser (1.064 μ) at 59.1 nm. Radiation at still shorter wavelengths can be obtained by using higher order processes. To investigate this,

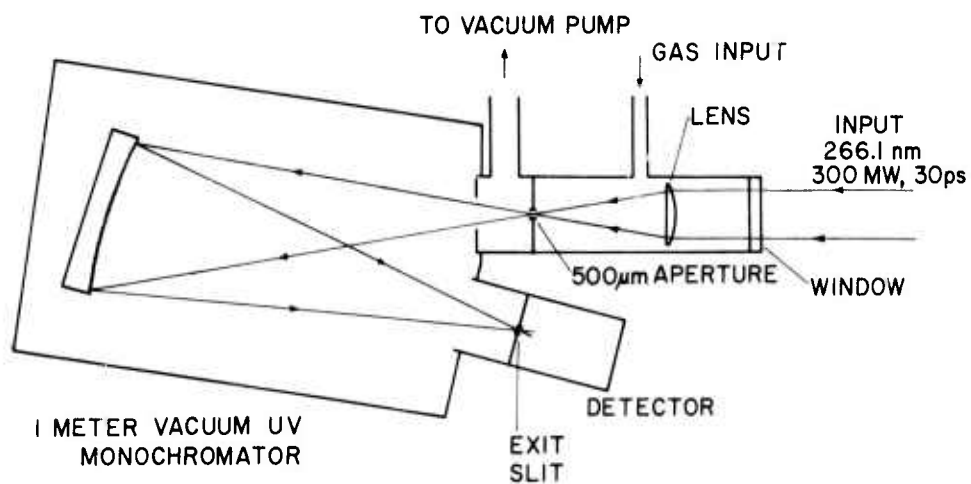


Fig. 14 — Experimental arrangement used for generating and detecting the fifth and seventh harmonic of 266.1 nm radiation

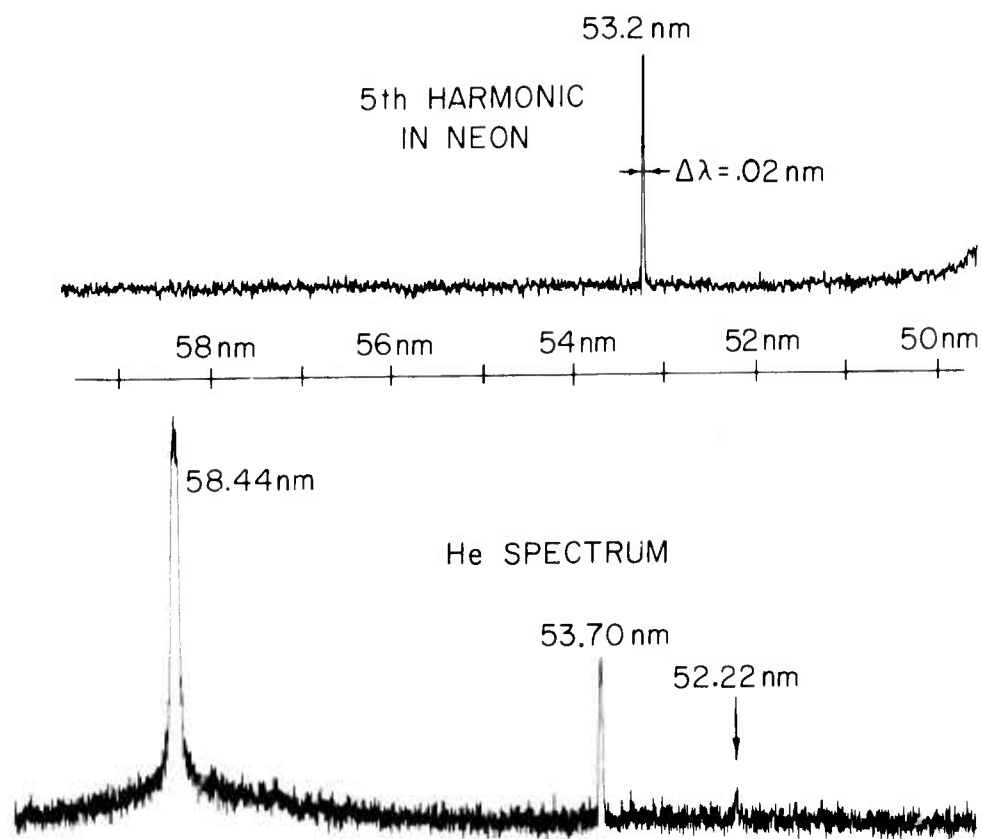


Fig. 15 — Densitometer trace of photograph of spectrum of fifth harmonic radiation (top) and He discharge (bottom) between 50 and 60 nm

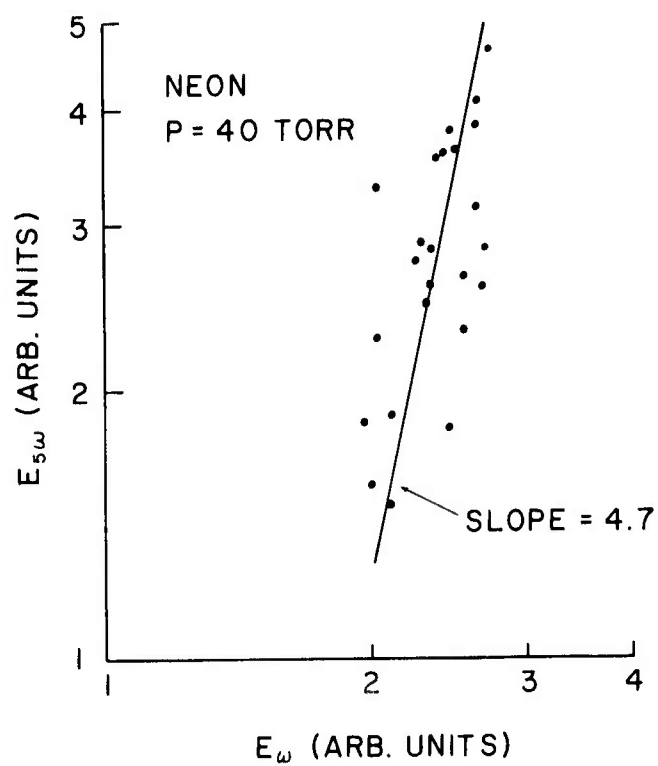


Fig. 16 — Variation of strength of fifth harmonic signal with input intensity showing good agreement with fifth power law dependence

radiation at 38 nm was produced by seventh harmonic conversion of the 266.1 nm pulses in He (Fig. 17). In this case the generated radiation lies in the ionizing continuum, although the absorption cross section is only one-half of that in Ne for 53.2 nm radiation. The conversion efficiency was considerably less than the fifth harmonic process, and the signal levels were in the noise of the photomultiplier detector. Nevertheless, clear evidence of radiation at 38 nm by tuning the spectrometer grating while recording signals with the photomultiplier (Fig. 18) was obtained.

The results reported in this section demonstrate clearly that nonlinear conversion processes of higher order than third can be useful in generating coherent radiation in the XUV region of the spectrum. Further pursuit of this study seems justified in order to develop this capability into a useful tool for tunable spectroscopy, short wavelength photography, materials analysis, and plasma diagnostics. Our results are due in large part to the quality of the laser radiation at 1.064 μ and 266 nm which is generated by the laser system developed and described earlier in this program.

The efficiency of the conversion process depends not only on the peak intensity of the beam in the focus, but also on the total power. A beam of relatively low power which is focused to give comparable intensity to a more intense source will have a shorter beam waist and therefore a shorter interaction region in which conversion can take place. The success of these experiments therefore depends strongly on the development of a laser source with superb spatial and temporal quality. This was accomplished in the early phases of this program. In addition, the optimization of the second harmonic processes was vital to provide sufficient total power in the UV pump pulses. Such a capability (described in an earlier section of this report) has already demonstrated its usefulness and should prove extremely valuable for future research in this area.

III. ELECTRON-COLLISIONAL PUMPING

III. A. MODELING OF 3p-3s LASING SCHEMES

III. A.1. INTRODUCTION

The study of 3p-3s ion laser schemes was undertaken mainly because of two important features which made production of a short-wavelength laser by this method seem feasible; (a) The scheme showed the possibility of quasi-cw lasing, (b) It represented an isoelectronic extrapolation of lasers already existing in the visible and near UV¹. Quasi-cw lasing in the 3p-3s scheme is obtained as indicated in the diagram in Fig. 19. Electron-collisional pumping from 2p to 3p is followed by 3p-3s lasing, with the 3s lower laser level more rapidly depopulated by radiative dipole decay to the 2p ground state, thereby maintaining the inversion. Lasing time is thus limited only by the time during which the required

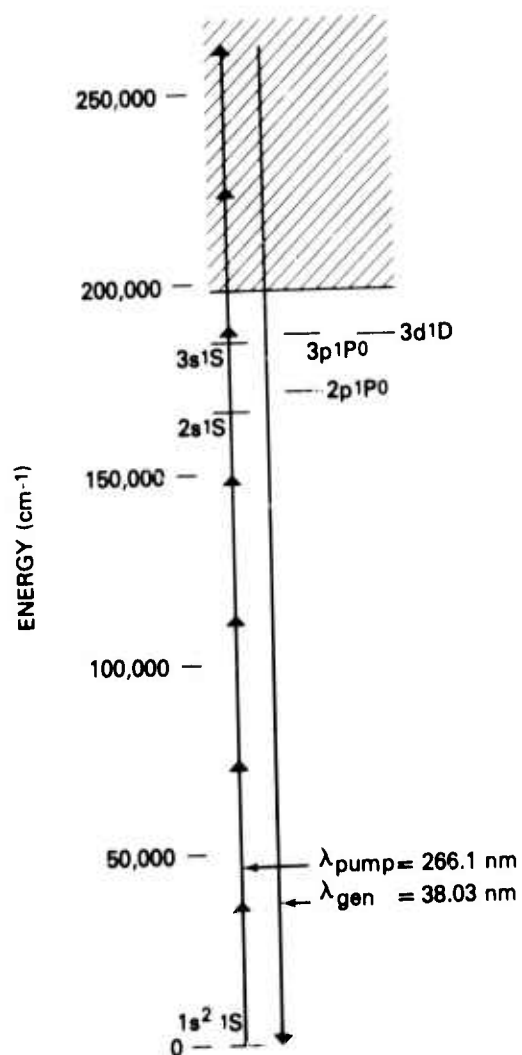


Fig. 17 — Partial energy level diagram of He showing energy levels involved in seventh harmonic conversion of 266.1 nm radiation

SEVENTH HARMONIC SIGNAL IN H₂

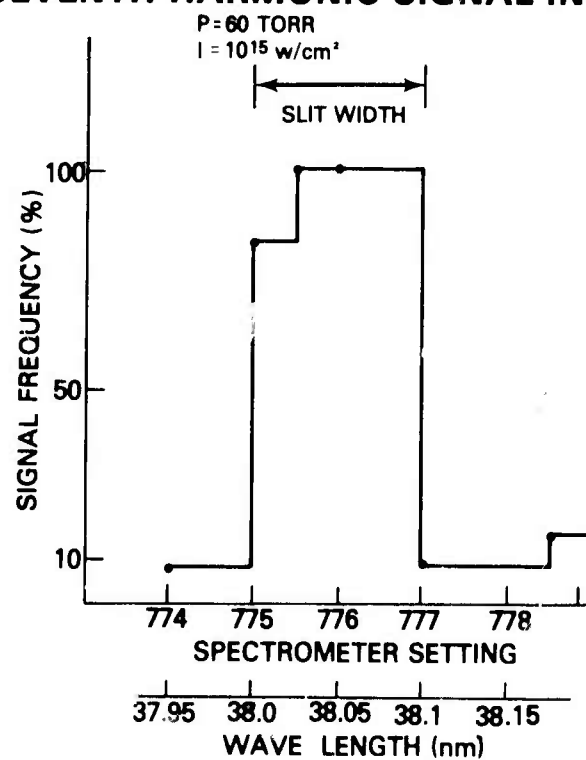


Fig. 18 — Dependence on spectrometer wavelength setting of frequency of detection of 38 nm signal. Data shows presence of signal at 38 nm with a turning width equivalent to the slit width.

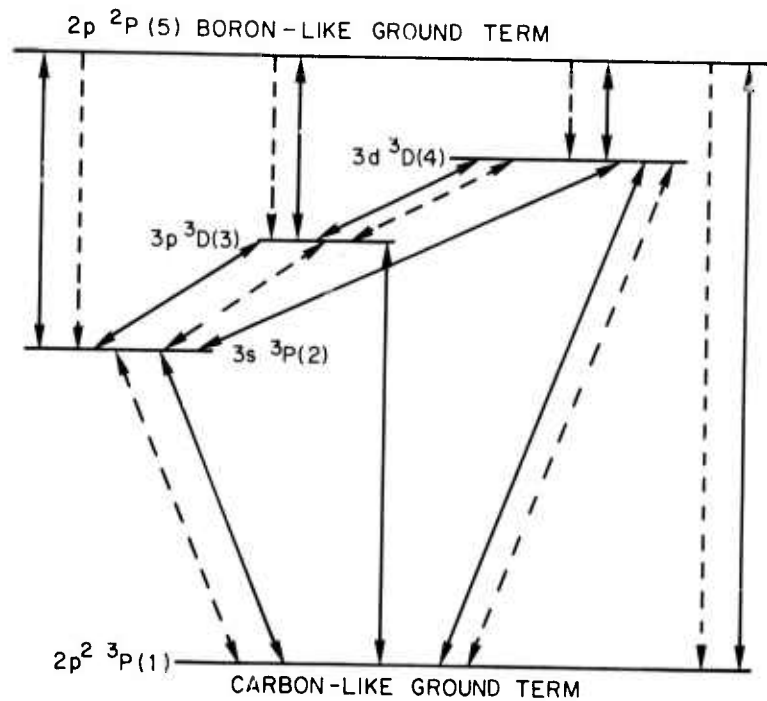


Fig. 19 — Term diagram for 3p→3s lasing scheme in carbon-like ions showing important terms and transitions used in numerical modeling results described. Dashed arrows designate radiative transitions; solid arrows represent electron-collisional transitions.

plasma conditions can be maintained. The effects of transitions to and from other atomic levels in the same and in neighboring species on the upper and lower laser level populations are taken into account in the modeling when they are important. The purpose of the modeling was to provide guidance and rationale in the understanding, selection, operation, and interpretation of near-term laboratory experiments.

III. A.2. ANALYTICAL ESTIMATES

The $3p \rightarrow 3s$ scheme was originally treated with a simplified three-level analytical model², which indicated the feasibility of extrapolating successful near-UV schemes into the vacuum-UV region. Single-pass amplification was predicted in a laser-produced plasma of reasonable length, pump power, and pump rise time, especially for plasmas of high electron temperature. The analytical estimates were later extended³ to plasmas of higher densities where it was shown that inversion on shorter wavelength transitions is attainable for highly stripped ions of the carbon isoelectronic sequence.

III. A.3. TIME-DEPENDENT NUMERICAL MODELING

The $3p \rightarrow 3s$ scheme was first modeled numerically using a "Hot Spot" model⁴ which used time-dependent rate equations to solve for the populations of relevant atomic levels on the assumption that the plasma is pumped by a subnanosecond laser pulse. This code, which was well tested by successfully modeling x-ray generation in laser plasmas⁵, neglects plasma motion and assumes that densities and temperatures are spatially homogeneous although the electron and ion temperatures change with time due to energy balance. The hot spot code was applied to model the doubly ionized oxygen ion (O III) in order to compare its predictions with laser experiments⁶ and initial analytical estimates² for $3p \rightarrow 3s$ lasing. The results of this modeling not only showed strong lasing in the $3p \rightarrow 3s$ transition but also agreed with scaling laws predicted by the analytical studies.

In an effort to model better the present short-wavelength laser scheme, a time dependent code (named XRL-1) more suitable for the modeling of x-ray lasers was developed. This code provided detailed output describing level populations and transitions between the levels as a function of time and gave insight into the physical processes important in obtaining population inversion. Specifically, it was determined that ionization and recombination affected the upper and lower laser level populations (mainly by depletion of the total lasing species density) in such a manner as to reduce the predicted value of the gain by a factor of 2 to 5; nevertheless, a reasonable and observable gain was predicted.

III. A.4. STEADY-STATE MODELING

The need to scan entire isoelectronic sequences to determine which

ions would give the best gain for a given set of plasma conditions required the development of a steady-state computer code which was applied to carbon-like ions and a variety of rather high density plasmas obtainable with present day technology. The steady-state code assumed temporally and spatially constant densities and temperatures and included all relevant collisional and radiative transitions (including important radiative trapping effects). It should be noted that although the modeling described here concentrates exclusively on six-electron ions, the results are expected to be similar for all ions having at least one outer 2p electron in the ground configuration from the boron-like to the neon-like sequences.

This code and its results are described in detail in reference 7, the full text of which is contained in the appendix of this report. The code was sufficiently economical and uncomplicated to allow a large array of elements and plasma conditions to be studied. Much insight into the relative importance of the atomic processes resulting in or inhibiting population inversion and some important scaling laws could be gained by studying the output of this simplified code. The use of the steady-state code was justified by the excellent agreement of its predictions with more detailed time-independent codes⁴, analytical estimates^{2,3}, and experiments⁶.

The results of these steady-state calculations indicate significant gain products for 3p-3s ionic transitions in quasi-cw emission in an amplified spontaneous emission mode, i.e., without a resonant cavity, in an equilibrium plasma model. Such gain products may be observed in high-density plasmas containing carbon-like ions of atomic number $Z \approx 20$ such as produced by laser irradiation of pellets or electromagnetically driven high-density pinch devices. Even more spectacular gain products are computed when the steady-state model is run in a simulated transient mode by maintaining the population density of the lasing species at one third of the total ion density rather than a few percent which would exist under equilibrium conditions at high temperatures. Some gain products computed for this "transient" behavior are graphed in Fig. 20. With enhanced electron temperatures typical of transient plasma heating, gains approaching saturation levels are predicted. Therefore, vacuum UV lasing at wavelengths between 500 and 1000 Å using existing high-density discharge devices appears promising for a near-term proof of feasibility of lasing in plasmas at short wavelengths.

REFERENCES

1. W. B. Bridges and A. N. Chester, in Handbook of Lasers, R. J. Pressly, ed. (Cleveland: Chemical Rubber Co., 1971), Chapter 7.
2. R. C. Elton, Appl. Opt. **14**, 97 (1975). The present numerical results are consistent with the analytical results in this paper when adjustments for density and improved rates are made.

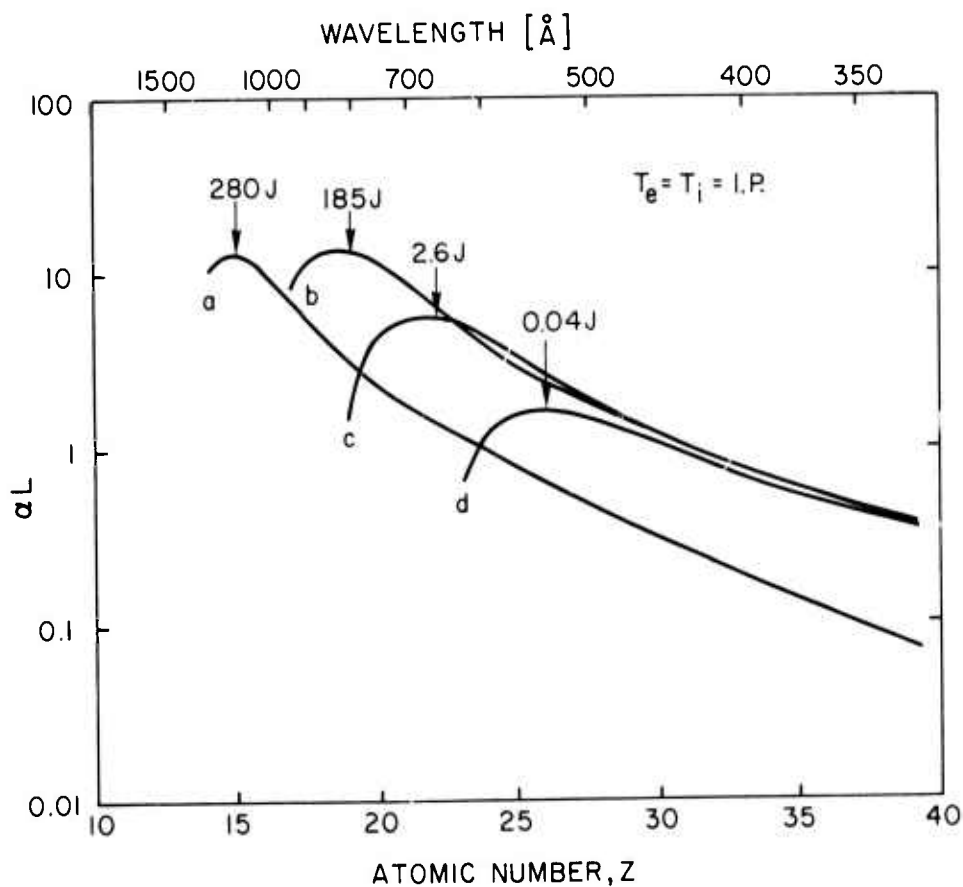


Fig. 20 — Computed gain products αL versus atomic number and wavelength for 6-electron carbon-like ions at enhanced nonequilibrium temperatures T_e, T_i equal to the ionization potential. Curves a through d correspond respectively to electron densities of $10^{19}, 10^{20}, 1$ and 10^{22} cm^{-3} and to relevant plasma diameters of 3, 1, 0.1 and 0.01 mm. The required plasma energies in Joules are indicated for each curve at peak gain.

3. R. C. Elton, in Progress in Lasers and Laser Fusion, B. Kursunoglu, A. Perlmutter, and S. M. Widmayer, eds. (New York: Plenum Press, 1975).
4. K. G. Whitney and J. Davis, J. Appl. Phys. 45, 5294 (1974).
5. K. G. Whitney and J. Davis, Appl. Phys. Lett. 24, 509 (1974).
6. Y. Hashino, Y. Katsuyama, and K. Fukuda, Jap. J. Appl. Phys. 11, 907 (1972); 12, 470 (1973).
7. L. J. Palumbo and R. C. Elton, to be published J. Opt. Soc. Am. (in press) (See Appendix).

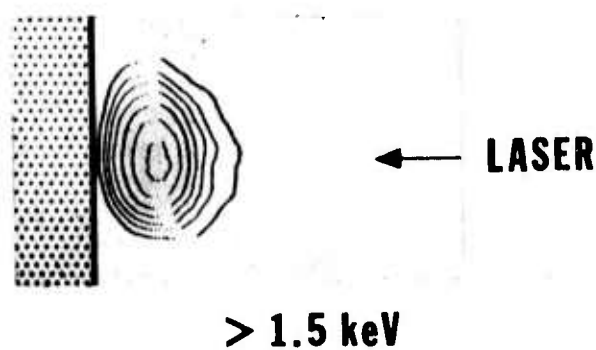
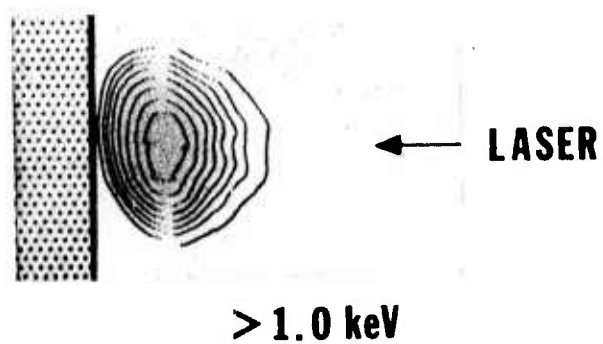
III. B. LASER-PLASMA INTERACTION EXPERIMENTS

III. B.1. INTRODUCTION

One potential method for demonstrating a short-wavelength laser is to use electron collisional pumping of multiply ionized atoms. The electron collisional pumping may be achieved by rapid heating of a relatively cool but dense plasma with picosecond laser pulses. The initial experimental efforts have been directed towards a basic physics understanding of laser-plasma interactions in order to explore the possibility of enhanced plasma heating. Spectroscopic studies of laser-produced plasmas have been made in order to determine plasma parameters as a function of time and the ionic species produced. The results are described in Section 2 below. The dual laser system and the experimental results are described in Sections 3 and 4, respectively. It is realized that the success of this approach is very much dependent on the appropriate selection of a spatial location in the expanding plasma where the picosecond (heating) laser pulse is to be focused. Therefore, independent of a particular inversion atomic model, knowledge of the spatial distribution of electron density and plasma expansion characteristics in the initial plasma is vital for directing and synchronizing the pumping laser pulse. Interferometric studies of the laser-produced plasma have been made in an attempt to obtain such information, and the results are described in Section 5.

III. B.2. SPECTROSCOPIC STUDY OF LASER-PRODUCED PLASMAS

The mode-locked Nd:YAG laser beam of 25 ps in pulse duration is directed into a vacuum chamber ($p \leq 10^{-4}$ torr) and then focused onto various slab targets (Na, Mg, Al and Si) using a 30 cm focal length lens. The focal spot has an elliptical shape of 30 μm by 70 μm and the laser power density at the focus is estimated to be 10^{14} W/cm². X-ray pinhole images and spectra from plasmas produced by this power density were measured. An expanding, x-ray emitting plasma (aluminum) is photographed using a double-pinhole x-ray camera. Fig. 21 shows



100 μm

Fig. 21 — Pinhole x-ray photographs taken simultaneously with two different absorbers to detect the x-ray energies indicated in keV

microdensitometer scans (showing density contour) of such x-ray photographs taken simultaneously, one through 0.5 mil and the other through 1.5 mil beryllium absorbers. The size of the initial hot plasma is estimated to be 50 μm in diameter.

The plasma radiation is spectrally analyzed using a flat Rubidium Acid Phthalate (RAP) crystal ($2d = 26.121 \text{ \AA}$) and the spectra are recorded on No Screen medical x-ray film through 12 μm beryllium foil to protect the film from visible radiation. Although the potential lasing wavelengths conceivable with the laser power density available here would lie well above 100 \AA , the spectral region of 5 \AA - 12 \AA is relatively clear of line radiation, and consequently more convenient for line identification. Figs. 22 through 25 indicate microdensitometer scans of the x-ray spectra thus obtained from Na-, Mg-, Al-, and Si-plasmas, respectively. All four spectra show very strong $1s2p \rightarrow 1s$ resonance transition lines and the other Rydberg series lines of He-like ion species, i.e., Na X, Mg XI, Al XII, and Si XIII. Free-to-bound recombination edges are also seen at the series limits. For Na-, Mg-, and Al-plasmas, even H-like (Na XI, Mg XII, and Al XIII) Lyman- α lines appear, decreasing in intensity with increasing atomic number. But the trend is reversed for blends of long wavelength satellite lines of the He-like resonance line, $1s2l2p \rightarrow 1s^2 2l$. This is understandable in view that when the laser-heated plasma temperature is high enough to ionize up to H-like ion species for lower Z atoms, the temperature is too high for Li-like ion species to be highly populated (burn out).

Assuming that the electron density does not exceed the critical value ($\approx 10^{21} \text{ cm}^{-3}$) for laser light penetration, the high stages of ionization observed with such a short heating pulse are difficult to understand using a thermal model of the plasma, because the thermal ionization time required is longer than the laser pulse. The situation here may be explained however using a spherical "hot spot" model. This numerical model assumes a stationary, uniform plasma sphere at the laser focus (neglecting magnetohydrodynamic plasma motion during the time of interest) and also assumes that the major plasma cooling is by radiative and thermal-conductive mechanisms. It is also assumed that the laser light is absorbed in a small volume of $\sim 10^{-6} \text{ cm}^{-3}$ predominantly through the process of inverse bremsstrahlung, and its energy is deposited directly as thermal energy into the electron gas. The electrons then share their energy with the ions through collisions that heat, excite, and ionize the ions. The excitation and subsequent radiative decay of the hydrogen-like and helium-like ionization stages are modeled in some detail to allow computation of the K-like ($np \rightarrow 1s$, $n \geq 2$) emission spectrum that is observed in the laser-heated plasma. Fig. 26 indicates the computed electron and ion temperatures as a function of time for Al-plasma. One notes that a large T_e/T_i with $kT_e \sim 1 \text{ keV}$ exists for an initial time period of $\sim 50 \text{ ps}$. The temporary non-equilibrium situation which exists here is desirable, because the high T_e is most effective in producing a high inversion, whereas a lower T_i reduces the Doppler linewidth — both effects increasing

25ps:0.1 J
Nd:YAG Laser

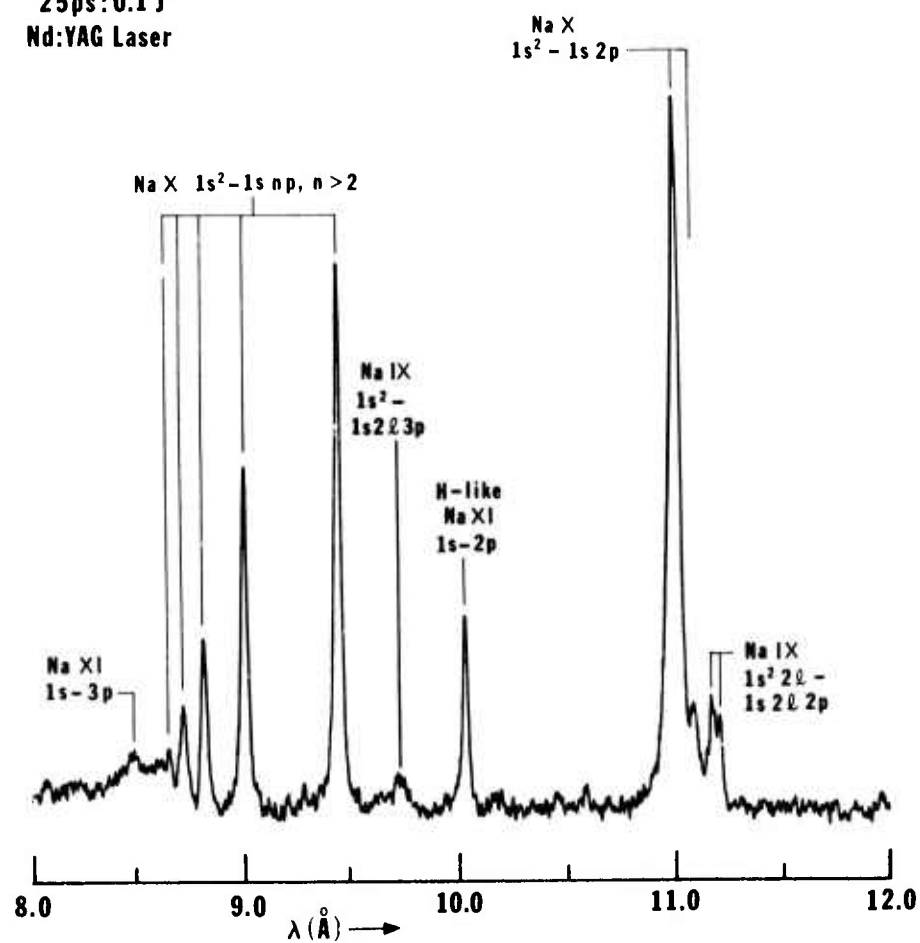


Fig. 22 — X-ray spectrum taken with Na-target

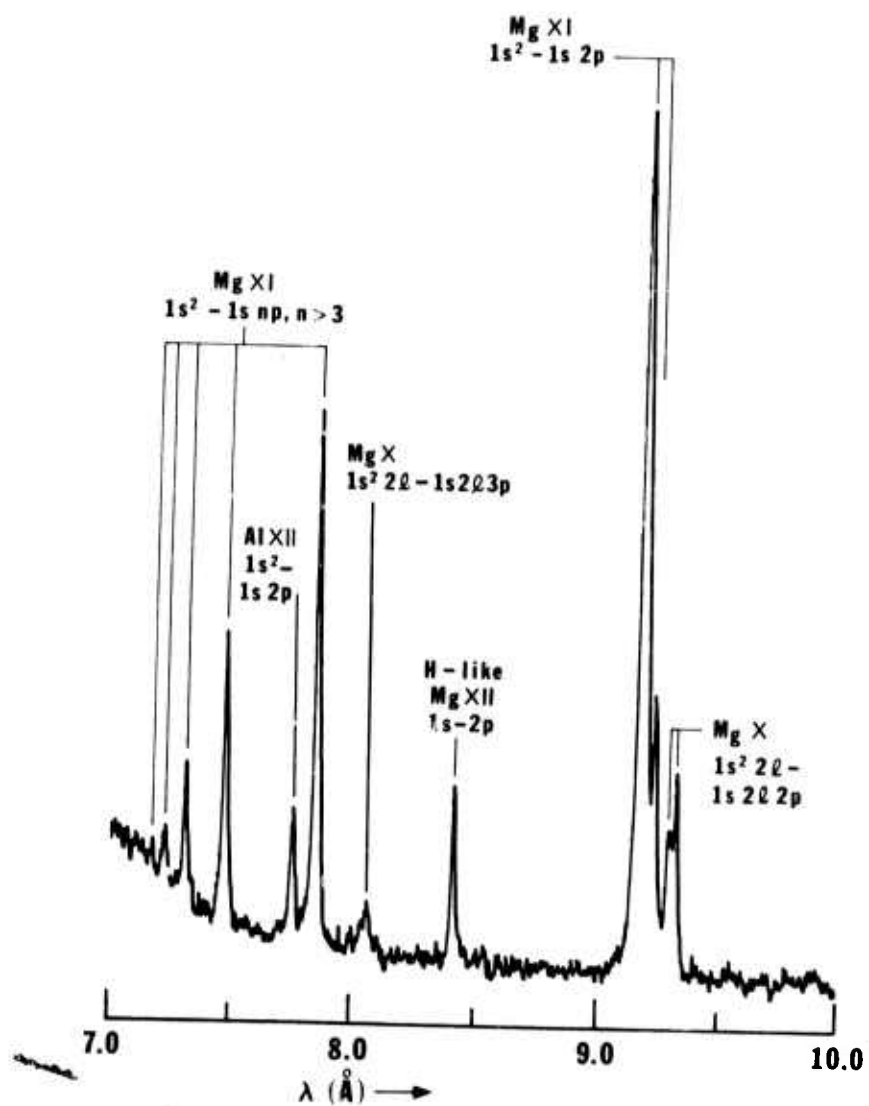


Fig. 23 — X-ray spectrum taken with Mg-target

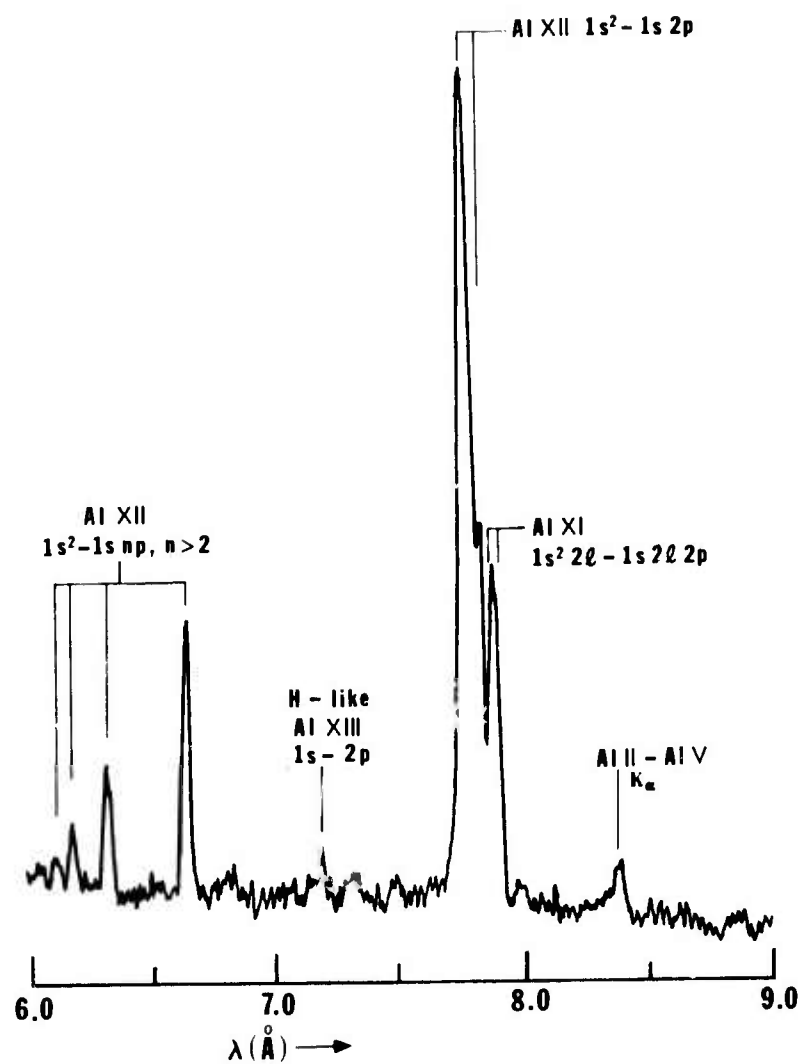


Fig. 24 — X-ray spectrum taken with Al-target

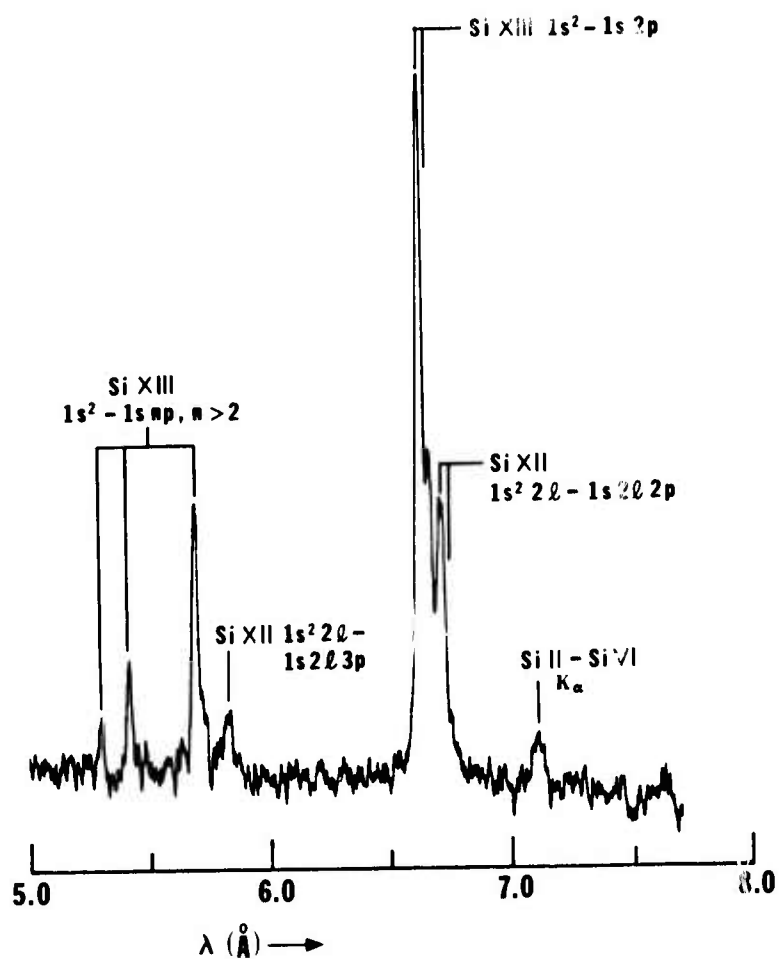


Fig. 25 — X-ray spectrum taken with Si-target

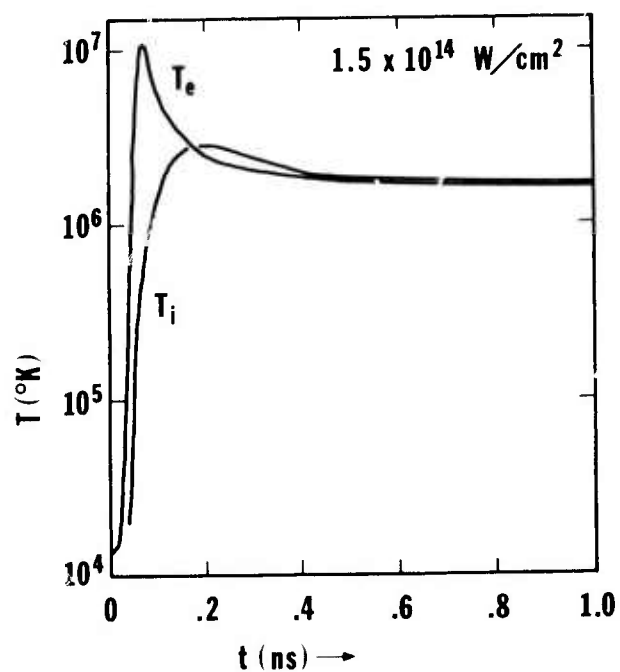


Fig. 26 — Computed electron and ion temperatures as a function of time

any gain. Fig. 27 shows ground population densities of Al XI, Al XII, Al XIII, and Al XIV, where the populations of electrons and Al XII are nearly constant due to the assumptions made. Li-like Al XI, however, dips sharply after a peak due to the burn-out and then gradually increases, caused mainly by the recombination of Al XII ions. Time-resolved power densities of line radiation due to Al XII $1s^2-1s2p$, Al XII $1s^2-1s3p$, and H-like Al XIII $1s-2p$ transitions are shown in Fig. 28 and a time integrated K-x-ray spectrum of Al XII and Al XIII ions is compared with that of the experimentally obtained spectrum in Fig. 29. The experimental points are relative values with arbitrary units and are normalized to the computed value of the $1s^2-1s4p$ line overall agreement is good between the two; however, a definite tendency towards lower experimental values in $1s^2-1s3p$, $1s^2-1s2p$, is noted. This discrepancy is interpreted to be due to the fact that these lines may be optically thick, an effect not yet included in the numerical model.

The spectral features observed so far indicate that the plasma electrons are heated to a temperature somewhere between 300-600 eV. However, precise temperature measurement is essential for further investigation. This will be done using two approaches, i.e., from the intensity ratio of He-like $1s^2-1s2p$ to H-like $1s-2p$ resonance lines and by using the x-ray absorption method. The latter technique may also be used to obtain the bremsstrahlung profile of the plasma.

The original experimental scheme proposed is to make a line focus on a slab target so that a cylindrical expanding plasma is formed. This plasma is subsequently heated and pumped by an axial laser beam of short pulse duration. Detailed plasma diagnostics and spectroscopic study in the two-laser-beam operation will be made using low-Z targets. The spectroscopic study will be extended to the vacuum UV region where $3p \rightarrow 3s$ lasing is likely to occur.

III. B.3. DUAL PULSE LASER SYSTEM

A dual pulse laser system was developed under this program both as a tool to study the properties of laser-produced plasmas and as a pumping source for the two-pulse laser heating experiments. The laser system consisted of a mode-locked Nd:YAG laser and a Q-switched Nd:YAG glass laser which were synchronized by a technique developed under the program. The details of the design of the individual lasers as well as the synchronizing system have been given in previous semiannual technical reports. The salient features of this system are 1) a single mode-locked pulse at 1.06μ of 30 psec duration and containing up to 200 mJ of energy, 2) a Q-switched pulse variable in duration from 1 nsec to 10 nsec at a peak power of 1 GW, and 3) synchronization between these two pulses with a jitter time of ± 120 psec. This is the first time two independently pulsed lasers have been synchronized with this degree of accuracy.

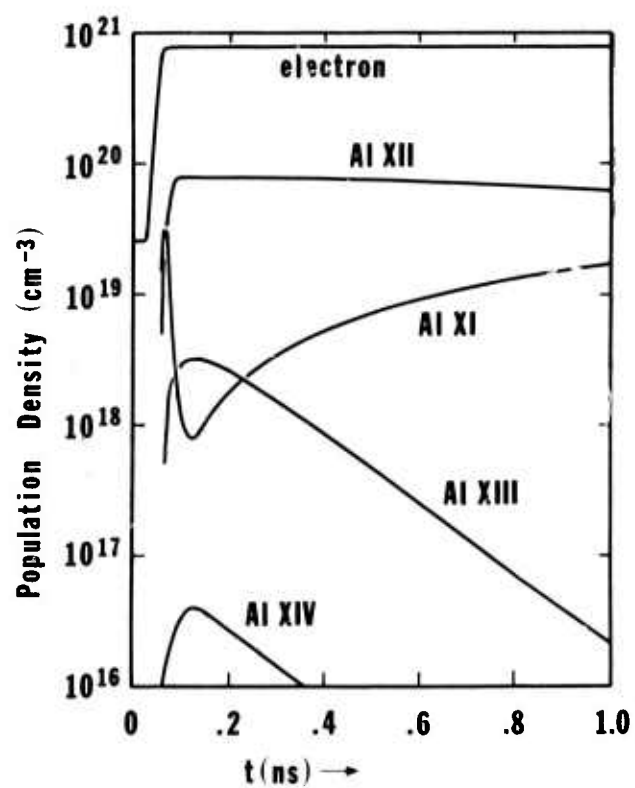


Fig. 27 — Ground state population densities of Al XI, Al XII, Al XIII and Al XIV ions

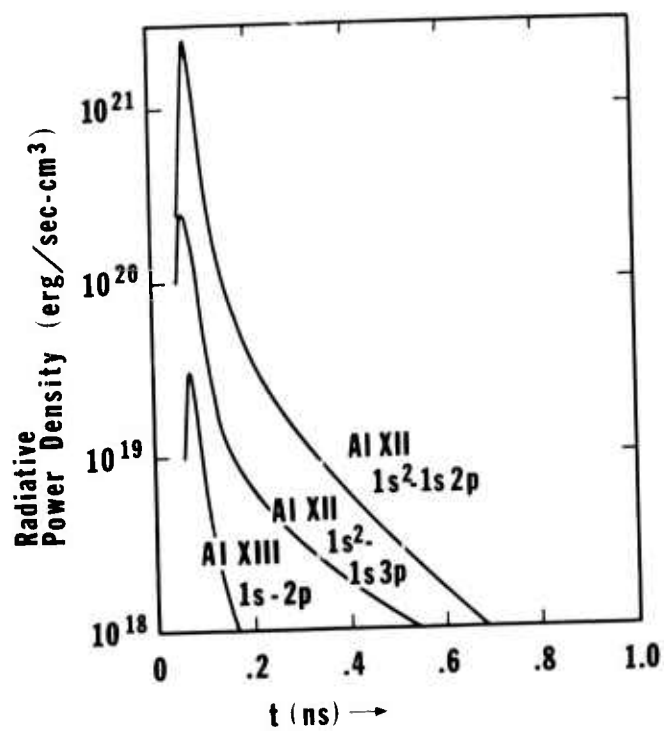


Fig. 28 - Computed time histories of Al XII $1s^2 - 1s2p$, Al XII $1s^2 - 1s3p$, and Al XIII $1s - 2p$ transition line

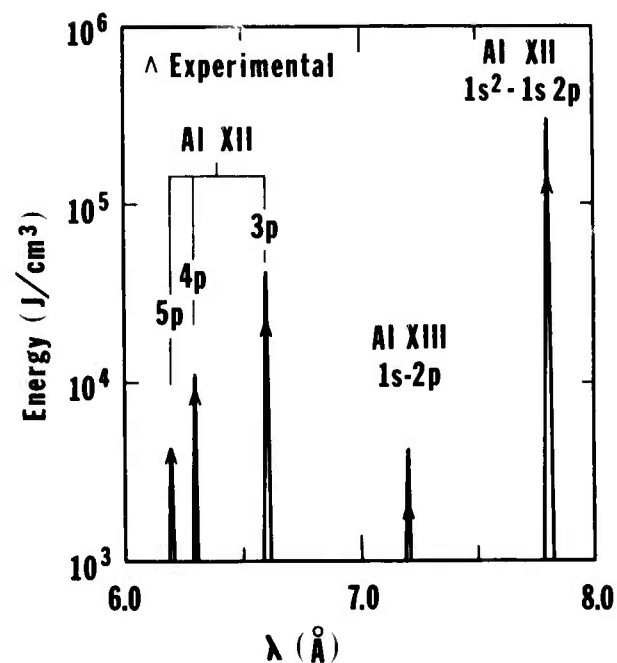


Fig. 29 — Comparison of computed spectral line intensities of aluminum and that obtained from the experiment

III. B.4. DUAL-LASER EXPERIMENT

The dual-laser experimental concept is shown schematically in Fig. 30 and has been discussed in previous semiannual reports and elsewhere recently^{1,2}. The basic idea is to prepare a suitable plasma ion environment with a laser-target combination, and to subsequently pump a population inversion on the ions with a very fast rising second laser pulse. At its present stage of development it consists of a plasma generated by point focusing a 2.0 J Q-switched glass laser pulse onto a magnesium slab target, and injection of a synchronized mode-locked 25 ps, 150 mJ Nd:YAG laser into the Mg-plasma after a certain delay time. The properties of the state-of-the-art laser system are summarized in the previous section. The initial laser beam is focused with a 30 cm focal length, f/15 lens and the focal spot size is measured using a silicon diode array, yielding the results shown in Fig. 31. First observations have been directed towards detection of enhanced emission indicating increased electron heating with the short-pulse laser and associated enhanced pumping.

Meanwhile, the ionic composition of the expanding plasma as well as the temperature can be appreciated using x-ray photography and spectroscopy³. Figs. 32a and 32b illustrate images of the x-ray emitting initial plasma obtained, respectively, with a 50 μm pinhole and through a bundle of 5 cm long metallic tubes (i.d. = 400 μm), both of which recorded x-ray photons of 1 to 1.5 keV. While the former shows only the most intense x-ray emitting region ($\sim 250 \mu\text{m}$) in the vicinity of the target; the latter also records rather faint x-rays originating from tenuous expanding plasma which extends as far as 1 mm along the target and 1.8 mm away from the target. A peak electron temperature of the Mg-plasma produced by the Q-switched glass laser may be estimated^{4,5} from the line intensity ratio of H-like Mg XII $2p \rightarrow 1s$ to He-like Mg XI $1s2p \rightarrow 1s^2$ lines, assuming a coronal model. The x-ray spectrum is obtained using a flat RAP ($2d = 26.121 \text{ \AA}$) analyzing crystal and a microdensitometer scan of the spectrum obtain is shown in Fig. 33. The main line features in the spectrum are those which arise from He-like Mg XI and Li-like Mg X ions. The spectrum is typical⁴ of a plasma where the electron temperature is about 100 eV. In this arrangement the spectral line width is determined by the size of the radiating source ($\sim 250 \mu\text{m}$).

A possible ionic inversion scheme involves lasing on $3p \rightarrow 3s$ transitions following pumping from $2p$ levels and final rapid depopulation from $3s \rightarrow 2p$. This is a proven transition in the near ultraviolet, and extrapolation to the vacuum UV region has been described in previous semiannual reports and elsewhere⁸. Recent advances in numerical modeling of this scheme for ions in the carbon isoelectronic sequence are described in Section V.A. This is a possible quasi-stationary inversion scheme, and the first stage will be to seek evidence of population inversion, since significant gain will require absorption of considerable pumping energy. For ascertaining the existence of an inverted population density between $3p$ and $3s$ levels, measurements of $3p \rightarrow 3s$ and $3s \rightarrow 2p$

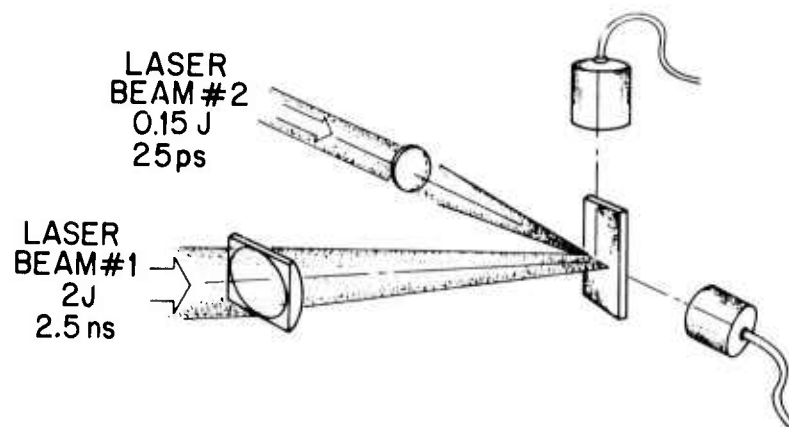


Fig. 30 — Schematic of experiment designed to verify gain on transitions pumped by electron collisions in a plasma

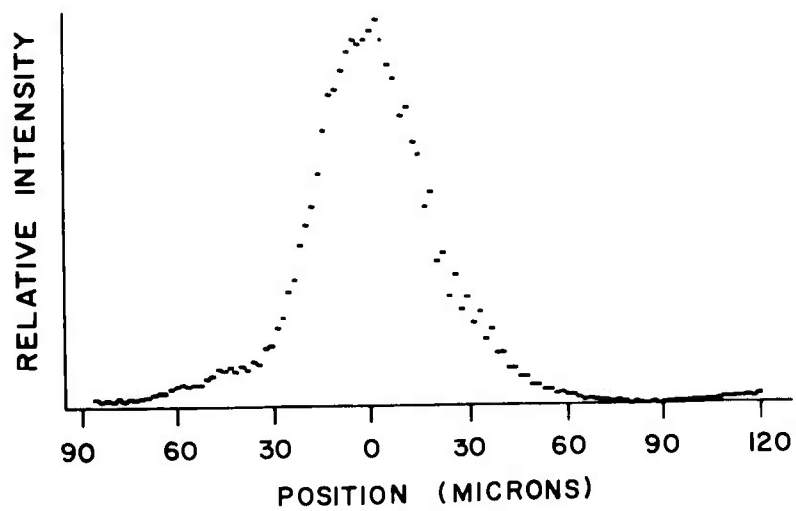
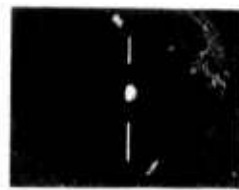


Fig. 31 — Measurement of focal spot size using silicon diode array.
Spatial resolution is $25\ \mu\text{m}$

X-RAY (1-1.5 keV) PHOTOGRAPHS

a) PINHOLE (50 μm)



1 mm

Mg

← LASER

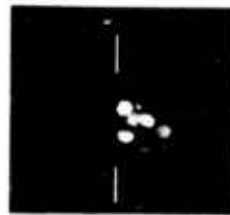
$E=2\text{ J}$

$\Delta t=2.5\text{ ns}$

$d=100\text{ }\mu\text{m (POINT)}$

$p/a=10^{13}\text{ W/cm}^2$

b) TUBULAR
(5 cm \times 400 μm)
COLLIMATOR



1 mm

← LASER

Fig. 32 — Time integrated x-ray image of expanding plasma (a) using a 50 μm pinhole, and (b) using a bundle of 5 cm long metallic tubes of which inner diameter is 400 μm

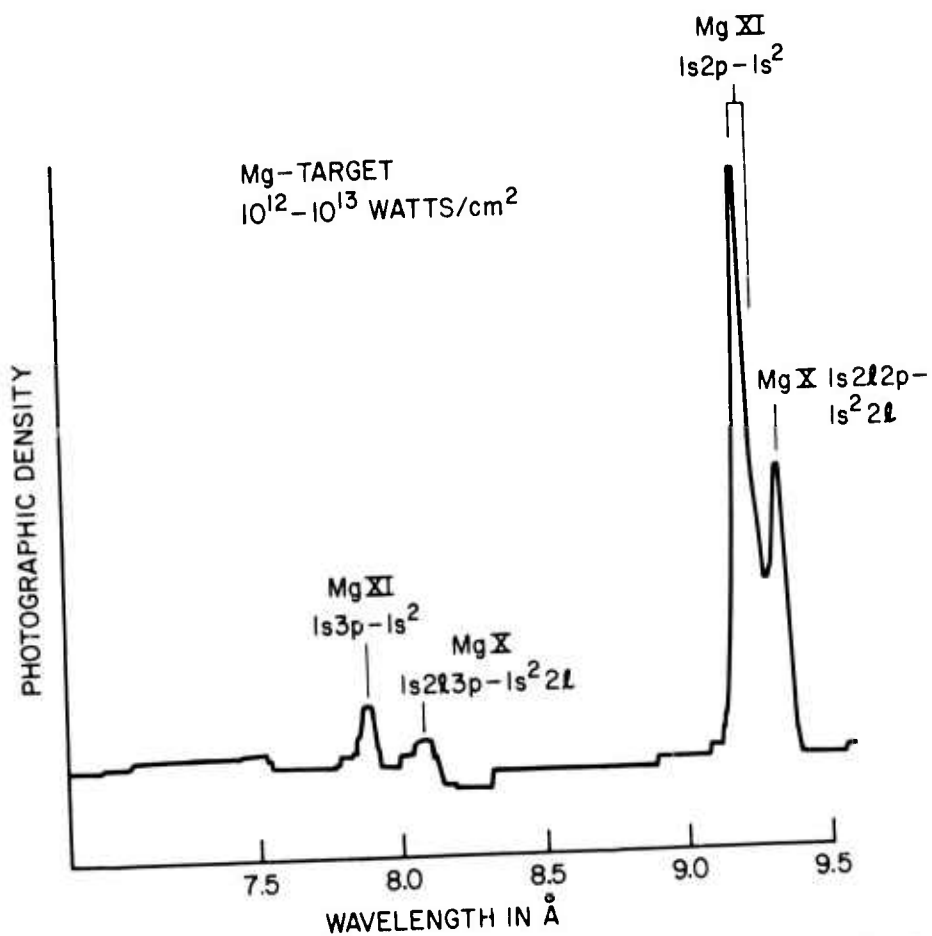


Fig. 33 — K-x-ray spectrum of Mg-plasma obtained with RAP analyzing crystal. Q-switched glass laser is focused onto a Mg-target to form a 100 μ m diam. focal spot.

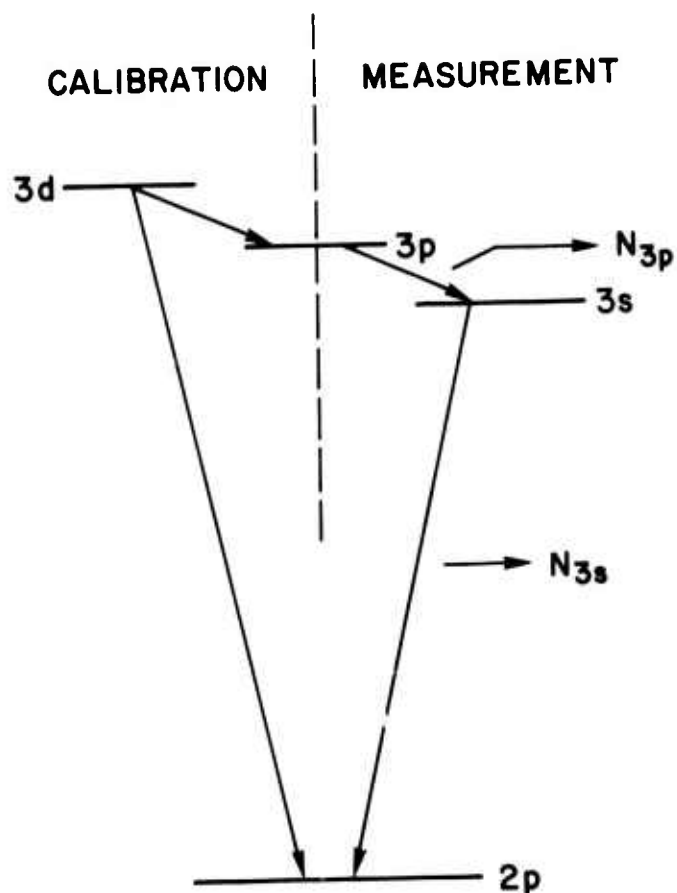


Fig. 34 — Transitions involved in determining the population inversion ratio N_{3p}/N_{3s} from relative line intensities, using branching transitions shown from the 3d level for instrumental calibration.

lines will be made, with the latter occurring at about 1/10 the wavelength of the former. In order to bridge this gap in instrument sensitivity, the 3d→3p and 3d→2p nearby pairs of lines will also be measured for a branching ratio calibration, since they originate from the same upper level. This approach is indicated in Fig. 34.

The ion chosen for initial studies is Mg^{6+} (Mg VIII). The expected wavelength of the 2p3s ^3P laser line has been determined by extrapolating the known wave numbers in the CI isoelectronic sequence for carbon through neon. Fig. 35 shows the plot of wave numbers for the carbon-like ionic species (up to Ar XIII), and one sees that the wavelength for Mg VII falls at $1625 \pm 10 \text{ \AA}$. A 1-meter normal-incidence vacuum UV spectrometer with a 1,200 lines-per-millimeter ruled grating (blazed at 1200 \AA) has been set up for the spectroscopic analysis, and the target chamber is mounted directly on the front of the entrance slit assembly. The distance between the target focal spot to the entrance slit is 11 cm. Fig. 36 shows a microdensitometer scan of a typical time-integrated spectrum in the region of 1400 to 1800 \AA , taken with a 20 shot (Q-switched glass laser only) exposure. The Mg-target used in this particular exposure contained aluminum and carbon as impurities; the $\text{Al II } 3s^2 3p^1 \text{ } ^1\text{P} - 3s^2 1\text{S}$ line at 1670.8 \AA and the $\text{C IV } 2p^2 \text{ } ^2\text{P} - 2s^2 \text{ } ^2\text{S}$ doublets at 1550.8 \AA and 1548.2 \AA providing excellent references. Some of the lines identified so far are listed in Table 2. The spectrum consists of mostly lines arising from Mg IV and Mg III ions in this spectral range; however, it is conceivable that some of the unidentified lines are those which originate from Mg ions of higher stages of ionization. For example, a weak line at 1625 \AA may be the Mg VII ($2p3p \text{ } ^3\text{D} - 2p3s \text{ } ^3\text{P}$) transition as predicted. The shorter wavelength 3s→2p (and 3d→2p) lines for Mg VII require grazing incidence spectroscopy. Preliminary space-resolved measurements on a separate system (charge transfer experiment described in Section III) indicate the presence and resolution of these lines in magnesium.

III. B.5. INTERFEROMETRIC STUDY

The laser scheme also requires a rather careful selection of the time-when, and the location-in the expanding plasma where the second (plasma heating) laser pulse is injected. This restriction results from a combination of a maximum electron density (depending on the element) above which the level coupling becomes collision dominated and, perhaps more importantly, on a sufficiently high density to absorb the pump radiation from the short-pulse laser in a finite plasma length. The last condition implies densities approaching the "critical" value. It is therefore essential to have detailed information on the characteristics of the expanding plasma, including the electron density profile as a function of time. Unfortunately, no previous work in this direction has been made, particularly for the case of the line focus. The dual-pulse laser system was used for interferometric studies of laser-produced plasmas in order to obtain such experimental data. The interferometer probe was done⁷ with the second harmonic of the mode-locked laser pulses, providing spatial resolution of 15 μm and temporal

TABLE 2: Extrapolation of Lasing Transitions on Carbon-Like Ions.

ION SPECIES	λ in Å	CONFIGURATION
Mg III	1738.8	$2p^5 3p^3 D - 5p^5 3d^3 F$
Mg IV	1736.8	$2p^4 3s^2 P - 2p^4 3p^2 S$
Al II	1725	$3s 3p^3 P - 3s 3d^3 D$
Al II	$\left. \begin{matrix} 1721.2 \\ 1721.3 \end{matrix} \right\}$	
Al II	1670.8	$3s^2 1S - 3s 3p^1 P$
Mg VII	1625 ?	$2p 3s^3 P - 2p 3p^3 D$
Al III	1611.9	$3p^2 P - 3d^2 D$
Mg IV	1611.2	$2p^4 3s^2 D - 2p^4 3p^2 D$
Mg IV	1607.1	
Mg III	1586.2	$2p^5 3p^3 S - 2p^5 3d^3 P$
Mg III	1572.7	
C IV	1550.8	$2s^2 S - 2p^2 P$
C IV	1548.2	
Mg IV	1470.8	$2p^4 3p^2 P - 2p^4 3d^2 D$
Mg IV	1459.6	$2p^4 3s^4 P - 2p^4 3p^4 S$
Mg IV	1437.5	$2p^4 3p^2 D - 2p^4 3d^2 F$
Mg IV	1409	$2p^4 3p^2 F - 2p^4 3d^2 G$
Mg IV	1404.7	

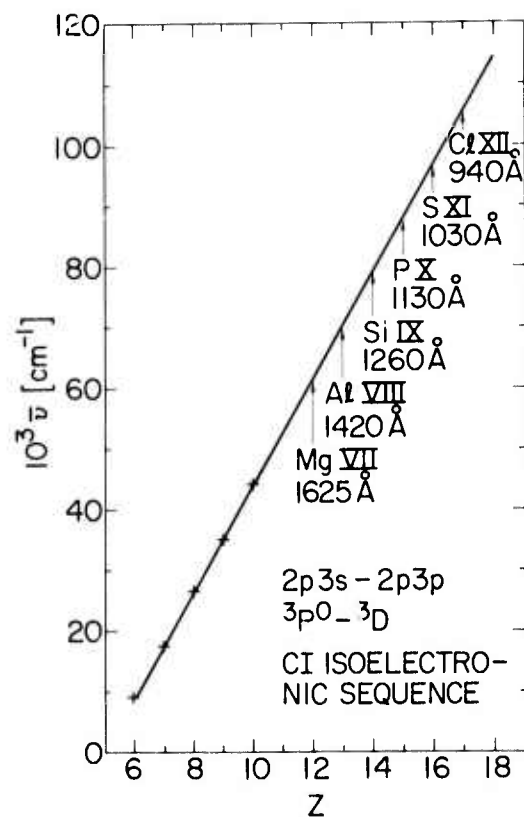


Fig. 35 — Extrapolation of $2p3p\ ^3D - 2p3s\ ^3P$ transition lines in carbon-like isoelectronic sequence

Mg - TARGET
 Q - SWITCHED GLASS LASER,
 1GW, 2.5ns
 FOCAL SPOT SIZE: 100 μ m IN DIA.

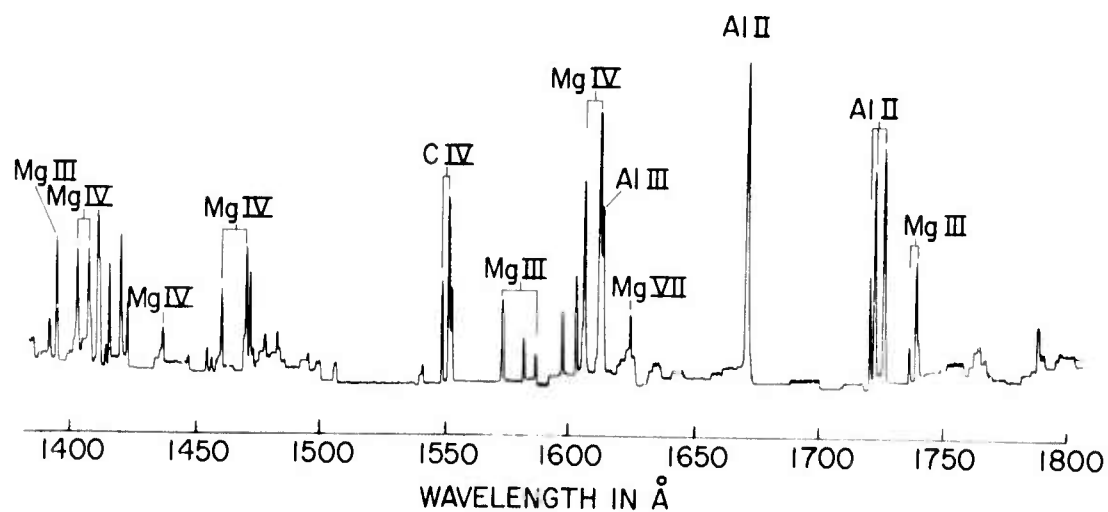


Fig. 36 - Vacuum UV spectrum of laser (Q-switched glass laser) produced Mg-plasma

resolution of 30 psec. Because the picosecond pulse was synchronized with a longer Q-switched pulse which was used to generate the plasma, the plasma could be studied interferometrically during its heating, expansion, and cooling phases. Interferometer studies were made for several different Q-switch pulse durations and target materials. The expansion properties of plasmas created with a line focus were also investigated.

Observation of the expansion characteristics of the plasmas showed a rapid expansion with a velocity of $\sim 4 \times 10^7$ cm/sec during the heating pulse, followed by a slower expansion and recession in some instances after the end of the heating pulse. The initial expansion velocity was found to be independent of target material and did not change significantly as the laser intensity was varied over two orders of magnitude. Spreading of the plasma along the target surface was observed in a pattern similar to the current distribution recently inferred by Drouet and Pépin⁸. The patterns observed here suggest a distortion of the current paths in the plasma resulting in a lowered inductance.

Expansion characteristics of a plasma from a line focus were compared with those from a point focus. The plasmas generated from the line focus have the same initial expansion velocity as those from the point focus. The elongated nature of the line focus is retained in the plasma during and after the heating pulse, although transverse expansion of the short dimension is somewhat faster than that of the long dimension. In general, the plasmas thus produced appear to remain uniform and free of instability on the scale of 15 μ m for the range of time delays which were used.

Electron density profiles were determined for the plasmas generated from the line focus at several times during and after the heating pulse. The electron density distribution was found to decay exponentially away from the target at all times, while the scale length increases at later times. Density gradients up to 10^{21} cm⁻³/cm are observed at distances of the order of 100 μ m from the target. Extrapolation of the measurements shows that the density distribution must rise faster in the vicinity of the target than exponentially, if the critical density is to be reached in front of the original target surface.

Comparison of the plasma expansion from a polyethylene target with that from the heavier metallic target shows an identical expansion velocity, but no tendency for the expansion to slow down after the heating pulse ends. (More experimental details are contained in the previous semiannual technical report [NRL Memo Report 3241]).

III. B.6. CONCLUSION

A 30 ps, 150 mJ Nd:YAG laser pulse is capable of producing a rapidly heated plasma of 300-600 eV when focused onto a slab target. The physical mechanism involved is primarily inverse bremsstrahlung heating.

Strong $2p \rightarrow 1s$ transition lines arising from the He-like Al XII and Si XIII ions and the H-like Na XI and Mg XII ions are observed with the appropriate targets. A numerical model (hot-spot model) has been used in conjunction with these experiments to study the time variation of ion and electron temperatures and the ionic population densities. The results indicate a non-thermal equilibrium state in the early phase of the plasma expansion.

In the dual-laser experiments, possible $3p \rightarrow 3s$ lasing lines of the carbon-like Mg VII ion in the expected spectral region with and without the heating laser pulse injection have been surveyed. The results show neither detectable enhancement of these lines nor any detectable heating of the plasma. This indicates the heating pulse is not effectively absorbed by the plasma. The interferometric study of the expanding plasma produced at either point or line foci of the nanosecond glass laser beam revealed a detailed picture of time-evolving electron density profile and other expansion characteristics. Observation of the critical density surface was not possible due to a severe refraction of the probing laser pulse at the region of high electron density gradient. The critical density layer probably remains within a distance much less than $10 \mu\text{m}$ from the target surface. Observation of the plasma in this region would require the use of a probe beam with a shorter wavelength than the one used here. It is clear that the heating pulse at $1.06 \mu\text{m}$ in the dual-pulse experiment will not interact with the plasma at the critical density where energy absorption should be most efficient.

The interferometric studies also showed quite clearly that with a line focus the region of high density of interest for these experiments was extremely narrow ($\leq 1 \mu\text{m}$) and further, that this region tended not to be linear. These results indicate that the picosecond heating of a preexisting line focus laser plasma approach would be extremely difficult at best, if not impossible.

A second approach to the problem is to use a single laser pulse for both creation and heating of the plasma. A simple estimation indicates that probably a laser pulse of 10^{12} Watt or greater may be necessary in order to have meaningful amplification in the elongated laser-plasma medium. Such a laser system is equivalent to or greater in power than most existing fusion research laser facilities.

These results have lead to a change in approach for producing the required plasma. Laser heating has been abandoned in favor of more conventional plasma pinch technology. This modified approach is described in the next section.

REFERENCES

1. R.C. Elton, in Progress in Lasers and Laser Fusion, p. 117 (Plenum Press, New York, 1975).
2. R. A. Andrews in Progress in Lasers and Laser Fusion, p. 235 (Plenum Press, New York, 1975).
3. D. Mosher, Phys. Rev. A 10, 2330 (1974).
4. T. N. Lee and D. J. Nagel, J. Appl. Phys. (Sept. 1975).
5. J. F. Reintjes, T. N. Lee, R. C. Eckardt, R. C. Elton and R. A. Andrews, Bull. Am. Phys. Soc. 20, 1336 (1975); Bull. Am. Phys. Soc. 21 (1976).
6. R. C. Elton, Appl. Optics 14, 97 (1975); L. J. Palumbo and R. C. Elton, J. Opt. Soc. Am. (in press).
7. J. F. Reintjes, T. N. Lee, R. C. Eckardt, and R. A. Andrews, J. Appl. Phys. 47, 4457 (1976).
8. M. G. Drouet and H. Pépin, Appl. Phys. Letters 28, 426 (1976).

III. C. HYPOCYLOIDAL PINCH DEVICE

Referring to Fig. 20, at lower Z, the two longer wavelength curves pertain to the lower densities and larger diameters more typical of electromagnetically driven pinch devices. The efficiencies of such

devices are in the percent range in contrast to laser-produced plasmas (tenths of percent at high temperatures) and make direct use of capacitive energy storage systems in the 10's of kJ to mJ ranges with existing and reliable technology. It thus seems prudent to pursue the near-term goals of electron collisionally pumped vacuum-UV lasers below 1000 Å with a suitable electrically driven plasma pinch device. Fortunately, a device has just recently been developed¹ at NASA Langley and Vanderbilt University that appears ideal for this application. The device is shown schematically in Fig. 37. It is a cylindrically symmetrical version of the well-known plasma focus principle, in which the plasma implodes radially (inverse pinch) to form a high-density (reportedly $\geq 10^{19} \text{ cm}^{-3}$) high-temperature ($\sim 1500 \text{ eV}$) plasma on axis in a cylindrical (mm's in diameter, cm's in length) configuration desirable for lasing. The hypocycloidal current configuration originally inspired the name for this device.

A duplicate of the NASA/Vanderbilt successful device has been built for NRL (Figs. 37 and 38), and the first experiments are planned with an argon filling for lasing near 900 Å as indicated in Fig. 20. Actually, various ions in such as boron-like through neon-like should span the 800-1000 Å region, and accurate calculations are underway through the courtesy and cooperation of Dr. R. D. Cowan of Los Alamos Scientific Laboratory. The required temperature of $\sim 600 \text{ eV}$ for argon is quite realistic for this device. Amplification will be verified by orthogonal axial and radial spectroscopic simultaneous measurements with two normal incidence vacuum-UV spectrometers.

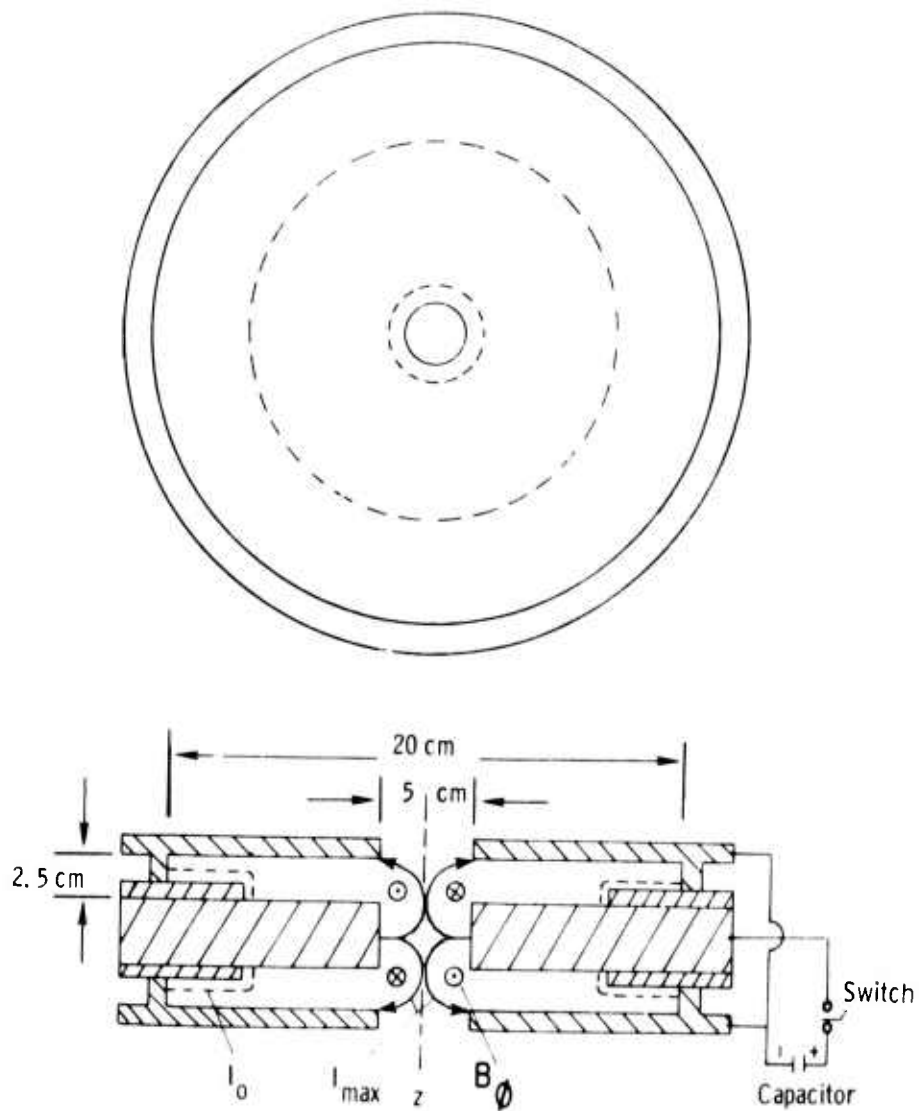
Work on this approach, i.e., 3p-3s lasing using a plasma pinch device for plasma heating, is continuing despite the termination of this ARPA program. The work is being supported by NRL.

REFERENCES

1. J. H. Lee, D. R. McFarland, and F. Hohl, "Dense Plasma Focus Production in a Hypocycloidal Pinch," NASA Technical Note NASA TN D-8116, December 1975 (to be published).

IV. RESONANT CHARGE TRANSFER PUMPING

The resonant charge transfer process¹ for populating excited states of ions was chosen for investigation as a possible x-ray laser pumping mechanism for several reasons: (a) the cross section is orders of magnitude higher than other processes, (b) the process is selective for certain excited states of ions, (c) it is the one process identified for which the pumping rate coefficient actually increases² at shorter wavelength ($\lambda^{-5/4}$). While total cross section experimental data are available for this process, the final excited states populated have not been measured in classical cross beam experiments.



HYPOCYCLOIDAL PINCH

Fig. 37 — Schematic of radially driven focused plasma pinch device invented by Lee, McFarland and Hohl (Ref. 8). The geometry is cylindrically symmetrical with the disc cathodes shown separated by approximately 6 cm. Note that both ends are conveniently accessible for injection and observation.

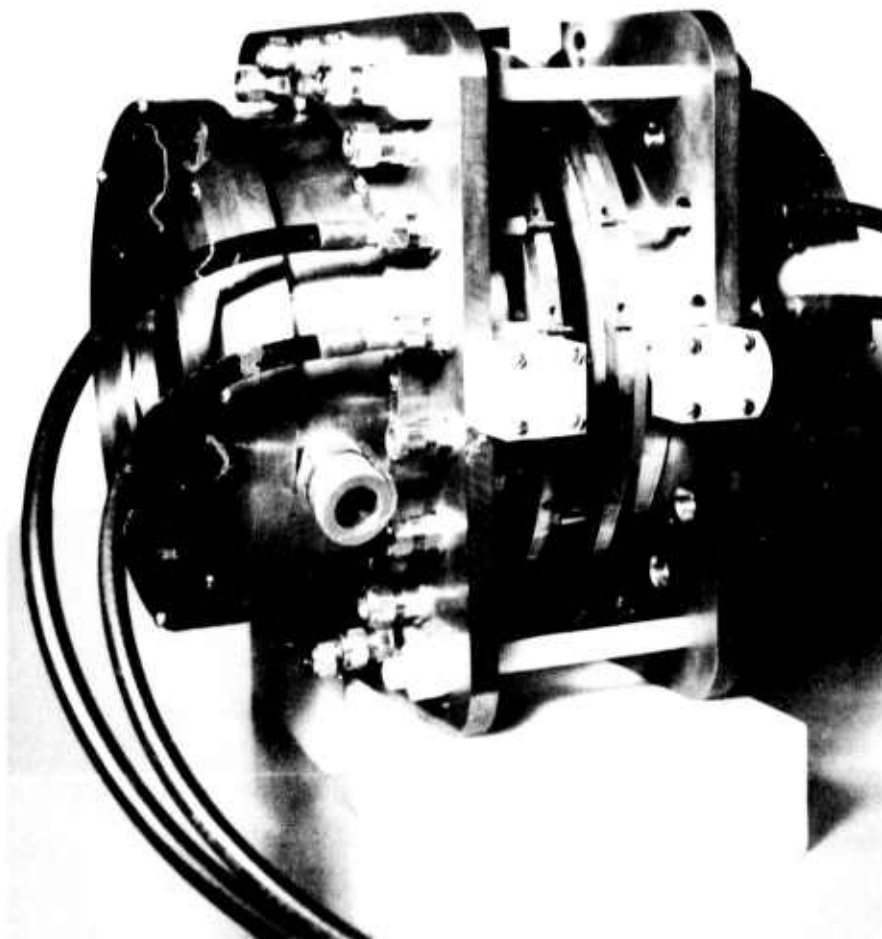


Fig. 38 — Photograph of the assembled hypocycloidal pinch device constructed for NRL. Two of the cables are shown connected in this photograph.

The resonance charge transfer process proceeds most efficiently by ion/atom interactions. For net gain at short wavelengths, a high density of interacting particles is required, although again due to the favorable wavelength scaling and magnitude of the rate, the densities required are orders of magnitude less than for other processes at short wavelengths^{1,2}. The plasma dynamic theory required for predicting particle densities in the ion/atom interaction zone is formidable compared to the experiment envisioned, so that an experimental search for evidence of resonance charge transfer pumping was undertaken. However, some classical Landau-Zener calculations were carried out³⁻⁵ to predict the energy levels expected to be preferentially populated for a thermal plasma, with the results indicating $n=3-4$ most favorable with $n=2$ and 5 possibilities. Again, the process is ion-velocity sensitive and these predicted levels can be expected to deviate for any significant non-thermal distributions.

The conceptually simple experiment^{2,3,5} is illustrated in Fig. 39. Targets of carbon, boron and nitrogen were irradiated⁶ by a laser beam with power up to 400 MW (8 J, 20 ns) in a point focus, and spectra of one- and two-electron ions were observed with a grazing incidence spectrograph^{7,8}. The line emission was spatially resolved along an axis normal to the target by the addition of a second orthogonal slot as shown in Fig. 39. Initial observations (phase one) with this laser and a point focus were intended to gather evidence of preferential level population from the observation of anomalously intense spectral lines in the resonance series (from transitions originating on the pumped levels). These experiments were to be followed by a line focus series in a later phase of the program, using the large NRL terrawatt laser facility.

The first experiments were performed with expansion into a vacuum environment, and the decay of the spectral line emission and width with distance from the target was recorded^{7,8}. The relative intensities of the resonance series lines was found to be normal except very close to the target where self absorption of the strongest members was observed, as was to be expected.

The addition of a gaseous atmosphere in the pressure range of 1-10 torr (significant absorption occurred at higher pressures for the longer wavelengths) required the addition of gas puffing apparatus and special valves for isolating and back-flushing the entrance slit of the spectrograph to eliminate clogging by debris. When this was accomplished, both visible and soft x-ray spectra revealed a distinct zone of enhanced density and illumination centered up to 1 cm from the target surface⁶ and not present on the spectra obtained with expansion into a vacuum environment^{7,8}. The distance of this zone from the target was found to be directly related to the laser power and inversely related to the gas pressure. It was present with carbon as well as boron nitride targets⁸ and gases of hydrogen, helium, neon and argon. The electron density increased to $\sim 10^{17} \text{ cm}^{-3}$ in the center of this zone before

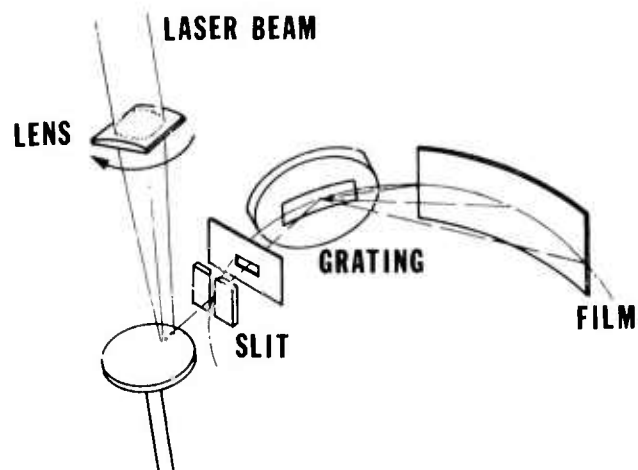


Fig. 39 — Schematic diagram of the NRL resonance charge transfer experiment, including the grazing incidence vacuum spectrograph. The horizontal slot provides spatial resolution along the direction of plasma expansion from the target surface. Rotation of the lens permits both axial and radial viewing. The background (atomic) gas is not indicated.

decreasing again further out; this was estimated from the Stark broadening of HeII and CIII spectral lines in the visible region. From visible time-integrated photographs it has been determined that this zone of enhancement is arc-shaped radially from the point of target irradiation — and possibly initiated at a particular velocity yet to be ascertained. The particular levels populated may be associated with a nonthermal radial ion velocity component not uncommon to such plasmas; such may be determined from time- and space-resolved spectroscopic measurements.

Distinct features in the CV (helium-like two-electron ion) resonance series spectra were enhanced emissions from the third and fourth members originating on $n=4$ and 5 levels when a helium background gas was present, as shown in Fig. 40. This only was observed in the outer regions of the interaction zone, near 1.5 cm from the target when the helium pressure was 1 torr. It also was present at a pressure of 5 torr, from data obtained so far. This indicates that indeed there exists an enhanced relative population of these two particular levels in the region of enhanced conditions associated with the presence of helium. Preferred population by resonance charge transfer is suggested as a possible electron capture mechanism favoring these levels, and this explanation would be consistent with the apparent velocity selective nature of the distinct zone of enhancement for the helium atmosphere experiments. However, other mechanisms (e.g., dielectronic capture and collisional recombination followed by cascade) cannot yet be ruled out without further parametric studies. Clearly, however, the goal of the first phase of this experiment, namely to identify a region of interaction and evidence of preferential level population has been fulfilled and the milestone reached on schedule.

Although this program has been terminated, the charge transfer work will continue at NRL under sponsorship of NRL and ERDA. The goals will be changed in order to address the problems of interest to ERDA, i.e., the physics of charge transfer between hydrogen and heavy ions in environments typical of magnetic fusion.

REFERENCES

1. "Review of Short Wavelength Laser Research," R. W. Waynant and R.C. Elton, Invited Paper, Proc. IEEE 64, 1059 (1976).
2. "X-Ray Laser Research: Guidelines and Progress at the Naval Research Laboratory," R. C. Elton and R. H. Dixon, Annals of the New York Academy of Sciences 267, 3 (1976).
3. "Three Quasi-CW Approaches to Short Wavelength Lasers," R. C. Elton, in Progress in Lasers and Laser Fusion, edited by B. Kursunglu, A. Perlmutter, and S. M. Widmayer (Plenum Press, Inc., New York, 1975).
4. "ARPA/NRL X-Ray Laser Program — Semiannual Technical Report for 1 Jan 1974 - 30 Jun 1974," NRL Memorandum Report 2910 (October 1974).

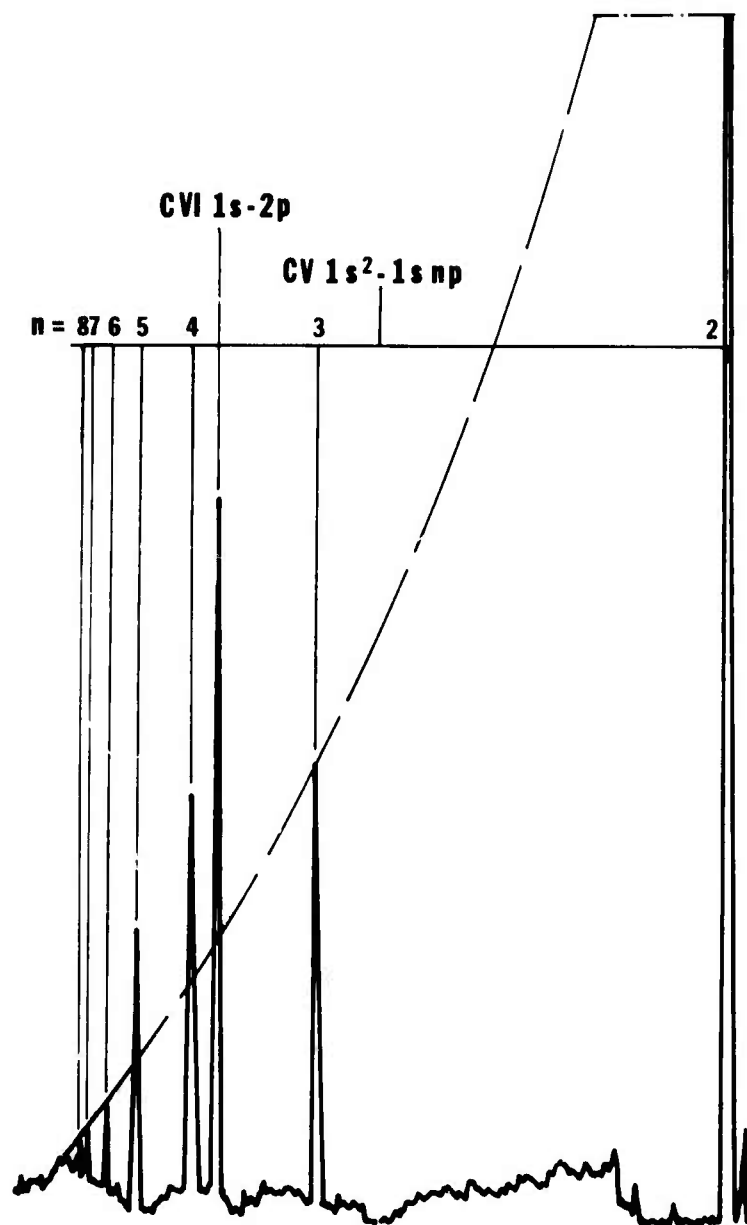


Fig. 40 — Microdensitometer tracing of C V and C VI resonance spectra in 30-40 Å region. Broken line indicates expected envelope for CV series peak intensities; anomalous emission from n=4 and n=5 levels is indicated.

5. "ARPA/NRL X-Ray Laser Program — Semiannual Technical Report for 1 Jul 1974 - 31 Dec 1974," NRL Memorandum Report 3057 (May 1975).
6. "ARPA/NRL X-Ray Laser Program — Semiannual Technical Report for 1 Jul 1975 - 31 Dec 1975," NRL Memorandum Report 3241 (March 1976).
7. "ARPA/NRL X-Ray Laser Program — Semiannual Technical Report for 1 Jan 1975 - 30 Jun 1975," NRL Memorandum Report 3130 (1975).
8. "Spectroscopy of Plasmas for Short Wavelength Lasers," R. C. Elton and R. H. Dixon, Proc. IVth Int'l Conf. on Beam Foil Spectroscopy, Gatlinburg, Tenn., Sept. 1975; published in Beam Foil Spectroscopy, Vol. 2, edited by I. A. Sellin and D. J. Pegg (Plenum Press, Inc., New York, 1976).

V. TRAVELING-WAVE PUMPED VUV LASERS

V. A. INTRODUCTION

The concept of traveling wave (or swept gain) excitation, when coupled to low inductance flat-plate Blumlein discharge circuitry, produces a unique technological advantage for excitation of vacuum ultraviolet laser transitions. This concept, originated by Shipman¹ at the Naval Research Laboratory, has been utilized to produce high-power amplified superfluorescent emission from atoms, molecules, ions and excimers covering the wavelength region from 6000 Å to 1161 Å. In addition, it is likely that numerous infrared laser lines were simultaneously produced, but these were not studied.

The concept of traveling-wave excitation becomes vital for generation of real gain below 1000 Å. Scully has given the concept its first theoretical treatment terming it "swept-gain" and has shown the effects of gain on the emission characteristics. Some of these characteristics have been observed in our laboratory (see previous semiannual technical report, NRL Memo Report 3241), but the need for a more exhaustive experimental investigation is required. The concepts of laser lethargy, pulse narrowing, and the group velocity of a pulse in a uniformly or non-uniformly inverted amplifying medium are important for short-wavelength lasers.

V. B. MOLECULAR AND ION LASER RESEARCH

The apparatus used to produce traveling-wave excitation is described in publications on the hydrogen laser²⁻⁶ and vacuum ultraviolet CO laser emission⁷. This system needs no further description except to point out that the present technology for producing high-quality traveling-wave discharges is not yet suitable for high repetition rates. At relatively long wavelengths (> 2000 Å) some sacrifice in risetime and uniformity to simplify construction and increase the repetition rate can be tolerated without loss of performance, but at shorter wavelengths

these qualities cannot be sacrificed without serious loss of output power.

The traveling-wave system produced a bit of serendipity also. It was found that at low pressures in the presence of rare gas backgrounds that carbon atoms, probably from the $(C_2 H_2)_n$ insulator on which the electrodes rested, were being ionized (C^{+8} or CIV) and excited to give superfluorescence at 1550 \AA . Efforts to understand the mechanism of the inversion have not been successful. The carbon lines which would yield information on the inversion process lie too far into the VUV to be observed with a normal incidence spectrograph. Possible mechanisms for inverting the 2p-2s resonance lines observed to be lasing are based on transient events only. One possible mechanism requires that excitation take place from the ground state of the atom or lower stage of ionization directly to the excited state of the ion. This is not a phenomenon new to lasers. Bennett proposed this direct excitation process and showed that it was most probable with rapid excitation⁹. In an experiment quite similar to this CIV lasing experiment, Norton and Wooding¹⁰ have generated these stages of ionization in carbon by surface discharge across $(C_2 H_2)_n$ and propose that these stages of ionization will be collisionally velocity selected with excited species of each ion having greater velocity than the ground state of that ion stage, i.e., CIV(2p) has greater velocity than CIV(2s). This creates a region of predominantly CIV(2p) which can amplify a spontaneously emitted photon without the resonance absorption present when CIV(2s) ions are present. This explanation would be ideally suited for traveling-wave excitation which would reduce the inversion density required for threshold by two orders of magnitude. The exploitation of ions in the vacuum ultraviolet has hardly begun. There is no reason why many lasers should not be produced from ions in this spectral region. The process will not likely be very efficient, because the quantum efficiency will be very low and rapid excitation still will be required. Further work is required to understand the inversion mechanism of ion lasers and to exploit new ion lasers in the VUV/x-ray region. The concept of "velocity selection" is especially important and could ease short-wavelength laser development if it can be produced.

V. C. RARE-GAS HALIDE EXCIMER LASER RESEARCH

The new class of laser species - excimers - offers several advantages for operation in the vacuum ultraviolet: 1) they exist as molecules only in the excited state and are not self-terminating; 2) they have a broad emission bandwidth and offer some tunability; and 3) they offer the possibility of high efficiency and high power. These quasi molecules can be discharge pumped by Blumlein systems and may make ideal amplifiers for low-level pulses from the nonlinear mixing upconversion processes discussed previously. Numerous transitions in the vacuum ultraviolet have been suggested as possible laser candidates by Ewing and Brau¹¹. Table 3 shows some of these candidates and an estimate of the wavelength at which lasing might be expected.

TABLE 3

<u>Excimer</u>	<u>λ (Å)</u>	<u>Observed</u>
Xe I	2560	yes
Xe Br	2920	yes
Xe Cl	3240	yes
Xe F	3860	yes
Kr I	1850	no*
Kr Br	2030	yes*
Kr Cl	2190	yes
Kr F	2560	yes
Ar Br	1610	no*
Ar Cl	1720	yes*
Ar F	2670	yes
Ne F	1050	no*

*Indicates this report contains new results on these excimers

The rare-gas halide excimers have a definite attraction both as amplifiers for upconverted signals and as direct sources. The traveling-wave Blumlein system was modified to take higher pressures and to excite larger gas volumes in a more uniform discharge free from arcs. These modifications worked sufficiently well to generate lasing in Xe F, Kr F, Kr Cl, and Ar F (see Fig. 41). These gases had been shown to lase previously and were investigated only to provide an indication of how well the system would operate. Details of the operation are provided in the preprint¹² of the report (see Appendix) of the successful production of Ar Cl laser emission at 1750 Å. Similar operation of the system with a few Torr of Br generated lasing in Kr Br at 2065 Å. (see Fig. 42), but no success was obtained with Ar Br. It should be pointed out that all of the laser emission observed was without resonators, i.e., superfluorescent emission. Considerable improvement would be expected if a resonant cavity was used, and it may make lasing occur in Ar Br. The same might be said for Kr I and Ne F, which also did not lase. In the case of Kr I it was further hindered by the difficulty of maintaining a sufficient Iodine vapor pressure inside the laser chamber. Ne F was probably hindered by the poor transmittance of LiF windows in the 1000 Å region. Some data were taken without LiF windows, but other difficulties in operating the system with a He purged spectrograph may be responsible for the lack of lasing. In summary, all of the rare-gas halide combinations which did not lase might be made to do so if the experimental conditions could have been improved.

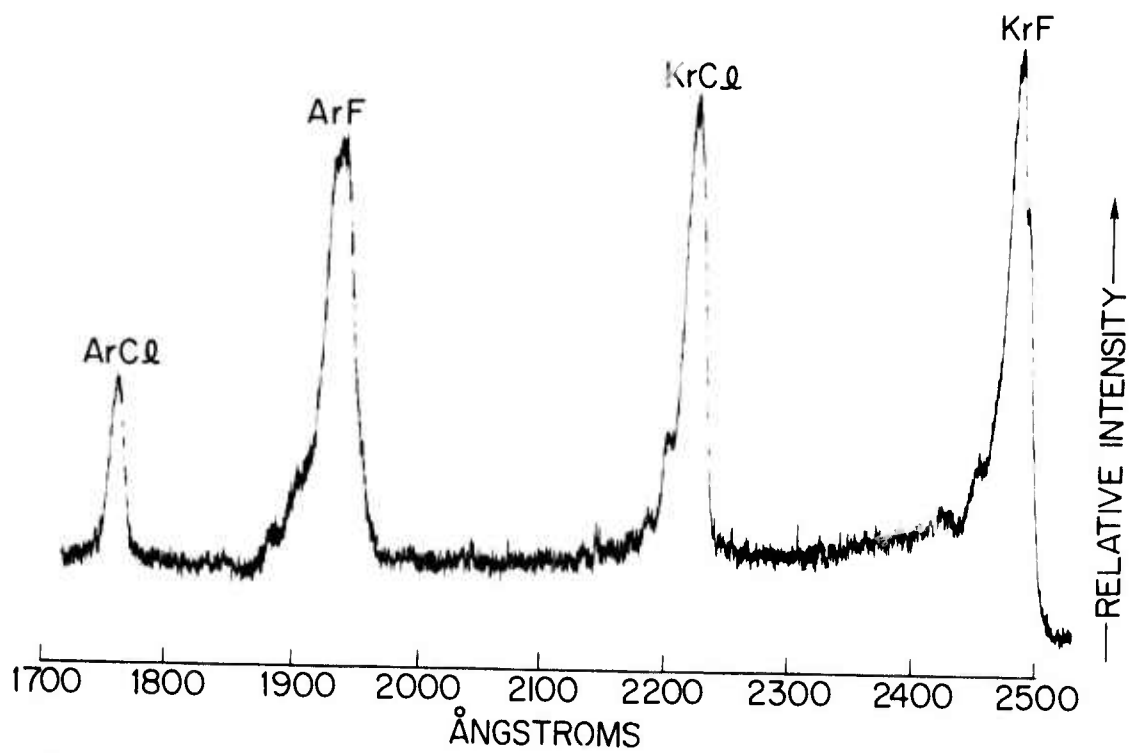


Fig. 41 — Rare gas-halide laser spectra produced by mirrorless Blumlein excitation system

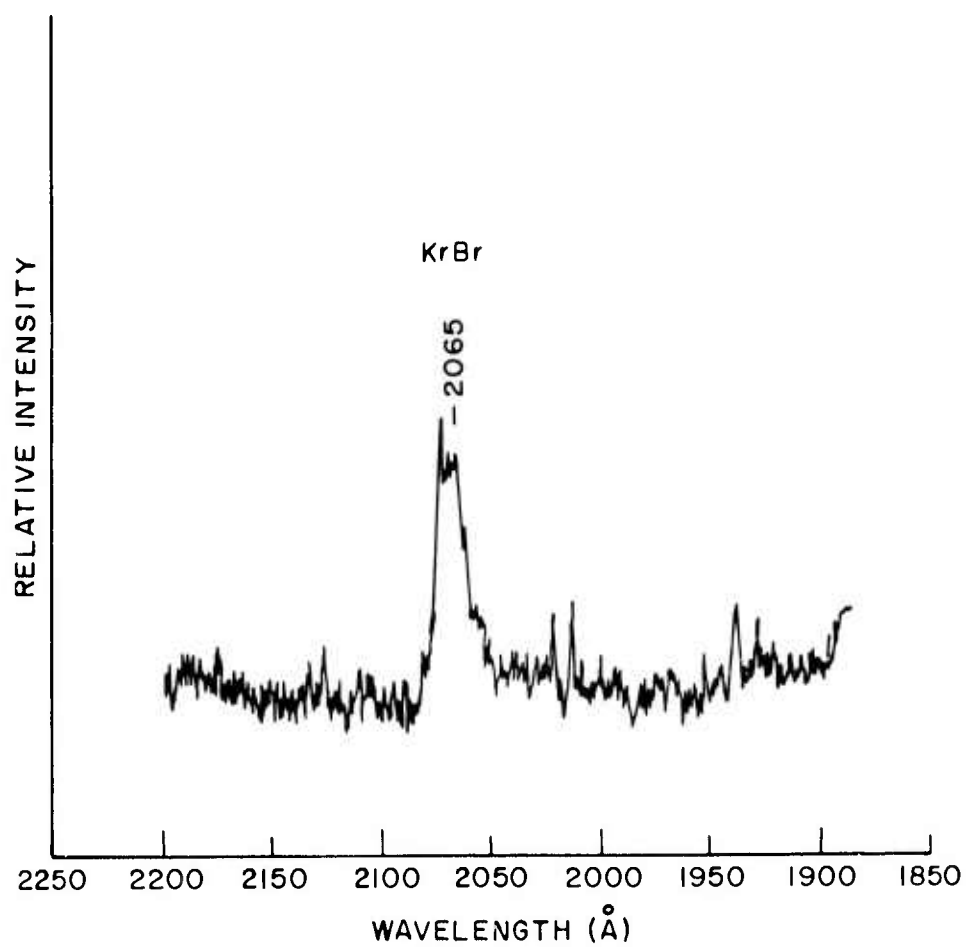


Fig. 42 — Spectrum from KrBr when excited by fast discharge system

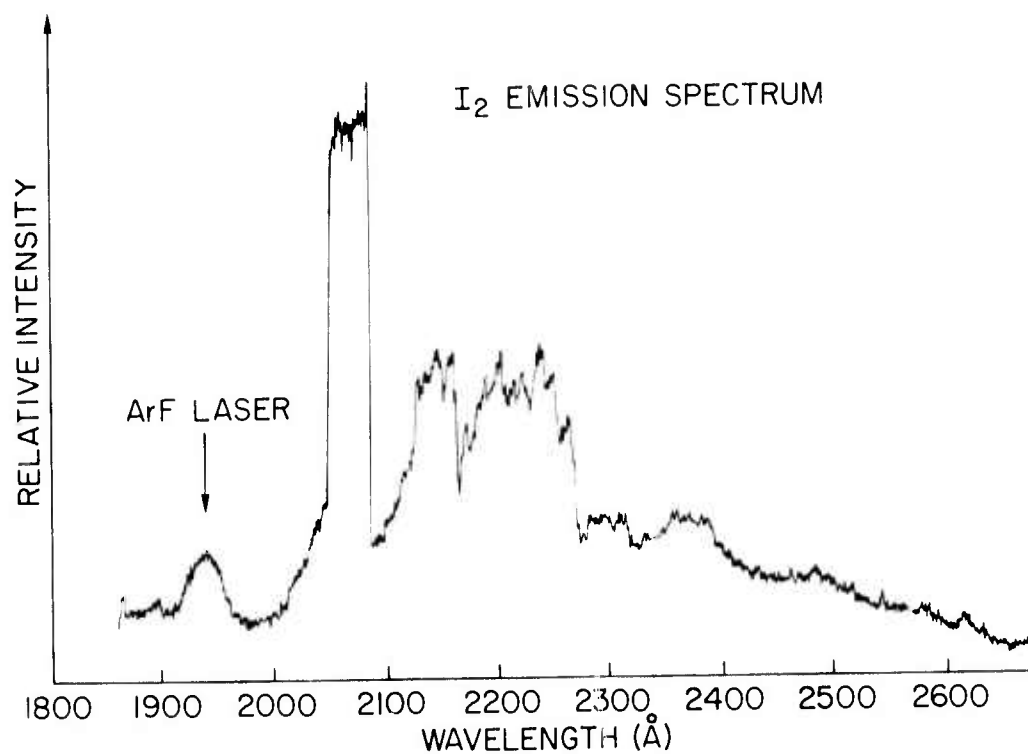


Fig. 43 — Emission spectrum from molecular iodine when excited by a longitudinally focused pulse of ArF laser radiation and observed along the axis of excitation

In an initial attempt to utilize the rare-gas halide lasers as pumps to produce tunable laser radiation, Ar F was used to pump I₂ vapor. This idea was proposed by Murray and Powell at the Third Colloquium on Electronic Transition Lasers¹³ and follows earlier experiments by Byer¹⁴ in which 5320 Å radiation was used to pump the B-X transitions in I₂ producing many laser lines in the 5400 Å - 1.3 μ region. In this case an Ar F pulse (at 1930 Å) was focused into I₂ vapor (~100 M Torr) in front of a one-meter vacuum spectrograph. The 1930 Å radiation populates the D state of I₂, and inversion exists on D-X transitions where the upper vibrational levels of the X states are the lower laser levels. Emission in the 2000-2700 Å region results (see Fig. 43). At present the evidence of lasing is the narrow beam of emission falling on the spectrograph slit. It should be easy to produce a cavity laser using a grating for tuning by using a cylindrical lens for pumping. This is an extremely clean method of pumping, and it produces wavelengths of importance in photochemistry.

Another application involves the use of rare-gas halide lasers as pumps for rare-earth doped crystals in a manner similar to that suggested by Yang¹⁵ for H₂ laser pumping. The Ar Cl laser lines observed could be a possible pumping source for some doped-crystal tunable lasers, but the attainment of lasing in Ar Br may be an exact match to the trifluoride crystals already studied.

In summary, the discharge laser research conducted on this contract has resulted in new lasers in the vacuum ultraviolet which fill needs in other areas of research and which contribute to the understanding of principles and techniques required for the realization of an x-ray laser.

REFERENCES

1. J. D. Shipman, Jr., Appl. Phys. Lett. 10, 3 (1967).
2. R. W. Waynant, J. D. Shipman, Jr., R. C. Elton, and A. W. Ali, Appl. Phys. Lett. 17, 383 (1970).
3. R. W. Waynant, J. D. Shipman, Jr., R. C. Elton, and A. W. Ali, Proc. IEEE 59, 679 (1971).
4. R. W. Waynant, A. W. Ali, and P. S. Julienne, J. Appl. Phys. 42, 3406 (1971).
5. R. W. Waynant in Proc. Electro-Optical Systems Design Conf. - '71 West, M. S. Kiver, ed. (Kiver Publishing Co., Chicago, Ill) pp 1-5.
6. R. W. Waynant, Phys. Rev. Lett. 28, 533 (1972).
7. R. W. Waynant, (unpublished).
8. R. W. Waynant, Appl. Phys. Lett. 22, 419 (1973).

9. W. R. Bennett, Jr., Appl. Opt. Suppl. 2, 3 (1965).
10. B. A. Norton and E. R. Wooding, Phys. Rev. A 11, 1689 (1975).
11. J. J. Ewing and C. A. Brau, Appl. Phys. Lett. 26, 350 (1975).
12. R. W. Waynant, (to be published).
13. J. R. Murray and H. T. Powell, (to be published).
14. R. L. Byer, R. L. Herbst, and H. Kildal, Appl. Phys. Lett. 20, 463 (1972).
15. K. H. Yang and J. A. DeLuca, Appl. Phys. Lett. 29, 499 (1976).

VI. MISCELLANEOUS ANALYSES

A vital part of this program was the systematic analyses of a number of proposed pumping schemes based upon available atomic and ionic data. The purpose was to provide direction to the experimental program. Indeed, it was a direct result of such searching that the favorable electron collisional pumping of 3p-3s quasi-cw inversions (described above) was identified and now pursued actively at a number of laboratories in the U.S. and abroad, including the Soviet Union.

Considerable analysis was carried out on the photoionization of K-shell electrons, and the resulting inversion on K-alpha transitions at very short wavelengths, which may be assured by ion-line shifting compared to the absorbing K-alpha line^{1,2}. This is basically a self-terminating laser scheme, limited in inversion intervals by recombination rates. New gains were predicted and the fundamental limitation was identified to be photoionization losses to the beam due to outer valence electrons. Intense, well-tuned pump sources are required. As more and more innershell processes were included in the considerations for this approach, it became increasingly difficult to envision a first generation x-ray laser evolving from such a complex system. Detailed rate equation numerical analysis similar to those successfully developed for the 3p-3s outershell scheme would be extremely complex and the processes quite uncertain. Therefore this approach was not followed experimentally but may be reconsidered at some future time, particularly if a method is developed for efficiently transferring intense x-radiation to small linear targets in very short bursts.

Some numerical modeling¹ was also carried out for photoionization of alkalis such as sodium. The modeling was on a time-resolved basis both with an exploding wire pump source and a traveling-wave device.

It has been suggested that the absorption of intense line radiation by overlapping lines of other species may be an efficient way of pumping particular upper laser levels preferentially³⁻⁵. Some very attractive

and important aspects of this approach are: (a) lasing occurs in a single species and is thus regenerative, so that cw operation is possible, (b) no Auger energy losses are present as valence electrons are pumped, (c) photoionization losses can be avoided, (d) the intense resonance lines appropriate for pumping are generally well identified and the transitions understood, (e) some line overlapping is recurrent so that extrapolations to shorter wavelengths may be possible, and (f) hybrid schemes incorporating the best features of photo- and electron-collisional excitation may be combined. Some necessary requirements of this approach are: (a) very close overlap of the pumping and the pumped transition is required for efficient coupling. When not so close, both Stark and opacity broadening have been suggested. These usually lead to very high densities ($\sim 10^{22} \text{ cm}^{-3}$ typically) and/or thick plasmas, with many particles required to be heated and large pump energy inputs required. Also, (b) as with photoionization pumping, the coupling between the pump and the pumped regions must be good, and ideally the two species should coexist in the same plasma. This requires very close Z's or at least ionization potentials. Since an intense blackbody pump source is required, (c) hydrogenic ion resonance lines are often considered as are helium-like lines. These as well as neon-like ions are also desirable (for pulsed plasma devices) since they tend to have extended lifetimes associated with increased ionization potentials.

In considering and analyzing the photoexcitation pumping approach, two particular schemes were analyzed and the details are included in a paper entitled "Resonant Photoexcitation Pumping in Hydrogenic Ions," which is included in Appendix A. The first ions considered were hydrogenic, where a "natural" overlap in wavelength occurs between an $n=2$ to $n=1$ Lyman- α pump line from an ion of nuclear charge Z and an $n=2$ to $n=4$ absorption line for a $2Z$ ion. This is a hybrid (or "photon assist") scheme, where the $n=2$ level of the lasant is pumped by electron collisions (which complicates the analysis considerably). A list of potential laser $n=4$ to $n=3$ wavelengths for ions of beryllium through krypton extending from 1172 \AA to 14 \AA is given in Table 1 of the paper in Appendix A. The gains calculated are at best marginal since the overlap is not exact when relativistic corrections are included for the calculated wavelengths; and also close coupling between a very dense pump and a more tenuous lasant is required which does not lend itself obviously to convenient experiments. Nevertheless, calculations are completed for a Mg XII lasant pumped by C VI Lyman- α radiation.

Also analyzed in Appendix A is a much more promising combination of a hydrogenic C & XVII lasant pumped from $n=1$ to $n=4$ (Lyman- α) by a Lyman- α line of K XIX with potential $n=4$ to $n=3$ lasing at 65 \AA . The reported wavelengths are within 3 m\AA and the Z's are sufficiently close to coexist in a common plasma. Electron collisional pumping is not required nor is Stark broadening so that the analysis is more exact and gains of 44 cm^{-1} are calculated. This is a very promising scheme and will be pursued at NRL in the hypocycloidal pinch⁶

device designed to produce cylindrical plasmas of centimeter length at high density and high temperature. While this is a gaseous discharge device, it has recently been shown that efficient injection of metallic ions by laser vaporization is possible.

The close K-C α overlap is coincidental but encouraged a systematic search for other promising combinations. Starting from the Ryberg formula for hydrogenic ions up to Z=20 and requiring a wavelength decrement $\delta\lambda \leq 0.05 \text{ \AA}$ a simple computer program produced 68 candidates. A number of these are particularly attractive, with wavelength decrements less than 10 m\AA which can be accommodated with Doppler broadening. It is intended to investigate these systematically in the new hypocycloidal pinch device⁶. Also, it is important to recognize that uncertainties exist in tabulated wavelengths in the 1-10 m \AA range, particularly between elements investigated by different laboratories. For this reason it is intended that the most promising candidates will be remeasured under high resolution on a single experiment and perhaps other less promising candidates will be reinvestigated for closer coincidences than previously suspected.

In summary, photoexcitation pumping between species in a single medium appears very promising under the proper conditions. The energies required to heat a sufficient density of ions becomes again a practical limitation so that it is imperative that as efficient coupling as possible be made between the pumping and the lasing ions. New and precise checks are required on promising coincidences and are indeed planned here and in the Soviet Union, (see note in proof, p. 4).

REFERENCES

1. "ARPA/NRL X-Ray Laser Program — Semiannual Technical Report for 1 Jan 1974-30 Jun 1974," NRL Memorandum Report 2910 (October 1974).
2. "Quasistationary Population Inversion on K α Transitions," R. C. Elton, Appl. Opt. 14, 2243 (1975); Physica Fennica 9, Suppl. S1, p. 397 (1974), and NRL Memorandum Report 2906 (October 1974).
3. B. A. Norton and N. J. Peacock, J. Phys. B: Atom. Molec. Phys. 8, 989 (1975).
4. A. V. Vinogradov, I. Yu. Skobelev, I. I. Sobel'man, and E. A. Yukov, Sov. J. Quant. Electron. 5, 1192 (1976).
5. "Review of Short Wavelength Laser Research," R. W. Waynant and R. C. Elton, Proc. IEEE 64, 1059 (1976).
6. J. H. Lee, D. R. McFarland, and F. Hohl, "Dense Plasma Focus Production in a Hypocycloidal Pinch," NASA Technical Note, NASA TN D-8116, December 1975 (to be published).

VII. SUMMARY

During the last reporting period the shortest wavelength coherent radiation ever achieved has been generated. Also major steps have been made in narrowing the approach and concept for moving to even shorter wavelengths. Unfortunately a major segment of the program ends here due to the abrupt cancellation of the effort by ARPA.

The major accomplishments during this period (since 1 January 1976) have been:

Nonlinear Mixing

1. The shortest wavelength coherent radiation ever reported has been generated at 53 and 38 nm. This was accomplished via a nonlinear mixing process which was resonantly enhanced. The measured efficiency for generation of 53 nm from 266 nm (fourth harmonic of Nd:YAG at 106 μ m) was 10^{-5} . This work represents the first demonstration of higher order mixing process in gases.
2. Extremely high efficiencies have been achieved for the fourth harmonic generation of 266 nm from 1.06 μ m in ADP and KD* P. The highest efficiencies yet reported, 85%, for conversion of 532 nm to 266 nm has been achieved. The problem has been analyzed and modeled. It is now possible to specify all the parameters to achieve the optimum conversion efficiency.
3. A complete cancellation of self-phase modulation in 1.06 μ m pulses propagating through cesium vapor has been observed. This represents the first time this has been accomplished. The negative nonlinear refractive index responsible for this effect has been measured as $n_2/N = -(2.5 \pm .5) \times 10^{-30}$ esu, in good agreement with theory.

Electron-Collisional Pumping

4. Interferometric measurements have been made of point and line focus laser produced plasmas with a spatial resolution of 1 μ m and a temporal resolution of 30 psec. These studies have shown that due to large plasma density gradients the high density region required for laser heating is very thin and usually not in a linear configuration. Hence the laser heating approach has been abandoned in favor of a more conventional plasma pinch device.
5. A hypocycloidal pinch device has been constructed and is ready for testing. This device should be capable of producing the required high density plasmas in a linear configuration.

Resonant Charge Transfer

6. Early experiments indicate a region of enhanced density and illumination for specific spectral lines centered up to 1 cm from the target surface which may be due to charge transfer. This is supported by both visible and soft x-ray measurements.

TW Pumping

7. The first observations have been made of laser action in ArCl excimers pumped by a high voltage, fast risetime Blumlein discharge circuit. The new laser emits at 175 nm and operates at atmospheric pressure.

Analysis

8. An analysis has been made of resonant photoexcitation pumping in hydrogenic ions. Two schemes are analyzed both based on a four-level laser lasing on $4 \rightarrow 3$ transitions in hydrogenic ions of medium Z . One involves collisional excitation followed by photo-assist pumping. The other, more promising, takes advantage of a wavelength coincidence for pumping directly from $n=1$ to $n=4$ in, e.g., Cl^{16+} by Lyman- α radiation from K^{18+} . This latter scheme is being pursued experimentally with the hypocycloidal pinch device.

It is unfortunate that the ARPA program is terminated at this point since the overall approach has been narrowed and supported by considerable analysis and numerical modeling. However, relevant work will continue on the magnetic pinch device and the resonant charge transfer under the support of NRL and ERDA, respectively. The goals and priorities, will change, however, particularly for the latter.

Reprints of the major presentation abstracts and published papers are collected in Appendix B. Only those for the last half of FY 76 and FY 76T appear. Many others have appeared in previous semiannual technical reports. A total of 122 presentation and publication have resulted from the work done under this program.

VIII. APPENDICES

Appendix A: Resonant Photoexcitation Pumping in Hydrogenic
Ions by R. C. Elton. 92

Appendix B: Presentations and Publications for the
Reporting Period as follows:

Presentations

"K X-Ray Emission Spectra From a High Power-Density Plasma,"
by T. N. Lee, Int'l Conf. on the Physics of X-Ray Spectra,
August 1976. 115

"Compensation of Self Phase Modulation by Cesium Vapor,"
by R. H. Lehmborg, J. Reintjes, and R. C. Eckardt, Proc. 1976
Int'l Quantum Electronics Conf., Amsterdam, June 1976. 118

"An Electron-Collision Pumped Quasi-CW Soft X-Ray Laser Using
Helium-Like Ions", by L. J. Palumbo, Int'l Conf. on the Physics
of X-Ray Spectra, Aug. 1976. 123

"Diagnosis of a Traveling-Wave Surface Discharge as a Source
of Short Wavelength Stimulated Emission," by R. W. Waynant,
T. N. Lee and R. C. Elton, Bull. Am. Phys. Soc. 21, 597
(1976). 125

"Shortest Wavelength Laser from Harmonic Generation", by J. Reintjes,
R. Eckardt, N. Karangelen, R. C. Elton and R. Andrews, Physics
Today, December 1976, p. 17. 126

"Review and Status of X-Ray Laser Research," by R. W. Waynant,
Invited Paper, Int'l Conf. on the Physics of X-Ray Spectra,
Aug. 1976. 129

"Study of Expansion Characteristics of Laser Produced Plasmas
Using Microinterferometry," by J. F. Reintjes, T. N. Lee,
R. C. Eckardt, R. C. Elton, and R. A. Andrews, Bull. Am.
Phys. Soc. 21, 854 (1976). 132

"Comparison of Efficient Harmonic Generation from 532 nm to
266 nm in ADP and KD*P," by J. F. Reintjes and R. C. Eckardt,
Proc. 1976 Int'l Quantum Electronics Conf., Amsterdam,
June 1976. 133

"Gain Calculations for Electron Collision Pumped X-Ray
Lasers," by L. J. Palumbo, Int'l Conf. on the Physics of
X-Ray Spectra, NBS, Gaithersburg, Aug. 1976. 137

"Beam Divergence of Vacuum Ultraviolet Lasers," by R.W. Waynant, Annual Meeting of the Optical Society of America; J. Opt. Soc. Am. (1976).	140
"K X-Ray Emission Spectra from a High Power Density Plasma," by T. N. Lee, Int'l Conf. on the Physics of X-Ray Spectra, August 1976.	141
"Time-Dependent Calculations of Harmonic Conversion from 532 nm to 266 nm in ADP," by R. C. Eckardt and J. Reintjes, Annual Meeting of the Optical Society of America; J. Opt. Soc. Am. (1976).	142
"High-Efficiency Harmonic Conversion to 266 nm in ADP and KD*P," by J. Reintjes (introduced by R. C. Eckardt) and R. C. Eckardt, Annual Meeting of the Optical Society of America; J. Opt. Soc. Am. (1976).	143
"X-Ray Spectra of Multiply Ionized High-Z Atoms From a Vacuum-Spark Plasma," by T. N. Lee and R. C. Elton, 18th Annual Plasma Physics Meeting of the American Physical Society, 15-19 Nov 1976, San Francisco, Calif.	144
"Observation of Coherent Radiation at 53.22 nm by Fifth Harmonic Conversion," by J. Reintjes, R. C. Eckardt, C. Y. She, N. E. Karangelen, and R. A. Andrews, International Conference on the Physics of X-Ray Spectra, 30 Aug - 2 Sep 1976, National Bureau of Standards, Gaithersburg, Md.	145
"Generation of Coherent Radiation at 38 nm and 53 nm Using High-Order Optical Nonlinearities," by J. Reintjes, C. Y. She, R. C. Eckardt, N. E. Karangelen, R. C. Elton and R. A. Andrews, Postdeadline paper, Annual meeting of the Optical Society of America, 18-22 October 1976, Tucson, Arizona.	146
"Requirements, Methods and Results for Absolute Radiometry from Extended Sources in the 12-25 Å and 500-3000 Å Spectral Regions," by R. C. Elton, Workshop on the Use of XUV and X-Ray Radiometry in Plasma Diagnostics 5 eV to 10 keV, National Bureau of Standards, Gaithersburg, Md., 29-30 Nov 1976.	152
"Emission Measurements in the 3 Å Region from a Point Plasma Source with Potential as a Transfer Standard," T. N. Lee, Workshop on the Use of XUV and X-Ray Radiometry in Plasma Diagnostics 5 eV to 10 keV, National Bureau of Standards, Gaithersburg, Md., 29-30 Nov 1976.	153

Publications

- "Calculations for Short-Wavelength Lasers Pumped by Thermal Electron Collisions in Carbon-Like and Helium-Like Ions," by L. J. Palumbo and R. C. Elton, J. Opt. Soc. Am. (1977). 154
- "Interferometric Study of Laser-Produced Plasmas," by J. F. Reintjes and T. N. Lee, J. Appl. Phys. (1976). 182
- "Efficient Harmonic Generation From 532 nm to 266 nm in ADP and KD*P," by J. F. Reintjes and R. C. Eckardt, submitted to Applied Physics Letters, Aug. 1976. 212
- "Short-Wavelength Laser Calculations for Electron Pumping in Carbon-Like and Helium-Like Ions," by L. J. Palumbo and R. C. Elton, Appl. Opt. (1976). 222
- "Generation of Coherent Radiation at 53.2 nm by Fifth-Harmonic Conversion," by J. Reintjes, R. C. Eckardt, C. Y. She, N. E. Karangelen, R. C. Elton and R. A. Andrews, Phys. Rev. Letters (1976). 250
- "Complete Compensation of Self-Phase Modulation in Cesium Vapor at 1.06 μ ," by R. H. Lehmberg, J. Reintjes and R. C. Eckardt, Phys. Rev. Letters (1976). 261
- "A Discharge-Pumped ArCL Superflorescent Laser at 175.0 nm," by R. W. Waynant, Appl. Phys. Letters (1976). 274

APPENDIX A

Resonant Photoexcitation Pumping in Hydrogenic Ions

R. C. Elton

I. INTRODUCTION

A. BACKGROUND

Many short-wavelength laser approaches depend on self-terminating inversion schemes, in which population inversion densities are pumped and lasing is obtained in times shorter than relaxation times. This places such severe requirements on pump sources as well as detectors, that many such schemes appear impractical for the x-ray region with present technology. CW operation is approached when rapid lower laser state depletion is possible and terminates either when the pump source is removed or when the initial electron sink is depleted and not sufficiently rapidly replenished, as for photoionization schemes -- hence "quasi-cw" operation.

CW operation for the duration of the pump pulse is the most desirable mode and is best understood for levels in a single atom or ion, i.e., excitation pumping from a "reservoir" level followed by lasing and rapid lower-level depletion to the original level. This scheme has proven very successful for visible/uv ion cw-lasing between levels with the same principle quantum number such as $3p-3s$, and indeed appears most promising for extrapolation into the vacuum-uv region.² For shorter x-ray wavelengths, transitions between levels with different principle quantum number are required, such as $3-2$ in one or two electron ions. However, simple collisional pumping from $1s$ ground state does not yield sufficient gain coefficients for non-cavity lasing, except perhaps at very high densities. Here again, radiative trapping enters and further depletes the inversion obtained.

Inversions in simple 1, 2, and 3 (bound) electron ions are particularly attractive because of the simplicity of the spectra obtained and the general lack of lossy Auger effects.³ It is clear, however, that external pumping in addition to collisional from plasma electrons is required; and since selective pumping to a particular upper laser level is desired, resonance or near-resonance line absorption is most desirable. Also, line absorption is most efficient from a pump source viewpoint compared, for

* Two schemes are included here. The second (KC ℓ) is the more promising and is an object of an experiment. The first "hybrid" scheme (C,Mg) is very sensitive to quite uncertain collisional rates, and the absolute numbers given are still in considerable doubt; hence, no experiment is proposed for scheme (1).

example, to a continuum source. Such resonance pumping based upon coincidental near-overlapping lines has been suggested,^{4,5} but the wavelength matching has not always been sufficiently close for realistic coupling of the pump and absorbing lines.⁴ Also, the schemes are usually not obviously extrapolated to shorter wavelengths, since they are often based upon coincidences.

B. PRESENT SCHEMES

Two schemes are discussed below, each based on a four-level analysis and leading to lasing on 4→3 transitions in hydrogenic ions of medium Z. The first⁽¹⁾ to be discussed involves a hybrid of collisional excitation followed by photon-assist pumping and requires the more detailed analysis. It is quite sensitive to collisional rates, but also offers a variety of laser wavelengths (e.g., see Table 1).

The first scheme is based upon the very nearly exact overlap in hydrogenic ions between 2-4 absorption (pumping) transition in an ion of atomic number Z and a 2-1 Lyman-α pump line from an ion of atomic number Z/2. This is indicated most simply by the formula

$$\Delta E_{\ell m} = Ry Z^2 \left[\frac{1}{\ell^2} - \frac{1}{m^2} \right]_{\ell-m}, \quad (1)$$

where

$$Z^2 \left[\frac{1}{4} - \frac{1}{16} \right]_{2-4} = \left(\frac{Z}{2} \right)^2 \left[1 - \frac{1}{4} \right]_{1-2}. \quad (2)$$

(More exact calculations have been published by Garcia and Mack.⁶) Referring to the energy-level diagram in Fig. 1 and assuming degenerate sublevels at high densities, electrons collisionally excited into the n=2 state of ion Z are transferred to n=4 by absorption of Lyman-α radiation from ion Z/2, creating a population inversion between 4 and 3 with a rapid 3-2 rate assuring cw operation. The n=2 population is, in the lasing ion, enhanced by radiative trapping effects of its own Lyman-α radiation; and the n=3 population is reduced by the very lack of such trapping on the (Stark) broader Lyman-β line, providing plasma densities are properly adjusted. Due to the near-exact transition matching in hydrogenic ions, this scheme can be widely extrapolated for all even-Z lasing ions. Some ion examples are listed along with the 4-3 lasing wavelengths in Table 1.

The second scheme (2) takes advantage of fortunate wavelength coincidence⁵ for photon pumping directly from n=1 to n=4 in, e.g., Cl^{16+} by Lyman-α radiation from K^{18+} , thus avoiding collisional pumping (see Fig. 2). Wavelengths are extrapolated for ions which are multiples of Z=17, 19, as indicated in []'s in Table 1 also.

Table 1. Possible Laser Lines

Lasant	Pump	Laser Wavelength [\AA]
Be IV	He II	1172
C VI	Li III	521
O VIII	Be IV	293
Ne X	B V	187
Mg XII	C VI	130
Si XIV	N VII	95
[Ca XVII]	[K XIX] ^a	[65] ^a
Fe XXVI	Al XIII	28
[Se XXXIV] ^a	[Sr XXXVIII] ^a	[16] ^a
Kr XXXVI	Ar XVIII	14

^aApplies to second scheme (2).

These are the first truly quasi-cw scheme to be proposed for the soft x-ray region which are also amenable to extrapolation to shorter wavelengths through recurring resonance pumping processes. Also, in these schemes, the lasing photon energy is insufficient to cause photoionization from the excited states involved. Furthermore, the pumping line radiation source cannot photoionize the $n=2$ level and does not appreciably photoionize the $n=3,4$ levels of the lasing ions, as will be shown in the analysis below.

Lasing on 3-2 transitions following $n=2$ pumpout (2-4 by $Z/2$ Lyman- α and 2-6 by Lyman- β) is another possibility suggested but requires significantly more pumping power. Supplemental pumpout of $n=3$ electrons into $n=6$ which could assist the 4-3 lasing would also be provided by Lyman- α radiation from $Z/3$ ions, again according to Eq. (1), in a 3-element scheme.

To summarize some attractive highlights of the present schemes:

- a. The "hybrid" approach combines the best features of electron collisional pumping with resonance photoexcitation enhancement;
- b. The pumping resonance is recurrent so that the scheme can be extrapolated to shorter wavelengths;
- c. CW operation is assured which eliminates the short pump pulse risetime requirements and/or large replenishment rates -- invites various plasma devices;

- d. No Auger losses are present in one-electron ions;
- e. No photoionization losses are present, particularly to the laser beam;
- f. The physics and spectroscopy of hydrogenic ions is relatively simple, near-exact, and reliable;
- g. The resonance line pump source is nearly monoenergetic and therefore highly efficient;
- h. Respectable gain coefficients under conditions compatible with existing technology (and often independent of Z , N_e) are expected;
- i. The devices envisioned should be compact and amenable as a tool for probing.

In the following sections the schemes are analyzed using established hydrogen-like ion physics for particular cases: (1) magnesium/carbon and (2) chlorine/potassium. These combinations were chosen from a number because of particular compatibility with current high-density plasma devices; other combinations can be modeled by computer. Energy requirements are also included, and experimental arrangements based upon established plasma principles and existing technology are described to complete the requirements for reasonable experimentation.

II. ANALYSIS

An analysis based upon a steady-state solution of the relevant rate equations follows, along with resulting estimates of the net gain coefficient that can be expected.

A. RATE EQUATION MODELING

Referring again to Figs. 1 and 2, the rate equations affecting the population densities N in the three levels (labeled by subscripts) involved in the lasing can be written in terms of the $n=1$ reservoir density, which is assumed to be constant. Denoting electron collisional rates by C , radiative rates by A , photon-induced rates by P , and total depopulation rates for a particular level by D , the rate equations are given by [(1) and (2) superscripts refer to the respective schemes.]

$$\frac{dN_2}{dt} = N_1 C_{12} + N_3 (A_{32} + C_{32}) + N_4 (A_{42} + P_{42}^{(1)} + C_{42}) - N_2 D_2 = 0, \quad (3)$$

$$\frac{dN_3}{dt} = N_1 C_{13} + N_2 C_{23} + N_4 (C_{43} + A_{43}) - N_3 D_3 = 0, \quad (4)$$

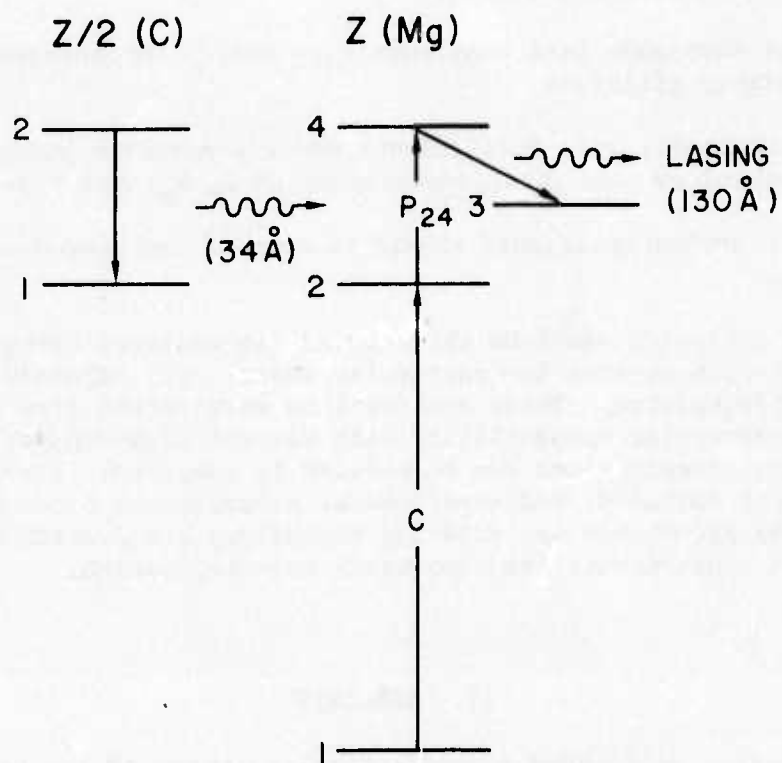


Fig. 1 — Energy-level diagram for Z and $Z/2$ hydrogenic ions showing principle processes essential to the present scheme. Characteristics for the Mg/C combination are indicated. Other processes are included in the rate-equation analysis in the text.

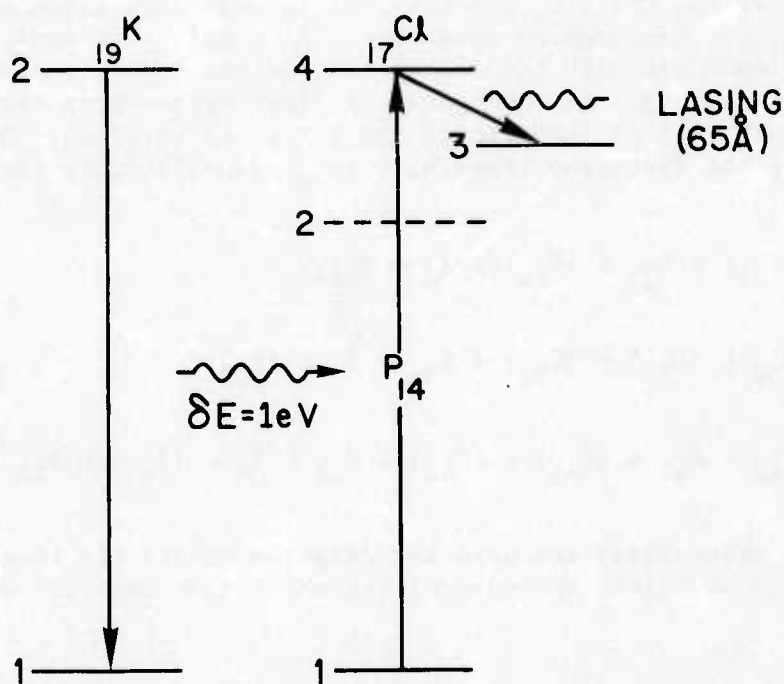


Fig. 2 — Energy-level diagram for hydrogenic ions of potassium and chlorine showing principle processes essential to the present photon pumping scheme. Note the almost exact overlap of the optically thick Lyman- α pump line and the Lyman- γ absorption line.

and

$$\frac{dN_4}{dt} = N_1 C_{14} + N_2 (C_{24} + P_{24}) + N_3 C_{34} - N_4 D_4 + N_1 P_{14}^{(2)} = 0. \quad (5)$$

Furthermore, in writing the D's, electron collisional ionization rates are denoted by I, photoionization rates by I_p ; $A' = Ag(\tau_0)$ is used, where $g(\tau_0)$ (not to be confused with the statistical weight factor g or the effective Gaunt factor $\langle g \rangle$) is the "escape factor" approaching zero with large optical depth (τ_0) at line center and unity for optically thin lines of small τ_0 [only the resonance lines have $g(\tau_0)$ significantly less than unity]. Thus

$$D_2 = A'_{21} + (C_{21}) + C_{23} + (C_{24}) + I_2 + P_{24}, \quad (6)$$

$$D_3 = A'_{31} + A_{32} + (C_{31}) + (C_{32}) + C_{34} + I_3 + (I_{p3}), \quad (7)$$

and

$$D_4 = A'_{41} + A_{42} + A_{43} + (C_{41}) + (C_{42}) + C_{43} + I_4 + (I_{p4}) + P_{42}^{(1)} + P_{41}^{(2)} \quad (8)$$

In Eqs. (6)-(8), parentheses are used to designate relatively insignificant rates for the numerical analyses of the particular cases chosen.

B. FORMULAS

The following formulas and sources were used in deriving the necessary rates for the above equations:

1. Electron Collision Induced Rates.

The collisional excitation rates for $\Delta n \neq 0$ derived from the Coulomb-Born "effective Gaunt factor" formulation

$$C_{lm} = N_e \frac{1.6 \times 10^{-5} f_{lm} \langle g \rangle \exp(-\Delta E_{lm}/kT)}{\Delta E_{lm} \sqrt{kT}} \text{ sec}^{-1}, \quad (9)$$

where f_{lm} is the absorption oscillator strength, $\langle g \rangle$ is the appropriate Gaunt factor, and the excitation energy ΔE_{lm} and kT are in eV. For 1-2 as well as 1-3 and 1-4 transitions, the C's were scaled up according to more detailed calculations.^{8,9} Corresponding deexcitation rates were found from detailed balancing according, e.g., to

$$C_{21} = C_{12} (g_1/g_2) \exp(\Delta E_{12}/kT) \quad (10)$$

with g_1, g_2 the statistical weights $2n^2 = 2, 8$, respectively.

*Also, Landshoff & Perez, Phys. Rev. A, 13, 1619 (1976) and Davis & Whitney, J. Appl. Phys. 47, 1426 (1976) for scheme (2) rates in Table 5.

Collisional ionization from excited states n were calculated from⁷

$$I_n = N \frac{9 \times 10^{-7}}{e^{\chi_n / \sqrt{kT}}} \beta \exp(-\chi_n / kT) \text{ sec}^{-1}, \text{ for } \beta = 3 \quad (11)$$

with the ionization potential $\chi_n = Z^2 Ry/n^2$ and χ_n, kT again in eV units. These ionization rates are in close agreement with cross-section calculations for carbon ions.¹⁰

2. Radiative Rates with Trapping.

It is important that there be strong radiative trapping on the Mg Lyman- α line to increase the $n=2$ source level population density. Likewise, it is important that trapping be reduced for the Lyman- β line to reduce lower laser level population density. These are achieved with Stark broadening, since the Lyman- β line is considerably more Stark broadened at increased charged-particle densities.

Radiative trapping effects may conveniently be introduced¹¹ with a modified spontaneous decay rate $A' = Ag(\tau_0)$, where $g(\tau_0)$ is the so-called "escape factor" derived from the optical depth at line center τ_0 . The latter is given for a lower level density N_ℓ by

$$\tau_0 = (2\pi^2 r_0 c) f_{\ell m} N_\ell L(\omega_0) d. \quad (12)$$

Here d is the (least) depth of the plasma in cm and $L(\omega)$ is the line shape factor at the central angular frequency ω_0 , which for Doppler broadening is

$$L(\omega_0) = \frac{\lambda_0^2}{2\pi c} \left(\frac{\ln 2}{\pi} \right) \frac{1}{w_D(\lambda)} \approx 0.47 \frac{\lambda_0^2}{2\pi c} \frac{1}{w_D(\lambda)}, \quad (13)$$

where $w_D(\lambda)$ is the half-half-width of the line.

For Stark broadening

$$L(\omega_0) = S(\alpha_0) \left(\frac{d\alpha}{d\lambda} \right) \left(\frac{d\lambda}{d\omega} \right) = \frac{\lambda_0^2}{2\pi c F_0} S(\alpha_0), \quad (14)$$

where $S(\alpha_0)$ is the reduced Stark profile parameter at line center in terms of $\alpha \equiv |\Delta\lambda|/F_0$ and $F_0 = 2.61eN^{2/3}$. This can be rewritten as

$$L(\omega_0) = \frac{\lambda_0^2}{2\pi c} \frac{(\alpha_0^{1/2})_H}{w_s(\lambda)} S_H(\alpha_0) \approx 0.26 \frac{\lambda_0^2}{2\pi c} \frac{1}{w_s(\lambda)}, \quad (15)$$

where the subscript H refers to tabulated hydrogenic values, since $S(\alpha_0)$ scales approximately as Z^5 and $\alpha_{1/2}$ as Z^{-5} . (Actually He^+ values were used.) Therefore, from Eq. (12)

$$\frac{\tau_o}{d} \approx \frac{\pi r_o f N_\ell \lambda_o^2 (0.25)}{w_s(\lambda) + 0.5 w_D(\lambda)} \text{ cm}^{-1} . \quad (16)$$

From this may be found τ and then $g(\tau)$ from the graph in Fig. 3. The depth remains a variable^o here and can be adjusted to give the desired ratio of escape factors for the Lyman- α and - β lines, within reasonable experimental limits.

3. Line Widths.

The line widths are not only important for ascertaining the optical depths of the resonant lines as above, but also for the laser line in the gain equation and for overlapping and matching the absorption line with the pump line.

The Doppler half-half-width in Å units is given by⁷

$$w_D(\lambda) = 3.8 \times 10^{-5} \lambda (\#T/\mu)^{1/2} , \quad (17)$$

where in this case the wavelength λ is in Å units, $\#T$ is in eV, and μ is the atomic mass number.

For Stark widths associated with perturbers p , it is at present necessary to scale from calculated values for hydrogen and ionized helium as follows:

$$w_s \propto \lambda^2 \frac{Z_p}{Z_i} \left(\frac{N_e}{Z_p} \right)^{2/3} \propto \frac{Z_p^{1/3}}{Z_i^5} N_e^{2/3} \propto \alpha F_o . \quad (18)$$

But $\alpha \propto N_e^{1/3}$ from the tabulated values, probably due to additional electron broadening at high densities. Therefore, it is assumed that

$$w_s \propto N_e / Z^5 . \quad (19)$$

High-density calculations for He^+ (and H) then yield the values listed in Tables 2 and 3 by extrapolation.

4. Photoexcitation Pumping and Photo-Deexcitation Rates.

The very important resonance absorption pumping process occurs at a rate $P_{\ell 4}$ given by (ℓ being the lower level)

$$P_{\ell 4} = N_o \int c \sigma_{\ell 4}(\nu) d\nu , \quad (20)$$

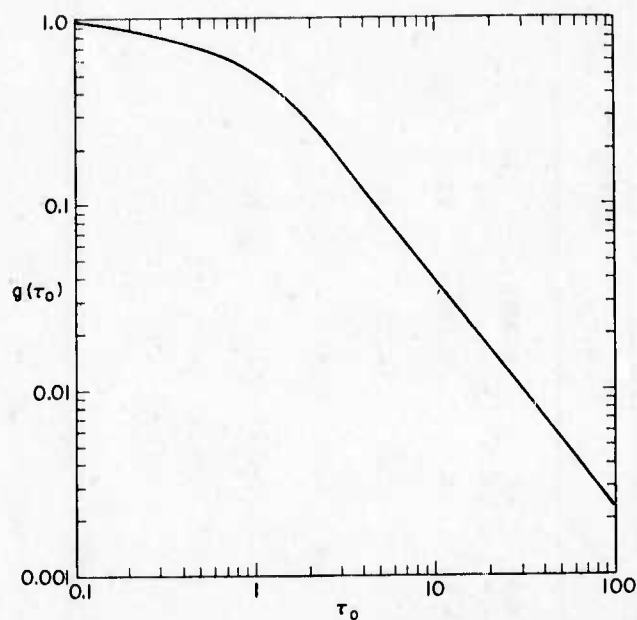


Fig. 3 — The “escape factor” $g(\tau_0)$ as a function of the optical depth τ_0 . This factor relates the transition probability A_{lm} to A'_{lm} and is important for high-opacity conditions.

SOME UNCERTAINTIES EXIST IN DRAFT NUMBERS

Table 2. Radiative Parameters for Scheme (1): e,C → Mg

Transition	$(10^{20} Z^5 / N_e) w_s$	$10^4 w_s^a$	$10^4 w_D^a$	τ_o / d	τ_o	$g(\tau_o)$	$10^{-10} A^b$	$10^{-10} P^b$
2-1	7.8	0.94 (1000) ^c	25 (64) ^c	1400 (90) ^c	42 (1.7) ^c	0.0067	3.2	
3-1	170	21	21	71	2.8	0.19	23	
4-1	450	54	23	12	0.48	0.70	19	
3-2	1600	190	130	3.6	0.16	1	91	
4-2	6700	810	100	0.15 ^d	0.0045	1	17	3.5
4-3	32000	3800	386	0.18 ^d	0.0054	1	19	
2-4								14

^a Widths in Å units. $Z = 12$, $N_e = 3 \times 10^{20} \text{ cm}^{-3}$, $T = 1460 \text{ eV}$, $d = 400 \mu\text{m}$

^b Rates in sec^{-1} units

^c Values for $Z = 6$, $N_e = 10^{22}$, $T = 300 \text{ eV}$, $d = 200 \mu\text{m}$

^d Anticipating lower state densities from results

Table 3. Radiative Parameters for Scheme (2): K-Cℓ

Transition	$(10^{20} Z^5 / N_e) w_s$	$10^4 w_s^a$	$10^4 w_D^a$	τ_o / d	τ_o	$g(\tau_o)$	$10^{-10} A^b$	$10^{-10} P^b$
2-1	7.8	0.055 (0.31) ^c	24 (18) ^c	26 (20) ^c	2.6 (2) ^c	0.2	109	
3-1	170	1.2	22	4.6	0.46	0.7	210	
4-1	450	3.2	20	1.3	0.13	0.9	100	5.7
3-2	1600	11	133	1.3	0.13	0.9	340	
4-2	6700	47	98	1.4 ^d	0.14	0.9	64	
4-3	32000	225	380	1.1 ^d	0.11	1	75	
1-4								91

^a Widths in Å units. $Z = 17$, $N_e = 10^{20} \text{ cm}^{-3}$, $T = 2000 \text{ eV}$, $d = 1 \text{ mm}$.

^b Rates in sec^{-1} units.

^c Values for $Z = 19$.

^d Anticipating lower-state densities from results.

where $\sigma(\nu)$ is the absorption cross section for the ℓ -4 transition and N_e is the pumping photon density assumed constant over the absorption line profile and also assumed to originate from a blackbody source of uniform intensity over the absorption line and at a temperature T_B . The absorption integral may be written as:

$$\int \sigma_{\ell 4}(\nu) d\nu = \frac{g_4}{g_\ell} \frac{A_{4\ell} c^2}{8\pi\nu^2} \quad (21)$$

The photon density N_p may be obtained from the blackbody flux Φ [ergs/Hz-ster-sec-cm²] formula as

$$N_p = \frac{1}{h\nu} \cdot \frac{2\pi}{c} \cdot \Phi = \frac{2\pi}{hc\nu} \cdot \frac{2h\nu^3}{c^2} [\exp(h\nu/kT_B) - 1]^{-1}, \quad (22)$$

where a 2π collection solid angle is assumed. Thus from Eq. (20)

$$P_{\ell 4} = \frac{1}{2} \frac{g_4}{g_\ell} A_{4\ell} [\exp(h\nu/kT_B) - 1]^{-1}, \quad (\text{see Tables 3 and 4}), \quad (23)$$

where $g_4/g_\ell = 4$ or 16 for schemes (1) and (2), respectively,

Photo-deexcitation $P_{4\ell}$ from 4 to ℓ , or induced emission, is also possible, for the which the cross section is related by

$$\sigma_{4\ell} = \sigma_{\ell 4} (f_{4\ell}/f_{\ell 4}) = \sigma_{\ell 4} (g_\ell/g_4) \quad (24)$$

Thus from Eqs. (21) and (23),

$$P_{4\ell} = \frac{A_{4\ell}}{2} \exp[(h\nu/kT_B) - 1]^{-1}, \quad \text{also in Tables 2 and 3.} \quad (25)$$

It is important in using these rates that pump and absorption line overlap be maintained, and the plasma parameters were carefully chosen with this in mind as discussed in Section II.C.

5. Photoionization Loss Rates.

Photoionization from the upper lasing state or from the source state, labeled 4 and 2 respectively here, are potential losses that must be considered in any short wavelength laser scheme. Both the pump source and the lasing emission are potential sources for consideration. The laser photon energy

$$h\nu_{43} = Z^2 \text{Ry} \left[\frac{1}{9} - \frac{1}{16} \right] = 0.049 Z^2 \text{Ry} \quad (26)$$

is clearly less* than the ionization energy $Z^2 \text{Ry}/n^2$ for either $n=2$ or $n=4$ so that photoionization by the laser beam is impossible. The pump source photon energy is given by

*Even considering ionization energy lowering.

$$h\nu_p = \zeta^2 \text{ Ry} \left[1 - \frac{1}{4} \right], \text{ where } \zeta = Z/2^{(1)} \text{ or } 19Z/17^{(2)}, \quad (27)$$

and could cause photoionization from $n=4$ as well as $n=3$ with ionization energies $0.06 Z^2 \text{ Ry}$ and $0.11 Z^2 \text{ Ry}$, respectively. The latter will be more probable [see Eq. (28)] and in fact could assist in lowering the density N_3 (if the rate were of sufficient magnitude). Thus, the rates I_{p4} and I_{p3} are included in Eqs. (7) and (8) and need evaluation here.

For hydrogenic ions, the Kramer's formula suffices so that

$$\sigma_{n\infty} = \frac{64\pi^4 e^{10} m Z^4}{3\sqrt{3} c h^6 v g_n^3} \quad (28)$$

and equals $2 \times 10^{-17} n^{-5}$ for $Z = 17$, or 6×10^{-20} and 2×10^{-20} for $n=3$ and $n=4$, respectively -- small values. Following Eqs. (20)-(23), the photoionization rate due to the pump source radiation becomes

$$I_{pn} = \frac{256 \pi^5 e^{10} m Z^4}{3\sqrt{3} c^2 h^6 v g_n^3} [\exp(h\nu/kT_B) - 1]^{-1}, \quad (29)$$

or

$$I_{pn} = \frac{660 Z^4}{n^5} \exp[(h\nu/kT_B) - 1]^{-1} \quad (30)$$

which is negligible.

C. ENVIRONMENTAL PARAMETERS

1. Scheme (1): e, c^{5+} pumping Mg^{11+}

In order to evaluate the above rate formulas for the specific $Z=12$, $Z/2=6$ combination, the electron density N_e , the (equal) electron and ion temperatures T , and the diameter d must be specified. The length L also becomes a consideration when the gain and pump power are estimated.

For the Mg plasma lasant,

$$h\nu = 1460 \text{ eV} = h\nu_{12}$$

$$N_e = 3 \times 10^{20} \text{ cm}^{-3}$$

$$d = 400 \text{ } \mu\text{m}$$

$$L = 5 \text{ mm}$$

were chosen. The temperature was so designated for maximum collisional excitation rates and consistent with optimum concentration of Mg^{11+} ions. The electron density was chosen at a value below critical density at which interferometric measurements should be possible; high values are desirable for increasing the $n=2$ source level population density. Another reason for limiting N_e to $3 \times 10^{20} \text{ cm}^{-3}$ is to prevent excessive Stark broadening of the $2-4^e$ transition which must be pumped by a normally rather narrow C VI Lyman- α line. The separation of these lines is 0.04 \AA so that some Stark broadening of the Mg line is necessary, and the density chosen was thus a compromise for these particular ions. (Table 2 shows actual widths.) The diameter was chosen as $400 \text{ }\mu\text{m}$ to make the Mg Lyman- α line optically thick to maximize radiative trapping and thereby reduce the effective $n=2$ decay rate through a lowered $g(\tau_0)$. Effective cylindrical geometry then dictated a length of about 5 mm .

For the C VI pump plasma,

$$kT_B = 300 \text{ eV}$$

$$N_e = 10^{22} \text{ cm}^{-3}$$

$$d = 200 \text{ }\mu\text{m}$$

were chosen for maximum blackbody emission and sufficient optical depth. Further increases in T_B depletes the fraction of C^{5+} ions compared to stripped ions which is estimated by the Saha relation at these densities by

$$\frac{N(C^{5+})}{N(C^{6+})} = N_e \left(\frac{2\pi h^2}{m kT} \right)^{3/2} \exp(\chi_n / kT) = 3.2 \times 10^{-3}. \quad (31)$$

Sufficient optical depth is necessary to again achieve both a blackbody level and overlap between the Mg $2-4$ absorbing transition, which has a half-half-width of 0.09 \AA according to Table 2, and the 0.1 \AA Stark broadened C VI line shifted by 0.04 \AA . For a Lorentzian wing profile, the width of the optically thick C VI Lyman- α line scales approximately as $\tau_c^{1/2}$ so that the requirement is

$$0.1\sqrt{\tau_c} \geq 0.09 + 0.04. \quad (32)$$

For $\tau/d = 90$, from Eq. (16) and including Eq. (31), this sets the diameter of the carbon plasma, as $\sim 200 \text{ }\mu\text{m}$. If larger dimensions prove feasible, T_B could be raised for greater gain.

It is with these parameters that the collisional rates listed in Table 4 and the radiative rates listed in Table 2 are calculated for scheme (1).

SOME UNCERTAINTIES EXIST IN DRAFT NUMBERS

Table 4. Electron Collisional Rate Coefficients and Rates^a For Mg^b [Scheme (1)]

Transition	$10^{10} (C/N_e)^c$	$10^{-10} C^d$	$10^{10} (I/N_e)^c$	$10^{-10} I^d$
1-2	0.23	0.73		
2-1	0.16	0.49		
1-3	0.032	0.097		
3-1	0.010	0.030		
1-4	0.012	0.095		
4-1	0.0032	0.0097		
2-3	1.9	5.6		
3-2	0.98	2.9		
2-4	0.21	0.63		
4-2	0.065	0.2		
3-4	7.5	22		
4-3	4.5	13		
2-∞			1.0	3.0
3-∞			2.8	8.4
4-∞			5.3	16

^a For $N_e = 3 \times 10^{20} \text{ cm}^{-3}$

^b $\lambda_T = 1460 \text{ eV}$

^c Units: $\text{cm}^3 \text{ sec}^{-1}$

^d Units: sec^{-1}

2. Scheme (2): K^{18+} Pumping Cl^{16+}

A particular attraction of this scheme is the closeness of the Z-values and the possibility of using a single plasma mixture, as well as the close wavelength match. The parameters chosen for analysis are

$$kT = 2000 \text{ eV}$$

$$N_e = 10^{20} \text{ cm}^{-3}$$

$$d = 1 \text{ mm}$$

$$L = 1 \text{ cm}$$

The wavelength difference between the K XIX Lyman- α pump line and the C XVII Lyman- γ absorption line is very small, namely $23 \times 10^{-4} \text{ \AA}$, and sufficient overlap ($\sim \frac{1}{3}$) is achieved by Doppler broadening as indicated in Table 3; this factor was included in calculating P_{14} and P_{41} from Eqs. (23) and (25). Also, at a density of 10^{20} cm^{-3} the collision limit⁷ is above $n=7$ and coronal ionization equilibrium conditions apply.¹³ Under such conditions, a temperature of $kT=2000 \text{ eV}$ results in about 40% abundance^{7,13} of the desired ionic species for each of the two elements involved, the remainder being in helium-like chlorine and stripped potassium ions. A diameter of 1 mm was chosen to assure that the pump line becomes optically thick ($\tau=2$, Table 3) for the blackbody model chosen; the factor $[1-\exp(-\tau)] = 0.86$ was also included in P_{14} and P_{41} . Again, a reasonable aspect ratio requires a length of about 1 cm.

With these parameters, the collisional rates listed in Table 5 as well as certain radiative rates given in Table 3 were calculated for scheme (2).

Table 5

Electron Collisional Rate Coefficients and Rates ^a for Cl ^b [Scheme (2)]						
Transition	$10^{10}(C/N_e)^c$	<u>a</u>	$10^{-10}C^d$	$10^{10}(I/N_e)^c$	<u>a</u>	$10^{-10}I^d$
1-2		0.070				
2-1		0.078				
1-3		0.011				
3-1		0.0065				
1-4		0.0050				
4-1		0.0019				
2-3		1.44				
3-2		0.84				
2-4		0.26				
4-2		0.097				
3-4		6.8				
4-3		4.1				
2- ∞					0.37	
3- ∞					1.1	
4- ∞					2.2	

^a For $N_e = 10^{20} \text{ cm}^{-3}$

^b $kT = 2000 \text{ eV}$

^c Units: $\text{cm}^3 \text{ sec}^{-1}$

^d Units: sec^{-1}

[See footnote p. 7 also.]

D. EVALUATIONS

1. Scheme (1): e, C^{5+} Pumping Mg^{11+}

The steady state solution of the three rate equations (3), (4), and (5) for the three unknowns N_4/N_1 , N_3/N_1 , and N_2/N_1 is straightforward and will not be written out here. The numerical results for scheme (1) are†

$$\frac{N_4}{N_1} = 1.0 \times 10^{-2} \quad (33)$$

$$\frac{N_3}{N_1} = 8.1 \times 10^{-4} \quad (34)$$

$$\frac{N_2}{N_1} = 3.8 \times 10^{-2} \quad (35)$$

The first two are the critical density ratios for inversion and enter the gain coefficient (α) equation as

$$\begin{aligned} \alpha_{43} &= \frac{1}{8\pi} \frac{\lambda_{43}^2}{\Delta\nu} A_{43} N_1 \left[\frac{N_4}{N_1} - \frac{g_4}{g_3} \frac{N_3}{N_1} \right]^* \\ &= \frac{\lambda_{43}^4}{8\pi c} \frac{A_{43}}{2w_{43}} N_1 \left[\frac{N_4}{N_1} - \frac{16}{9} \frac{N_3}{N_1} \right]^*, \end{aligned} \quad (36)$$

where N_1 is the ground state density of Mg^{11+} ions, related to N_e and the stripped-ion density N_s by

$$N_e \approx (Z - 1) N_1 + Z N_1 (N_s/N_1). \quad (37)$$

If coronal equilibrium relations are applied, $N_s/N_1 \approx 3$ is found, so that

$$N_1 = N_e/47 = 6.4 \times 10^{18}. \quad (38)$$

Equation (36) gives†

$$\alpha_{43} \approx 5 \text{ cm}^{-1} \quad \text{at} \quad \lambda_{43} = 130 \text{ \AA} \quad (39)$$

and

$$I/I_0 = \exp(\alpha L) = 12 \quad (40)$$

for $L = 0.5 \text{ cm}$.

* For Stark broadening, α_{43} can be shown to be approximately constant and independent of density and Z .

† The absolute numbers given in Eqs. (33)-(35) and (39)-(40) are still uncertain at this writing — see top of next page.

This gain coefficient could change with more careful optimization of temperature, density, and the blackbody-pump temperature; which is a job for a computer model, particularly since so many rates enter.

2. Scheme (2): K^{18+} Pumping Cl^{16+}

The numerical results from solution of the rate equations [and corresponding Eqs. (33), (34), and (35) for scheme (1)] are

$$\frac{N_4}{N_1} = 3.4 \times 10^{-1} \quad (41)$$

$$\frac{N_3}{N_1} = 4.7 \times 10^{-2} \quad (42)$$

$$\frac{N_2}{N_1} = 3.8 \times 10^{-1} \quad (43)$$

which are considerably larger than for the hybrid scheme and much less dependent on collisional rates; hence, more reliable.

The gain coefficient for Cl XIX is calculated from Eq. (36) where $N_1 = 0.4 N_T$ and N_T is defined as the density for either chlorine or potassium in equal proportions. Thus

$$N_e/N_T \approx \underbrace{0.4(16) + 0.6(17)}_{Cl} + \underbrace{0.4(18) + 0.6(19)}_{K} \quad (44)$$

or

$$N_1 = 0.4 N_e/35 = 1.1 \times 10^{18} \text{ cm}^{-3} \quad (45)$$

[corresponding to Eq. (38) for scheme (1)]. For the narrower Doppler-broadened line here, the gain coefficient becomes

$$\underline{\alpha \approx 44 \text{ cm}^{-1}} \text{ at } \underline{\lambda_{43} = 65 \text{ \AA}} \quad (46)$$

and

$$\underline{I/I_0 = \exp(\alpha L) = e^{44} \text{ (saturated)}}$$

for $L = 1\text{cm}$. This large gain coefficient indicates a considerable degree of flexibility in design.

III. DEVICE REQUIREMENTS

The device parameters listed in Section II. C. center around a laser and a pump source, with the former "seeing" at least 2π solid angle of the latter. Several approaches for generating appropriate high-density small plasmas suggest themselves, particularly since cw operation removes the short risetime requirements.

The energy densities stored in the plasmas are given in ergs/cm³ for scheme (1) by

$$\text{Mg: } (N_e + N_i) kT + N_i \chi = 8.4 \times 10^{11} \quad (47)$$

$$\text{C: } (N_e + N_i) kT_B + N_i \chi = 7.2 \times 10^{12} \quad (48)$$

and for scheme (2) by

$$\text{KCl: } (N_e + N_i) kT + N_i \chi \approx 3.7 \times 10^{11} \quad (49)$$

which are equivalent to the plasma pressures. These may be compared to the pressure exerted by a 10 MG magnetic confinement field (same units)

$$\frac{B^2}{8\pi} = 4 \times 10^{11}. \quad (50)$$

In spite of the difference in pressures for the carbon and magnesium plasmas in scheme (1), the expansion velocities v and the radial expansion times t_r (to desired radii) at peak temperatures

$$\text{Mg: } v \approx 10^7 \text{ cm/sec, } t_r \approx 2 \text{ ns} \quad (51)$$

and

$$\text{C: } v \approx 6 \times 10^6 \text{ cm/sec, } t_r \approx 1.7 \text{ ns} \quad (52)$$

are comparable. This is important for expanding-plasma inertial confinement devices.

Multiplying by the volumes given in Section II. C., the plasma energy requirements become from Eqs. (47) through (49)

$$\text{Mg: } E = 53 \text{ J} \quad (53)$$

$$\text{C: } E_{\min} = 110 \text{ J}$$

$$\text{KCl: } E = 1200 \text{ J (radius} = 1 \text{ mm)}$$

For electromagnetically driven pinch devices such as proposed here, these are very reasonable energies and pressures; since a conversion efficiency from capacitor to plasma of 4 percent can be expected with state-of-the-art technology,¹⁴ and multi-megagauss fields are not uncommon. For laser-produced solid-target plasmas, the conversion efficiency drops sharply with laser power after plasma temperatures in the 300 eV range are reached, so that kJ lasers can be expected to be required.

IV. SUMMARY

In brief, these analyses indicate that photon assist of electron-collisional pumping is marginally promising at best, since collisional effects tend to dominate at the high densities required both to capitalize on Stark broadening and to achieve wavelength overlap of the transitions involved. Also, the lower blackbody temperature associated with the Z/2 pump source limits the amount of photon pumping available.

On the other hand, purely photon pumping is most promising in a situation such as found for K+Cl, where an almost exact wavelength match occurs. The density can be lowered, with Doppler broadening providing overlap, and collisions become of minor importance. The analysis is more accurate and reliable then. Also, the higher-Z potassium pump source produces a higher blackbody line and more inversion along with higher gains. This scheme therefore looks very promising. Other such coincidental overlaps have recently been found to occur and will be of future investigations.

V. REFERENCES FOR APPENDIX A

1. For a "Review of Short Wavelength Laser Research" as of October 1975, see: R. W. Waynant and R. C. Elton, Proc. IEEE (in press).
2. R. C. Elton, Appl. Optics 14, 97 (1975). See also NRL Memorandum Reports 2910, 3057, 3130, and 3241 for progress summaries.
3. R. C. Elton, Appl. Optics 14, 2243 (1975).
4. B. A. Norton and N. J. Peacock, J. Phys. B: Atom. Molec. Phys. 8, 989 (1975).
5. A. V. Vinogradov, I. Yu. Skobelev, I. I. Sobel'man, and E. A. Yukov, Sov. J. Quant. Electron. 5, 1192 (1976).
6. J. D. Garcia and J. E. Mack, J. Opt. Soc. Am. 55, 654 (1964).
7. R. C. Elton, in Methods of Experimental Physics, Plasma Physics, vol. 9A, edited by H. R. Griem and R. H. Lovberg, Chapter 4, (Academic Press, N. Y., 1970).
8. A. Burgess, D. G. Hummer, and J. A. Tully, Phil. Trans. Roy. Soc. London 266, 225 (1970).
9. A. H. Gabriel and C. Jordan, in Case Studies in Atomic Collision Physics, vol. 2, Chapter 4, edited by McDaniel and McDowell, (North Holland Publ. Co., 1972).
10. I. L. Beigman and L. A. Vainshtein, Sov. Astron. 11, 712 (1968).
11. R. W. P. McWhirter, in Plasma Diagnostic Techniques, Chapter 5, edited by R. H. Huddlestone and S. L. Leonard, (Academic Press, N.Y., 1965).
12. H. R. Griem, Spectral Line Broadening by Plasmas, (Academic Press, N.Y., 1974).
13. T. F. Stratton, in Plasma Diagnostic Techniques, Chapter 8, edited by R. H. Huddlestone and S. L. Leonard, (Academic Press, N.Y., 1965).
14. J. H. Lee, D. R. McFarland, and F. Hohl, "Dense Plasma Focus Production in a Hypocycloidal Pinch," NASA Technical Note, NASA TN D-8116, December 1975.

K X-RAY EMISSION SPECTRA FROM A HIGH POWER DENSITY PLASMA

T. N. Lee

U.S. Naval Research Laboratory
Washington, D.C. 20375

Vacuum spark discharges have been used as a source of EUV and x-radiation since at least the 1890's [1]; however, in spite of its long history, this extremely simple device still finds a place in the modern laboratory. In general, when such a device is operated with an increased energy input, it is known [2], [3], [4] to emit the K x-ray radiation of highly stripped, high-Z atoms. This line radiation originates from one or more small ($\sim 10^{-9}$ - 10^{-7} cm³), high-temperature ($\sim 10^7$ - 10^8 °K) plasmas. The x-ray energy density (in both line and bremsstrahlung radiation) in such a plasma volume reaches a value of 10^6 - 10^8 J/cm³ in a time interval of about 5×10^{-9} sec, giving a power density of 10^{14} - 10^{16} watts/cm³ [5]. In addition to the highly concentrated hot plasmas, the discharge also produces somewhat cooler, low-energy-density plasmas. Accordingly, the integrated spectral contributions from all the components of different plasma temperatures and states makes it difficult to unambiguously interpret the spectra obtained, unless one can also produce spatially resolved spectra with a resolution of a few tens of micrometers. Another difficulty in understanding the x-ray spectrum obtained with multiple discharge exposures is a consequence of the shot-to-shot nonreproducibility of the discharge, i.e., such spectrum is an integration of a large variety of spectral features emitted by individual discharges.

In this study, space-and-time-resolved K x-ray line spectra emitted by a vacuum spark plasma are analyzed in order to better understand the physics of the x-ray spectrum. These spectra are obtained with a single discharge exposure. The vacuum spark source used here is a laser-pulse-triggered discharge and is essentially the same device used in the previous investigation [6]. The capacitive discharge takes place between a bullet-shaped anode tip and a relatively flat cathode which is separated from the anode by a gap of approximately 5 mm. The anode material used here is iron. After triggering, the discharge current reaches its maximum value of 250 kA in about 2 μ sec. A flat LiF analyzing crystal is used, and the spectrum is recorded on Polaroid film in an XR-7 film back. Spatially resolved (in an axial direction) spectra of the discharge x-ray emission is obtained by simply mounting a 150 to 250 μ m-wide slit (oriented perpendicular to the discharge axis) onto the x-ray window (125 μ m-thick Be-foil). Pinhole (50 μ m in size) x-ray photographs are also taken simultaneously with each spectral exposure to aid in the interpretation of the spectral data. Fig. 1 shows three microdensitometer tracings taken by scanning across three different axial locations of the discharge gap in a space-resolved spectrum. The three locations correspond respectively to a plasma cloud near the anode tip (1st trace) and two axially well-separated (600 μ m in distance) point plasmas which constitute the main x-ray emitting plasmas in this particular run. The 1st tracing suggests that the plasma cloud emits

predominantly K α -type transition lines mainly from Fe II through about Fe X, according to the normal line intensity ratio between a K α and K β line. One of the point plasmas (2nd trace) is hot enough to produce the 2p \rightarrow 1s transition lines of Fe XXIV, Fe XXV, and H-like Fe XXVI ions; whereas the other point plasma (3rd trace, the farthest from the anode tip) does not emit these lines. Negligibly weak K β -type (3p \rightarrow 1s) lines in the 3rd trace, however, indicates that this relatively cool point plasma emits predominantly K α -type lines arising from Fe XI through Fe XVIII ions. It is likely that the main contribution to this feature may be Fe XVIII ions which are produced by innershell ionizations of Ne-like closed-shell Fe XVII ions. Examination of a number of pinhole x-ray photographs and spectra obtained indicate that a single, isolated hot point plasma is rarely produced but generally accompanies a cooler point plasma (or a small cloud) occurring in the immediate vicinity ($\leq 25 - \sim 100 \mu\text{m}$). For instance, the point plasma which produced the spectrum indicated in the 2nd tracing of Fig. 1 is surrounded by a small plasma cloud, according to the monitoring x-ray pinhole photograph. However, on several occasions, we were able to obtain spectra emitted by

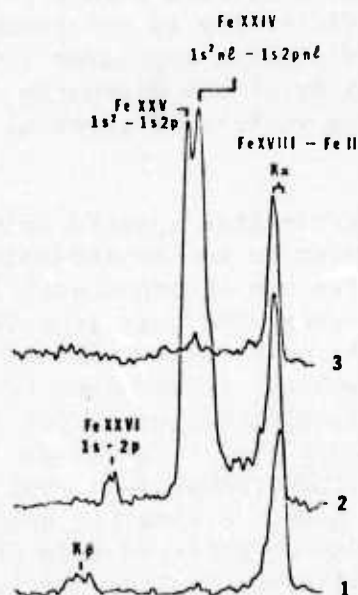


Fig. 1 - Microdensitometer scans of a space-resolved K x-ray spectrum of iron. Scan 1 is taken at the plasma cloud near the anode, and scans 2 and 3 are at two separated ($600 \mu\text{m}$) point plasmas, respectively.

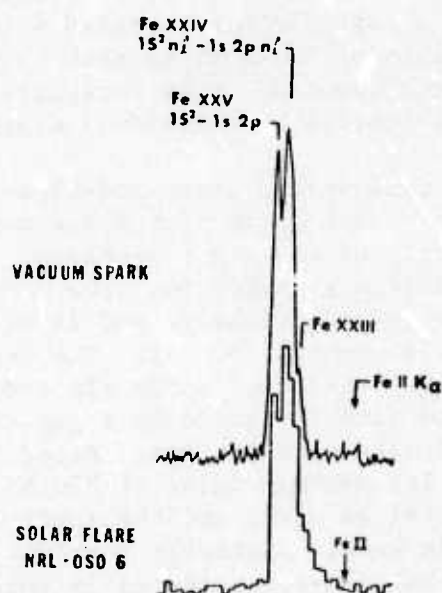


Fig. 2 - Microdensitometer scan of a space-resolved K x-ray spectrum emitted by a well-isolated point plasma. Also shown is a corresponding Fe x-ray spectrum [7] of the solar flare for comparison. Note the negligibly weak Fe II K α line in both cases.

what is believed to be an isolated point plasma. Such a spectrum is shown in Fig. 2, where a microdensitometer scan of the point plasma is shown along with a corresponding Fe spectrum [7] of the solar flare (NRL-OSO 6) for comparison. Note the strong Fe XXV $1s2p \rightarrow 1s^2$ and Fe XXIV $1s2p \text{ nl} \rightarrow 1s^2 \text{ nl}$ lines with negligibly weak emission of the Fe II - Fe XVIII $K\alpha$ and $K\beta$ lines. This result contradicts the previous assumption [8] that a laboratory transient plasma inevitably produces K transition lines of lower stages of ionization due to the extremely transient ionizing condition (in this experiment, $\sim 10^{-9}$ sec). On the other hand, the result is in good agreement with a recent study by Feldman, et al. [9], who deduced the spectral contributions from a two-temperature plasma based on space-resolved x-ray absorption measurements. Time-resolved x-ray line radiation of Fe XXV $1s2p \rightarrow 1s^2$ and its satellite lines are obtained by properly positioning an x-ray detector and a slit at the film plane of the crystal spectrometer. The data is analyzed by comparing the signals with the simultaneously obtained pin-hole x-ray photographs or the space-resolved spectra (time integrated) obtained with the second LiF analyzing crystal. The result will be described.

I would like to thank Mr. R. H. Dixon for reading the paper and Dr. R. C. Elton for helpful discussions.

- [1] R. W. Wood, Phys. Rev. V, no. 1, p. 1 (1897).
- [2] L. Cohen, U. Feldman, M. Swartz, and J. H. Underwood, J. Opt. Soc. Am. 58, 843 (1968).
- [3] T. N. Lee and R. C. Elton, Phys. Rev. A 3, 865 (1971).
- [4] J. L. Schwob and B. S. Fraenkel, Space Sci. Rev. 13, 589 (1972).
- [5] T. N. Lee, Ann. New York Acad. Sci. 251, 112 (1975).
- [6] T. N. Lee, Astrophys. J. 190, 467 (1974).
- [7] G. A. Doschek, J. F. Meekins, R. W. Kreplin, T. A. Chubb, and H. Friedman, Astrophys. J. 170, 573 (1971).
- [8] A. H. Gabriel, M.N.R.A.S. 160, 99 (1972).
- [9] U. Feldman, S. Goldsmith, J. L. Schwob, and G. A. Doschek, Astrophys. J. 201, 225 (1975).

Accepted for 1976 International Quantum Electronics Conference, Amsterdam.

COMPENSATION OF SELF PHASE MODULATION BY CESIUM VAPOR*

R. H. Lehmberg, J. Reintjes and R. C. Eckardt
Naval Research Laboratory, Washington, D.C. 20375
(202) 767-2730

ABSTRACT

We have observed a significant reduction of Nd:YAG laser-generated self phase modulation by propagating the output pulses through a cesium vapor cell. The limitations of this technique are discussed, and a related pulse shaping experiment will be described.

*Work supported by U.S. ERDA and ARPA.

Recently, we reported the observation of self defocusing of mode locked 1.06 μ pulses in cesium vapor, and attributed it primarily to the nearby two photon resonance with the 6s-7s levels.¹ The corresponding negative value of n_2 was measured at -1.4×10^{-30} N, in reasonable agreement with the calculated value of -2.62×10^{-30} N. Since the useful output power of large Nd laser systems is ordinarily limited by self focusing and self phase modulation (SPM), the existence of this negative n_2 raises the possibility of increasing the power by using Cs vapor for compensation. Here, we report the first observation of partial compensation of the SPM generated in a Nd:YAG laser system.

The laser radiation consisted of single pulses of FWHM duration $t_p = 50$ psec, as measured by a 5 psec resolution streak camera. The bandwidths were broadened to $2-5$ cm^{-1} by SPM in the YAG amplifiers, and the integrated spectra had the double-humped appearance (Fig. 1a, c) expected for a chirp of this magnitude.² The collimated beam, with a peak on-axis intensity $I \approx 1.9$ GW/cm², propagated through a total path length $L = 200$ cm in Cs vapor. Its diameter was relatively large (1 cm) in order to avoid whole-beam self defocusing effects.¹ The integrated spectra of the input and output pulses were recorded by directing a portion of the center of each beam through a 1-m grating spectrograph onto an image converter camera operating in the streak mode adjusted for a 1 nsec resolution and 10 nsac/cm sweep rate. A 12.5 nsec pulse separation allowed the input and output spectra to be compared on the same film (e.g. Fig. 1). The spectral resolution is $.2$ cm^{-1} .

In Fig. 1c, the phase modulated spectrum of the incident pulse gives a maximum chirp width of $\Delta\nu_c = 4.5$ cm^{-1} , which corresponds to a peak on-axis phase shift $\Phi = 2\pi \Delta\nu_c t_p / 2.66 \approx 8.5$. In the output pulse, the double-hump

has disappeared, and $\Delta\omega_c$ has been reduced to 2.7 cm^{-1} ; hence, $B_{\text{out}} \approx 5.3$. The phase reduction $B_{\text{out}} - B \approx -3.2$ is in reasonable agreement with the value $\Delta B = 8\pi^2 n_2 I L / \lambda c \approx -4.9$ calculated from $n_2 = -1.4 \times 10^{-30} \text{ N}$ measured previously.¹

The asymmetry in these spectra arises from asymmetry in the laser pulse shape. Since the pulse changes shape within the laser, the output intensity variation - dI/dt does not correspond exactly to the instantaneous chirp frequency. Moreover, some beam degradation due to small scale self focusing was evident in the more intense pulses. It is therefore unlikely that the SPM can be completely cancelled by a single Cs cell at the output, i.e., one should compensate after each amplifier stage before self focusing and pulseshape changes become appreciable.⁵

Additional experiments are in preparation to do the initial pulse chirping with CS_2 rather than in the amplifiers. This will allow better control of small scale self focusing and will ensure that the pulseshape remains the same in the chirping and compensating elements; hence, a nearly complete phase compensation should be attainable. In a second experiment, the negative SPM due to the cesium cell alone will be used to study pulse squaring effects in a grating pair.

REFERENCES

1. R. H. Lehmberg, J. Reintjes, and R. C. Eckardt, Appl. Phys. Lett. 25, 374 (1974); Phys. Rev. A (March 1976).
2. R. C. Eckardt, C. H. Lee, and J. N. Bradford, Opto-electronics 6, 67 (1974).
3. R. H. Lehmberg, J. Reintjes, and R. C. Eckardt, NRL Memo Rpt. 5150 (Sept 1975) p. 25-30.

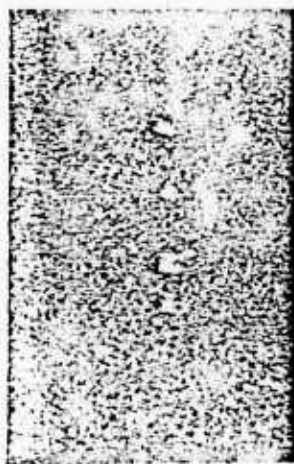
FIGURE CAPTIONS

FIGURE 1 Integrated spectra of pulses at the Cs cell input (lower traces) and output (upper traces): (a) empty cell; (b) $N = 3.7 \times 10^{16} \text{ cm}^{-3}$ with a small double pulse ($I < .15 \text{ GW/cm}^2$) which remains essentially time-bandwidth limited; (c) $N = 3.7 \times 10^{16} \text{ cm}^{-3}$, showing a reduction of the SPM bandwidth of a pulse of intensity 1.9 GW/cm^2 .

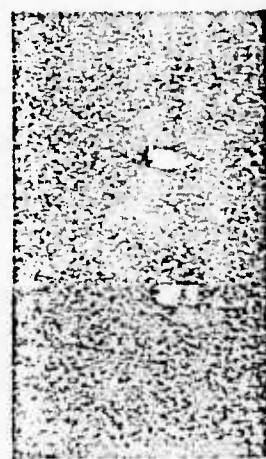
→ | | ← 10 cm⁻¹



(a)



(b)



(c)

cathode at the appropriate angle for Rowland circle focussing.

Initially when there is no population inversion the transitions are very intense. Population inversion occurs at a later stage of expansion and cooling when the $Ly\alpha$ and $Ly\beta$ intensities are much reduced. The extremely high sensitivity of the VUV streak camera [4] makes it possible to record the subnanosecond scale temporal variation of the $Ly\alpha$ and $Ly\beta$ intensities through to the inversion phase.

References

- [1] Based on calculations described by M.H. Key at the Gordon Conf. on Laser produced plasmas, Tilton, USA (1973), which were developed from earlier work by L. Gudzenko and L. Shelepin, *Sov. Phys. Doklady* 10 (1965) 147, and paper by S. Slutz, G. Zimmerman, W. Lokka, G. Chapline, L. Wood at APS Monterey Conf. (1972).
- [2] J.P. Christiansen, D.E.T.F. Ashby, K.U. Roberts, *Computer Phys. Commun.* 7 (1974) 271.
- [3] T.P. Donaldson, R.J. Hutcheon, M.H. Key, *J. Phys. B. Atom. Molec. Phys.* 6 (1973) 1525.
- [4] D.J. Bradley, A.G. Roddie, W. Sibbett, M.H. Key, M.J. Lamb, C.L.S. Lewis, P. Sachsenmaier, *Optics Commun.* 15 (1975) 231.

R4 AN ELECTRON-COLLISION PUMPED QUASI-CW SOFT X-RAY LASER USING HELIUM-LIKE IONS

L.J. PALUMBO and R.C. ELTON

Naval Research Laboratory, Washington, D.C. 20375, USA

A steady-state analytical plasma model has been applied to a quasi-cw electron-collisional pumping scheme for producing soft x-ray lasing on the $3s^1S \rightarrow 2p^1P$ transition in helium-like ions. The estimates of pump power requirements, gain coefficient, and optimum element indicate that lasing may be obtained in the 20–70 Å region with a gain of $> 10 \text{ cm}^{-1}$ in moderate-Z plasmas under conditions existing in present and forthcoming pellet fusion experiments. The $1s3s^1S$ upper laser level is pumped by electron collisional excitation from the $1s^2^1S$ ground level, lasing takes place by transitions into $1s2p^1P$, and rapid $1s2p^1P \rightarrow 1s^2^1S$ decay prevents self termination, i.e., quasi-cw operation is expected. The upper laser level is also depopulated by electron-impact excitation into the nearby $1s3p^1P$ term, which imposes an upper limit on the electron density for a given element. A population inversion is maintained, even though the electron-impact excitation rates from the ground state into both the $3s$ and $2p$ levels are comparable, because rapid $2p \rightarrow 1s$ decay prohibits accumulation in the $2p$ level while the $3s$ level is not dipole coupled directly to the ground state.

The equations for the steady-state population densities, N_3 and N_2 , of the upper and lower laser levels are,

$$N_3 = \frac{N_1 N_e X_{13}}{A_{32} + N_e (X_{32} + X_{34})},$$

$$N_2 = \frac{N_1 N_e X_{12} + N_3 (A_{32} + N_e X_{32})}{A_{21}},$$

where the subscripts 1 through 4 refer to the $1s^2^1S$, $1s2p^1P$, $1s3s^1S$, and $1s3p^1P$ levels, respectively. The A 's are spontaneous radiative decay rates, the X 's are electron collisional excitation or deexcitation rate coefficients, and the N 's are the population densities with N_e being the electron density. The deexcitation rate coefficient, X_{32} , is computed from X_{23} by detailed balancing. Required energy level spacings, etc. were taken from published data and scaled appropriately with spectrum number. The ground state density, N_1 , was obtained from N_e by assuming charge neutrality, 100% abundance of helium-like ions, and small fractional populations of excited levels.

Fig. 1 shows some results of gain at two (high) electron densities. A gain coefficient, α , of $> 10 \text{ cm}^{-1}$ is desired because, even with very large pump laser systems, it may be difficult to form a plasma of the required temperature and density with a length of more than a few millimeters. These curves are typical of those computed over a wide range of electron density and temperature. The curves show an increase in gain with N_e , an optimum Z at a given density, a rapid decrease in α for Z larger than this optimum, and a Z_{min} cutoff below which the computed inversion density is negative. The gain scales analytically as $\sim (Z-1)^{-2.5}$ when collisional processes dominate the $3s^1S$ level depopulation (low Z or closely spaced energy levels) and as $\sim (Z-1)^{-8.5}$ when the prominent mode of depopulation is by spontaneous laser-line emission. For a given Z , the highest gain is attained when the electron temperature is approximately twice the $1s \rightarrow 3s$ excitation energy, ΔE_{13} . This is a consequence of the fact that $N_e X_{13}$, the rate for the dominant process populating the upper laser level, reaches a peak at $kT_e \approx 2\Delta E_{13}$; for higher temperatures, this rate falls off slowly and the laser pumping rate decreases. An ion temperature less than the electron tem-

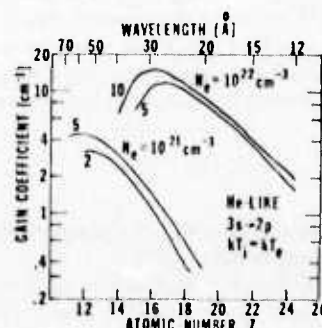


Fig. 1. Calculated gain for $3s^1S \rightarrow 2p^1P$ lasing in helium-like ions plotted vs. atomic number for two electron densities. For each density, electron temperatures were chosen which yielded the highest gain and their values in keV are indicated by numbers next to each curve.

perature, which may occur in a transient laser plasma, would increase the gain in the plotted curves by a factor of $(T_e/T_i)^{1/2}$ due to a reduced Doppler width.

The production of a plasma with the density and temperature required to produce reasonable gains on this transition would require a pump laser with a power density $\sim 10^{17}$ W/cm² over an area of largest dimension ≥ 1 mm on a cylindrical pellet-like target to avoid temperature decrease by thermal conductivity. Such lasers and targets are currently being developed in the laser fusion programs. Results from a micro-interferometric diagnostic experiment [1] using a Nd:YAG 30 psec probe laser synchronized with a Nd:glass 2 nsec plasma producing laser to study the evolution of a high-density critical layer at $N_e \approx 10^{21}$ cm⁻³ will be described.

References

- [1] J.F. Reintjes, T.N. Lee, R.C. Eckardt, R.C. Elton, and R.A. Andrews, *Butl. Am. Phys. Soc.* (1975) 1336.

R5 INTERACTION OF POWERFUL MILLISECOND LASER PULSES WITH MATTER

V.B. FEDOROV

Lebedev Physical Institute, Leninsky Prospekt 53, Moscow, USSR

The paper treats the problems of evaporation and heating of strongly absorbing solid targets (particularly metals) under high-energy ($\sim 10^4 - 10^2$ J) and long-duration ($10^{-3} - 10^{-6}$ sec) laser pulses.

The solid target evaporation and optical discharges supported by the laser beam near solid targets (and in gaseous targets) are studied in the intensity range of incident laser radiation $I \sim 10^7 - 10^9$ W/cm². Results on the mechanisms of the processes taking place near the targets, on the gasdynamic structure of the optical discharges and plasma heating are presented.

The possibility to advance experiments with long-duration laser pulses into high-intensity range of laser radiation up to $I \sim 10^{11} - 10^{13}$ W/cm² is demonstrated. The first experiments in this range have shown that reflection from dense, near critical optical discharge plasma results in laser Q-switching and corresponding self-consistent, high temperature plasma heating.

R6 MULTIPHOTON IONIZATION PROCESSES AT VERY HIGH LASER INTENSITY

L.A. LOMPRE, G. MAINFRAY and C. MANUS

Service de Physique Atomique, Centre d'Etudes Nucléaires de Saclay BP No 2, 91190 Gif-sur-Yvette, France

The purpose of this paper is to present some preliminary results of the first investigation of multiphoton ionization of

rare gases at very high laser intensity (10^{15} W/cm²).

The laser used in the present experiment is a mode-locked Nd:YAG oscillator using a Kodak 9740 saturable dye. A single pulse is selected from a train of 10 pulses by the well-known method of Pockels switch. The laser pulse width was measured to be 28 ± 2.5 ps by using a picosecond streak camera [1]. This single pulse is amplified to an energy up to 1 J. The laser radiation is linearly polarized and is centered at 10 643.5 Å, with a linewidth of 0.8 Å. The laser pulse is then focused into a vacuum chamber by an $f/3$ aspheric lens corrected for spherical aberrations. The gas under investigation is released into the chamber at a pressure of 10^{-4} torr. The ions resulting from the laser interaction with atoms at the focal point are extracted with a transverse electric field of 500 V/cm, and then detected with an electron multiplier.

The experiment consists of measurements of the number of ions N_i formed as a function of the laser intensity I . In a log-log plot, the experimental points form a straight line with a slope

$$K = \frac{\partial \log N_i}{\partial \log I}$$

Within the experimental errors, the K values for the five rare gases are in good agreement with the corresponding K_0 values. K_0 is the next integer greater than the ionization energy of the atom divided by the laser photon energy. This would mean that no resonant multiphoton ionization processes have taken place at this laser wavelength. Previous experiments have shown that K can have values smaller or larger than K_0 depending on the laser wavelength, when there is a resonant multiphoton excitation of an atomic level [2].

An important conclusion can be derived from the experimental results obtained for helium atoms at a laser intensity of $(3 \pm 2) \times 10^{15}$ W/cm², that is a peak laser electric field of 1.5×10^9 V/cm. No lowering of the slope $K = 22 \pm 2$ is observed. Consequently, possible tunnel effect does not play any role at this laser intensity. Ionization of helium atoms seems to result only from a "pure" 22-photon process. This result is in contradiction with the very few theoretical calculations which predict that tunnel effect should appear in this laser intensity range [3-4].

References

- [1] L.A. Lompre, G. Mainfray and J. Thebaud, *Appl. Phys. Lett.* 26 (1975) 501.
 [2] B. Held, G. Mainfray, C. Manus, J. Morellec, and F. Sanchez, *Phys. Rev. Lett.* 30 (1973) 423
 [3] L.V. Keldysh, *Zh. Eksp. Teor. Fiz.* 47 (1964) 1945. [*Sov. Phys. JETP* 20 (1965) 1307].
 [4] G.J. Pert, *J. Phys. B* 8 L173 (1975).

Abstract Submitted
for the Washington, D.C. Meeting of the
American Physical Society

26-29 April 1976

Physics and Astronomy
Classification Scheme
Number 52

Bulletin Subject Heading
in which Paper should be
placed Plasma Diagnostics

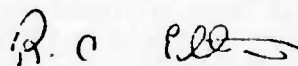
Diagnosis of a Traveling-Wave Surface Discharge
as a Source of Short Wavelength Stimulated Emission.*
R. W. WAYNANT, T. N. LEE, and R. C. ELTON, Naval Research
Laboratory--A possible laser emission from CIV resonance
lines at 1548.2 and 1550.8 Å has been previously report-
ed¹ using a low pressure, traveling wave discharge.
However, a specific physical process which is responsible
for the population inversion in the resonance transition
is not well known. In view of the low pressure involved,
the discharge is believed to be associated with a surface
breakdown over a polyethylene insulating sheet which is
exposed to the discharge. The purpose of the present
study is a first attempt to understand, through a diag-
nosis of the device, the processes with which the ablated
material is multiply ionized and the radiation is ampli-
fied. The diagnostics include spectroscopy as well as
high-speed optical and x-ray measurements. The possi-
bility of association with a velocity selection popula-
tion mechanism² is considered.

*Work supported in part by DARPA

¹R. W. Waynant, Appl. Phys. Letters 22, 419 (1973).

²B. A. Norton and E. R. Wooding, Phys. Rev. A 11, 1689
(1975).

Submitted by



Signature of APS Member

R. C. Elton
Code 5520
Naval Research Laboratory
Washington, D.C. 20375

search & discovery

Nobel prize to Richter and Ting for discovery of J/psi

The 1976 Nobel Prize in Physics has been awarded to Burton Richter of SLAC and Samuel C. C. Ting of MIT "for their pioneering work in the discovery of a heavy elementary particle of a new kind." Their surprising and far-reaching discovery of the J/psi particle was announced in November 1974 (PHYSICS TODAY, January 1975, page 17). The prize of \$160 000, to be shared equally by Richter and Ting, was scheduled to be awarded on 10 December in Stockholm.

The J/psi with a lifetime 1000 times greater than expected for a particle as massive as 3.1 GeV, did not fit into the three-quark classification scheme. Two years after the discovery, nine or ten particles related to the J/psi have been found. All the members of the J/psi family of mass below 3.7 GeV (the threshold for the associated production of charmed mesons) have remarkably small widths, typically a few hundred kilovolts or smaller, whereas particles with comparable mass were expected to have widths of several hundred MeV. By now it is widely believed that all the J/psi particles are bound states of a charmed quark and its antiquark. Further confirmation of the existence of charm has come from the discovery of charmed mesons and charmed baryons.

Richter collaborated on the experiment with a large team of experimenters led by himself, Martin Perl (SLAC), William Chinowsky, Gerson Goldhaber and



TING



RICHTER

George Trilling (Lawrence Berkeley Laboratory). The experimenters used the large solenoidal magnetic detector at SPEAR, the electron-positron colliding-beam device at SLAC. It was Richter who led the drive to construct SPEAR, after his pioneering efforts with an electron-electron device done with W. C. Barber, Bernard Gittelmann and Gerard K. O'Neill.

The SLAC-LBL team had been studying the behavior of the total cross section for e^+e^- annihilation as a function of energy, varying the total energy in 200-MeV steps. They observed an anomalously high cross section at 3.2 GeV.

When the California experimenters returned to this energy region and varied the energy in much finer steps, using a nuclear magnetic-resonance spectrometer to monitor the ring energy, they found¹ a cross section for hadron production at 3.105 GeV that was greater than 100 times the cross section outside the peak. The full width at half maximum was less than or equal to 1.3 MeV.

The actual discovery of the particle the group called " $\psi(3105)$ " took place in one frantic weekend (9-10 November 1974). By the next day the news had traveled far and wide. On 21 November the SLAC-

continued on page 19

Shortest wavelength laser from harmonic generation

Records for the shortest wavelength at which coherent radiation has been achieved in the search for an x-ray laser system are falling with remarkable speed:

► It was only in June that Henry Hutchinson, C. C. Ling and Daniel Bradley (Imperial College, London) reported¹ at the Amsterdam Quantum Electronics Conference that they had extended the range of generation of coherent radiation into the extreme ultraviolet at 570 Å.

► After a preliminary paper in August, at the International Conference on the Physics of X-ray Spectra, John Reintjes, Robert Eckardt, Nicholas Karagelen, Raymond Elton and Ronald Andrews of

the Naval Research Laboratory (Washington, DC) and Chiao-Yao She of Colorado State University report in a current Letter² that they pushed the record down to 532 Å.

► Now, at the Tucson meeting of the Optical Society in October, the NRL group reported preliminary results indicating they had reached 380 Å.

The methods used by the two groups are quite similar: Both used the nonlinear susceptibilities of noble gases to generate harmonics of an incident laser beam. These methods are extensions of initial work done in 1973 by Stephen Harris and his colleagues at Stanford. The Imperial College group used argon to frequency-triple the radiation from a xenon excimer

laser (one in which the active medium consists of excited short-lived Xe_2 molecules). The NRL group obtained the fifth (and, in their latest work, seventh) harmonic of pulses that were already fourth harmonics of Nd-YAG laser light. The noble gases they used were helium, neon and argon, Reintjes told PHYSICS TODAY.

The NRL experiment. The primary radiation wavelength of 2661 Å was obtained from the 1.06-micron output of a Nd-YAG laser by two successive stages of frequency doubling, first in a crystal of potassium dihydrogen phosphate and then in one of potassium dideuterium phosphate. The NRL experimenters then converted this 2661-Å radiation of

the fifth harmonic by a process that can be pictured as follows:

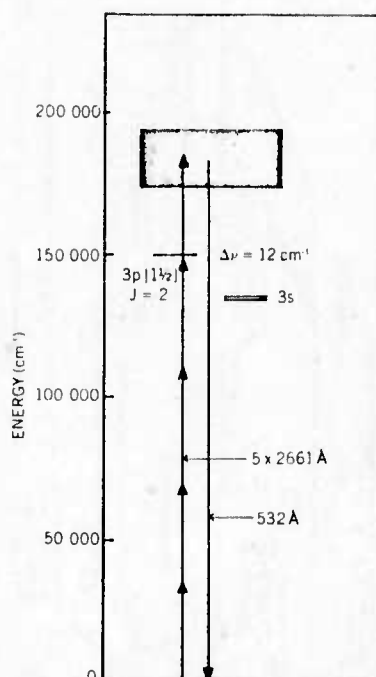
A sequence of virtual transitions of a ground state electron with the absorption of five pumping photons at 2661 Å generates a dipole moment that causes the emission of a single photon at one fifth of the driving wavelength. Such high-order nonlinear processes tend to be inefficient. However, the NRL group took advantage of an accidental near-resonance in neon, which has a $3p\ [1\frac{1}{2}], J = 2$, line located within 12 cm^{-1} of four-photon resonance with the 2661-Å input, which enhanced the five-photon emission process. Although this effect tends to increase the conversion efficiency, the improvement can be offset by absorption resulting from photoionization in the neon gas. A similar situation exists in the Imperial College group's experiment on third-harmonic generation in argon.

In the NRL team's experimental arrangement, the 2661-Å beam was focussed (by a calcium-fluoride lens) to a spot in a 500-micron hole in the gas-vacuum wall, which took the place of the entrance slit of a 1-m vacuum-uv monochromator. The 30-psec input pulses with a peak power of 330 MW were formed by the lens into a spot 10 microns in radius and with a depth of 2 mm, later reduced, Reintjes said, to a 5-micron spot size with a depth of 0.5 mm (by switching from a lens of 10-cm focal length to a 5-cm lens). The 532-Å radiation was detected both photographically and photoelectrically. Because for the neon the generated radiation is in the ionizing continuum, efficient conversion requires that the interaction length (focal depth) be kept less than the 0.7-mm absorption length for a neon pressure of 40 Torr.

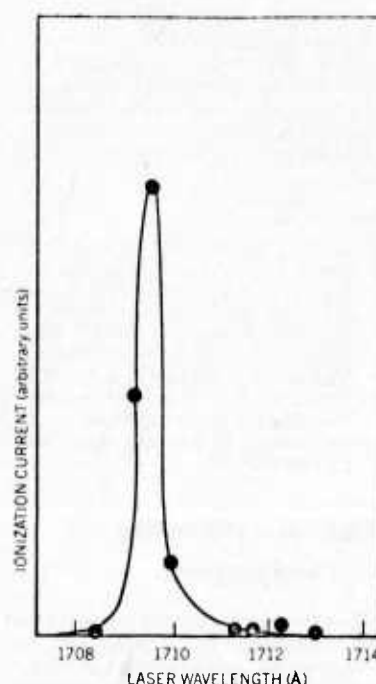
This difficulty was avoided by the NRL team in the helium experiment, because there the generated photon energy lies below the continuum, radiating from a level 1760 cm^{-1} above the $3p$ state. Although the four-photon resonance is not nearly as exact as in neon, the net conversion efficiency (in the range of 10^{-6} – 10^{-5}) was higher in helium. This is because of its transparency at 532 Å, and because its negative dispersion allows phase matching by a tight-focussing procedure. The group has also seen fifth-harmonic conversion in argon at pressures of 10 Torr, Reintjes told us.

The latest result of the NRL group, mentioned above, is the generation of the seventh harmonic of the 2661-Å light in helium. In this experiment, in which the 380-Å output originated from a level in the ionizing continuum of helium, the 5-cm lens was used for focussing. Because the experimental arrangements are the same, the fifth and seventh harmonics are generated simultaneously, but conversion is considerably less for the seventh-order process.

The Imperial College work. Short wavelengths can be obtained not only by going



The five-photon process in neon, with a near-resonance at the four-photon level, used to generate 532-Å coherent radiation at NRL.



Efficiency of third-harmonic generation peaks at 1709.4 Å in argon to produce 570-Å coherent output in an experiment at Imperial College.

to higher-order processes but also by pumping with a laser of shorter wavelength. The Imperial College group did the latter, making use of the availability of the xenon excimer laser, which at 1710 Å is already in the vacuum-uv region. A single stage of frequency tripling in argon, enhanced by two-photon resonance with the $5p$ state, was therefore sufficient to produce the coherent extreme-uv radiation at 570 Å. The narrow-band tunability of the Xe_2 laser made accurate tuning to the resonance possible, and the experimenters were able to plot the relative efficiency of the process as a function of the laser's wavelength.

The Imperial College experimenters pumped with 10-nsec, 15-mJ pulses with a bandwidth of 1 Å, from the Xe_2 laser. With a barium-fluoride lens of 3-cm focal length, they focussed the beam just in front of a 250-micron aperture in the focal plane of a 1-m normal-incidence vacuum spectrograph. The bandwidth of the 570 Å coherent radiation was an instrument-limited 0.8 Å. As compared with the NRL pulses, the longer-duration lower-power pulses of the Imperial College experiment make saturation of the resonant transition less serious, Bradley said.

Bradley and his collaborators indicate that coherent radiation at even shorter wavelengths than theirs could be attained with other noble-gas-excimer lasers and appropriate isotropic nonlinear media.

Another development at Imperial College is the generation of pulses as short

as 0.3 psec by I. S. Ruddock and Bradley. The extremely short pulses, practically bandwidth limited, were obtained by mode locking a cw dye laser with two saturable absorbers. The pulses are significant for their hyperbolic-secant-squared intensity profiles, so that they are stationary pulses, that is, solitons. This makes it possible for them to propagate through materials without changing shape, according to Bradley. Because the pulses contain only 150 optical cycles (at 6000 Å), the Imperial College pulses are nearly at the lower limit of pulse duration set by the frequency of the laser. The arrangement used an argon-ion pumping laser, a saturable absorber dye cell and a resonant cavity, near the center of which passed a free-flowing jet of a rhodamine dye. Such short pulses are useful in the study of the interactions of matter on a very short time scale; for example, in ultrahigh-speed photography, stopping the motion of crystals and macromolecules.

As pumping lasers of increasing power are developed, will it become possible to obtain converted coherent radiation of higher and higher orders, and so of shorter and shorter wavelengths? Reintjes answered our question with a qualified yes. It turns out that there are certain effects that may limit conversion, in particular electrical breakdown of the gas. Such a breakdown was already seen in Reintjes's lab, in neon at 60 Torr. In this region an increase in pressure (needed for efficient conversion) lowers the breakdown threshold.

If soft x rays may be said to begin at 100 Å, some people believe that coherent x rays are likely to become a reality soon. The uses of such radiation would include the study of crystals and biomolecules, and photolithographic techniques for producing super-miniaturized electronic microcircuits.

—HRL

References

1. M. H. R. Hutchinson, C. C. Ling, D. J. Bradley, *Optics Comm.* 18, 203 (1976); D. J. Bradley, M. H. R. Hutchinson, C. C. Ling, in *Tunable Lasers and Applications* (A. Mooradian, T. Jaeger, P. Stokseth, eds.), Springer, New York (1976), page 40.
2. J. Reintjes, R. C. Eckardt, C. Y. She, N. E. Karagelen, R. C. Elton, R. A. Andrews, *Phys. Rev. Lett.* (to be published).
3. I. S. Roddick, D. J. Bradley, *Appl. Phys. Lett.* 29, 296 (1976).

New values for boiling and freezing points

The values assigned to the temperatures of the boiling point of water and the freezing points of tin and zinc on the International Practical Temperature Scale of 1968 appear to be significantly higher than thermodynamic values. The new measurements, done by Leslie Guildner and Robert Edsinger with a very carefully built gas thermometer at the National Bureau of Standards, may lead to a redefinition of the International Practical Temperature Scale.

Although experimenters have made temperature measurements for many years with classical gas thermometers, Ralph P. Hudson, chief of the Bureau's Heat Division, says "They were polishing a slightly rotten apple. We decided to do it right." The project began about 20 years ago, with both Guildner and Edsinger working on it almost from the beginning. Their first determination was the thermodynamic temperature of the steam point, which they found to be 99.975 °C, a discrepancy with the IPTS-68 (the most recent revision) of -0.025 °C. Subsequently they found the tin and zinc freezing points to be 231.924 °C and 419.514 °C, which are lower than the values on the IPTS-68 by 0.045 °C and 0.66 °C, respectively.

The 1968 revision is based primarily on gas thermometry, the work most immediately preceding being done at the Physikalische Technische Bundesanstalt in Braunschweig by Helmut Moser and Wilhelm Thomas and at the National Research Council in Ottawa by Hugh Preston-Thomas and Chris Kirby.

The NBS results differ from and are thought to be more accurate than earlier gas-thermometry values for two reasons: First, the NBS group developed instrumentation to allow the highest level of metrology for the measurement processes such as thermal expansion, thermomole-



NBS precision mercury manometer has a total uncertainty in pressure ratios of 1.5 ppm.

cular pressure and the realization of pressure ratios, Hudson told us. For example, the precision mercury manometer has a total uncertainty in pressure ratios of only 1.5 ppm. Second, the effect of sorption, which is thought to be the principal source of systematic bias between the NBS work and earlier gas thermometry, is believed to be insignificant in the new results because of a comprehensive effort to minimize it.

The next step for the NBS team will be to measure the freezing point of aluminum, near 660 °C. Eventually they are aiming for measurement at the gold point near 1064 °C to incorporate in a new version of the IPTS. The latter was revised in 1948, 1968, and will be revised again in the not-too-distant future, perhaps as early as 1983, according to one member of the Advisory Committee on Thermometry; this group reports to the International Committee of Weights and Measures.

—GBL

Nobel prize

continued from page 17

LBL group found a second narrow resonance decaying to hadrons, simply by scanning the entire region in 1-MeV steps. The new resonance had a mass of 3.695 GeV.

Much later, Richter said: "It has been particularly satisfying to have witnessed the birth of a new class of particles; the ψ 's with their unexpected properties. Every experimentalist dreams of making the great discovery—a discovery which will change the direction of scientific thought. I don't know yet if the colliding-beam machines and the new particles we have discovered with them will cause a sharp change in that direction, but surely they have bent it a bit."

Ting and his Brookhaven-MIT collaborators (Ulrich Becker, Min Chen and others) had been studying quantum electrodynamics, photoproduction of vector mesons and e^+e^- pair decay of vector mesons for the last ten years at DESY, where they developed techniques to identify electron-positron pairs from a background of millions of hadrons. They started their experiment at the Brookhaven AGS, searching for new particles in the reaction $p + \text{Be} \rightarrow e^+ + e^- + X$ with a precise pair spectrometer that had a mass resolution of 5 MeV. They saw a sharp peak at 3.1 GeV with a width consistent with zero (consistent with their mass resolution). They called it the "J" particle. The peak was first observed in August 1974, Ting recalls.³ The group decided to make many experimental checks, such as decreasing the magnet current. They then spent late October and the first week in November measuring the anomalous e^+/π^+ ratio, hoping that the J could explain this number.

On 6 November Ting decided to publish⁴ the work on the J. On 11 November Ting, who was visiting SLAC for a Program Advisory Committee meeting, went to W. K. H. Panofsky's office and told him and Richter of the MIT results. Richter reciprocated with the SLAC-LBL results. Within a short time the Adone storage ring in Frascati also discovered the J/ ψ particle. "It was the shot heard 'round the world,'" at least in the circles traveled by particle physicists.

Biographies. Richter earned his BS and PhD at MIT. In 1956 he went to Stanford University and in 1963 joined the staff of SLAC, where he has been a professor since 1967.

Ting got his bachelor's and doctorate at the University of Michigan. In 1963 he went to CERN and then joined Columbia University's physics department the following year. He went to MIT in 1967, where he became a professor in 1969. Since 1966 Ting has been doing experiments at DESY.

—GBL

References

1. J.-E. Augustin, A. M. Boyarski, M. Breidenbach, F. Bulos, J. T. Dakin, G. J. Feldman, G. E. Fischer, D. Fryberger, G. Hanson, B. Jean-Marie, R. R. Larsen, V. Luth, H. L. Lynch, D. Lyon, C. C. Morehouse, J. M. Paterson, M. I. Perl, B. Richter, P. Rapidis, R. F. Schwitters, W. M. Tanenbaum, F. Vannucci, G. S. Abrams, D. Briggs, W.

Review and Status of X-Ray Laser Research

Ronald W. Waynant
U. S. Naval Research Laboratory
Washington, D. C. 20375

The possibility of developing lasers in the x-ray region of the spectrum has attracted serious attention over the past few years. This attention has occurred for several reasons: (1) the success of generating vacuum ultraviolet laser wavelengths as short as 1100 Å; (2) the success of nonlinear tripling and mixing processes to up-convert existing laser frequencies to attain wavelengths as short as 887 Å; (3) the construction of extremely powerful laser systems to study laser fusion; and (4) the occurrence of results which have been attributed to stimulated emission from several x-ray experiments. Along with these developments numerous ideas for advancements have been made. This discussion collects the last results and proposals and places them within the framework of basic x-ray laser theory. Limitations of experimental technology and the lack of needed theoretical data are discussed.

Construction of lasers below 1000 Å is impeded by the lack of conventional optics. Window and reflector materials are used to make resonators in the visible, but below 1000 Å no material transmits until the 10-50 Å region is reached and the reflectance of metal coatings is usually below 50%. It is possible to use Bragg reflectors, but these are very difficult to align in practice. Distributed feedback also would be a possibility for obtaining resonance in an x-ray oscillator, but the intense pump power required may destroy the delicate lattice spacing required. Because of these practical limitations x-ray lasers are likely to resemble the single-pass, high-gain, mirrorless amplified spontaneous emission (ASE) lasers developed in the uv and vuv. Further study of the general properties of ASE lasers likely will indicate the operating characteristics of x-ray lasers.

Single-pass lasers of length L have gain given by $\exp(\alpha L)$ where α , the small signal gain coefficient, is given by

$$\alpha = \frac{\lambda^2 A N}{8\pi \Delta \nu}.$$

Here λ is the wavelength, $\Delta \nu$ is the linewidth in frequency units, A is the transition probability, and N is the inversion density. Substituting the wavelength dependency for Doppler broadening, the gain factor scales approximately as λ^3 . The pumping power per unit volume (W-cm^{-3}) scales as λ^{-4} . Typical values for $\alpha = 5$, $L = 1$ cm and particle velocity of 10^7 cm/sec are shown in Table I. This table shows the extremely high

TABLE I

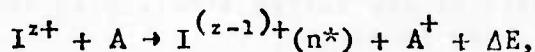
$\lambda[\text{\AA}]$	1	10	100	1000	2000
$P[\text{W-cm}^{-3}]$	10^{19}	10^{16}	10^{11}	10^7	10^6

power densities required in the 1-10 Å wavelength region. At present only high-power focused lasers can approach this power density.

The rate coefficients for energy transfer depend on the specific pumping process involved. Most of the excitation processes have rates which scale inversely with wavelength, the exception being resonance charge transfer. The use of metastable states to store excitation prior to rapid transfer to radiative states may alleviate the requirement for rapid excitation.

Perhaps the most important pumping process is electron collisional excitation. All of the vacuum ultraviolet lasers generated have been excited by electron collision, primarily collisions with molecules. It does not seem likely that molecules can be used in this manner to produce wavelengths much below 600 Å, however. Progress toward x-ray lasers will involve collisions with ions. One such proposal utilizes the electron-collision excitation process to invert the 3p-3s levels in ions. Since this transition has lifetimes connected with it that make lasing rather easy to produce in the visible and near uv, it may be possible to reach short wavelengths by following the isoelectronic ion sequence to higher stages of ionization. For example, the 3p-3s transition of U^{+85} gives a wavelength of 11 Å.

Various electron attachment processes can lead to population inversion. Three-body collisional recombination preferentially fills upper ion levels leading to population inversion with respect to the lower levels. This process is dependent on rather high densities to achieve a high pumping rate and may be best achieved in laser-produced plasmas. Some observations of population inversion in expanding laser plasmas have already been made. Dielectronic capture, where a free electron is captured and a second electron excited, is a possible means of creating a population inversion. Charge transfer interactions proceed as



where an ion, I^{z+} , interacts with a neutral atom, A, reducing the ionic charge, z, by removing an electron from A and promoting the remaining ion to an excited level, n^* . Charge transfer occurs spontaneously only when the defect energy, ΔE is exothermic. Stimulated charge transfer with the defect energy supplied by a laser also has been considered. Charge exchange experiments are presently underway.

Photoabsorption has been considered for the production of a population inversion because of the possibility of tuning the pumping source to produce a specific innershell vacancy. Both K α and full-shell vacancies in alkalis have been studied. The alkalis have the advantage of only one outershell electron and therefore no Auger effects. The analysis of both the alkalis and the K α laser proposals are positive provided photoionization losses of the laser frequency can be minimized and provided a strong pumping source can be found. Such a source could come from a suitably tailored laser-produced plasma.

Other means of possible x-ray laser production include the use of nuclear transitions and the use of stimulated Compton scattering. Serious consideration of nuclear transitions is definitely increasing and could produce an early breakthrough if methods are found to reduce the lifetime of long-lived isomers or if the shorter-lived excited nuclei can be rapidly assembled into a laser configuration. Stimulated Compton scattering has also received increased attention, but the attainment of wavelengths much below 200 Å does not seem possible due to the present limitations of electron and photon beams.

It must be pointed out that the verification of gain becomes very difficult in the far ultraviolet and soft x-ray regions. This is especially true for the very small, single-pass lasers anticipated. Techniques for the verification of gain will likely require the ability to vary the length or other geometry of the gain region as well as the ability to control the pumping intensity. Methods of examination for gain can follow those used for single-pass longer-wavelength vuv lasers, but it is essential that gain be measured to insure that laser action is present.

Many of the above difficulties can be avoided by starting with a powerful infrared laser and using the nonlinear susceptibility of vapors to generate harmonic frequencies or to sum several frequencies. These techniques avoid the pumping intensities required at shorter wavelengths and transfer much of the high-quality spatial and temporal characteristics from the infrared to the far ultraviolet. The extremely low efficiencies associated with nonlinear processes have been improved greatly by using materials with resonances near the incoming laser frequencies or their harmonics. Wavelengths as short as 887 Å have been generated, and mixing of tunable visible or near uv wavelengths has produced tunable vacuum uv in the 1000-2000 Å region. Conversion efficiencies range from 10^{-3} to 10^{-7} for these processes. Some prospects exist for the generation of shorter wavelengths via nonlinear processes employing higher-order harmonics in ionized vapors. It may also be possible to start with high-power vacuum-uv lasers rather than infrared lasers. Nonlinear processes will be available for mixing and tuning of x-ray laser wavelengths when these lasers are developed.

While it is difficult to predict the impact that an x-ray laser is certain to have on future research, it is likely to be most valuable in materials research. Its coherence will be valuable in producing x-ray holograms having high resolution. Its temporal and spatial properties also will be quite valuable in many areas. It is likely that the most important applications have not been anticipated at this time.

References

R. W. Waynant and R. C. Elton, "Review of Short Wavelength Laser Research," Proc. IEEE, vol. 64, pp. 1059-1092 (July 1976) and the 268 references therein.

APS News - p. 722

bulletin

OF THE AMERICAN PHYSICAL SOCIETY

MAY 1976

INCLUDING THE PROGRAM OF THE
1976 CAP-APS-SMF JOINT CONGRESS

14-17 JUNE 1976

Vol. 21, p. 854, 1976

E-3 Study of Expansion Characteristics of Laser Produced Plasmas Using a Micro-Interferometry*. J. F. REINTJES, T. N. LEE, R. C. ECKARDT, R. C. ELTON, and R. A. ANDREWS, Naval Research Laboratory--High quality interferograms of laser produced plasmas with spatial resolution of 15 micrometers are obtained using a relatively simple Jamin-type interferometer and a precisely timed 30 ps probing laser pulse from a mode-locked Nd:YAG laser, frequency doubled to 0.53 μm . The spatial resolution attainable with the present arrangement is limited by the velocity of the expanding plasma and the finite duration of the probing pulse. The plasmas are produced by focusing a Nd:glass Q-switched laser pulse (0.5 GW, 10^{11} - 10^{13} Watts cm^{-2}) onto slab targets of Al, Mg, and CH_2 . Time-dependent behaviors of electron density distribution, plasma dimension, and expansion velocity for both point and line foci are made as a function of time delay between the mode-locked and the Q-switched laser pulses. The results thus obtained with different durations of the heating (Q-switched) pulse and with the various target material are compared.

*Work supported by DARPA Order No. 2694.

854

PUBLISHED FOR THE AMERICAN PHYSICAL SOCIETY
BY THE AMERICAN INSTITUTE OF PHYSICS

COMPARISON OF EFFICIENT HARMONIC GENERATION
FROM 532 nm TO 266 nm IN ADP AND KD*P

J. F. Reintjes and R. C. Eckardt
Naval Research Laboratory
Washington, D C. 20375

ABSTRACT

Second harmonic generation in ADP and KD*P from 532 nm to 266 nm with 85% conversion is reported. Effects of nonlinear absorption and crystal length on high-level conversion are investigated.

COMPARISON OF EFFICIENT HARMONIC GENERATION
FROM 532 nm TO 266 nm IN ADP AND KD*P†

J. F. Reintjes and R. C. Eckardt
Naval Research Laboratory
Washington, D.C. 20375

Efficient generation of the fourth harmonic Neodymium lasers provides a convenient source of high-power ultraviolet pulses for a variety of experiments. Significant discrepancies have been reported, however, between maximum experimental conversion efficiencies in 90° phase-matched ADP, which are typically 30%, and corresponding theoretical predictions of 60-80%.¹ These differences have been ascribed to such varied processes as linear or nonlinear absorption at 266 nm, distortion of the phase matching condition resulting from optical absorption or imperfect phase matching.²

Using mode-locked pulses from a Nd YAG laser we have measured various aspects of fourth-harmonic generation and nonlinear transmission at 266 nm in KD*P and ADP. Our results demonstrate that harmonic conversion efficiencies approaching the theoretical limit can be obtained when the full spectral width of the pump pulse ($\lambda = 532$ nm) is phase matched, but that conversion is limited by parametric interactions between the pump and harmonic pulses ($\lambda = 266$ nm) when the phase matching is incomplete.

Conversion efficiency measurements were made by monitoring the incident and transmitted pump pulses along with the harmonic pulse, thus allowing limiting processes due to nonlinear absorption to be distinguished from those due to incomplete phase matching. Conversion efficiency was observed to increase with crystal length until the spectral width of the phase matching peak became comparable to that of the pump pulse (0.9 Å in our experiments) and decreased for longer crystals. This result indicates that the major limitation on high conversion of picosecond pulses is group velocity dispersion between pump and harmonic pulses. This effect is further confirmed in spectral measurements which clearly show the restricted phase matching which occurs in longer crystals. In these experiments ADP and KD*P gave virtually identical results.

†Supported by the Defense Advanced Research Projects Agency, DARPA Order 2694

"...Efficient Harmonic Generation...", J. F. Reintjes and R. C. Eckardt

Conversion efficiency was then measured as a function of pump intensity in 4 mm samples of both materials (Fig. 1). Energy conversion up to 85% was observed in ADP (80% in KD*P) with pump intensities of $8 \times 10^9 \text{ W/cm}^2$. Comparison with theoretical expectations for conversion of a monochromatic plane wave weighted with Gaussian spatial and temporal distribution shows excellent agreement and indicates we have actually achieved the theoretical limit of conversion at these powers.

We present the first quantitative measure of nonlinear absorption at 266 nm in these materials. Values of the two-photon absorption coefficient were $6.5 \times 10^{-11} \text{ W/cm}$ for ADP and $1.5 \times 10^{-11} \text{ W/cm}$ for KD*P. The linear absorption coefficient was $.035 \text{ cm}^{-1}$ for both materials. These results indicate that optical absorption is negligible in limiting high-conversion harmonic generation of single pulses in short crystals, although it can be significant in longer crystals used as parametric converters.

Finally, we report observation of the effects of parametric interaction between the pump pulse and the harmonic pulse which occur in longer crystals and result in the generation of spectral structure and new frequencies which appear as sidebands on the transmitted pump and harmonic pulses (Fig. 2).

Time-dependent calculations, which include the effects of group velocity dispersion and phase modulation on these effects, are presented and compared with the experimental results.

1. K. Kato, Optics Comm. 13, 361 (1975).
2. V. D. Volosov, V. N. Krylov, V. A. Serebryakov, and D. V. Sokolov, JETP Lett. 19, 23 (1974).

"...Efficient Harmonic Generation..." J. F. Reintjes and R.C. Eckardt

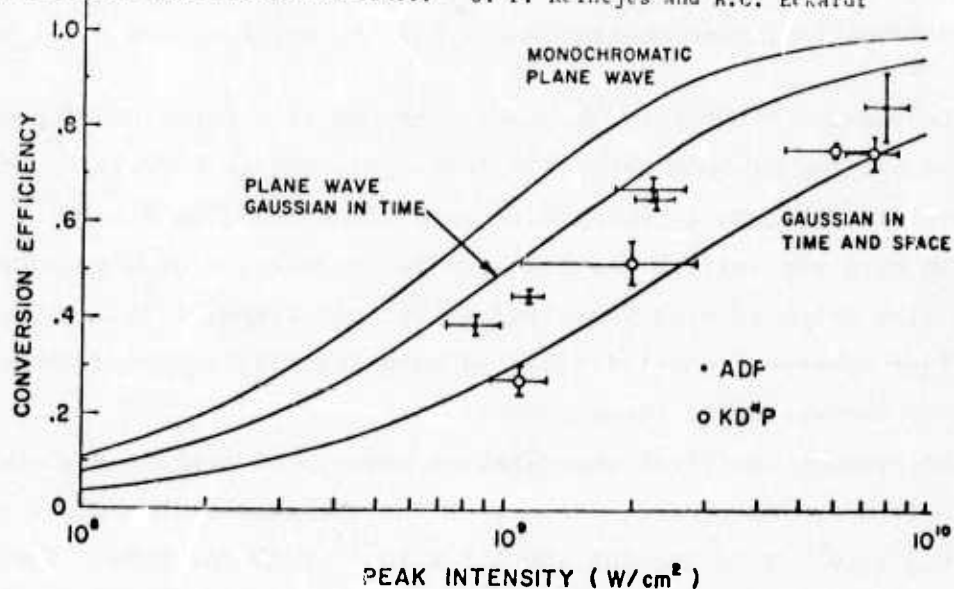


Fig. 1 - Energy conversion vs peak incident pump intensity in 0.4 cm ADP and KD*P. Theoretical curves are calculated for ADP, accounting for profiles of the pump in time and space as indicated. Data agrees well with a spatial profile between a square top and a Gaussian, which is representative of the beam used for measurements.

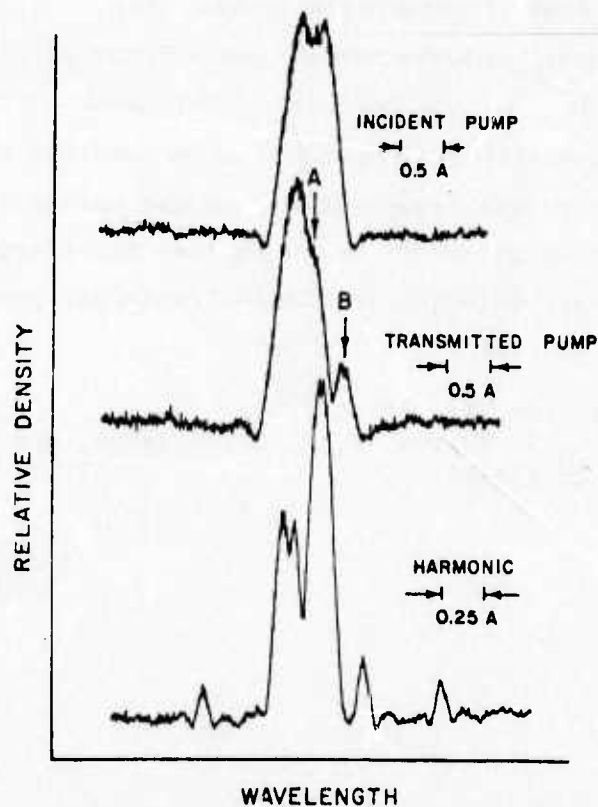


Fig. 2 - Spectral distribution of incident and transmitted pump and harmonic pulses in 2 cm KD*P showing partial conversion of the pump (A) and resulting structure in the transmitted pump (B) and harmonic.

GAIN CALCULATIONS FOR ELECTRON COLLISION PUMPED X-RAY LASERS*

L. J. Palumbo
Naval Research Laboratory
Washington, D.C. 20375

A steady-state computer model for estimating atomic level population densities and short-wavelength laser gain has been developed and applied to electron-collisionally pumped, single-ion, quasi-cw lasing schemes in the carbon-like and helium-like isoelectronic sequences. The carbon-like scheme is an isoelectronic extrapolation to higher atomic number ions and shorter wavelengths of transitions observed [1] to lase in the near UV. The analysis described here is a detailed extension of previous analytical estimates [2] for $3p \rightarrow 3s$ lasing following electron collisional pumping from a $2p$ ground-state reservoir; important refinements include the addition of ionization equilibrium and radiation trapping, extension to high densities [3], the inclusion of more energy levels and more mixing transitions, and the solution for the relevant population densities by simultaneous rate equations.

Because of the close similarity between the carbon-like scheme and another electron-collisional pumping scheme involving $3s \rightarrow 2p$ lasing (collisionally pumped $1s \rightarrow 3s$) in the 10-50 Å range in moderate-Z helium-like ions, the computer code developed for the carbon-like ions was also used with minor modifications to model this two-electron scheme.

In both of these schemes, the lower laser term is rapidly depleted by spontaneous dipole emission into the ground term, while the upper laser term can decay spontaneously only via the lasing transition and is pumped from the ground "reservoir." Such "single-ion" schemes in which the relevant levels are all the same ionization stage result in a maintenance of population inversion independent of atomic lifetimes and ionic regeneration; thus, gain occurs for as long as appropriate plasma conditions can be maintained, and the population inversion is said to be quasi-cw.

A set of steady-state rate equations, each of the form

$$\frac{dN_j}{dt} = 0 = \sum_{k \neq j} N_k W_{kj} - N_j \sum_{k \neq j} W_{jk},$$

was solved for the population densities, N_j , of the levels considered in the present model. The W 's in this equation represent the rates for appropriate atomic processes involving transitions between levels j and k and include electron collisional excitation and deexcitation, electron collisional ionization and (three-body) recombination, spontaneous photoemission, photoabsorption (through an escape-factor treatment of radiation trapping [4], and radiative recombination. Photoionization and transitions induced by ion collisions were negligible in all important cases considered here. In order to allow efficient computation, simple analytical estimates [5], [6] and semi-empirical fits [7] were used to

derive rates needed in the above equations, and the necessary energy-level spacings and oscillator strengths were extrapolated from published tables [8] by scaling appropriately with atomic number. For both the carbon-like and the helium-like schemes, a set of rate equations was solved for the population densities of five levels which included the term ($3d^3D$ in C-like ions and $3p^1P$ in He-like ions) most strongly collisionally coupled to the upper laser term and also strongly coupled by dipole emission to the ground reservoir term, the ground term of the lasing species, and the ground term of the next higher ionization stage.

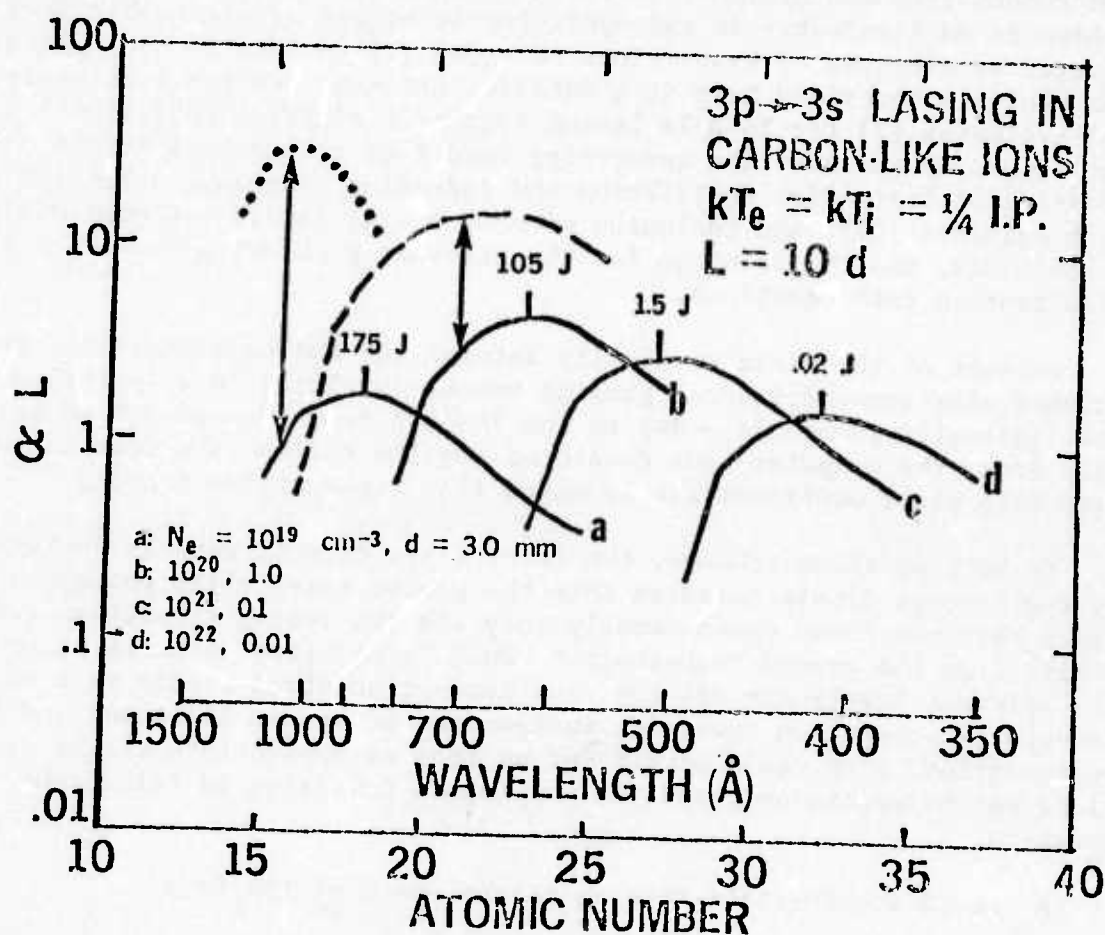


FIGURE 1. Computed product of gain coefficient, α , times plasma length, L , versus atomic number for ions of the carbon isoelectronic sequence at a temperature of one-fourth the ionization potential (for most cases). Solid curves are plotted for various practical electron density (N_e)/plasma diameter (d) combinations. The required plasma particle kinetic energy plus ionization energy is indicated for each curve. The dashed curve indicates the strong effect on curve (b) of varying the $3s - 3p$ collisional mixing rate by decreasing the effective Gaunt factor from 0.75 to 0.2. Also, the effect of increasing the electron temperature by a factor of four while limiting the ionization rate to maintain an abundance of the carbon-like species equal to one-third the total ion density (as might be the case in a transient heating phase) is indicated for curve (a) by the dotted curve.

Computations were performed for a variety of electron densities and plasma diameters (the size alters the populations through optical depth effects) selected to model conditions presently attainable by plasma discharges or by high-power laser/target interaction. For most of the carbon-like runs, a temperature of one-fourth the ionization potential was selected to assure adequate abundance of the lasing species while still maintaining a high $2p \rightarrow 3p$ pumping rate. Some typical gains calculated for carbon-like ions in a cylindrical plasma of length ten times its diameter are shown in Fig. 1, where curves (a) and (b) represent plasmas created in high-density discharge devices and curves (c) and (d) are typical of smaller high-density laser plasmas. Similar curves generated for helium-like ions under a variety of conditions exhibit population inversion on $3s \rightarrow 2p$ transitions yielding lasing in the 10-50 Å range, but the computed gains in plasmas of reasonable length are two to three orders of magnitude less than those shown in Fig. 1.

*Supported in part by the Defense Advanced Research Projects Agency, DARPA Order 2694.

- [1] Y. Hashino, et al., Jap. J. Appl. Phys. 11, 907 (1972); 12, 470 (1973).
- [2] R. C. Elton, Appl. Opt. 14, 97 (1975).
- [3] R. C. Elton, in Progress in Lasers and Laser Fusion, eds., B. Kursunoglu, A. Perlmutter, and S. M. Widmayer (New York: Plenum Press, 1975).
- [4] T. Holstein, Phys. Rev. 72, 1212 (1947); 83, 1159 (1951).
- [5] R. C. Elton, in Methods of Experimental Physics, Volume 9A, Plasma Physics, eds., H. R. Griem and R. H. Lovberg (New York: Academic Press, 1970) Chapter 4.
- [6] H. R. Griem, Plasma Spectroscopy, (New York: McGraw-Hill, 1964).
- [7] H. J. Kunze, Phys. Rev. A 3, 937 (1971).
- [8] W. L. Wiese, et al., Atomic Transition Probabilities - Volume I: Hydrogen through Neon, NSRDS-NBS-35 (Washington, D.C.: U.S. Government Printing Office, 1971).

SUMMARY

(TYPE DOUBLE SPACE IN A SINGLE PARAGRAPH. ADDRESS SHOULD BE AS BRIEF AS POSSIBLE, BUT SUFFICIENT FOR POSTAL SERVICE.)

"Beam Divergence of Vacuum Ultraviolet Lasers"

(Title of paper. Capitalize only the first letter of each principal word.)

Ronald W. Waynant

(Author)

Optical Sciences Division, Naval Research Laboratory

(Department)

(Institution)

Washington, D.C.

20375

(Number)

(Street)

(City)

(State)

(Zip)

The near field, far field and focusing patterns of vacuum ultraviolet lasers become important when interaction applications are contemplated. Time-integrated studies of the emission patterns from hydrogen at 1600 Å and at 1160 Å, from CO at 1800 Å and from C IV at 1550 Å have been made when these gases were excited by a fast-rising, traveling-wave discharge produced in a flat-plate Blumlein laser. Near-field and far-field intensity distributions were recorded on photographic film using bandpass interference filters and LiF optics. The intensity patterns show a surprisingly complicated structure which proved partially attributable to reflection and interference effects from the dielectric insulator which was tangent to the discharge electrodes. Placement of a rough, non-reflecting dielectric surface over the polyethylene insulator did not completely eliminate the structure. Addition of a second dielectric surface to constrict the discharge from above helped produce some smoothing of the intensity distribution and enabled high-pressure (> 300 Torr) operation of H₂ with an accompanying higher power. This constriction made no improvement in the output of the other materials.

Annual Meeting of the Optical Society of America; J. Opt. Soc. Am. (1976)

Abstract Submitted
For the International Conference on the Physics of
X-ray Spectra.

Aug. 30 - Sept. 2 1976

K X-RAY EMISSION SPECTRA FROM A HIGH POWER-DENSITY PLASMA

Tong-Nyong Lee
U.S. Naval Research Laboratory
Washington, D.C. 20375

ABSTRACT

A laser-triggered vacuum spark discharge¹ generates one or more small (10^{-7} - 10^{-8} cm³), high temperature ($\sim 10^6$ K) plasmas. The x-ray energy density (in both line and bremsstrahlung radiation) in such a plasma volume reaches a value of $\sim 10^5$ J/cm³ in a time interval of about 10^{-9} sec, giving a power density of $\sim 10^5$ watts/cm³. K-x-ray emission spectra obtained from the plasma include a number of K α -type ($2p \rightarrow 1s$) transition lines arising from Fe II through Fe XXIII ions in addition to relatively strong He-like Fe XXV $1s2p \rightarrow 1s^2$ and Li-like Fe XXIV $1s2\ell2p \rightarrow 1s^22\ell$ transition lines. Particularly strong is what appears to be a blend of K α -type lines arising from ions in stages below Fe XVIII. The purpose of the study is to identify the particular stages of ionization which contribute predominantly to this K α -line blend. The line intensity ratios between K α ($2p \rightarrow 1s$) and K β ($3p \rightarrow 1s$) type transition lines are determined respectively from the x-ray spectra which are obtained using a flat LiF crystal diffractometer. Since the minute plasma often accompanies less hot plasma components, a spatially resolved spectrum with a single discharge exposure is required in order to avoid ambiguity. Present results suggest that the strong blended feature emitted by the high energy-density plasma is predominantly due to Fe XVIII $1s2s^22p^6 - 1s^22s^22p^5$ transitions as evidenced by unusually weak K β -type lines. The upper state of this transition is believed to be populated by the innershell ionization of the closed shell Ne-like Fe XVII ions rather than the dielectronic recombination process because of the extremely weak Fe XIX-K α line.

¹T. N. Lee, Astrophys. J. 190 467 (1974)

T. N. Lee
Code 5520
Naval Research Laboratory
Washington, D.C. 20375

SUMMARY

(TYPE DOUBLE SPACE IN A SINGLE PARAGRAPH. ADDRESS SHOULD BE AS BRIEF AS POSSIBLE, BUT SUFFICIENT FOR POSTAL SERVICE.)

"Time-Dependent Calculations of Harmonic Conversion from 532 nm to 266 nm in ADP"
(Title of paper. Capitalize only the first letter of each principal word.)

R. C. Eckardt and J. Reintjes

(Author)

Optical Sciences Division, Naval Research Laboratory

(Department)

(Institution)

Washington, D.C.

20375

(Number)

(Street)

(City)

(State)

(Zip)

Time-dependent calculations of harmonic generation with dispersion and depletion of the pump pulse are presented. Conversion of intense, 30 psec duration pulses from 532 nm to 266 nm in ADP is considered. Numerical solutions of the coupled propagation equations for harmonic generation were obtained using a second-order Runge-Kutta method and fast Fourier transforms. The difference of group velocities causes the more slowly propagating harmonic pulse to "walk through" the fundamental pulse. The presence of phase modulation on the input pulse or central frequency phase mismatch then disturbs the phase relationship between harmonic and fundamental, causing the harmonic pulse to drive the fundamental pulse through the inverse parametric process. The result is limitation of conversion efficiency, generation of new frequencies, and distortion of both the harmonic and transmitted fundamental pulses. The calculations showed that either intensity-dependent phase modulation with a peak value of 0.4π or phase mismatch of $\Delta k = 0.1\pi \text{ cm}^{-1}$ would reduce conversion efficiency of a 10^9 W/cm^2 peak intensity pulse to 26% in a 2 cm crystal length after a peak conversion of 88% had been reached at 1 cm crystal length. Only in the case of perfect phase matching with no phase modulation does the conversion efficiency increase monotonically.

Annual Meeting of the Optical Society of America; J. Opt. Soc. Am. (1976)

SUMMARY

(TYPE DOUBLE SPACE IN A SINGLE PARAGRAPH. ADDRESS SHOULD BE AS BRIEF AS POSSIBLE, BUT SUFFICIENT FOR POSTAL SERVICE.)



"High-Efficiency Harmonic Conversion to 266 nm in ADP and KD*P"
(Title of paper. Capitalize only the first letter of each principal word.)

J. Reintjes (introduced by R. C. Eckardt) and R. C. Eckardt
(Author)
Optical Sciences Division, Naval Research Laboratory
(Department) (Institution)
Washington, D.C. 20375
(Number) (Street) (City) (State) (Zip)

We present results of an experimental study of high-efficiency second-harmonic generation in KD*P and ADP from 532 nm to 266 nm using frequency-doubled pulses from a mode-locked Nd:YAG laser. We have made measurements of conversion efficiency as a function of crystal length, input power, and wavelength, and have investigated the effects of nonlinear absorption and phase modulation on conversion efficiency. In addition, we present the first quantitative measurements of two-photon absorption at 266 nm in these materials. Measurements of conversion vs crystal length show decreasing efficiency beyond an optimum length. Such observations have been used elsewhere to infer the importance of nonlinear absorption. Our simultaneous measurements of transmitted fundamental and harmonic energies show no evidence of optical losses. Spectral measurements show that the limited conversion in long crystals ($l > 1$ cm) is due to group velocity dispersion in the crystal combined with small amounts of phase modulation on the pump pulse. Conversion was then measured in short crystals where these effects are minimal and efficiency up to 85% was observed. The measurements are in excellent agreement with theoretically calculated conversion efficiencies. Measurements of two-photon absorption shows that it should not be effective in limiting conversion below about 80%.

Annual Meeting of the Optical Society of America; J. Opt. Soc. Am. (1976)



Abstract Submitted

for the 18th Annual Plasma Physics Meeting of the

American Physical Society

Nov. 15-19 1976

Physics and Astronomy
Classification Scheme
Number 52.70

Bulletin Subject Heading
in which Paper should be placed
32. Diagnostics

X-Ray Spectra of Multiply Ionized High-Z Atoms From a Vacuum-Spark Plasma. T. N. LEE and R. C. ELTON, Naval Research Lab.--Newly observed x-ray emission lines arising from highly stripped high-Z atoms are obtained from a single-discharge spectroscopy on a laser-pulse triggered two-electrode vacuum spark discharge¹. The spectra obtained include the H-like Lyman- α line of the Zn XXX ion as well as the He-like resonance line of the Zn XXIX ion and its satellite lines. Because of the rare occurrence of such ions, these lines have apparently been obscured in previous multiple exposure data. The x-ray spectrometer used consists simply of a LiF analyzing crystal and a slit (150-500 μm in width) placed at the x-ray window and oriented perpendicular to the discharge axis in order to obtain spatial resolution. The spectra were recorded on Polaroid film in a XR-7 mount. The spectral lines arising from highly ionized atoms originate from one or more minute plasmas ($\leq 25 \mu\text{m}$ in size) with a power density as high as 10^{15} W/cm^2 . The probability of forming such minute plasma in a discharge is found to decrease rapidly with the increase of atomic number of plasma ions.

¹T. N. Lee, *Astrophys. J.*, 190, 467 (1974).

Submitted by

T. N. Lee

T. N. LEE

Naval Research Laboratory, Code 5520

Washington, D.C. 20375

Note: We would like to present this paper as a ten-minute talk.

POSTDEADLINE ABSTRACT

To be presented as part of first review paper in Session 11

Observation of Coherent Radiation at 53.22 nm
by Fifth Harmonic Conversion*

J. Reintjes, R. C. Eckardt, C. Y. She,
N. E. Karangelen, and R. A. Andrews

Naval Research Laboratory
Washington, D.C. 20375

We report observation of coherent radiation at 53.22 nm, the shortest wavelength at which coherent radiation has been reported. It was generated in He and Ne at pressures of 40 torr by four-photon, resonantly enhanced fifth harmonic conversion of mode-locked laser pulses at 266.1 nm (the fourth harmonic of a Nd:YAG laser). The pump radiation was focused with a 10 cm calcium fluoride lens to a spot size of $\sim 10 \mu\text{m}$ at the center of a 500 μm diameter aperture which replaced the entrance slit of a normal incidence vacuum spectrometer. The radiation at 53.22 nm was observed both photoelectrically (with an EMI photomultiplier and a sodium salicylate scintillator) and photographically (on Kodak 101-01 film). The estimated conversion efficiency is in the range of 10^{-7} for a focused intensity at 266.1 nm of $3 \times 10^{14} \text{ W/cm}^2$. The generation of coherent radiation at 38 nm with seventh order mixing processes will also be discussed.

*This work was supported in part by the Defense Advance Research Projects Agency under DARPA Order 2694.

"Generation of Coherent Radiation at 38 nm and 53 nm
Using High-Order Optical Nonlinearities"*

J. Reintjes (introduced by R. C. Eckardt), C. Y. She, R. C. Eckardt,
N. E. Karangelen, R. C. Elton, and R. A. Andrews

Naval Research Laboratory
Washington, D.C. 20375

The generation of coherent vacuum ultraviolet radiation by means of optical frequency upconversion using third order nonlinearities has attracted considerable interest in recent years. The use of higher order nonlinear processes is especially attractive for the generation of coherent radiation at wavelengths in the extreme ultraviolet because such interactions allow larger steps along the frequency scale to be taken. Recently, we have reported preliminary observations of coherent light generated at 53.2 nm by fifth harmonic conversion of laser pulses at 266.1 nm. In this paper we announce the extension of available coherent radiation to 38.0 nm through seventh harmonic conversion of the 266.1 nm pulses in helium. This is the shortest wavelength coherent radiation reported to date. In addition, we describe further investigations of the fifth harmonic conversion at 53.2 nm. The conversion efficiency is now in the 10^{-5} to 10^{-6} range, about ten times larger than our earlier measurements. We have observed fifth harmonic conversion in argon in addition to helium and neon, with signal strengths comparable to those generated in neon. Finally, we report the generation of coherent light at 59.1 nm in helium, resulting from a combination of four photons at 266.1 nm and one photon at 532.2 nm.

*Work supported in part by Defense Advanced Research Projects Agency under ARPA Order 2694.

SUMMARY

"Generation of Coherent Radiation at 38 nm and 53 nm Using High-Order Optical Nonlinearities"*

J. Reintjes, C. Y. She, R. C. Eckardt,
N. E. Karangelen, R. C. Elton, and R. A. Andrews
Naval Research Laboratory
Washington, D.C. 20375

Optical frequency upconversion has proven to be an important method for generating coherent radiation in the vacuum ultraviolet region of the spectrum¹. Third order processes (chiefly third harmonic generation) have been used to generate coherent light at wavelengths as short as 57 nm². The use of higher order nonlinearities has been proposed for generation of light at still shorter wavelengths since such interactions allow larger steps along the frequency scale to be made in a single conversion process³.

In this paper we describe experimental investigations of fifth and seventh order frequency conversion processes in the rare gases. We report the generation of coherent radiation at 38.0 nm in helium through seventh harmonic conversion of laser pulses at 266.1 nm. This is the shortest wavelength coherent radiation reported to date. This work also represents the first observation of a seventh order frequency conversion process. We have previously reported⁴ preliminary observations of fifth harmonic conversion of the 266.1 nm pulses to 53.2 nm in helium and neon. Here we described a more detailed study of this process, reporting an increase of tenfold in conversion efficiency and extension of our observation to conversion in argon. Finally, we report the generation of more frequencies in this region of the spectrum through six wave mixing processes utilizing other harmonics of the Nd YAG laser radiation.

*Work supported in part by Defense Advanced Research Projects Agency under ARPA Order 2694.

The pump pulses for these experiments were derived from a mode-locked Nd:YAG laser operating at $1.06\text{ }\mu\text{m}$ followed by two successive stages of second-harmonic generation with about 70% conversion in each stage. Quartz prisms were used to separate the fourth-harmonic pulses from the fundamental and second-harmonic pulses. The pump pulses entered a sample cell through a MgF_2 window. The cell was attached to a 1 m normal incidence vacuum spectrometer which was equipped with a 1200 g/mm aluminum grating. A CaF_2 lens was used to focus the radiation at the center of a $500\text{ }\mu\text{m}$ diameter aperture which replaced the entrance slit of the spectrometer. The gas used for nonlinear mixing was flowed into the cell and was differentially pumped behind the entrance aperture. The energy in the pump pulses was measured with a calibrated joule meter after the focusing lens, indicating a peak power of 330 MW.

In our previous experiments on fifth harmonic conversion to 53.2 nm we recorded the fifth harmonic signal on Kodak 101-01 film through a single $1200\text{ }\text{\AA}$ thick Al filter. In the current experiments we have used an EMI 9750 QA photomultiplier and a sodium salicylate scintillator along with two Al windows for detection. The photoelectric detection allows us to obtain quantitative comparison of signals and is more sensitive than the film at 38 nm where the reflectivity of the Al grating is quite low.

Seventh harmonic conversion to 38 nm was observed in helium at a pressure of 60 torr with a focused beam intensity at 266.1 nm of about 10^{15} W/cm^2 . Helium is of course transparent to the pump radiation at 266.1 nm while the generated radiation lies in the photoionizing continuum approximately 65000 cm^{-1} above the discrete series limit. The absorption cross section

of 4 Mb at this wavelength results in an absorption length of 1 mm, slightly longer than the confocal parameter of 0.5 mm of the pumping beam.

A coarse survey with a 2 mm exit slit showed radiation only in a narrow region near 38 nm. Wavelength identification was then done by varying the spectrometer wavelength setting around 38 nm while using an exit slit width of 150 μm , corresponding to a full spectral width of about 0.1 nm. Absolute calibration of the spectrometer dial to an accuracy of $\pm .05$ nm was done with a He discharge spectrum. Photoelectric signals were observed when the spectrometer was tuned to 38.02 nm. No signals were detected when the spectrometer was tuned by .07 nm to either side. This behavior indicated that the observed radiation consisted of a single narrow line at 38.02 nm, in good agreement with the expected value of 38.03 nm. No signals were observed either when the cell was evacuated or when the helium pressure was dropped below 40 torr. A preliminary survey also showed no detectable seventh harmonic signals in neon.

We have also extended our study of fifth harmonic conversion to 53.2 nm in the rare gases. Conversion efficiency in helium is now in the range of 10^{-6} to 10^{-5} , about ten times larger than our original measurements. This increase was obtained through use of a shorter focusing lens, which raised the focused intensity to 10^{15} W/cm². We have also observed fifth harmonic conversion in argon in addition to helium and neon. There is a near three photon resonance in argon between the pump radiation and the $3p^6 - 3d[3\frac{1}{2}]^0 J=3$ transition. Conversion in argon appeared to be comparable to that in neon.

It is possible to generate other wavelengths in this region of the XUV through six wave mixing processes utilizing other harmonics of the Nd:YAG

laser. As a preliminary step in this direction we have successfully generated the eighteenth harmonic of the YAG radiation at 59.1 nm in neon. This was done by combining four photons at 266.1 nm with one photon at 532.2 nm in Ne. This wavelength lies in a transparent region of the neon spectrum below the continuum. For these measurements, the dispersing prisms were removed and the entire beam was sent into the spectrometer. The experimental detection was done with the photomultiplier in a manner similar to that described for seventh harmonic detection. Again a single narrow spectral feature was observed centered on the expected wavelength of 59.1 nm. The conversion level was below that for the fifth harmonic, presumably because of the reduced intensity of the laser second harmonic at 532 nm.

REFERENCES

1. A. H. Kung, J. F. Young, G. C. Bjorklund and S. E. Harris, Phys. Rev. Lett. 29, 985 (1972); R. T. Hodgson, P. P. Sorokin and J. J. Wynne, Phys. Rev. Lett. 32, 343 (1974); A. H. Kung, Appl. Phys. Lett. 25, 653 (1974).
2. M. H. R. Hutchinson, C. C. Ling and D. J. Bradley, Postdeadline Paper S.1, IXth International Quantum Electronics Conference, Amsterdam, The Netherlands, 1976.
3. S. E. Harris, Phys. Rev. Lett. 31, 341 (1973).
4. International Conference on the Physics of X-Ray Spectra, National Bureau of Standards, Gaithersburg, Md., August 1976.

Requirements, Methods and Results for Absolute Radiometry from
Extended Sources in the 12-25 Å and 500-3000 Å Spectral Regions

R. C. Elton

Naval Research Laboratory
Washington, D.C. 20375

Techniques developed at the Naval Research Laboratory for intensity calibration of instrumentation in the vacuum ultraviolet and soft x-ray spectral regions will be described. The emphasis will be placed on in-situ techniques from extended radiation sources.

Emission Measurements in the 3 \AA Region from a Point
Plasma Source with Potential as a Transfer Standard

T. N. Lee

Naval Research Laboratory
Washington, D.C. 20375

The utility of concentrated small plasmas as intense sources of short-wavelength radiation for point source radiometry will be discussed. The utility as secondary calibration standards will also be point out.

Short-Wavelength Laser Calculations for Electron Pumping
in Carbon-Like and Helium-Like Ions

L. J. Palumbo and R. C. Elton
Naval Research Laboratory
Washington, D.C. 20375

A steady-state computer code has been used to compute population densities of excited terms in carbon-like and helium-like ions. It is shown that an inversion between terms of the $1s^2 2s^2 2p^3 p$ and $1s^2 2s^2 2p^3 s$ configurations sufficient to produce observable laser gain can be obtained in high-density plasmas such as produced by laser irradiation of pellets or electromagnetically driven pinch discharges. Such inversions in elements of atomic number $Z = 15-40$ give rise to lasing in the 1200-300 Å range. Shorter wavelength lasing (80-5 Å) on $1s^3 s \rightarrow 1s^2 p$ transitions in helium-like ions of $Z = 10-40$ is also modeled; but significant gain is probably not possible with current plasma devices.

I. INTRODUCTION

An intense effort has been underway for the past several years to find methods for generating coherent radiation at wavelengths shorter than 1000 \AA , as is evidenced by the large number of experimental and theoretical publications in this field. Details are treated in a recent review paper¹ and in references therein. Barring some fortuitous discovery, short-wavelength lasing will most likely be attained by a progressive step-by-step process, possibly working from known lasing schemes in the UV to shorter and shorter wavelengths into the soft x-ray spectral region. A straightforward approach would be the isoelectronic extrapolation of a known lasing scheme in the visible or near-UV involving a neutral atom or a low stage of ionization²⁻⁴, and attaining vacuum-UV lasing using higher stages of ionization as created in a plasma. As a precedent, a number of ions have recently been shown⁵ to lase in the near-UV region in Z-pinch plasma devices; extrapolation to non-cavity amplification is the first challenge.

This article reports on a scheme for achieving lasing below the 1000 \AA "barrier" by the isoelectronic extrapolation of a transition which is responsible for a large number of known visible and near-UV ion lasers, many of which have been shown to lase in the cw mode, i.e., with steady-state population inversion. This is of great importance for vacuum-UV lasers, where self-terminating inversions require very short pump risetimes^{1,6}. The method and results reported here represent primarily a refinement of previous analytical calculations for $3p \rightarrow 3s$ lasing in six-electron carbon-like ions, following electron collisional pumping from a $2p$ ground state reservoir⁷. Initial extrapolations to high densities⁸ are expanded upon. Also, the multiple ionic energy levels and the atomic transitions between them are considered in increased detail here through the use of a computer program which solves coupled steady-state rate equations to obtain energy-level population densities for given plasma conditions. The addition of ionization and recombination, as well as radiative trapping, represent other important advances in the present results.

Because of the close similarity between the carbon-like scheme and another electron-collisional pumping scheme involving $3s \rightarrow 2p$ lasing (collisionally pumped $1s \rightarrow 3s$) in the $30\text{-}100 \text{ \AA}$ range in moderate-Z helium-like ions, the computer code developed for the carbon-like ions was also used to model this two-electron

scheme. Although population inversions were computed and are presented for a wide range of plasma conditions and for a number of elements in the helium isoelectronic sequence, the resulting net gain calculated is insignificant at densities and dimensions available in state-of-the-art plasma devices.

Both of these schemes operate over transitions of insufficient energy to cause photoionization losses in the amplifying medium, in contrast to innershell schemes proposed for short-wavelength lasing where such losses can be the limiting factor^{1,9}.

Descriptions of the physical model and computer code are given in the next section, results for the carbon-like and helium-like schemes are presented and described in Section III, and the feasibility of these schemes for producing short-wavelength lasing is discussed briefly in Section IV.

II. NUMERICAL MODEL

A. Pumping Scheme

As diagrammed in Fig. 1 for the six-electron carbon-like species and mentioned in the Introduction, the $3p\ ^3D$ upper laser term is assumed⁷ to be pumped by electron collisional excitation from the $2p\ ^3P$ ground term on the same ion¹⁰. Radiative coupling of these two terms is dipole forbidden, so that spontaneous and stimulated emission into the $3s\ ^3P$ lower laser term is favored. Also, the population density in this latter term is rapidly depleted to the $2p\ ^3P$ ground "reservoir" term by dipole decay, resulting in a possible steady-state population inversion and quasi-cw lasing. The terminology "quasi" here refers to possible transient lasing conditions associated with environmental plasma changes; and not to self-termination often associated with short-wavelength laser schemes and caused by lack of either lower laser term depletion or reservoir state replenishment. The latter is a common problem with many schemes based upon pumping by ionization or recombination and is eliminated in a single-ion scheme such as modeled here, where the initial reservoir term is rapidly replenished by dipole decay from the lower laser term, with continuous lasing resulting.

At the increased densities required for amplification without multiple pass cavities, collisional mixing between terms becomes an important process competing with radiative transitions, and the nearby $3d\ ^3D$ term is the most important. This term is strongly dipole coupled to the ground term (as is the lower laser term) and is included in the modeling. This strong radiative coupling also requires the inclusion of resonance trapping effects for both terms in the numerical model. The total density of lasing ions in the plasma, and hence the net gain, would be affected by significant ionization or recombination. For example, at the high temperatures desired for large collisional pumping the former is a concern for creating significant densities of boron-like ions. Hence, ionization and recombination rates between carbon-like and boron-like ions are included.

In close analogy to this $3p \rightarrow 3s$ model, the $3s\ ^1S$ term in helium-like ions is assumed to be pumped from the $1s\ ^1S$ ground term by collisions, with lasing taking place on $3s\ ^1S \rightarrow 2p\ ^1P$ transitions followed by rapid $2p\ ^1P \rightarrow 1s^2\ ^1S$ resonance decay. The detailed term structure is shown in Fig. 2.

B. Rate Equation Code

In the most general case, the populations of the excited and ground levels of an atomic species in a plasma can be determined at each point in time by the simultaneous solution of a set of rate equations which express the time rate of change of the population density of each atomic energy level as the sum of the rates which populate this level by transitions from all other levels, minus the sum of the rates which reduce the population of the given level by transitions into all other (higher or lower) levels. If the rate at which plasma conditions (temperature and density) change is much smaller than the dominant transition rates in the time-dependent rate equations, then each rate of population density change can be neglected (set to zero); this yields a coupled set of time-independent or steady-state rate equations, each of the form

$$\frac{dN_k}{dt} = 0 = \sum_{j \neq k} N_j W_{jk} - N_k \sum_{j \neq k} W_{kj}, \quad (1)$$

where t is the time, N_j and N_k are population densities of levels j and k ,

and W_{jk} (similarly for W_{kj}) represents the sum of the rates for all atomic processes which populate level k from level j . An equation of type (1) is required for each level, k , considered. In general, levels j and k may be in the same or in different ionization stages, and the W 's are functions of the ionization species, the temperature, the density, and the radiation field intensity at each point in the plasma.

For a precise dynamical plasma model, one must solve a large set of time-dependent rate equations, taking into account all important excited and ground levels for each stage of ionization of each element found in the plasma. All significant atomic processes affecting the population densities of these levels (including ionization and recombination) must be included in the computation, as well as the possibility that the populations may vary not only temporally but also spatially due to boundary effects, plasma motion, plasma structure, radiation transport, etc. It was not the aim of the present effort to produce such a full-scale plasma model. Rather, the purpose was to introduce certain simplifying plasma assumptions into a model to estimate the conditions required to produce population inversions in plasma ions, to look for optimum plasma conditions, to identify promising elements and ionization stages for producing lasing in existing plasmas, and to gain physical insight into the processes resulting in or hindering the achievement of short-wavelength lasing in highly stripped ions.

In the present code, the population densities of the levels of interest and the electron and ion densities are assumed to be spatially homogeneous; they are also assumed to be time independent in order to avoid the solution of a set of coupled differential equations, rendered nonlinear by the inclusion of radiation trapping as discussed below. Thus the inversion and gain computed here would be valid for a homogeneous portion of a larger plasma and would be applicable to plasmas which maintain their conditions for a reasonably long time. Similarly, all other relevant plasma parameters, such as the electron temperature, T_e , and the ion temperature, T_i (which is assumed in most cases to be equal to T_e under the equilibrium conditions achieved rapidly at high densities), are assumed constant in time. Plasmas in existing devices which satisfy this condition are mentioned below.

The credibility of the present calculations is enhanced by the agreement between the results reported here and experimental results⁵ for similar ionic configurations. In a sense, the present steady-state model yields mainly minimum lasing requirements. Transient conditions can be defined during a heating phase in which enhanced inversion densities (and gains) can be achieved at higher temperatures before significant ionizing depopulation of the desired species occurs; this possibility is analyzed below for the carbon-like ions.

It should be noted here that although the present analysis for $3p \rightarrow 3s$ lasing concentrates on carbon-like ions, the computed population inversions and gain should be comparable for $3p \rightarrow 3s$ transitions in the boron-like through the neon-like sequences, i.e., where $2p$ valence electrons exist. The six-electron ion was chosen as a model because it was expected⁷ to produce slightly (but not significantly) more gain than other ions of more or fewer electrons. In fact, boron-like ions may produce a simpler spectrum, and neon-like ions may be advantageous due to the extended lifetime association with rare gas type ionic species of increased ionization energy¹¹.

The set of equations (1) is solved when reduced to a finite and tractable number by considering only the most relevant levels in the carbon-like or helium-like ion. For the triplet terms in the carbon-like ion, the levels corresponding to a particular J value are assumed to be populated in proportion to their statistical weights. This is plausible since collisional mixing is rapid between these closely spaced levels for the large electron densities required to achieve observable single-pass gain along the small plasma lengths attainable with present-day devices. Hence, in computing the carbon-like population densities, the levels of a given term are lumped together and the averaged term-to-term transition rates are used in Eq. (1). However, because the width of the lasing line is less than the $3p \rightarrow 3s$ multiplet splitting, the gain is computed only for the strongest component of the multiplet. Also, only those terms of the ground and excited configurations which are expected to have the largest effect on the population inversion are considered. The energy levels and the important transitions between them are included in Figs. 1 and 2.

Thus, a coupled set of five equations of type (1) are solved for population densities of the following carbon-like terms, where the numbers in parentheses are the respective subscripts used in subsequent equations and in Fig. 1: (1) the ground term, $2p^2\ ^3P$; (2) the lower laser term, $2p3s\ ^3P$; (3) the upper laser term, $2p3p\ ^3D$; (4) the nearest competing term, $2p3d\ ^3D$; and (5) the ground term of the next higher ionization stage (boron-like ion). Transitions from the ground term into other excited triplet terms deplete the ground reservoir term population by at most a few percent for the conditions which show appreciable population inversion, and are thus ignored. The three terms of the ground configuration of the carbon-like ions (under most plasma conditions of interest here) contain most of the population, and it is assumed that this population is divided among these terms in proportion to their statistical weights; with 60% [P in Eq. (17)] of the total population density in the triplet system (shared by the 3P ground term and the sparsely populated excited triplet terms) and the remainder shared between the $2p^2\ ^1S$, $2p^2\ ^1D$, and excited singlet terms. The total ion density is tied to the electron density through charge neutrality.

Because it is desired to operate at a high temperature for maximum pumping, only ionization equilibrium with the next higher ionic species is considered. The gain is optimized by selecting a temperature for rapid pumping without excessive lasing-species depletion by ionization. Analogously, for the helium-like ions, a set of five coupled rate equations is solved with subscripts 1 through 5 designating the following singlet terms: (1) the ground term, $1s^2\ ^1S$; (2) the lower laser term, $2p\ ^1P$; (3) the upper laser term, $3s\ ^1S$; (4) the nearest competing term, $3p\ ^1P$; and (5) the $1s\ ^2S$ ground term of the next higher (hydrogenic) ionization stage. The fraction of the total helium-like ion density which occupies the triplet system is expected to be small for the high Z 's and high densities considered here.

C. Rates Applied

In computing the rates (W 's) in Eq. (1), estimates of all important collisional radiative processes between the five terms mentioned above were included where applicable. Specifically included for the lasing ion were electron-collisional excitation and deexcitation, electron-collisional ionization and

(three-body) recombination, spontaneous photoemission, photoabsorption (through a radiation trapping treatment), and radiative recombination. Photoionization was negligible in all important cases here. For efficient computation, simple analytical estimates for the rates of the various atomic processes were used in place of more accurate quantum mechanical calculations or published tabulations of such results (which are not available for all transitions, species, and ionization stages required in the present study). Most of these analytical formulas were obtained from collections included in References 12-14. A Maxwellian velocity distribution of electrons was assumed to hold for all calculations.

1. Excitation and Deexcitation

For the numerous transitions and ions included, the convenient¹⁵ effective Gaunt factor, or \bar{g} , analytical formula of Seaton¹⁶ and Van Regemorter¹⁷ was used to compute the collisional excitation rate, C_{jk} , for transitions from lower level j to upper level k

$$C_{jk} = N_e X_{jk} = 64\pi^2 \left(\frac{\pi}{3}\right)^{\frac{1}{2}} \frac{E_H}{h} a_0^3 N_e \left(\frac{E_H}{kT_e}\right)^{\frac{1}{2}} \left(\frac{E_H}{\Delta E_{jk}}\right) \times \quad (2)$$

$$f_{jk} <\bar{g}>_{jk} \exp(-\Delta E_{jk}/kT_e),$$

where N_e is the electron density, X_{jk} is the collisional excitation rate coefficient, h is Planck's constant, a_0 is the radius of the first Bohr orbit, E_H is the ionization potential of ground-state hydrogen (13.6 eV), k is the Boltzmann constant, T_e is the electron temperature, ΔE_{jk} is the energy gap between levels j and k , f_{jk} is the absorption oscillator strength for $j \rightarrow k$ transitions, and $<\bar{g}>$ is a Maxwellian-averaged effective Gaunt factor. The rates for collisional deexcitation, D_{kj} were computed from the rates for collisional excitation through detailed balancing,

$$D_{kj} = N_e X_{kj} = \frac{g_j}{g_k} C_{jk} \exp(\Delta E_{jk}/kT_e), \quad (3)$$

where X_{kj} is the collisional deexcitation rate coefficient and g_j and g_k are the statistical weights of levels j and k , respectively.

The energy-level spacings, ΔE_{jk} , were approximated by scaling either as z^2 or z for levels j and k of different or same principal quantum number, respectively, where z is the spectrum number or the charge seen by the outer (optical) electron. Scaling coefficients were estimated from tabulated energy levels^{18,19} and spectral lines²⁰, and the ΔE 's should be accurate to better than 15%. The oscillator strengths required for the modeling of the carbon-like scheme were assumed²¹ to be constant along the isoelectronic sequence for $\Delta n \neq 0$ transitions and to vary as Z^{-1} (where Z is the nuclear charge) for $\Delta n = 0$ transitions, with values extrapolated from limited data for low ionization stages published by Wiese, et al¹⁸. The more abundant data¹⁸ on helium-like ions allow the use of a much more accurate oscillator-strength estimate varying linearly with Z^{-1} . The Gaunt factor, $\langle \bar{g} \rangle_{jk}$, is a function of $x \equiv \Delta E_{jk}/kT_e$ obtained earlier from an empirical fit^{12,16,17} to existing data. An accumulation of experimental and theoretical results for scattered cases^{16,22} indicates that this empirical fit is approximately correct for $n=2$ to $n=3$ transitions. Thus, the data can be fitted in the relevant range of $x = 0.04$ to 1.0 by a power law expression,

$$\langle \bar{g} \rangle_{jk} = \alpha x^{-\beta}, \quad (4)$$

with $\alpha = 0.17$ and $\beta = 0.47$. For $x \geq 1.0$, a constant value of 0.17 is assumed. For $n=3$, $\Delta n=0$ transitions, it has become clear that the Gaunt factor is higher and, for the relevant range of $0.01 \leq x \leq 0.7$, a similar relation is assumed with $\alpha = 0.63$ and $\beta = 0.15$. This latter fit also appears to be approximately correct for the helium-like ion resonance transitions $n=1$ to $n=2,3$ which involve the $x = 0.1 - 1.0$ range. These expressions for $\langle \bar{g} \rangle_{jk}$ cannot be expected to be more accurate than a factor of two at present, and the separate expressions assumed are only significant for the larger values of x , where a common averaged expression would lead to an overly optimistic gain resulting from increased collisional pumping and decreased $n=3$ mixing.

The adopted oscillator strengths, Gaunt factors, and energy-level scaling relations are listed in Table 1. For computing the collisional excitation and deexcitation rates for the $\Delta n=1$ "dipole-forbidden" $2p^3P \rightarrow 3p^3D$ transition between terms of the same parity, Eqs. (2) through (4) were used with an oscillator strength assumed equal to that for the analogous $2p^3P \rightarrow 3s^3P$ dipole-allowed transition, so chosen according to guidance from both theoretical and experimental results²². For the $\Delta n=0$ quadrupole $3s^3P \rightarrow 3d^3D$ excitation rate both zero and a value equal to the $3s^3P \rightarrow 3p^3D$ dipole rate were assumed, as the true value is uncertain for the small energy gap involved. The effect on the computed peak gain values was $\leq 20\%$, so that a zero value was used.

2. Radiative Decay with Opacity

Spontaneous radiative decay rates, A_{kj} , were computed from the absorption oscillator strengths f_{jk} , by¹⁸

$$g_k A_{kj} = 8\pi^2 \frac{c r_0}{\lambda_{kj}^2} g_j f_{jk}, \quad (5)$$

where c is the velocity of light, r_0 is the classical electron radius, and λ_{kj} is the wavelength of the radiation emitted in a spontaneous transition from k to j . Induced emission²³ terms, $I_{\nu kj}$, can be ignored for $n=3$ to $n=2$ resonance transitions because $I_{\nu kj}/A_{kj} = [(g_k N_j / g_j N_k) - 1]^{-1} \approx 0.15$, for $\Delta E_{jk}/kT_e \approx 2$ at $kT_e = 1.0 \text{ eV}$. This is also the case for transitions between $n=3$ terms as long as the plasma is optically thin in the transverse direction, as is calculated for the conditions considered. Resonant photoabsorption in an optically thick plasma can be important in reducing the effective lower-laser-level radiative depletion rate and, hence, destroying the steady-state inversion; consequently, it must be considered in a model of this type. Since the only source of resonant radiation is assumed to be from spontaneous emission, resonant photoabsorption is accounted for by modifying the radiative decay rate with an "escape factor" $F_{kj}(\bar{\tau}_0)$ according to a method originally treated by Biberman²⁴ and Holstein²⁵ and conveniently summarized by McWhirter²³, where

$$F_{kj}(\bar{\tau}_0) = 1 - \frac{1}{\sqrt{\pi}} \int_{-\infty}^{\infty} \exp(-x^2) \{1 - \exp[-\bar{\tau}_0 \exp(-x^2)]\} dx. \quad (6)$$

Here $\bar{\tau}_0$ is the optical depth at line center, which for Doppler-broadened lines²⁶ is given by¹²

$$\bar{\tau}_0 = \left(\frac{\pi M_i c^2}{2kT_i} \right)^{\frac{1}{2}} r_0 \lambda_{kj} N_j f_{jk} r \quad (7)$$

with M_i the mass of the radiating ion, T_i is the ion temperature, and r the plasma radius. The escape factor, which is an inverse function of the optical depth (and hence of the lower-level population density), ranges between zero and unity and reduces the effect of the decay process at large depths. The explicit inclusion of this factor in Eq. (1) makes this set nonlinear, requiring a solution by iterative methods; this dictated a limitation to a reasonable number of levels included in the modeling. Since the optical depth depends upon the physical dimensions of the medium, the plasma diameter became an additional important parameter.

3. Ionization and Recombination

The most convenient formula for computing the rates, I_{j5} , of electron collisional ionization from the ground ($j=1$) and excited terms ($j=2,3,4$), respectively, of the lasing ion into the ground term (5) of the next higher species comes from a semi-empirical formula in a form given by Kunze²⁷ (which fits the data compiled by Lotz²⁸)

$$I_{j5} = 7.5 \times 10^{-8} \frac{qN_e}{\Delta E_{j5}} \left[\left(\frac{40kT_e}{\Delta E_{j5}} \right)^3 + 40 \right] \times \frac{(kT_e)^{\frac{1}{2}}}{\Delta E_{j5} + 3kT_e} \exp(-\Delta E_{j5}/kT_e) \text{ sec}^{-1}, \quad (8)$$

where q is the number of equivalent electrons in the outer shell and ΔE_{j5} is the ionization potential from term j . Both kT_e and ΔE_{j5} are in eV, while N_e is in cm^{-3} . For the helium-like ions, this formula is expected^{27,29} to be accurate to 15% for ground-state ionization and 25% for excited-state ionization. For ions other than hydrogenic and helium-like, this formula overestimates the

ionization rate by approximately a factor-of-two²⁹, and this correction was included in the carbon-like ion modeling. Rates for collisional (three-body) recombination, R_{5j}^c , into ground and excited terms were deduced from Eq. (8) using detailed balancing and the Saha relation to give

$$R_{5j}^c = \left(\frac{N_j}{N_5} \right)_{eq} I_{j5} = \frac{g_j}{g_5} \frac{h^3 N_e \exp(\Delta E_{j5}/kT_e)}{2 (2\pi m_e kT_e)^{3/2}} I_{j5}, \quad (9)$$

where $(N_j/N_5)_{eq}$ is the thermal equilibrium population ratio and m_e is the electron mass.

The rate of radiative recombination, R_{5j}^r , into either ground or excited terms is adopted from a formulation due to Griem³⁰ for the total recombination rate into hydrogenic levels of a given principal quantum number, n , with appropriate corrections through a multiplicative factor Q_j for nonhydrogenic behavior of the ground terms and for statistical weight partitioning into the various terms. The rate is given by

$$R_{5j}^r = \frac{64}{3} \left(\frac{\pi}{3} \right)^{1/2} N_e r_o^2 c z Q_j x^{3/2} E_1(x) \exp(x), \quad j=1,2,3,4, \quad (10)$$

where $x = \Delta E_{j5}/kT_e$ and $E_1(x)$ is the exponential integral of index one. The total recombination rate, R_{5j} , into term j is defined by

$$R_{5j} \equiv R_{5j}^c + R_{5j}^r. \quad (11)$$

4. Ion Collisional Rates

The rates for the important excitation and deexcitation processes due to ion collisions were estimated from the above electron collisional rates using a "guillotine factor" approach described by Weisheit¹³ and were found to be negligible for all conditions considered in the present modeling.

D. Explicit Rate Equations

Using the atomic rates defined in the above equations, one can write Eq. (1) explicitly:

$$\frac{dN_1}{dt} = 0 = -N_1 (C_{12} + C_{13} + C_{14} + I_{15}) + N_2 (A_{21} F_{21} + D_{21}) \quad (12)$$

$$+ N_3 D_{31} + N_4 (A_{41} F_{41} + D_{41}) + N_5 R_{51},$$

$$\frac{dN_2}{dt} = 0 = -N_2 (A_{21} F_{21} + D_{21} + C_{23} + C_{24} + I_{25}) + N_1 C_{12} \quad (13)$$

$$+ N_3 (A_{32} F_{32} + D_{32}) + N_4 D_{42} + N_5 R_{52},$$

$$\frac{dN_3}{dt} = 0 = -N_3 (D_{31} + A_{32} F_{32} + D_{32} + C_{34} + I_{35}) + N_1 C_{13} + N_2 C_{23} \quad (14)$$

$$+ N_4 (A_{43} F_{43} + D_{43}) + N_5 R_{53},$$

$$\frac{dN_4}{dt} = 0 = -N_4 (A_{41} F_{41} + D_{41} + D_{42} + A_{43} F_{43} + D_{43} + I_{45}) \quad (15)$$

$$+ N_1 C_{14} + N_2 C_{24} + N_3 C_{34} + N_5 R_{54},$$

and

$$\frac{dN_5}{dt} = 0 = -N_5 (R_{51} + R_{52} + R_{53} + R_{54}) + N_1 I_{15} \quad (16)$$

$$+ N_2 I_{25} + N_3 I_{35} + N_4 I_{45}.$$

These five equations are not linearly independent since, for the closed system of five levels, the sum of any four equations yields the fifth. However, an additional constraint imposed by the assumptions of charge neutrality and neglect of plasma motion (expansion or compression) yields an additional equation

$$N_e = \left(\frac{Z-6}{P}\right) (N_1 + N_2 + N_3 + N_4) + (Z-5) N_5 \quad (17)$$

which makes, for a selected electron density, the system soluble. Here P is the fraction of the lasing-species ions which occupies terms 1 through 4 and is set equal to 0.6 by assuming most of the population is in the ground terms of which N_1 represents the triplet contribution (Section II.B.).

Equations (12)-(17) were solved simultaneously for the five unknowns, N_k ($k=1$ through 5), by an iterative method. Since the escape factors for most conditions of interest were small perturbations, convergence was usually rapid.

III. CALCULATED RESULTS

A. Gain

The gain coefficients, α , for transitions $3p \rightarrow 3s$ 3P in carbon-like ions and $3s \rightarrow 2p$ 1P in helium-like ions were computed from the population densities, N_2 and N_3 , for a Doppler-broadened²⁶ line from³¹

$$\alpha = \left(\frac{\pi M_i c^2}{2 k T_i} \right)^{\frac{1}{2}} r_o \lambda_{32} g_2 f_{23} \left(\frac{N_3}{g_3} - \frac{N_2}{g_2} \right), \quad (18)$$

where g_2, g_3 are the statistical weights for terms 2 and 3, respectively. Such gain coefficients have been computed for several decades of electron densities and suitable corresponding plasma diameters. These parameters were selected to simulate plasmas which can be produced by presently available technology. For the carbon-like results shown in Fig. 3, an equilibrium electron kinetic temperature, kT_e , equal to one-third the ionization potential (I.P.) of the lasing species being modeled was used, with $T_e = T_i$; pre-equilibrium enhanced temperature results shown in Fig. 4 are discussed further in Section III.C. below. Equilibrium calculation results at $kT_e = kT_i = 0.7$ I.P. for helium-like ions are given in Fig. 5. In these figures, the gain product αL is plotted vs atomic number Z (and corresponding laser wavelength) and for several values of electron density N_e and plasma diameter d , with a fixed length $L = 10d$ chosen. The lower density curves, a and b, correspond to electrically driven dense pinch devices^{32,33} while the higher density curves, c and d, are more typical of laser-heated pellet conditions³⁴. The assumption $L = 10d$ is based upon an aspect ratio of 10:1 which is considered to be a reasonable maximum along a straight line axis in state-of-the-art plasma devices. The values chosen for d exceed those

below which severe diffraction losses would be expected to enter, i.e., $d \gg (\lambda L)^{1/2}$ or $d \gg 10\lambda$ for a 10:1 assumed aspect ratio. The computed gain products gL do not exceed 10 (corresponding to a single-pass gain of e^{10}) where it would be anticipated that saturation effects and particularly radial superfluorescence would enter as the product gd approaches unity. Thus, the choice of diameter d is dictated by a diffraction limit minimum and a radially thick maximum.

For clarity, the gain curves are shown as continuous lines, although computations were performed for integer values of Z . Significant gain products at higher Z values are achieved with the increased pumping rates associated with the higher electron densities. Each curve exhibits a minimum value of Z below which an inversion is not obtained because of dominant collisional mixing (the onset of Boltzmann equilibrium) between the upper and lower terms, which are closely spaced at these low Z values. (Negative gain values are not indicated on the $\log gL$ scale.) All curves reach a peak at a Z value somewhat higher than the collisional mixing cutoff due to a gradual reduction of the mixing effect resulting from the increased spacing of the laser levels with increasing Z . The decline in gain product as Z increases to values greater than this peak is due mainly to: (a) a reduced fractional population of excited terms resulting from a decreasing pumping rate for the larger pump energy gap, ΔE_{13} [see Eq. (2)], (b) a smaller number density of lasing ions at higher Z for a given electron density (from charge neutrality), and (c) the explicit linear scaling of the gain coefficient α with wavelength [see Eq. (18)].

The low- Z (long wavelength) cutoff, as well as the position and magnitude of the peak gain product have been found to be sensitive to plasma dimensions because of effects of radiative trapping such as the increased population of the lower laser term. The low- Z cutoff is also sensitive to the value of the $n=3$ laser level electron collisional mixing rate used in the modeling. The factor-of-two precision presently expected for the values used is reflected as ± 1 to ± 2 variation in the Z -cutoff values plotted in Figs. 3-5. However, for atomic numbers larger than those at the peak of the gL vs Z curve, the calculated results are no longer sensitive to the upper and lower laser term mixing rates, and the accuracy of the gain product plotted should be about as good as the accuracy of the pumping rates, i.e., about a factor-of-two.

B. Pump Energy Requirements

For steady-state inversion, it is the pump energy rather than power that becomes a stringent requirement for high gain. A lower limit on the amount of pump energy, E_p , required can be determined from the maintained plasma, ionization, and excitation energies, i.e.,

$$E_p = \left(\frac{3}{2} N_e kT_e + \frac{3}{2} N_i kT_i + N_i \bar{E}_i \right) V, \quad (19)$$

where \bar{E}_i is the average excitation plus ionization energy per ion and V is the plasma volume. Greater amounts of pump energy by factors of ~ 20 -1000 could be required to compensate for plasma-energy losses and coupling efficiency from the pump source. These stored energies are indicated in Figs. 3-5 for the peak gain point of each of the curves. Curves a and b in each figure correspond to conditions more typical of electrically driven pinch devices, where efficiencies of at least a few percent can be expected and energy storage systems of tens-of-kilojoules to megajoules are available; curves c and d correspond to laser-heated plasmas at high temperatures where the efficiency may be as low as 0.1 percent and much less energy (hundreds-of-Joules) is presently available.

C. Discussion

Under equilibrium temperature conditions with $kT_e = kT_i = \text{I.P.}/3$ and 0.7 I.P. for carbon-like and helium-like ions, respectively, the results for the former (shown in Fig. 3) are encouraging with gain products in the vacuum-UV region as high as $\alpha L = 1.6$ corresponding to net gains of $\exp(\alpha L) = 5$. For the latter (helium-like ions), the corresponding computed gain products plotted in Fig. 5 represent insignificant net gain, and at most a population inversion measurement could be expected for available plasma densities and dimensions such as represented here. Only with compressed laser-heated pellet plasmas of supra-solid density in a linear geometry could net amplification at high Z be conceived.

An increased electron temperature could have a significant effect both towards increasing the long-wavelength cutoff point as the $n=3$ laser level mixing rate decreases [Eq. (2) for $\Delta E_{jk}/kT_e$ very small] as well as increasing the gain

product as the $n=2$ to $n=3$ pumping rate increases. Electron temperatures considerably above the "equilibrium" values chosen here are not uncommon³⁵ under transient pre-equilibrium conditions of plasma heating in most fast-pulsed devices, and significantly increased gain is conceivable for the interval during which the desired ion is abundant. Such conditions are approximated within the present model for carbon-like ions, with the results plotted in Fig. 4 for N_e and d values corresponding to Fig. 3 but with temperatures increased by a factor of three. For these modified computations, a fixed laser-ion abundance of one-third the total was assumed, rather than an ionization-equilibrium value. Also, $T_e = T_i$ was again assumed, since the electron-ion energy equipartition times are generally less than the ion creation times at such high densities (if T_i were less than T_e , the gain products shown would increase as $T_i^{-1/2}$). Even for the somewhat conservative³⁵ temperature increase of $3\times$ assumed here, peak gain products of $\alpha L \approx 10$ are predicted, with a net gain of $\exp(\alpha L) \approx 2 \times 10^4$. Thus, only a modest transient temperature increase is required to saturate the gain (see Section III.A.).

Enhanced temperature calculations corresponding to the helium-like ion conditions of Fig. 5 continued to yield very small gain products (less than 10^{-3}) and therefore the results are not plotted.

IV. SUMMARY AND CONCLUSIONS

Population densities of ground and excited terms of carbon-like and helium-like ions in high-density plasmas were calculated by using the steady-state computer model described above. All important radiative and collisional transitions were included in the analysis and the laser gain product was derived from the computed population densities and the plasma length. The results of these calculations indicate significant gain products for $3p \rightarrow 3s$ ionic transitions in an amplified spontaneous emission (ASE) mode, i.e., without a resonant cavity, and for a quasi-equilibrium plasma model. With enhanced temperatures typical of a transient plasma heating phase, gains approaching saturation levels are predicted. The aspect ratio has been fixed throughout at $L/d = 10$; tandem operation³³ could conceivably increase this to 30 with a corresponding increase of a factor-of-three in the peak gain product,

with net equilibrium-mode gains ≥ 100 . Therefore, vacuum-UV lasing at wavelengths between 500 and 1000 Å using existing high-density discharge devices appears promising for a near term proof of feasibility of ASE in plasmas at short wavelengths.

Shorter wavelengths may subsequently evolve using smaller volumes heated by such high-power lasers as currently under development for compressed pellet fusion; here helium-like ion transitions might also become useful at very high densities.

V. REFERENCES

1. R. W. Waynant and R. C. Elton, *Proc. IEEE* 64, 1059 (1976).
2. P. K. Cheo and H. G. Cooper, *J. Appl. Phys.* 36, 1862 (1965).
3. W. B. Bridges and A. N. Chester, in *Handbook of Lasers*, ed. R. J. Pressley (Cleveland: Chemical Rubber Co., 1971), Chapter 7.
4. C. K. Rhodes, *IEEE J. Quant. Electron.* QE-10, 153 (1974).
5. Y. Hashino, Y. Katsuyama, and K. Fukuda, *Jap. J. Appl. Phys.* 11, 907 (1972); 12, 470 (1973).
6. R. C. Elton, R. W. Waynant, R. A. Andrews, M. H. Reilly, Naval Research Laboratory Report No. 7412, May 1972.
7. R. C. Elton, *Appl. Opt.* 14, 97 (1975). The present numerical results are consistent with the analytical results in this paper when adjustments for density and improved rates are made.
8. R. C. Elton, in *Progress in Lasers and Laser Fusion*, eds. B. Kursunoglu, A. Perlmutter, and S. M. Widmayer (New York: Plenum Press, 1975).
9. R. C. Elton, *Appl. Opt.* 14, 2243 (1975).
10. An alternate possibility of pumping by collisional ionization directly into excited states from the next lower ionization species is not considered here; a justification is agreement of the present model with existing experiments⁵.
11. T. N. Lee, Proceedings International Conference on the Physics of X-Ray Spectra, National Bureau of Standards, August 1976 (to be published).
12. R. C. Elton, in *Methods of Experimental Physics*, Volume 9A, *Plasma Physics*, eds. H. R. Griem and R. H. Lovberg (New York: Academic Press, 1970) Chapter 4.
13. J. C. Weisheit, *J. Phys. B* 8, 2556 (1975).
14. A. L. Merts, R. D. Cowan, N. H. Magee, Jr., Los Alamos Scientific Laboratory Report LA-6220-MS (March 1976).
15. For $n=3$, $\Delta n=0$ transitions an electron collisional rate⁷ derived from line broadening calculations yields results similar to the effective Gaunt factor formulation within the factor-of-two accuracy expected.
16. M. J. Seaton, in *Atomic and Molecular Processes*, D. R. Bates, ed. (New York: Academic Press, 1962) Chapter 11.

17. H. Van Regemorter, *Astrophys. J.* 136, 906 (1962).
18. W. L. Wiese, M. W. Smith, and B. M. Glennon, Atomic Transition Probabilities - Volume I: Hydrogen through Neon, NSRDS-NBS-4 (Washington, D.C.: U.S. Government Printing Office, 1969).
19. C. E. Moore, Atomic Energy Levels - Volume I, NSRDS-NBS-35 (Washington, D.C.: U.S. Government Printing Office, 1971).
20. R. L. Kelly with L. J. Palumbo, Atomic and Ionic Emission Lines below 2000 Angstroms - Hydrogen through Krypton, Naval Research Laboratory Report 7599 (Washington, D.C.: U.S. Government Printing Office, 1973).
21. W. L. Wiese, *Nucl. Instr. and Methods* 90, 25 (1970).
22. O. Bely, *Proc. Phys. Soc.* 88, 587 (1966); M. Blaha, *Astrophys. J.* 157, 473 (1969); H. -J. Kunze and W. D. Johnston, III, *Phys. Rev. A* 3, 1384 (1971), 4, 962 (1971); J. Davis and S. Morin, *J. Quant. Spectros. and Radiative Transfer* 11, 463 (1971); J. Davis, P. C. Kepple, and M. Blaha, Naval Research Laboratory Memorandum Reports 2939 and 3171, 1974 and 1975 (unpublished); J. Davis and K. G. Whitney, *J. Appl. Phys.* 47, 1426 (1976); R. U. Datla, M. Blaha, and H. -J. Kunze, *Phys. Rev. A* 12, 1076 (1975); R. K. Landshoff and J. D. Perez, *Phys. Rev. A* 13, 1615 (1976).
23. R. W. P. McWhirter, in Plasma Diagnostic Techniques, eds. R. H. Huddleston and S. L. Leonard (New York: Academic Press, 1965) Chapter 5.
24. L. M. Biberman, *Zh. Exp. Theor. Fiz.* 17, 416 (1947) [English transl: *Soviet Physics - JETP* 19, 584 (1949)].
25. T. Holstein, *Phys. Rev.* 72, 1212 (1947); 83, 1159 (1951).
26. Stark broadening is negligible for the present conditions, as computed from Eq. (526) of H. R. Griem, Spectral Line Broadening by Plasmas, (New York: Academic Press, 1974).
27. H. -J. Kunze, *Phys. Rev. A* 3, 937 (1971).
28. W. Lotz, *Astrophys. J. Suppl.* 14, 207 (1967); *Z. Physik* 216, 241 (1968).
29. R. U. Datla, L. J. Nugent, and H. R. Griem, *Phys. Rev. A* (in press, Sept. 1976).
30. H. R. Griem, Plasma Spectroscopy (New York: McGraw-Hill, 1964).
31. G. R. Fowles, Introduction to Modern Optics (New York: Holt, Rinehart, and Winston, Inc., 1968).
32. J. W. Mather, in Methods of Experimental Physics, Volume 9B, Plasma Physics, eds. H. R. Griem and R. H. Lovberg (New York: Academic Press, 1970), Chapter 15.

33. J. H. Lee, D. R. McFarland and F. Hohl, "Dense Plasma Focus Production in a Hypocycloidal Pinch," NASA Report TN-D-8116, December 1975 (unpublished).
34. T. P. Hughes, Plasmas and Laser Light (London: Halsted and New York: John Wiley, 1975).
35. K. G. Whitney and J. Davis, J. Appl. Phys. 45, 5294 (1974).

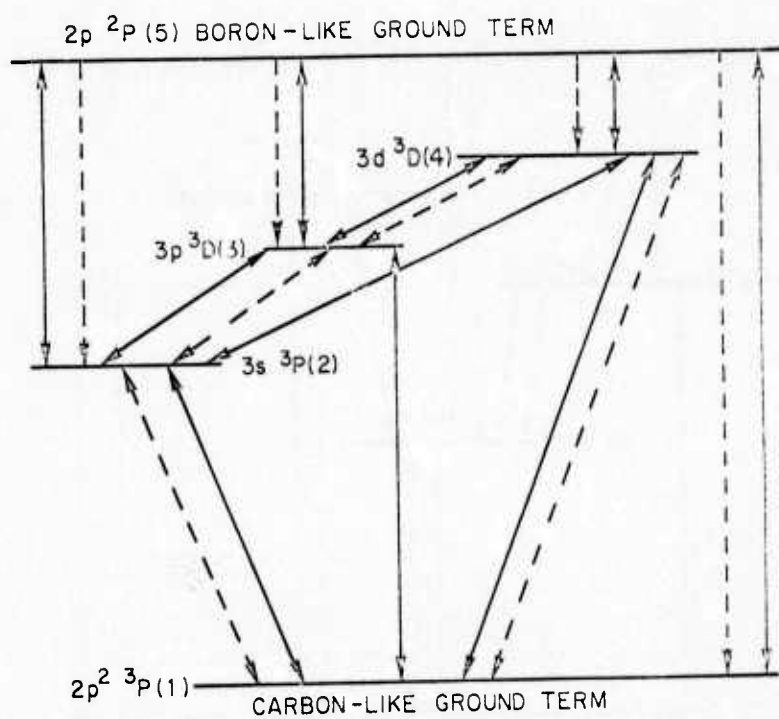
Table 1: Atomic Data Used in Calculations

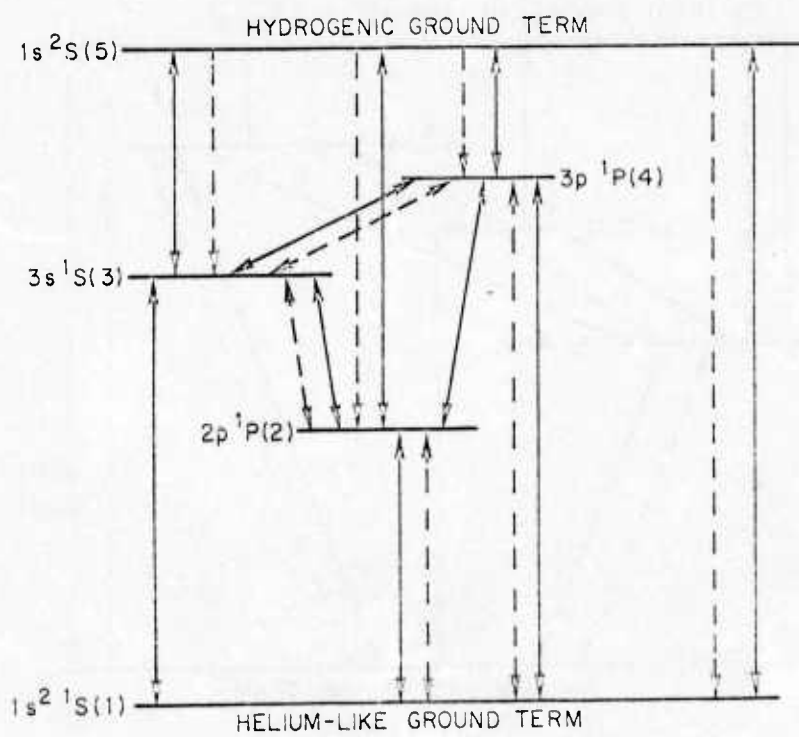
Carbon-Like Ions, $z = Z-5$				
lower term, j	upper term, k	ΔE_{jk}	f_{jk}	$\langle \bar{g} \rangle_{jk}$
$2p^2 \ ^3P$	$2p3s \ ^3P^0$	$2.35 \ z^2$	0.05	(e)
$2p^2 \ ^3P$	$2p3p \ ^3D$	(a)	0.05	(e)
$2p^2 \ ^3P$	$2p3d \ ^3D^0$	(a)	0.65	(c)
$2p3s \ ^3P^0$	$2p3p \ ^3D$	$1.10 \ z$	$2.9/z$	(d)
$2p3s \ ^3P^0$	$2p3d \ ^3D^0$	(a)	0.0 (b)	(d)
$2p3p \ ^3D$	$2p3d \ ^3D^0$	$1.38 \ z$	$0.75/z$	(d)
$2p^2 \ ^3P$	$2p \ ^2P^0 + e$	$3.75 \ z^2 \text{ (I.P.)}$	---	---
Helium-like Ions, $z = Z-1$				
lower term, j	upper term, k	ΔE_{jk}	f_{jk}	$\langle \bar{g} \rangle_{jk}$
$1s^2 \ ^1S$	$1s2p \ ^1P^0$	$10.9 \ z^2$	$0.83 - 1.1/z$	(d)
$1s^2 \ ^1S$	$1s3s \ ^1S$	(a)	$.032 - .022/z$	(d)
$1s^2 \ ^1S$	$1s3p \ ^1P^0$	$12.7 \ z^2$	$0.16 - 0.11/z$	(d)
$1s2p \ ^1P^0$	$1s3s \ ^1S$	(a)	$0.014 + .053/z$	(e)
$1s2p \ ^1P^0$	$1s3p \ ^1P^0$	(a)	$.21 - .26/z$	(e)
$1s3s \ ^1S$	$1s3p \ ^1P^0$	$0.184 \ z$	$1.04/z$	(d)
$1s^2 \ ^1S$	$1s \ ^2S + e$	$14.1 \ z^2 \text{ (I.P.)}$	---	---

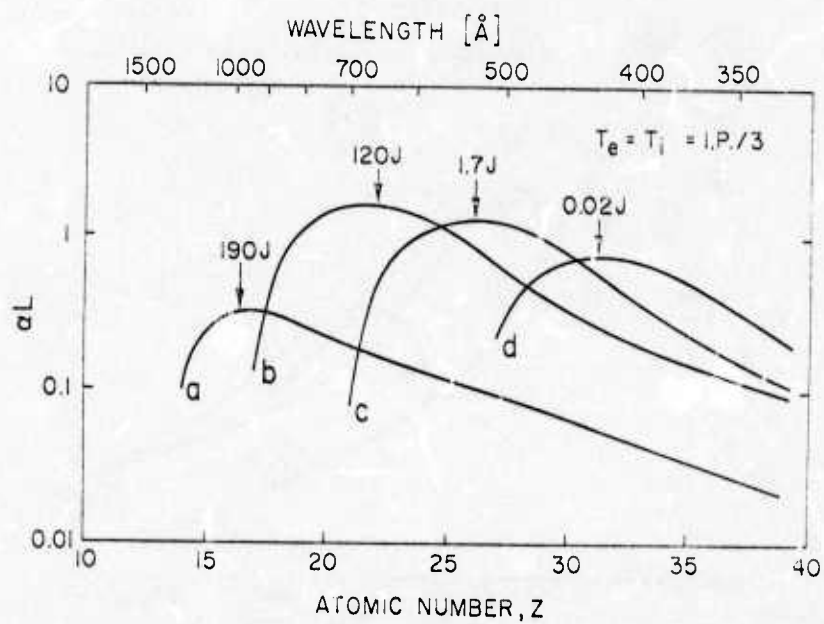
- (a) Energy gap computed from other gaps listed using $\Delta E_{ln} = \Delta E_{lm} + \Delta E_{mn}$, where $l, m,$ and n are any three terms. Sealing used is both predicted⁷ and typical of measurements²¹.
- (b) This quadrupole mixing is believed to be small and is taken to be zero. It has little effect on the computed gain for most cases even if it is assumed to be as large as the $3s \rightarrow 3p$ dipole rate.
- (c) Gaunt factor fitted to $\langle \bar{g} \rangle_{jk} = 0.17 (\Delta E_{jk}/kT_e)^{-0.47}$ for $\Delta E_{jk}/kT_e \leq 1$ and $\langle \bar{g} \rangle_{jk} = 0.17$ for $\Delta E_{jk}/kT_e > 1$.
- (d) Gaunt factor fitted to $\langle \bar{g} \rangle_{jk} = 0.63 (\Delta E_{jk}/kT_e)^{-0.15}$.
- (e) Derived from collisional rates for helium-like ions calculated by Landshoff and Perez²².

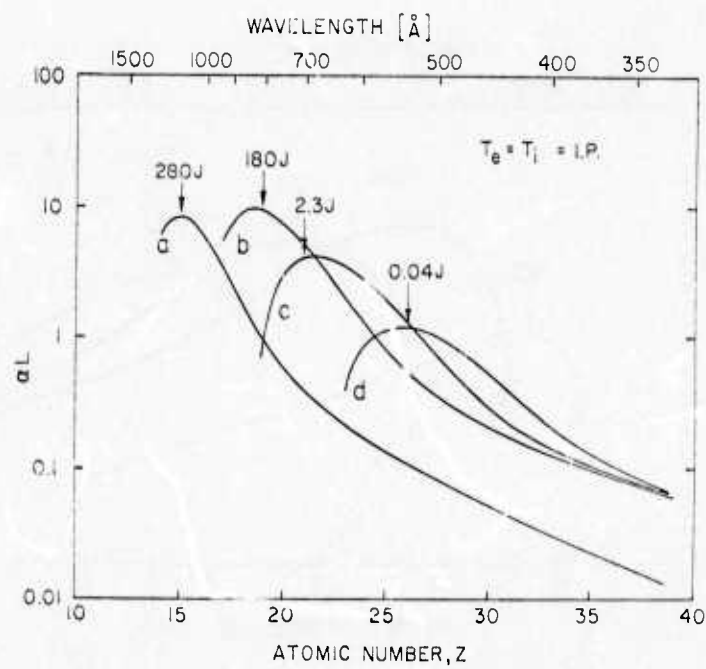
FIGURE CAPTIONS

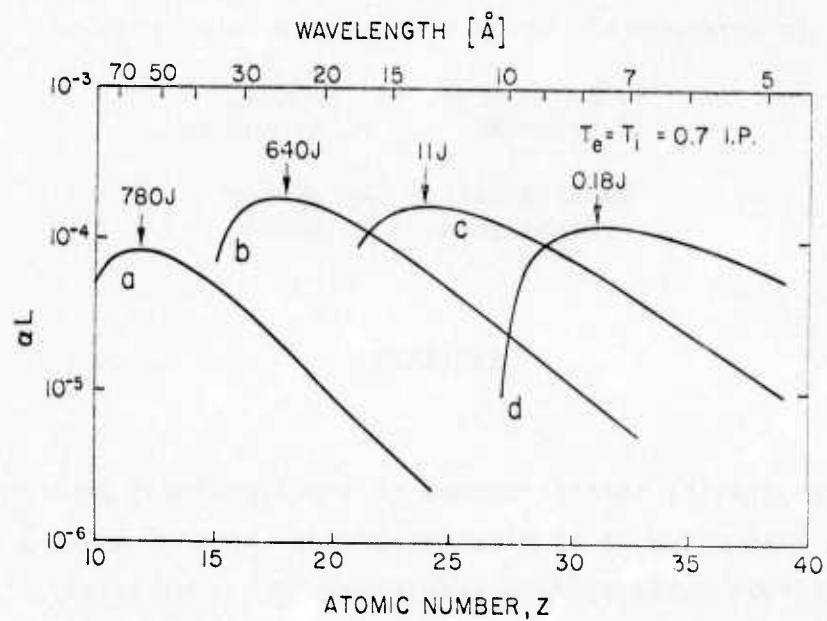
- Fig. 1 - Term diagram for 3p-3s lasing scheme in carbon-like ions showing important terms and transitions used in numerical modeling results described. Dashed arrows designate radiative transitions; solid arrows represent electron-collisional transitions. Numbers in parentheses correspond to subscripts in the text.
- Fig. 2 - Term diagram for 3s-2p lasing scheme in helium-like ions showing important terms and transitions used in numerical modeling results described. Dashed arrows designate radiative transitions; solid arrows represent electron-collisional transitions. Numbers in parentheses correspond to subscripts in the text.
- Fig. 3 - Computed gain products gL versus atomic number and wavelength for 6-electron carbon-like ions at temperatures T_e , T_i equal to one-third the ionization potential, I.P. (from Table 1). Curves a through d correspond respectively to electron densities of 10^{19} , 10^{20} , 10^{21} and 10^{22} cm^{-3} and to relevant respective plasma diameters of 3, 1, 0.1 and 0.01 mm. The required plasma energies in Joules are indicated for each curve at peak gain; lower values at higher densities reflect a volume decreasing as the third power of the diameter.
- Fig. 4 - Computed gain products gL versus atomic number and wavelength for 6-electron carbon-like ions at enhanced non-equilibrium temperatures T_e , T_i equal to the ionization potential, I.P. (from Table 1). As in Fig. 3, curves a through d correspond respectively to electron densities of 10^{19} , 10^{20} , 10^{21} and 10^{22} cm^{-3} and to relevant plasma diameters of 3, 1, 0.1 and 0.01 mm. The required plasma energies in Joules are indicated for each curve at peak gain; lower values at higher densities reflect a volume decreasing as the third power of the diameter.
- Fig. 5 - Computed gain products gL versus atomic number and wavelength for 2-electron helium-like ions at temperatures T_e , T_i equal to 0.7 times the ionization potential, I.P. (from Table 1). As in Figs. 3 and 4, curves a through d correspond respectively to electron densities of 10^{19} , 10^{20} , 10^{21} and 10^{22} cm^{-3} and to relevant plasma diameters of 3, 1, 0.1 and 0.01 mm. The required plasma energies in Joules are indicated for each curve at peak gain; lower values at higher densities reflect a volume decreasing as the third power of the diameter.











Interferometric Study of Laser-Produced Plasmas

J. F. Reintjes, T. N. Lee,
R. C. Eckardt, and R. A. Andrews

Naval Research Laboratory
Washington, D.C. 20375

ABSTRACT

High-quality interferograms of laser-produced plasmas with spatial resolution of 15 micrometers are obtained using a relatively simple Jamin-type interferometer and a precisely timed 30-psec probing laser pulse from a mode-locked Nd:YAG laser, frequency doubled to 532 nm. The spatial resolution attainable with the present arrangement is limited by the velocity of the expanding plasma and the finite duration of the probing pulse. The plasmas are produced by focusing a Nd:glass Q-switched laser pulse (0.5 GW , $10^{11} - 10^{13} \text{ Watts cm}^{-2}$) onto slab targets of Al, Mg, and CH_2 . The electron density distribution, plasma dimension, and expansion velocity for both point and line foci are studied as a function of time delay between the mode-locked and the Q-switched laser pulses. The results obtained with different durations of the heating (Q-switched) pulse and with the various target material are compared.

I. INTRODUCTION

The diagnostics of laser-produced plasmas is becoming of increasing importance for various applications, including laser-generated fusion. Among the various diagnostic techniques, interferometry has recently been shown¹⁻⁴ to be of great value in determining the electron density profiles and expansion characteristics of laser-produced plasmas. Since one is interested in time-and-space resolved information of a plasma, the probing laser pulse for such interferometric applications should be reasonably short to minimize blurring caused by the streaming motion of the plasma during the exposure. In addition, the small dimensions of the resulting plasmas require microscopic photography in order to obtain high spatial resolution.

In general, it has been the case in previous measurements that the probing laser pulse for illuminating the interferometer is obtained by diverting a portion of the main laser pulse (heating laser pulse) which generates the plasma. The probing time resolution in such an experiment is limited to times of the order of the main laser pulse. In such cases, the plasma expansion during the main laser pulse cannot be examined. Furthermore, measurements with high temporal and dynamical spatial resolution are limited by typical plasma streaming velocities ($\sim 10^7$ cm/sec) to plasmas generated with picosecond pulses.

In this paper we present interferometric measurements of plasmas generated with a Q-switched laser pulse of duration between 1.5 to 5.5 nsec. The interferometer is illuminated with a separate but synchronized mode-locked pulse from a Nd:YAG laser with a 20-psec duration. Such a combination enables us to probe plasmas with high temporal

and spatial resolution and to make measurements during the heating pulse. Interferometric studies were made for various target materials and durations of the heating laser pulse using both point and line foci of the main laser beam for plasma generation. In Section II, the experimental arrangements, including the laser synchronization scheme, are briefly described. The time-dependent plasma expansion for both the point and line foci, including electron density profiles and expansion velocities, are described in Section III.

II. EXPERIMENTAL ARRANGEMENT

A. Laser Synchronization.

The laser system used in these experiments is shown in Fig. 1. The plasma is created with the output of the Q-switched laser. The oscillator is a single-mode Nd:YAG Pockels cell Q-switched laser which generates a 20 mJ, 20 ns pulse. It passes through a Pockels cell shutter and is then amplified to a level of about 1 GW in three Nd:Glass amplifiers. A Pockels cell isolator is used between the last amplifier and the target to prevent reflections from the target from damaging the amplifier chain. The second mode-locked laser produces a train of 30 psec pulses, one of which is selected for amplification and conversion to the second harmonic at 532 nm.

The scheme used to synchronize the two laser oscillators is shown in Fig. 2. The primary problem in the synchronization of two independent lasers lies in the jitter inherent in the build-up of the oscillator pulses from the noise level. In the case of a passively mode-locked laser,

the jitter in build-up time of the pulse train is typically of the order of 1-10 μ sec from the time the flash lamps are fired. In the case of an actively Q-switched laser, jitter times of the order of 10-25 ns between the switching of the Pockels cell and the laser output pulse are typical. In order to overcome these problems, a three-step switching sequence is used in which each step is initiated by the appearance of an appropriate optical signal. The sequence is started with the arrival of the mode-locked pulse train. An early pulse in the train is used to trigger the Pockels cell in the Q-switched laser, with the timing adjusted so that the Q-switched pulse appears near the peak of the mode-locked pulse train. The only requirement on the Q-switched pulse build-up is that the delay and jitter not be larger than the duration of the entire mode-locked train (250 nsec). The leading edge of the Q-switched pulse is used to trigger the mode-locked pulse selector, gating out a pulse near the peak of the train for amplification. Selection of a pulse near the peak of the train will be reliable if the jitter of the Q-switch pulse build-up is of the order of a few interpulse spacings -- typically ~ 20 nsec. Finally, the selected mode-locked pulse is used to drive the Pockels cell shutter in the Q-switched laser gating out a segment of the oscillator pulse.

The accuracy of synchronization of the final output pulses is determined entirely by this last switching step. By greatly overdriving the last laser-triggered spark gap, the jitter in this last step is minimized. We have achieved typical stabilities of $\sim \pm 0.1$ nsec between the two pulses. The duration of the Q-switched pulse can be varied by adjusting the length of the charging cable in the pulse-forming network which drives the Pockels cell shutters. The output pulse intensity remains constant as the pulse

length is varied with longer pulses containing higher energy. This type of laser system has the advantageous characteristic that the two laser-pulse durations can be independently varied, allowing variable Q-switched pulse durations to be used for plasma generation while maintaining the same high degree of temporal and spatial resolution obtainable with the mode-locked pulse in the probing measurements.

B. Interferometer and Target Chamber.

The arrangement used for interferometry is shown in Fig. 3. A slab target is supported in the center of a vacuum chamber. The Q-switched pulse is focused with a 30 cm, f/15 lens onto the target, giving a focal spot 50 μm in diameter. For measurements with a line focus, a negative 400-cm-focal-length cylindrical lense was added in front of the 30 cm lens, giving a focus of 50 μm x 1 mm. Typical power densities on target were 10^{13} W/cm² for a point focus and 5×10^{11} W/cm² in a line focus. The mode-locked pulse is frequency doubled in a KDP crystal and is directed across the target at right angles to the path of the Q-switched laser. A Jamin interferometer is used, and the resulting interference pattern is photographed through a 10x, f/20 telescope imaged on the plane of the plasma with a spatial resolution of about 15 μm in the plane of the target. The time of arrival of the two pulses is changed by adjusting a variable-path delay in the mode-locked beam. The relative time of the two beams, along with the intensity of the Q-switched pulse, is monitored with a photodiode.

III. RESULTS

The interferograms of the expanding plasma were obtained as a function of time delay relative to the heating laser pulse. Because of the high

degree of accuracy in timing between the two lasers, the shot-to-shot reproducibility of the interferograms at a given delay time was excellent, thereby allowing measurements made on different laser shots at different times to be compared. A typical sequence is shown in Figs. 4a and 4b for a point focus on a 250- μm -thick aluminum target with a power density of approximately 10^{13} W/cm^2 . The main laser pulse is incident from the left, and the shadow of the target is clearly visible. The times shown on the bottom of the pictures indicate the time of arrival of the probing laser pulse relative to the 10% point on the rise of the Q-switched pulse. Controls for these measurements included insuring that no extraneous plasma effects were present when either the probing laser pulse was brought in before the Q-switched pulse or the Q-switched oscillator was blocked. As can be seen, during the early phase of the expansion ($t \leq 0.3 \text{ nsec}$), the plasma has a relatively well-defined hemispherical shape with a diameter of about 100 μm . It expands rapidly outward from the target until a time corresponding to the end of the laser pulse. At later times, the interference pattern from the denser regions of plasma flattens, while that from the more tenuous region shows continued expansion in a cone angle of about 90° . The flattening of the interference fringes suggests the development of a hollow core⁵ in the plasma as would result from Abel inversion analysis.

The extent of the plasma interference is determined by the minimum detectable fringe shift (about 1/4 fringe). The opaque region at the center of the plasma near the target corresponds to a region of high-electron-density gradient, which causes the probing laser beam to be deflected out of the telescope due to the high degree of refraction in this plasma region. The maximum detectable electron density gradient for the present system can be estimated¹ from the angular deflection of a ray passing through a plasma region of length l and density gradient $\frac{dn}{dx}$ by

$$\delta\theta = \frac{-e^2 \lambda^2}{4\pi m c^2} \frac{\partial n}{\partial x} \quad (1)$$

For an f/20 telescope, a wavelength of 532 nm, and a plasma dimension of 100 μm , Eq. (1) gives a maximum detectable electron density gradient of $3 \times 10^{22} / \text{cm}^{-3} / \text{cm}$. The study of plasmas in regions of greater electron density gradients requires the use of shorter wavelength probing pulses, e.g., third or fourth harmonics of the Nd laser^{3,8}.

An interesting feature in Fig. 4 is a sloping region of plasma near the target but outside of the area illuminated by the main laser pulse, which is seen in exposures taken after 1.5 nsec (indicated by arrow marks). This plasma region extends about 1 mm along the target surface at its peak and then recedes to the target surface at later times ($t \geq 5$ ns). Recently, the distribution of self-generated current flow in a laser-produced plasma has been measured⁶. Furthermore, Drouet and Pepin⁷, in an attempt to explain observations of a cathodic area much larger than the focal spot size, inferred that the current paths are spread out in the vicinity of the target surface. The sloping feature observed near the surface in the interferograms is very likely due to a plasma which is associated with such current paths. However, the time sequence of the plasma development as shown in Fig. 4 suggests that such a feature can arise from the natural tendency for the current in the plasma to take the least inductive path. Current which is constrained to flow normal to the target in the region illuminated by the laser pulse and along the target elsewhere would tend to develop paths in the plasma along the surface of the target in order to minimize inductance. Such behavior would result

in features similar to ones which are observed.

Interferograms (such as Fig. 4) which are taken without background fringes are found to be particularly useful for observing fine structure of extremely complicated plasma distributions. An example is illustrated in Fig. 5, showing jagged, turbulent features in an expanding plasma. In this particular sequence, the main laser beam consisted of a large number of closely clustered pulses of a few tens to a few hundred picosecond in duration which could only be partially resolved on the oscilloscope (Tektronix type 519) trace. Comparison with interferograms obtained with temporally smooth pulses indicates that such turbulent behavior is associated with pulse substructure.

The time sequence of interferograms of a plasma expanding from a line focus on a 1-mm-thick magnesium target is shown in Fig. 6. The intensity of the laser beam in this case was about $5 \times 10^{11} \text{ W/cm}^2$ at the target. The interferograms on the left view the plasma along the short dimension and those on the right along the long dimension of the focus. Background fringes have been added to the interferograms on the right to aid in the determination of electron densities.

During the early stages, the plasma expands rapidly in a manner similar to that observed with the point focus measurements. The plasma retains the ellipsoidal nature of the original line focus throughout the times covered in the measurement, although the transverse expansion of the short dimension is faster than that of the long dimension. Regions of uniform electron density are observed throughout the plasma which are parallel to the axis of the original focus. As the plasma expands such regions remain

uniform and apparently free of microscopic plasma instabilities on the scale of 15 μm .

Electron density profiles obtained from the line focus measurements along an axis perpendicular to the target through the center of the plasma are shown in Fig. 7. The analysis of electron density distributions from a line focus is simplified because the major contribution to the phase integral arises from a region of constant density through the center portion of the plasma. However, corrections arising from the nonuniform areas at both ends of the cylinder were included. Electron density distribution at four different times of the plasma expansion are shown.

The electron density distributions for all of the time measurements are observed to decay exponentially with distance from the target surface, and scale length of the density distribution increases with time. Measurement of the densities near the target is limited by the large electron density gradients. The maximum observed gradient is the same for all curves at $2 \times 10^{21} \text{ cm}^{-3}/\text{cm}$. This value is in agreement with the theoretical limit of the optical system as determined from Eq (1) for a plasma column 1 mm in length.

Extrapolation of the exponential curves taken at 0.5, 0.8, and 1.5 ns shows an intersection at the target surface at a density of $2 \times 10^{20} \text{ cm}^{-3}$. This implies the presence of a density gradient steeper than exponential in the vicinity of the target surface, if the electron density is assumed to reach the critical value ($\sim 10^{21} \text{ cm}^{-3}$) for the 1.06 μm laser.

The velocity of expansion can be determined by measuring the extreme detectable edge of the plasma at different times. This position in the

plasma is determined by the minimum detectable fringe shift ($\sim 1/4$ fringe) and corresponds to a density of about $2 \times 10^{18} \text{ cm}^{-3}$. Such a curve is shown in Fig. 8 for plasmas generated with a 2.5 nsec main laser pulse. Data are shown for a line focus on a Mg target (solid dots) at $5 \times 10^{11} \text{ W/cm}^2$; and for a point focus on Al targets of thickness 250 μm (open squares) and 25 μm (solid square) at an intensity of 10^{13} W/cm^2 . The expansion is fairly uniform during the main laser pulse with a velocity of about $4 \times 10^7 \text{ cm/sec}$. The velocity also appears to be independent of target material, as well as laser power density in the range covered here. The latter is in good agreement with recent results reported by McLean, et al.⁹ After the end of the pulse, the plasma expansion velocity decreases and, in the case of the 25 μm -thick Al target, the plasma actually recedes towards the target.

The slowing down of the expansion at the end of the pulse is typical of behavior observed here under a wide range of experimental circumstances, and coincides in time with the flattening of the observed interferometric pattern (see Fig. 4). This behavior is shown more clearly in Fig. 9 where plasma expansions for two different pulse durations are compared. A point focus was used on a 250 μm Al target with a power density of $\sim 10^{13} \text{ W/cm}^2$. Again initial velocity of $\sim 3.5 \times 10^7 \text{ cm/sec}$ and recession of the plasma after the laser pulse are observed. In this case, the difference in pulse duration results in a time difference at which the maximum extent from the target occurs.

The plasma expansion from a polyethylene target was also studied with a 1.5 ns main laser pulse, and results were compared with the data from an Al target (Fig. 10). The initial expansion velocity is the same from the two targets. However, the plasma from the lighter polyethylene target reaches a greater maximum extent from the target (1.8 mm) before slowing

in expansion than do the plasmas from the heavier metallic targets. It is unclear whether such behavior is related to the atomic number or electrical insulation property of the target material. In the latter case, this result may be associated with the possibility that current loops close within the target for conducting targets, but must close within the plasma for insulating targets.

IV. SUMMARY

Laser-generated plasmas have been studied interferometrically using a frequency-doubled probing pulse from a Nd:YAG mode-locked laser which gave a time resolution of 30 psec and a spatial resolution of 15 μm . The plasmas were generated with a pulse from a Q-switched Nd:Glass laser, with pulse duration variable from 1.5 to 5 nsec using both point and line foci on target. The laser pulses were precisely synchronized in time so that time-dependent characteristics of the plasma expansion could be studied. The use of independent laser pulses for this study allowed time-resolved information to be obtained about the plasma during the period that it was illuminated by the heating pulse.

Observation of the expansion characteristics of the plasmas showed a rapid expansion with a velocity of $\sim 4 \times 10^7$ cm/sec during the heating pulse, followed by a slower expansion and recession in some instances after the end of the heating pulse. The initial expansion velocity was found to be independent of target material and did not change significantly as the laser intensity was varied over two orders of magnitude. Spreading of the plasma along the target surface was observed in a pattern similar to the current distribution recently inferred by Drouet and Repin⁷. The

patterns observed here suggest a distortion of the current paths in the plasma resulting in a lowered inductance.

Expansion characteristics of a plasma from a line focus were compared with those from a point focus. The plasmas generated from the line focus have the same initial expansion velocity as those from the point focus. The elongated nature of the line focus is retained in the plasma during and after the heating pulse, although transverse expansion of the short dimension is somewhat faster than that of the long dimension. In general, the plasmas thus produced appear to remain uniform and free of instability on the scale of $15\text{ }\mu\text{m}$ for the range of time delays which were used.

Electron-density profiles were determined for the plasmas generated from the line focus at several times during and after the heating pulse. The electron-density distribution was found to decay exponentially away from the target at all times, while the scale length increases at later times. Density gradients up to $10^{21}\text{ cm}^{-3}/\text{cm}$ are observed at distances of the order of $100\text{ }\mu\text{m}$ from the target. Extrapolation of the measurements shows that the density distribution must rise faster in the vicinity of the target than exponentially, if the critical density is to be reached in front of the original target surface.

Comparison of the plasma expansion from a polyethylene target with that from the heavier metallic target shows an identical expansion velocity, but no tendency for the expansion to slow down after the heating pulse ends.

ACKNOWLEDGMENT

The authors would like to acknowledge Dr. R. C. Elton for his encouragement and for many helpful discussions.

REFERENCES

1. F. C. Jahoda and G. A. Sawyer, in Method of Experimental Physics
Plasma Physics, vol. 9, Part B, edited by R. H. Lovberg and H. R. Griem
(Academic Press, New York, 1971).
2. D. T. Attwood and L. W. Coleman, Appl. Phys. Lett. 24, 408 (1974).
3. D. T. Attwood, L. W. Coleman, and D. W. Sweeney, Appl. Phys. Lett.
26, 616 (1975).
4. J. N. Olsen and C. W. Mendel, Jr., J. Appl. Phys. 46, 4407 (1975).
5. K. Eidmann, M. H. Key, and R. Sigel, J. Appl. Phys. 47, 2402 (1976).
6. M. G. Drouet and R. Bolton, Phys. Rev. Lett. 36, 591 (1976).
7. M. G. Drouet and H. Pepin, Appl. Phys. Lett. 28, 426 (1976).
8. D. W. Sweeney, D. T. Attwood, and L. W. Coleman, Appl. Opt. 15,
1126 (1976).
9. E. A. McLean, B. H. Ripin, J. A. Stamper, H. R. Griem, and S. E. Bodner,
Bull. Am. Phys. Soc. 20, 1318 (1975), and also E. A. McLean, Bull. Am.
Phys. Soc. 21, 845 (1976).

FIGURE CAPTIONS

- Fig. 1 - Schematic diagram showing optics of both the probing (30 ps mode-locked Nd:YAG laser) and the heating laser (1.5 - 5.5 ns Q-switched Nd:Glass laser).
- Fig. 2 - Synchronization scheme between the Q-switched and the mode-locked laser.
- Fig. 3 - Schematic diagram showing laser focusing optics, frequency-doubled ($\lambda = 532$ nm) probing laser beam, Jamin interferometer, and recording system.
- Fig. 4 - Time evolution of expanding plasma as shown by no-background fringe interferograms. The plasma is produced by irradiating a 0.25-mm-thick Al target with 2.5 ns Q-switched laser pulse. Point focus is used. The time sequence is obtained with separate shots by varying the delay time between the heating laser and the probing laser pulse. An arrow mark indicates the sloping portion of plasma (see the text).
- Fig. 5 - Plasma interferogram showing jagged structure due to turbulence. The heating pulse in this particular run is believed to consist of closely clustered multiple pulses.
- Fig. 6 - Interferograms obtained with a line focus on a Mg target, where axial as well as side views of the cylindrical plasma are recorded. The interferograms taken along the axial view have background fringes. Small ripple in the fringes may be due to nonuniformity in the incident laser pulse.

Fig. 7 - Electron-density profiles of expanding cylindrical plasma for four different delay times. The heating laser pulse duration was 2.5 nsec, and the target material was magnesium.

Fig. 8 - Location of isoelectron density front as a function of time. The duration of the heating laser pulse was 2.5 ns, and the plasmas are produced by line focus onto 0.25 mm Al target (square) and also point focus onto 0.025 mm Al target (open circle), respectively.

Fig. 9 - Isoelectron density front of expanding plasma as a function of time. 0.25 mm Al target is irradiated by point focus of 5.5 ns (closed circle) and 1.5 ns (square) heating laser pulse, respectively.

Fig. 10- Location of expanding plasma front as a function of time. 0.25 mm Al (closed circle) and polyethylene (square) targets are irradiated by 1.5 ns main laser pulse.

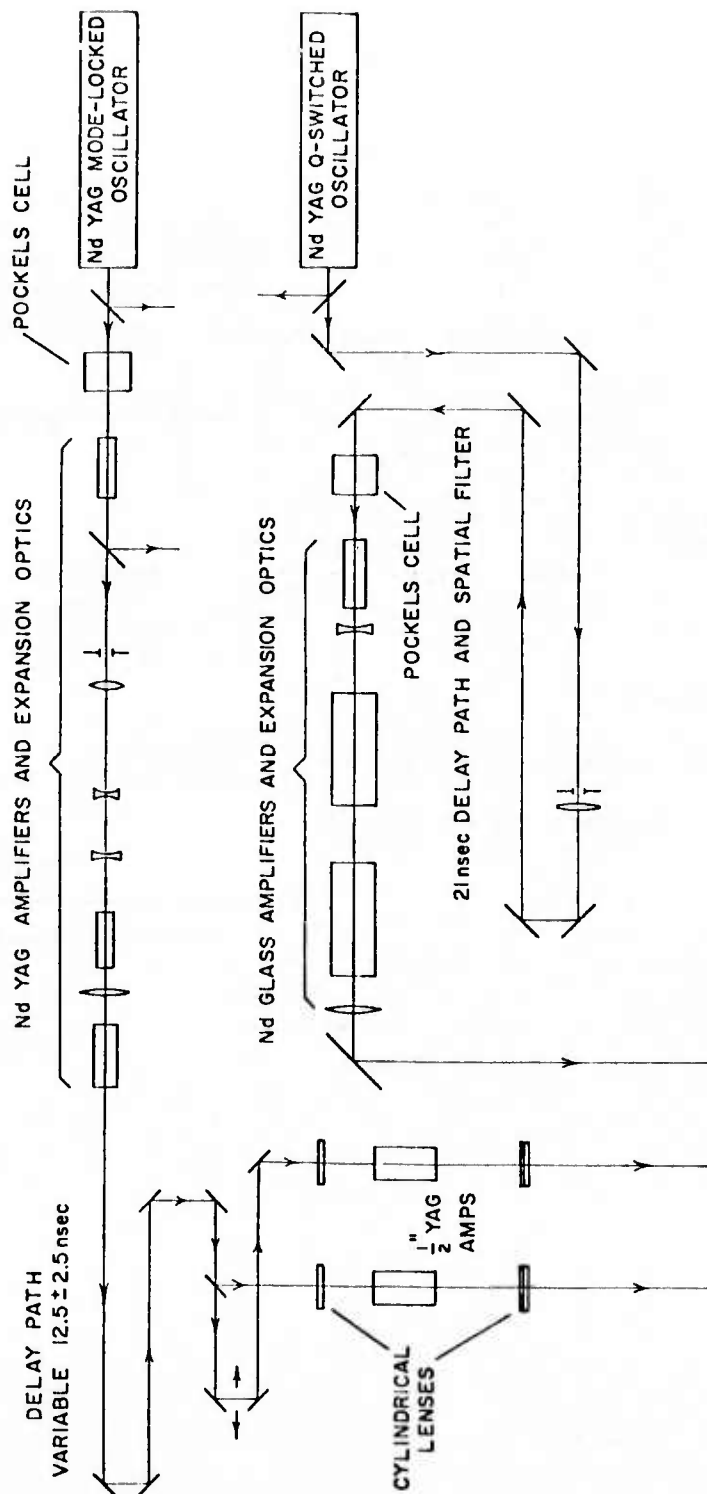


Figure 1

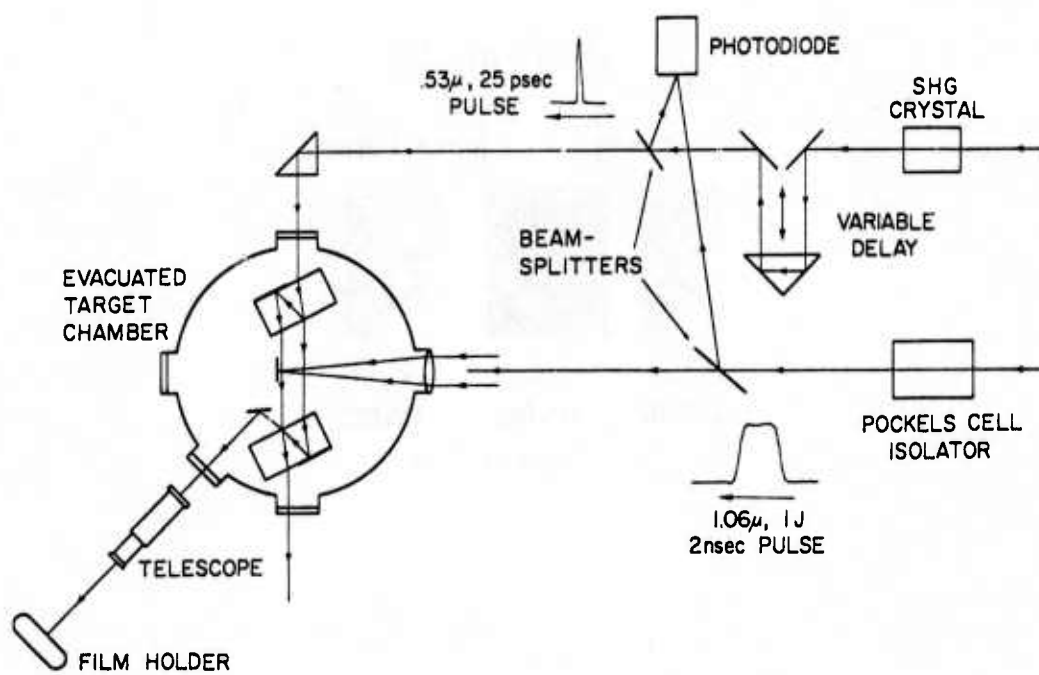


Figure 3

.010 in Al

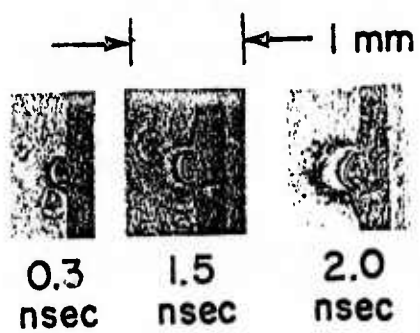


Figure 4a

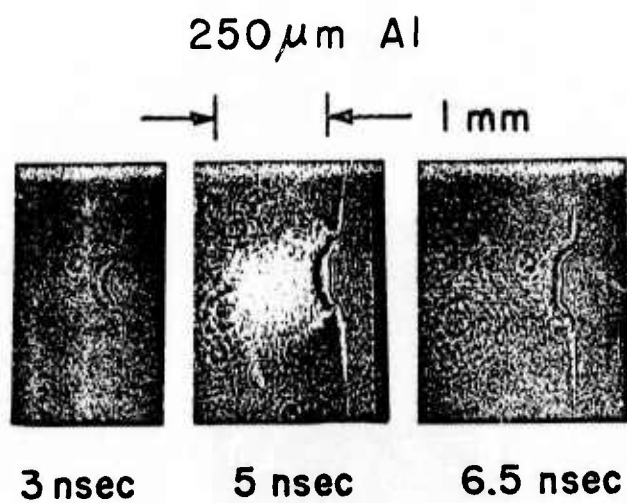


Figure 4b

1mm

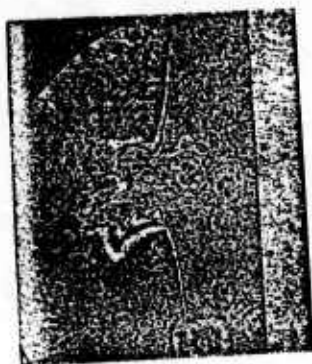



Figure 5

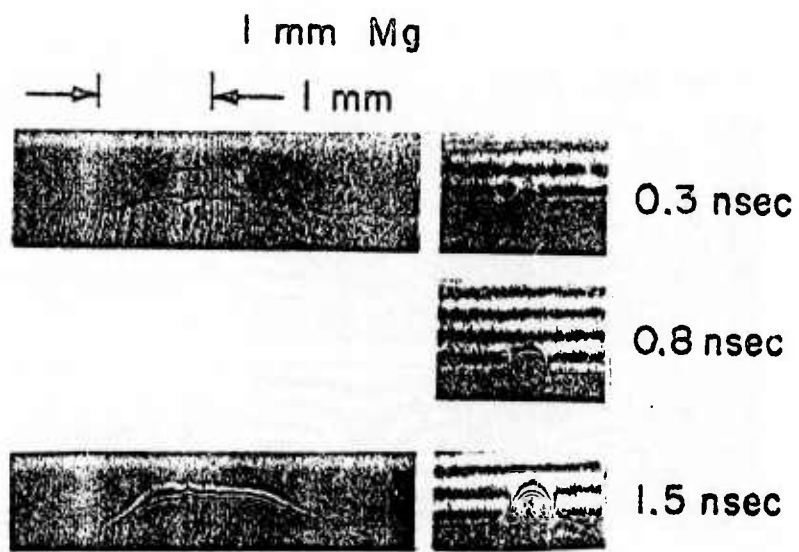


Figure 6a

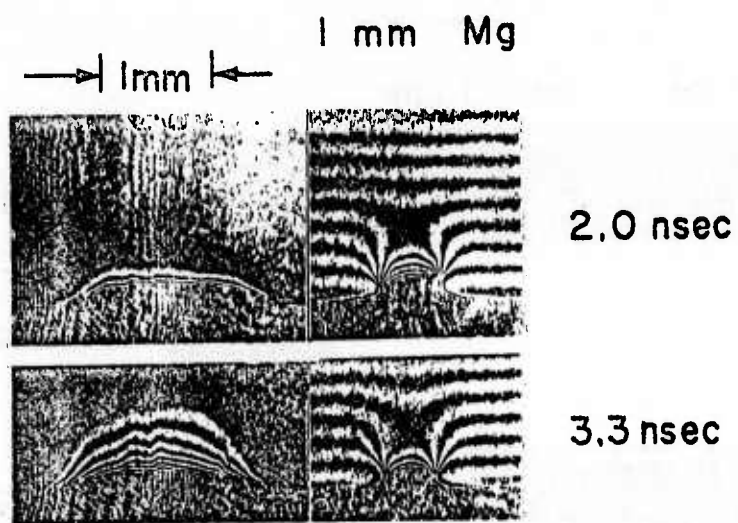


Figure 6b

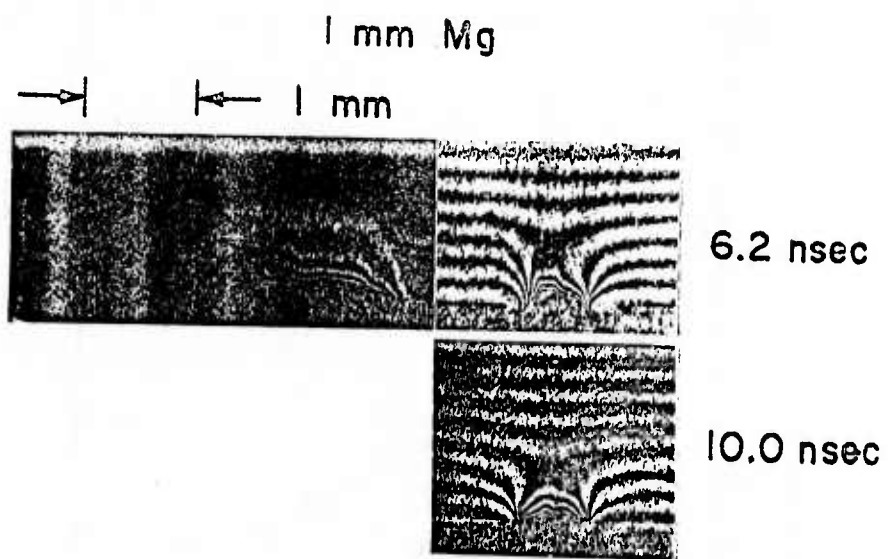


Figure 6c

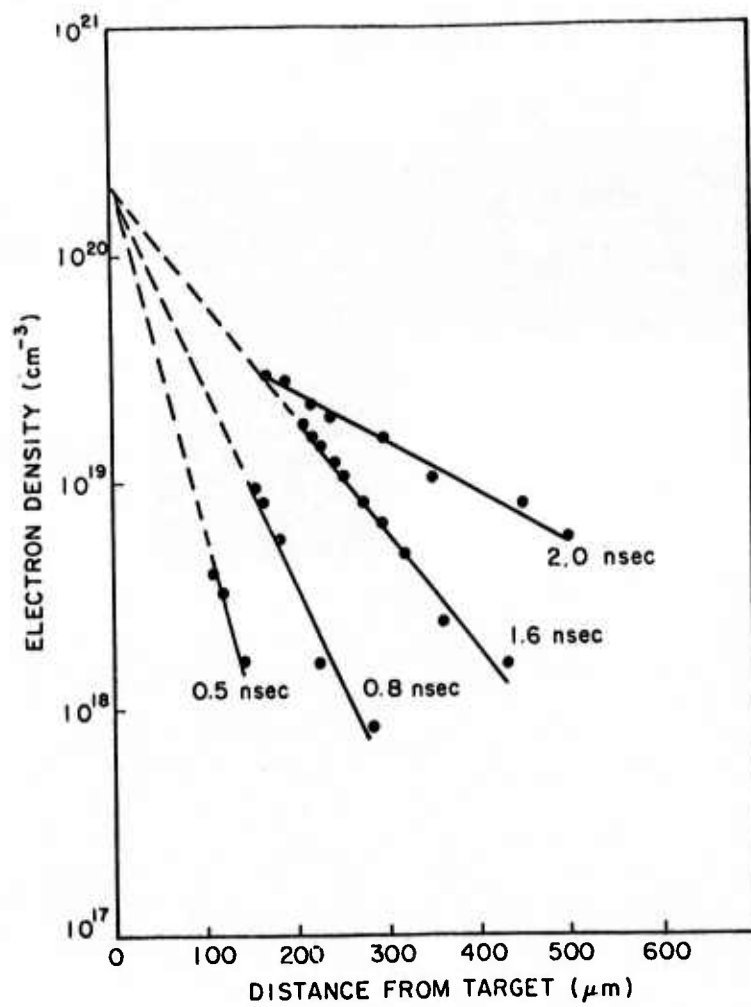


Figure 7

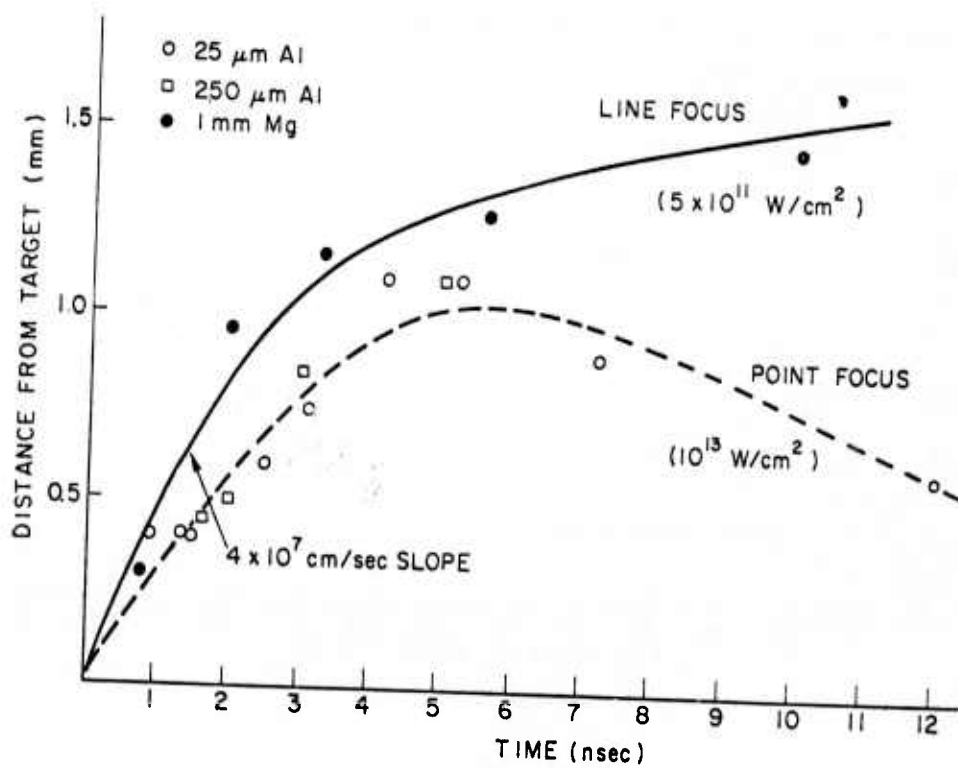


Figure 8

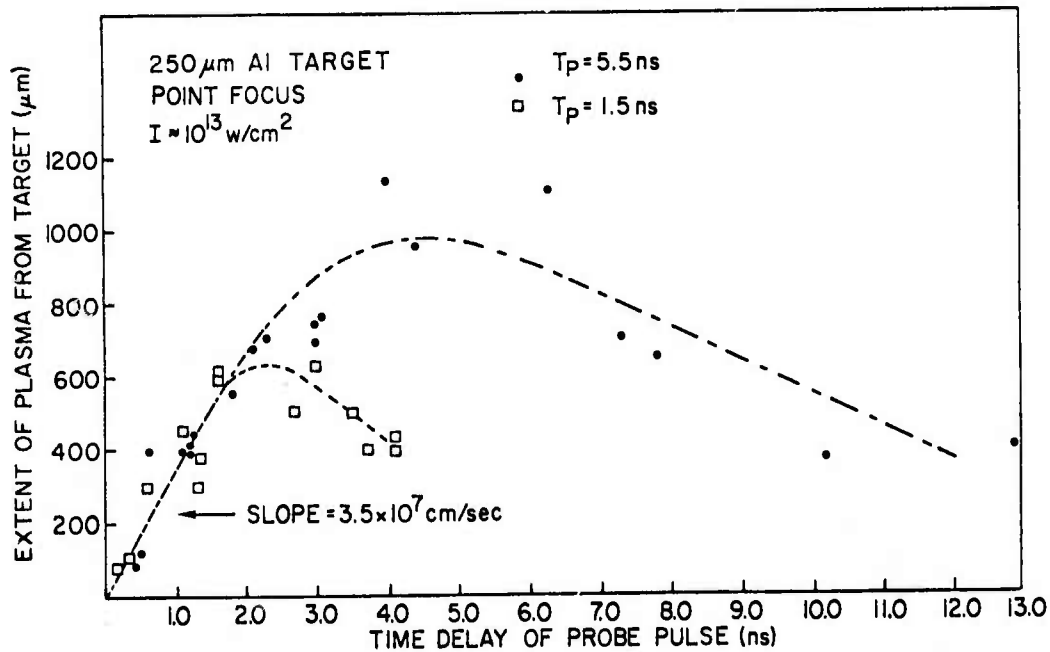


Figure 9

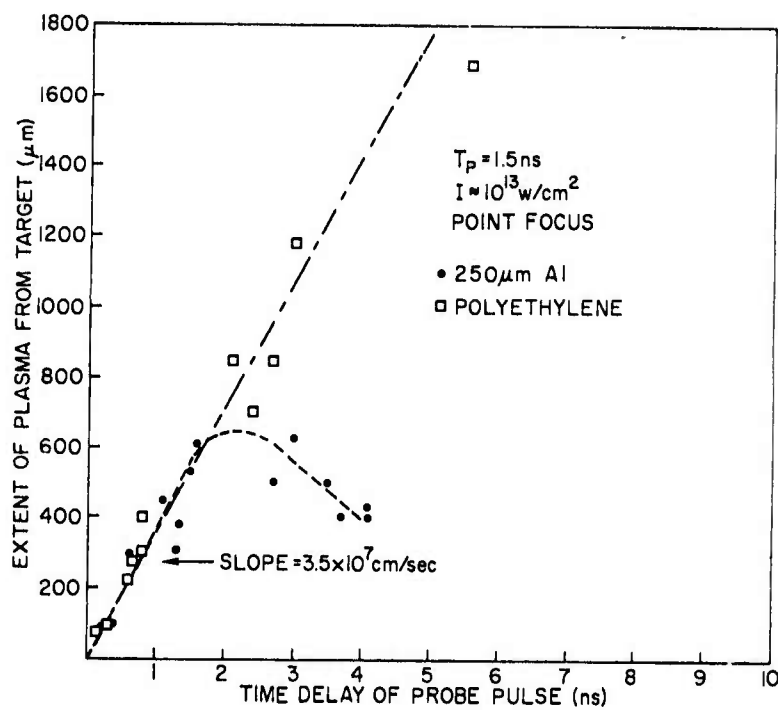


Figure 10

Efficient Harmonic Generation

From 532 nm to 266 nm in ADP and KD*P†

J. Reintjes and R. C. Eckardt
Naval Research Laboratory
Washington, D.C. 20375

Abstract

Second harmonic generation of mode-locked pulses in ADP and KD*P from 532 nm to 266 nm with 85% conversion is reported. Two-photon absorption coefficients are measured for the two materials and found to be relatively unimportant in the limitation of harmonic conversion compared to the effects of phase mismatch and dispersion.

†Work supported in part by Defense Advanced Research Projects Agency under ARPA Order 2694.

The generation of the fourth harmonic of Nd laser radiation by two successive stages of second harmonic generation provides a convenient source of high-power ultraviolet pulses for a variety of applications. In experiments involving high conversion levels, there have been significant discrepancies reported between theory and experiment in the conversion efficiencies of the second harmonic to fourth harmonic in crystals of ammonium dihydrogen phosphate (ADP) and potassium dideuterium phosphate (KD*P). Typical experimental values lie between 30 and 40% for a wide range of experimental conditions and pulse durations, while corresponding theoretical conversions are in the range of 70-80%. It has been pointed out that conversion of short laser pulses can be limited when dispersion in the group velocity reduces the spectral width of the phase matching peak below that of the laser pulse¹. The observed discrepancies in conversion efficiency have also been attributed in the literature to such varied processes as energy loss due to linear or nonlinear absorption at 266 nm, disturbance of the phase matching condition due to absorption followed by local heating, and improper or incomplete phase matching²⁻⁴.

In this letter we wish to report observation of high efficiency conversion of picosecond pulses from 532 nm to 266 nm in short crystals (4 mm in length) of both ADP and KD*P. Energy conversion efficiency up to 85%, the highest value yet reported at these wavelengths, has been observed in ADP, and comparison with theoretical calculations shows excellent agreement. We also investigated the relative importance of absorption losses and limited phase matching due to phase mismatch in the crystal or phase modulation of the pump pulse in limiting conversion efficiency.

The second harmonic conversion measurements were made using single amplified pulses of 30-psec duration from a mode-locked Nd:YAG laser. The infrared output pulses were frequency doubled to 532 nm in KDP with an efficiency of about 70%, and residual infrared radiation was prevented from reaching the uv generating crystal by a calcite polarizer. Typical green input energies of 15 mJ were measured with a calorimeter. The pump pulse duration was measured with a 5-psec resolution streaking camera which showed single pulses of 30-psec duration without amplitude substructure. Spectral measurements of the green pulse showed a width of .09 nm, corresponding to self-phase modulation of 0.8π which originated in the laser amplifier chain. The beam profiles as observed with a silicon photodiode array were elliptical-Gaussian clipped on the horizontal edges by a limiting aperture at the KDP crystal. Various telescopes were used to obtain different incident intensities of the pump pulse at the fourth harmonic crystal while maintaining constant energy.

Harmonic conversion efficiency from 532 nm to 266 nm was measured by monitoring simultaneously the incident and transmitted green pulses along with the generated harmonic pulse as the crystal was tuned through its phase-matching peak by varying either the angle or temperature. In addition to observing the harmonic generation and pump depletion, we observed the variation of the normalized sum of the harmonic pulses and transmitted green pulses

$$S = \frac{E_t}{E_o} + \frac{E_h}{E_o}$$

where E_t is transmitted green energy, E_h the harmonic energy, and E_o the incident green energy. A deviation of the sum from unity as the crystal is tuned across the phase matching peak indicates the presence of optical losses in the crystal.

Linear and nonlinear absorption at 266 nm were measured separately on several samples of each material. Linear absorption coefficients for both materials were 0.035 cm^{-1} . Two-photon absorption coefficients were determined to be $\beta = 6 \pm 1 \times 10^{-11} \text{ cm/W}$ for ADP and $\beta = 2 \pm 1 \times 10^{-11} \text{ cm/W}$ for KD*P. No significant sample-to-sample variations were observed.

We investigated the effect of crystal length on harmonic conversion efficiency using 4-mm, 12-mm, and 25-mm crystals of ADP and 4-mm, 12-mm, and 20-mm crystals of KD*P (the two shortest crystals of KD*P were 99% deuterated and the longest 90% deuterated). The 25-mm crystal of ADP was temperature tuned at 90° phase matching while the rest of the samples were angle tuned at room temperature. Peak intensity of the green pulse was 10^9 W/cm^2 for these measurements. For each material conversion efficiency first increased with crystal length and then decreased (Fig. 1). This behavior is similar to that reported elsewhere³ and has been used to infer the importance of nonlinear absorption in reducing the efficiency in longer crystals. In the present case, however, the constancy of the energy sum (see Fig. 1) shows that the effect of optical losses is negligible. This result is in agreement with calculations based on the measured absorption coefficients, which show that two-photon absorption is not effective in reducing conversion below 90% when the optimum crystal length is used.

The increased green transmission in the longer crystals indicates that the harmonic is driving the fundamental through a parametric back reaction, implying a loss of perfect phase matching. This effect was confirmed by spectral measurements which showed that considerable structure appeared on both the transmitted pump and generated harmonic pulses when the longer crystals were used (Fig. 2). This behavior is consistent with calculations of Karamizin and Sukhorukov⁵ which indicated that phase modulation in the presence of group velocity mismatch results in amplitude structure on the pulse. Our

calculations which take into account dispersion and parametric back reactions and which will be presented elsewhere in greater detail show that the conversion of phase-modulated pulses undergoes oscillation with crystal length. The result for a Gaussian phase-modulated pulse with the parameters of our input pulse is shown in Fig. 1. The experimental variation of conversion efficiency with crystal length is qualitatively accounted for by this calculation. Exact quantitative agreement for all crystal lengths would require precise knowledge of the phase structure of the input pulse.

If lack of perfect phase matching is the only limiting mechanism of conversion in longer crystals, optimum conversion should be obtained in shorter ones. Accordingly, we measured conversion as a function of pumping intensity for 4-mm samples of ADP and KD*P (Fig. 3). The energy conversion increased monotonically with intensity for both materials. Efficiencies up to 85% were observed in ADP and 75% in KD*P at pump intensities of $8 \times 10^9 \text{ W/cm}^2$. The measured values of energy conversion in ADP were compared with theoretical calculations using experimentally determined beam parameters and a value of $d_{\text{eff}} = .56 \times 10^{-12} \text{ m/V}$ for the second harmonic coefficient⁶. Theoretical curves are shown in Fig. 3 of harmonic conversion of pulses with Gaussian temporal shape and either uniform or Gaussian spatial profiles. The experimental points for ADP lie consistently between the theoretical values calculated for these two beam profiles. This indicates that good agreement between theory and experiment would be obtained for a spatial profile which is intermediate between the two forms which were considered here. Such an intermediate profile would be representative of the clipped elliptical beam actually used in our experiments. Thus we conclude that our experimentally determined conversion efficiencies are in substantial agreement with theory, with more exact quantitative agreement requiring more precise

knowledge of all beam characteristics. The consistently lower values of conversion efficiency for KD*P as compared to ADP can be accounted for by the lower tabulated value for the second harmonic coefficient.

The results presented in this letter demonstrate that the most efficient harmonic conversion of 30-psec pulses from 532 nm to 266 nm in ADP or KD*P is obtained in short crystals (< 1 cm) at high intensities ($> 10^9$ W/cm²). If nonlinear absorption were the dominant limiting mechanism, optimum conversion would require the use of long crystals and low intensities. However, our measurements show that absorption effects cause negligible energy loss for the harmonic generation in this experiment. Conversion efficiency in long crystals is limited by group velocity dispersion combined with small amounts of phase mismatch. Perhaps more important than decreased conversion is the appearance of spectral and temporal distortion of the harmonic pulses that occurs in longer crystals.

The use of picosecond-duration pulses limits this investigation to instantaneous effects. These results therefore can provide a useful basis for comparison of results obtained with longer-duration Q-switched pulses at high repetition rates in which instantaneous and long-term effects have not been unambiguously distinguished. Our measurement of two-photon absorption in ADP is consistent with the value which can be inferred from measurements with longer pulses³. Consequently, we do not expect this absorption to increase due to integrating effects. Thus, nonlinear absorption by itself is unlikely to effectively limit conversion of longer Q-switched pulses. It can however cause local heating, resulting in loss of phase matching as has been previously observed³.

A comparison of ADP and KD*P showed that the two materials behaved qualitatively similarly under short-pulse excitation. Conversion efficiency in the short crystals was slightly higher in ADP than KD*P for a given pumping intensity.

Measurements on longer crystals of both materials showed the same degree of spectral structure, indicating that the group velocity dispersion of KD*P is close to that of ADP in this wavelength range. KD*P has the advantage of better stability with small changes in temperature⁴, and the lower two-photon absorption coefficient could reduce local heating at higher average powers.

The authors thank David Anafi of Lasermetrics for use of the 20-mm KD*P crystal and J. M. McMahon, C. Y. She, and L. J. Palumbo for critical reading of this manuscript.

REFERENCES

1. W. H. Glenn, IEEE J. Quant. Electron. QE-5, 284 (1969).
2. V. D. Volosov, V. N. Krylov, V. A. Serebryakov, and D. V. Sokolov, ZhETF Pis. Red. 19, 38 [JETP Letters 19, 23-25 (1975)].
3. K. Kato, Optics Communication 13, 361 (1975).
4. Y. S. Liu, W. B. Jones, and J. P. Chernoch, Appl. Phys. Letters 29, 32 (1976).
5. Y. N. Karamzin and A. P. Sukhorukov, Krant. Electron. (Mosc.) 2, 912 (1975), [Sov. J. Quant. Electron. 5, 496 (1975)].
6. S. Singh, "Non-Linear Optical Materials," Handbook of Lasers with Selected Data on Optical Technology, Robert J. Pressley, Ed. (The Chemical Rubber Co., Cleveland, Ohio, 1971) p. 501. While a range of values of d are tabulated, the text lists a standard value of 0.57×10^{-12} m/V for the second harmonic coefficient of ADP. In the interests of standardization we have used this value for our calculations and have determined a value of $d_{\text{eff}} = d \times \sin \theta_{\text{PM}} = .56 \times 10^{-12}$ m/V for the effective coefficient of ADP at a room temperature phase matching angle of 80.3° .

FIGURE CAPTIONS

- Fig. 1 - Dependence of harmonic conversion efficiency (a) and energy sum (b) on crystal length. Experimental points are determined at the peak of the phase matching curve. The theoretical curve (solid line) is calculated for a phase modulated pulse with the parameters of our input pulse, taking into account group velocity dispersion and parametric back reactions. The dotted line is drawn through the experimental values of the energy sum.
- Fig. 2 - Spectral distribution of incident and transmitted pump and harmonic pulses in 25 mm ADP crystal.
- Fig. 3 - Dependence of harmonic conversion efficiency on peak pump intensity for 4-mm crystals of ADP and KD*P. The theoretical curves are calculated for ADP in the absence of dispersion for the indicated spatial profiles.

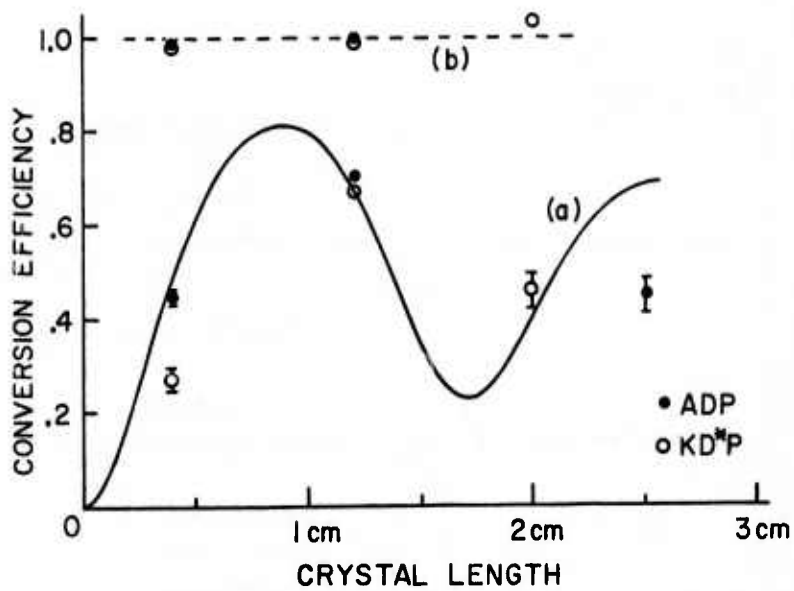


Figure 1

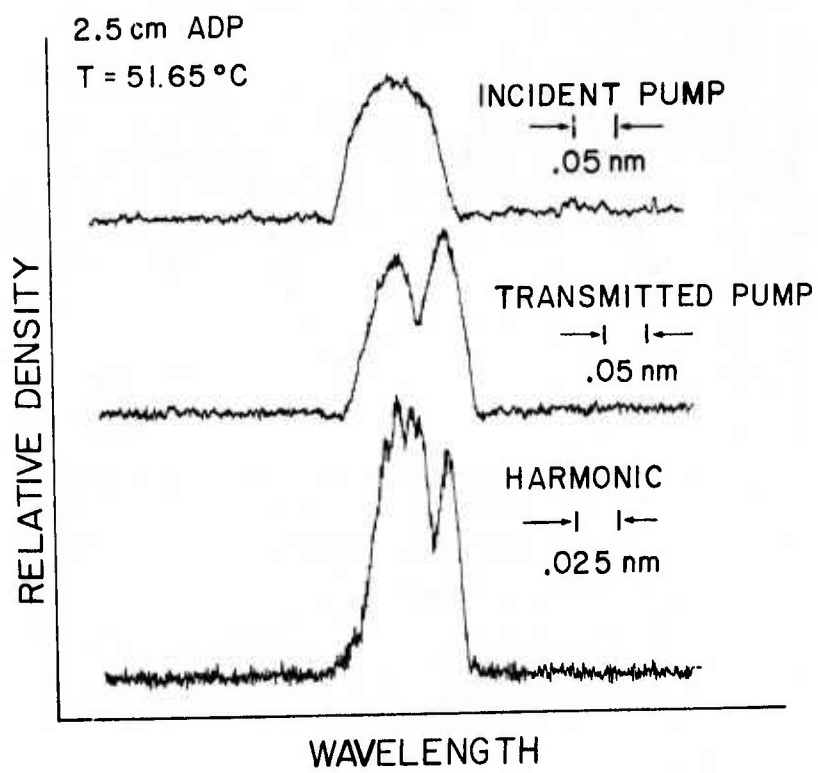


Figure 2

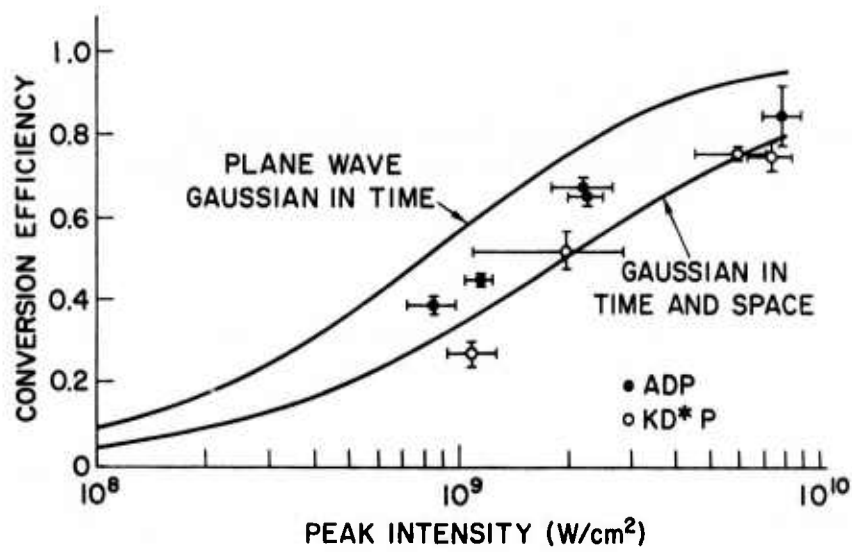


Figure 3

PREPRINT

Submitted to J. Opt. Soc. America

Short-Wavelength Laser Calculations for Electron Pumping
in Carbon-Like and Helium-Like Ions*

L. J. Palumbo and R. C. Elton
Naval Research Laboratory
Washington, D.C. 20375

A steady-state computer code has been used to compute population densities of excited terms in carbon-like and helium-like ions. It is shown that an inversion between terms of the $1s^2 2s^2 2p^3 p$ and $1s^2 2s^2 2p^3 s$ configurations sufficient to produce observable laser gain can be obtained in high-density plasmas such as produced by laser irradiation of pellets or electromagnetically driven pinch discharges. Such inversions in elements of atomic number $Z = 15-40$ give rise to lasing in the 1200-300 Å range. Shorter wavelength lasing (80-5 Å) on $1s^3 s \rightarrow 1s^2 p$ transitions in helium-like ions of $Z = 10-40$ is also modeled; but significant gain is probably not possible with current plasma devices.

*This work is part of the joint NRL/ARPA Soft X-Ray Laser Program (ARPA Order 2694).

This is a preprint of a paper intended for publication in a scientific journal. Since changes may be made prior to publication, please contact the authors before referencing any material contained herein.

I. INTRODUCTION

An intense effort has been underway for the past several years to find methods for generating coherent radiation at wavelengths shorter than 1000 Å, as is evidenced by the large number of experimental and theoretical publications in this field. Details are treated in a recent review paper¹ and in references therein. Barring some fortuitous discovery, short-wavelength lasing will most likely be attained by a progressive step-by-step process, possibly working from known lasing schemes in the UV to shorter and shorter wavelengths into the soft x-ray spectral region. A straightforward approach would be the isoelectronic extrapolation of a known lasing scheme in the visible or near-UV involving a neutral atom or a low stage of ionization²⁻⁴, and attaining vacuum-UV lasing using higher stages of ionization as created in a plasma. As a precedent, a number of ions have recently been shown⁵ to lase in the near-UV region in Z-pinch plasma devices; extrapolation to non-cavity amplification is the first challenge.

This article reports on a scheme for achieving lasing below the 1000 Å "barrier" by the isoelectronic extrapolation of a transition which is responsible for a large number of known visible and near-UV ion lasers, many of which have been shown to lase in the cw mode, i.e., with steady-state population inversion. This is of great importance for vacuum-UV lasers, where self-terminating inversions require very short pump risetimes^{1,6}. The method and results reported here represent primarily a refinement of previous analytical calculations for 3p-3s lasing in six-electron carbon-like ions, following electron collisional pumping from a 2p ground state reservoir⁷. Initial extrapolations to high densities⁸ are expanded upon. Also, the multiple ionic energy levels and the atomic transitions between them are considered in increased detail here through the use of a computer program which solves coupled steady-state rate equations to obtain energy-level population densities for given plasma conditions. The addition of ionization and recombination, as well as radiative trapping, represent other important advances in the present results.

Because of the close similarity between the carbon-like scheme and another electron-collisional pumping scheme involving 3s-2p lasing (collisionally pumped 1s-3s) in the 30-100 Å range in moderate-Z helium-like ions, the computer code developed for the carbon-like ions was also used to model this two-electron

scheme. Although population inversions were computed and are presented for a wide range of plasma conditions and for a number of elements in the helium isoelectronic sequence, the resulting net gain calculated is insignificant at densities and dimensions available in state-of-the-art plasma devices.

Both of these schemes operate over transitions of insufficient energy to cause photoionization losses in the amplifying medium, in contrast to innershell schemes proposed for short-wavelength lasing where such losses can be the limiting factor^{1,9}.

Descriptions of the physical model and computer code are given in the next section, results for the carbon-like and helium-like schemes are presented and described in Section III, and the feasibility of these schemes for producing short-wavelength lasing is discussed briefly in Section IV.

II. NUMERICAL MODEL

A. Pumping Schemes

As diagrammed in Fig. 1 for the six-electron carbon-like species and mentioned in the Introduction, the $3p\ ^3D$ upper laser term is assumed⁷ to be pumped by electron collisional excitation from the $2p\ ^3P$ ground term on the same ion¹⁰. Radiative coupling of these two terms is dipole forbidden, so that spontaneous and stimulated emission into the $3s\ ^3P$ lower laser term is favored. Also, the population density in this latter term is rapidly depleted to the $2p\ ^3P$ ground "reservoir" term by dipole decay, resulting in a possible steady-state population inversion and quasi-cw lasing. The terminology "quasi" here refers to possible transient lasing conditions associated with environmental plasma changes; and not to self-termination often associated with short-wavelength laser schemes and caused by lack of either lower laser term depletion or reservoir state replenishment. The latter is a common problem with many schemes based upon pumping by ionization or recombination and is eliminated in a single-ion scheme such as modeled here, where the initial reservoir term is rapidly replenished by dipole decay from the lower laser term, with continuous lasing resulting.

At the increased densities required for amplification without multiple pass cavities, collisional mixing between terms becomes an important process competing with radiative transitions, and the nearby $3d\ ^3D$ term is the most important. This term is strongly dipole coupled to the ground term (as is the lower laser term) and is included in the modeling. This strong radiative coupling also requires the inclusion of resonance trapping effects for both terms in the numerical model. The total density of lasing ions in the plasma, and hence the net gain, would be affected by significant ionization or recombination. For example, at the high temperatures desired for large collisional pumping the former is a concern for creating significant densities of boron-like ions. Hence, ionization and recombination rates between carbon-like and boron-like ions are included.

In close analogy to this $3p\text{-}3s$ model, the $3s\ ^1S$ term in helium-like ions is assumed to be pumped from the $1s\ ^1S$ ground term by collisions, with lasing taking place on $3s\ ^1S\text{-}2p\ ^1P$ transitions followed by rapid $1s\ 2p\ ^1P\text{-}1s\ ^1S$ resonance decay. The detailed term structure is shown in Fig. 2.

B. Rate Equation Code

In the most general case, the populations of the excited and ground levels of an atomic species in a plasma can be determined at each point in time by the simultaneous solution of a set of rate equations which express the time rate of change of the population density of each atomic energy level as the sum of the rates which populate this level by transitions from all other levels, minus the sum of the rates which reduce the population of the given level by transitions into all other (higher or lower) levels. If the rate at which plasma conditions (temperature and density) change is much smaller than the dominant transition rates in the time-dependent rate equations, then each rate of population density change can be neglected (set to zero); this yields a coupled set of time-independent or steady-state rate equations, each of the form

$$\frac{dN_k}{dt} = 0 = \sum_{j \neq k} N_j W_{jk} - N_k \sum_{j \neq k} W_{kj}, \quad (1)$$

where t is the time, N_j and N_k are population densities of levels j and k ,

and W_{jk} (similarly for W_{kj}) represents the sum of the rates for all atomic processes which populate level k from level j . An equation of type (1) is required for each level, k , considered. In general, levels j and k may be in the same or in different ionization stages, and the W 's are functions of the ionization species, the temperature, the density, and the radiation field intensity at each point in the plasma.

For a precise dynamical plasma model, one must solve a large set of time-dependent rate equations, taking into account all important excited and ground levels for each stage of ionization of each element found in the plasma. All significant atomic processes affecting the population densities of these levels (including ionization and recombination) must be included in the computation, as well as the possibility that the populations may vary not only temporally but also spatially due to boundary effects, plasma motion, plasma structure, radiation transport, etc. It was not the aim of the present effort to produce such a full-scale plasma model. Rather, the purpose was to introduce certain simplifying plasma assumptions into a model to estimate the conditions required to produce population inversions in plasma ions, to look for optimum plasma conditions, to identify promising elements and ionization stages for producing lasing in existing plasmas, and to gain physical insight into the processes resulting in or hindering the achievement of short-wavelength lasing in highly stripped ions.

In the present code, the population densities of the levels of interest and the electron and ion densities are assumed to be spatially homogeneous; they are also assumed to be time independent in order to avoid the solution of a set of coupled differential equations, rendered nonlinear by the inclusion of radiation trapping as discussed below. Thus the inversion and gain computed here would be valid for a homogeneous portion of a larger plasma and would be applicable to plasmas which maintain their conditions for a reasonably long time. Similarly, all other relevant plasma parameters, such as the electron temperature, T_e , and the ion temperature, T_i (which is assumed in most cases to be equal to T_e under the equilibrium conditions achieved rapidly at high densities), are assumed constant in time. Plasmas in existing devices which satisfy this condition are mentioned below.

The credibility of the present calculations is enhanced by the agreement between the results reported here and experimental results⁵ for similar ionic configurations. In a sense, the present steady-state model yields mainly minimum lasing requirements. Transient conditions can be defined during a heating phase in which enhanced inversion densities (and gains) can be achieved at higher temperatures before significant ionizing depopulation of the desired species occurs; this possibility is analyzed below for the carbon-like ions.

It should be noted here that although the present analysis for $3p\rightarrow 3s$ lasing concentrates on carbon-like ions, the computed population inversions and gain should be comparable for $3p\rightarrow 3s$ transitions in the boron-like through the neon-like sequences, i.e., where $2p$ valence electrons exist. The six-electron ion was chosen as a model because it was expected⁷ to produce slightly (but not significantly) more gain than other ions of more or fewer electrons. In fact, boron-like ions may produce a simpler spectrum, and neon-like ions may be advantageous due to the extended lifetime association with rare gas type ionic species of increased ionization energy¹¹.

The set of equations (1) is solved when reduced to a finite and tractable number by considering only the most relevant levels in the carbon-like or helium-like ion. For the triplet terms in the carbon-like ion, the levels corresponding to a particular J value are assumed to be populated in proportion to their statistical weights. This is plausible since collisional mixing is rapid between these closely spaced levels for the large electron densities required to achieve observable single-pass gain along the small plasma lengths attainable with present-day devices. Hence, in computing the carbon-like population densities, the levels of a given term are lumped together and the averaged term-to-term transition rates are used in Eq. (1). However, because the width of the lasing line is less than the $3p\rightarrow 3s$ multiplet splitting, the gain is computed only for the strongest component of the multiplet. Also, only those terms of the ground and excited configurations which are expected to have the largest effect on the population inversion are considered. The energy levels and the important transitions between them are included in Figs. 1 and 2.

Thus, a coupled set of five equations of type (1) are solved for population densities of the following carbon-like terms, where the numbers in parentheses are the respective subscripts used in subsequent equations and in Fig. 1: (1) the ground term, $2p^3\ ^3P$; (2) the lower laser term, $2p3s\ ^3P$; (3) the upper laser term, $2p3p\ ^3D$; (4) the nearest competing term, $2p3d\ ^3D$; and (5) the ground term of the next higher ionization stage (boron-like ion). Transitions from the ground term into other excited triplet terms deplete the ground reservoir term population by at most a few percent for the conditions which show appreciable population inversion, and are thus ignored. The three terms of the ground configuration of the carbon-like ions (under most plasma conditions of interest here) contain most of the population, and it is assumed that this population is divided among these terms in proportion to their statistical weights; with 60% [P in Eq. (17)] of the total population density in the triplet system (shared by the 3P ground term and the sparsely populated excited triplet terms) and the remainder shared between the $2p^2\ ^1S$, $2p^2\ ^1D$, and excited singlet terms. The total ion density is tied to the electron density through charge neutrality.

Because it is desired to operate at a high temperature for maximum pumping, only ionization equilibrium with the next higher ionic species is considered. The gain is optimized by selecting a temperature for rapid pumping without excessive lasing-species depletion by ionization. Analogously, for the helium-like ions, a set of five coupled rate equations is solved with subscripts 1 through 5 designating the following singlet terms: (1) the ground term, $1s^2\ ^1S$; (2) the lower laser term, $2p\ ^1P$; (3) the upper laser term, $3s\ ^1S$; (4) the nearest competing term, $3p\ ^1P$; and (5) the $1s\ ^2S$ ground term of the next higher (hydrogenic) ionization stage. The fraction of the total helium-like ion density which occupies the triplet system is expected to be small for the high Z 's and high densities considered here.

C. Rates Applied

In computing the rates (W 's) in Eq. (1), estimates of all important collisional radiative processes between the five terms mentioned above were included where applicable. Specifically included for the lasing ion were electron-collisional excitation, deexcitation, ionization, and recombination (three-body),

as well as spontaneous photoemission, resonance photoabsorption (through a radiation trapping treatment), and radiative recombination. The effects of photoionization and dielectronic recombination processes were insignificant. For efficient computation, simple analytical estimates for the rates of the various atomic processes were used in place of more accurate quantum mechanical calculations or published tabulations of such results (which are not available for all transitions, species, and ionization stages required in the present study). Most of these analytical formulas were obtained from collections included in References 12-14. A Maxwellian velocity distribution of electrons was assumed to hold for all calculations.

1. Excitation and Deexcitation

For the numerous transitions and ions included, the convenient¹⁵ effective Gaunt factor, or \bar{g} , analytical formula of Seaton¹⁶ and Van Regemorter¹⁷ was used to compute the collisional excitation rate, C_{jk} , for transitions from lower level j to upper level k

$$C_{jk} = N_e X_{jk} = 64\pi^2 \left(\frac{\pi}{3}\right)^{\frac{1}{2}} \frac{E_H}{h} a_0^3 N_e \left(\frac{E_H}{kT_e}\right)^{\frac{1}{2}} \left(\frac{E_H}{\Delta E_{jk}}\right) \times \quad (2)$$

$$f_{jk} <\bar{g}>_{jk} \exp(-\Delta E_{jk}/kT_e),$$

where N_e is the electron density, X_{jk} is the collisional excitation rate coefficient, h is Planck's constant, a_0 is the radius of the first Bohr orbit, E_H is the ionization potential of ground-state hydrogen (13.6 eV), k is the Boltzmann constant, T_e is the electron temperature, ΔE_{jk} is the energy gap between levels j and k , f_{jk} is the absorption oscillator strength for j - k transitions, and $<\bar{g}>$ is a Maxwellian-averaged effective Gaunt factor. The rates for collisional deexcitation, D_{kj} were computed from the rates for collisional excitation through detailed balancing,

$$D_{kj} = N_e X_{kj} = \frac{g_j}{g_k} C_{jk} \exp(\Delta E_{jk}/kT_e), \quad (3)$$

where X_{kj} is the collisional deexcitation rate coefficient and g_j and g_k are the statistical weights of levels j and k , respectively.

The energy-level spacings, ΔE_{jk} , were approximated by scaling either as z^2 or z for levels j and k of different or same principal quantum number, respectively, where z is the spectrum number or the charge seen by the outer (optical) electron. Scaling coefficients were estimated from tabulated energy levels^{18,19} and spectral lines²⁰, and the ΔE 's should be accurate to better than 15%. The oscillator strengths required for the modeling of the carbon-like scheme were assumed²¹ to be constant along the isoelectronic sequence for $\Delta n \neq 0$ transitions and to vary as Z^{-1} (where Z is the nuclear charge) for $\Delta n = 0$ transitions, with values extrapolated from limited data for low ionization stages published by Wiese, et al¹⁸. The more abundant data¹⁸ on helium-like ions allow the use of a much more accurate oscillator-strength estimate varying linearly with Z^{-1} . The Gaunt factor, $\langle \bar{g} \rangle_{jk}$, is a function of $x \equiv \Delta E_{jk}/kT_e$ obtained earlier from an empirical fit^{12,16,17} to existing data. An accumulation of experimental and theoretical results for scattered cases^{16,22} indicates that this empirical fit is approximately correct for $n=2$ to $n=3$ transitions. Thus, the data can be fitted in the relevant range of $x = 0.04$ to 1.0 by a power law expression,

$$\langle \bar{g} \rangle_{jk} = \alpha x^{-\beta}, \quad (4)$$

with $\alpha = 0.17$ and $\beta = 0.47$. For $x \geq 1.0$, a constant value of 0.17 is assumed. For $n=3$, $\Delta n=0$ transitions, it has become clear that the Gaunt factor is higher and, for the relevant range of $0.01 \leq x \leq 0.7$, a similar relation is assumed with $\alpha = 0.63$ and $\beta = 0.15$. This latter fit also appears to be approximately correct for the helium-like ion resonance transitions $n=1$ to $n=2,3$ which involve the $x = 0.1 - 1.0$ range. These expressions for $\langle \bar{g} \rangle_{jk}$ cannot be expected to be more accurate than a factor of two at present, and the separate expressions assumed are only significant for the larger values of x , where a common averaged expression would lead to an overly optimistic gain resulting from increased collisional pumping and decreased $n=3$ mixing.

The adopted oscillator strengths, Gaunt factors, and energy-level scaling relations are listed in Table 1. For computing the collisional excitation and deexcitation rates for the $\Delta n=1$ "dipole-forbidden" $2p\ ^3P-3p\ ^3D$ transition between terms of the same parity, Eqs. (2) through (4) were used with an oscillator strength assumed equal to 0.3 as deduced from calculations published by Vainshtein, et al.²² For the $\Delta n=0$ quadrupole $3s\ ^3P-3d\ ^3D$ excitation rate both zero and a value equal to the $3s\ ^3P-3p\ ^3D$ dipole rate were assumed. The true value is expected to be the smaller for the small energy gap involved. The effect of the comparison on the computed peak gain values was $\leq 20\%$ and a zero value was used.

2. Radiative Decay with Opacity

Spontaneous radiative decay rates, A_{kj} , were computed from the absorption oscillator strengths f_{jk} , by¹⁸

$$g_k A_{kj} = 8\pi^2 \frac{c r_0}{\lambda_{kj}^2} g_j f_{jk}, \quad (5)$$

where c is the velocity of light, r_0 is the classical electron radius, and λ_{kj} is the wavelength of the radiation emitted in a spontaneous transition from k to j . Induced emission²³ terms, $I_{\nu kj}$, can be ignored for $n=3$ to $n=2$ resonance transitions because $I_{\nu kj}/A_{kj} = [(g_k N_j / g_j N_k) - 1]^{-1} \approx 0.15$, for $\Delta E_{jk}/kT_e \approx 2$ at $kT_e = 1.0\text{ eV}$. This is also the case for transitions between $n=3$ terms as long as the plasma is optically thin in the transverse direction, as is calculated for the conditions considered. Resonant photoabsorption in an optically thick plasma can be important in reducing the effective lower-laser-level radiative depletion rate and, hence, destroying the steady-state inversion; consequently, it must be considered in a model of this type. Since the only source of resonant radiation is assumed to be from spontaneous emission, resonant photoabsorption is accounted for by modifying the radiative decay rate with an "escape factor" $F_{kj}(\bar{\tau}_0)$ according to a method originally treated by Biberman²⁴ and Holstein²⁵ and conveniently summarized by McWhirter²³, where

$$F_{kj}(\bar{\tau}_0) = 1 - \frac{1}{\sqrt{\pi}} \int_{-\infty}^{\infty} \exp(-x^2) \{1 - \exp[-\bar{\tau}_0 \exp(-x^2)]\} dx. \quad (6)$$

Here $\bar{\tau}_0$ is the optical depth at line center, which for Doppler-broadened lines²⁶ is given by¹²

$$\bar{\tau}_0 = \left(\frac{\pi M_i c^2}{2 k T_i} \right)^{\frac{1}{2}} r_0 \lambda_{kj} N_j f_{jk} r \quad (7)$$

with M_i the mass of the radiating ion, T_i is the ion temperature, and r the plasma radius. The escape factor, which is an inverse function of the optical depth (and hence of the lower-level population density), ranges between zero and unity and reduces the effect of the decay process at large depths. The explicit inclusion of this factor in Eq. (1) makes this set nonlinear, requiring a solution by iterative methods; this dictated a limitation to a reasonable number of levels included in the modeling. Since the optical depth depends upon the physical dimensions of the medium, the plasma diameter became an additional important parameter.

3. Ionization and Recombination

The most convenient formula for computing the rates, I_{j5} , of electron collisional ionization from the ground ($j=1$) and excited terms ($j=2,3,4$), respectively, of the lasing ion into the ground term (5) of the next higher species comes from a semi-empirical formula in a form given by Kunze²⁷ (which fits the data compiled by Lotz²⁸)

$$I_{j5} = 7.5 \times 10^{-8} \frac{q N_e}{\Delta E_{j5}} \left[\left(\ln \frac{40 k T_e}{\Delta E_{j5}} \right)^3 + 40 \right] \times \frac{(k T_e)^{\frac{1}{2}}}{\Delta E_{j5} + 3 k T_e} \exp (-\Delta E_{j5} / k T_e) \text{ sec}^{-1}, \quad (8)$$

where q is the number of equivalent electrons in the outer shell and ΔE_{j5} is the ionization potential from term j . Both $k T_e$ and ΔE_{j5} are in eV, while N_e is in cm^{-3} . For the helium-like ions, this formula is expected^{27,29} to be accurate to 15% for ground-state ionization and 25% for excited-state ionization. For ions other than hydrogenic and helium-like, this formula overestimates the

ionization rate by approximately a factor-of-two²⁹, and this correction was included in the carbon-like ion modeling. Rates for collisional (three-body) recombination, R_{5j}^c , into ground and excited terms were deduced from Eq. (8) using detailed balancing and the Saha relation to give

$$R_{5j}^c = \left(\frac{N_i}{N_5} \right)_{eq} I_{j5} = \frac{g_j}{g_5} \frac{h^3 N_e \exp(\Delta E_{j5}/kT_e)}{2 (2\pi m_e kT_e)^{3/2}} I_{j5}, \quad (9)$$

where $(N_i/N_5)_{eq}$ is the thermal equilibrium population ratio and m_e is the electron mass.

The rate of radiative recombination, R_{5j}^r , into either ground or excited terms is adopted from a formulation due to Griem³⁰ for the total recombination rate into hydrogenic levels of a given principal quantum number, n , with appropriate corrections through a multiplicative factor Q_j for nonhydrogenic behavior of the ground terms and for statistical weight partitioning into the various terms. The rate is given by

$$R_{5j}^r = \frac{64}{3} \left(\frac{\pi}{3} \right)^{1/2} N_e r_o^2 c z Q_j x^{3/2} E_1(x) \exp(x), \quad j=1,2,3,4, \quad (10)$$

where $x = \Delta E_{j5}/kT_e$ and $E_1(x)$ is the exponential integral of index one. The total recombination rate, R_{5j} , into term j is defined by

$$R_{5j} = R_{5j}^c + R_{5j}^r. \quad (11)$$

4. Ion Collisional Rates

The rates for the important excitation and deexcitation processes due to ion collisions were estimated from the above electron collisional rates using a "guillotine factor" approach described by Weisheit¹³ and were found to be negligible for all conditions considered in the present modeling.

D. Explicit Rate Equations

Using the atomic rates defined in the above equations, one can write Eq. (1) explicitly:

$$\begin{aligned} \frac{dN_1}{dt} = 0 = & -N_1 (C_{12} + C_{13} + C_{14} + I_{15}) + N_2 (A_{21} F_{21} + D_{21}) \\ & + N_3 D_{31} + N_4 (A_{41} F_{41} + D_{41}) + N_5 R_{51}, \end{aligned} \quad (12)$$

$$\begin{aligned} \frac{dN_2}{dt} = 0 = & -N_2 (A_{21} F_{21} + D_{21} + C_{23} + C_{24} + I_{25}) + N_1 C_{12} \\ & + N_3 (A_{32} F_{32} + D_{32}) + N_4 D_{42} + N_5 R_{52}, \end{aligned} \quad (13)$$

$$\begin{aligned} \frac{dN_3}{dt} = 0 = & -N_3 (D_{31} + A_{32} F_{32} + D_{32} + C_{34} + I_{35}) + N_1 C_{13} + N_2 C_{23} \\ & + N_4 (A_{43} F_{43} + D_{43}) + N_5 R_{53}, \end{aligned} \quad (14)$$

$$\begin{aligned} \frac{dN_4}{dt} = 0 = & -N_4 (A_{41} F_{41} + D_{41} + D_{42} + A_{43} F_{43} + D_{43} + I_{45}) \\ & + N_1 C_{14} + N_2 C_{24} + N_3 C_{34} + N_5 R_{54}, \end{aligned} \quad (15)$$

and

$$\begin{aligned} \frac{dN_5}{dt} = 0 = & -N_5 (R_{51} + R_{52} + R_{53} + R_{54}) + N_1 I_{15} \\ & + N_2 I_{25} + N_3 I_{35} + N_4 I_{45}. \end{aligned} \quad (16)$$

These five equations are not linearly independent since, for the closed system of five levels, the sum of any four equations yields the fifth. However, an additional constraint imposed by the assumptions of charge neutrality and neglect of plasma motion (expansion or compression) yields an additional equation

$$N_e = \left(\frac{Z-6}{P}\right) (N_1 + N_2 + N_3 + N_4) + (Z-5) N_5 \quad (17)$$

which makes, for a selected electron density, the system soluble. Here P is the fraction of the lasing-species ions which occupies terms 1 through 4 and is set equal to 0.6 by assuming most of the population is in the ground terms of which N_1 represents the triplet contribution (Section II.B.).

Equations (12)-(17) were solved simultaneously for the five unknowns, N_k ($k=1$ through 5), by an iterative method. Since the escape factors for most conditions of interest were small perturbations, convergence was usually rapid.

III. CALCULATED RESULTS

A. Gain

The gain coefficients, α , for transitions $3p\ ^3D+3s\ ^3P$ in carbon-like ions and $3s\ ^1S+2p\ ^1P$ in helium-like ions were computed from the population densities, N_2 and N_3 , for a Doppler-broadened²⁶ line from³¹

$$\alpha = \left(\frac{\pi N_1 c^2}{2 k T_1} \right)^{\frac{1}{2}} r_0 \lambda_{32} g_2 f_{23} \left(\frac{N_3}{g_3} - \frac{N_2}{g_2} \right), \quad (18)$$

where g_2 , g_3 are the statistical weights for terms 2 and 3, respectively. Such gain coefficients have been computed for several decades of electron densities and suitable corresponding plasma diameters. These parameters were selected to simulate plasmas which can be produced by presently available technology. For the carbon-like results shown in Fig. 3, an equilibrium electron kinetic temperature, kT_e , equal to one-third the ionization potential (I.P.) of the lasing species being modeled was used, with $T_e = T_i$; pre-equilibrium enhanced temperature results shown in Fig. 4 are discussed further in Section III.C. below.

Equilibrium calculation results at $kT_e = kT_i = 0.7$ I.P. for helium-like ions are given in Fig. 5. In these figures, the gain product αL is plotted vs atomic number Z (and corresponding laser wavelength) and for several values of electron density N_e and plasma diameter d , with a fixed length $L = 10d$ chosen. The lower density curves, a and b, correspond to electrically driven dense pinch devices^{32,33} while the higher density curves, c and d, are more typical of laser-heated pellet conditions³⁴. The assumption $L = 10d$ is based upon an aspect ratio of 10:1 which is considered to be a reasonable maximum along a straight line axis in state-of-the-art plasma devices. The values chosen for d exceed those

below which severe diffraction losses would be expected to enter, i.e., $d \gg (\lambda L)^{1/2}$ or $d \gg 10\lambda$ for a 10:1 assumed aspect ratio. The computed gain products gL do not exceed 10 (corresponding to a single-pass gain of e^2) where it would be anticipated that saturation effects and particularly radial superfluorescence would enter as the product gd approaches unity. Thus, the choice of diameter d is dictated by a diffraction limit minimum and a radially thick maximum.

For clarity, the gain curves are shown as continuous lines, although computations were performed for integer values of Z . Significant gain products at higher Z values are achieved with the increased pumping rates associated with the higher electron densities. Each curve exhibits a minimum value of Z below which an inversion is not obtained because of dominant collisional mixing (the onset of Boltzmann equilibrium) between the upper and lower terms, which are closely spaced at these low Z values. (Negative gain values are not indicated on the $\log gL$ scale.) All curves reach a peak at a Z value somewhat higher than the collisional mixing cutoff due to a gradual reduction of the mixing effect resulting from the increased spacing of the laser levels with increasing Z . The decline in gain product as Z increases to values greater than this peak is due mainly to: (a) a reduced fractional population of excited terms resulting from a decreasing pumping rate for the larger pump energy gap, ΔE_{13} [see Eq. (2)], (b) a smaller number density of lasing ions at higher Z for a given electron density (from charge neutrality), and (c) the linear scaling of the gain coefficient g with wavelength as predicted⁸ for high densities.

The low- Z (long wavelength) cutoff, as well as the position and magnitude of the peak gain product have been found to be sensitive to plasma dimensions because of effects of radiative trapping. With trapping included, the peak gain rises due to increased $3p\ ^3D$ population from the $3d\ ^3D$ level and the low- Z cutoff shifts slightly. The low- Z cutoff is also sensitive to the value of the $n=3$ laser level electron collisional mixing rate used in the modeling. The factor-of-two precision presently expected for the values used is reflected as ± 1 to ± 2 variation in the Z -cutoff values plotted in Figs. 3-5. However, for atomic numbers larger than those at the peak of the gL vs Z curve, the calculated results are no longer sensitive to the upper and lower laser term mixing rates, and the accuracy of the gain product plotted should be about as good as the accuracy of the pumping rates, i.e., about a factor-of-two.

B. Pump Energy Requirements

For steady-state inversion, it is the pump energy rather than power that becomes a stringent requirement for high gain. A lower limit on the amount of pump energy, E_p , required can be determined from the maintained plasma, ionization, and excitation stored energies, i.e.,

$$E_p = \left(\frac{3}{2} N_e kT_e + \frac{3}{2} N_i kT_i + N_i \bar{E}_i \right) V, \quad (19)$$

where \bar{E}_i is the average excitation plus ionization energy per ion and V is the plasma volume. Greater amounts of source energy by (factors of ~ 20 -1000) could be required to compensate for plasma-energy losses and coupling efficiency from the pump source. The stored energies E_p are indicated in Figs. 3-5 for the peak gain point of each of the curves. Curves a and b in each figure correspond to conditions more typical of electrically driven pinch devices, where efficiencies of at least a few percent can be expected and energy storage systems of tens-of-kilojoules to megajoules are available; curves c and d correspond to laser-heated plasmas at high temperatures where the efficiency may be as low as 0.1 percent and much less energy (hundreds-of-Joules) is presently available.

C. Discussion

Under equilibrium temperature conditions with $kT_e = kT_i = \text{I.P.}/3$ and 0.7 I.P. for carbon-like and helium-like ions, respectively, the results for the former (shown in Fig. 3) are encouraging with gain products in the vacuum-UV region as high as $\alpha L = 1.6$ corresponding to net gains of $\exp(\alpha L) = 5$. For the latter (helium-like ions), the corresponding computed gain products plotted in Fig. 5 represent insignificant net gain, and at most a population inversion measurement could be expected for available plasma densities and dimensions such as represented here. Only with compressed laser-heated pellet plasmas of supra-solid density in a linear geometry could net amplification at high Z be conceived.

An increased electron temperature could have a significant effect both towards increasing the long-wavelength cutoff point as the $n=3$ laser level mixing rate decreases [Eq. (2) for $\Delta E_{jk}/kT_e$ very small] as well as increasing the gain

product as the $n=2$ to $n=3$ pumping rate increases. Electron temperatures considerably above the "equilibrium" values chosen here are not uncommon³⁵ under transient pre-equilibrium conditions of plasma heating in most fast-pulsed devices, and significantly increased gain is conceivable for the interval during which the desired ion is abundant. Such conditions are approximated within the present model for carbon-like ions, with the results plotted in Fig. 4 for N_e and d values corresponding to Fig. 3 but with temperatures increased by a factor of three. For these modified computations, a fixed laser-ion abundance of one-third the total was assumed, rather than an ionization-equilibrium value. Also, $T_e = T_i$ was again assumed, since the electron-ion energy equipartition times are generally less than the ion creation times at such high densities (if T_i were less than T_e , the gain products shown would increase as $T_i^{-1/2}$). Even for the somewhat conservative³⁵ temperature increase of $3\times$ assumed here, peak gain products of $\alpha L \approx 10$ are predicted, with a net gain of $\exp(\alpha L) \approx 2 \times 10^4$. Thus, only a modest transient temperature increase is required to saturate the gain (see Section III.A.).

Enhanced temperature calculations corresponding to the helium-like ion conditions of Fig. 5 continued to yield very small gain products (less than 10^{-3}) and therefore the results are not plotted.

IV. SUMMARY AND CONCLUSIONS

Population densities of ground and excited terms of carbon-like and helium-like ions in high-density plasmas were calculated by using the steady-state computer model described above. All important radiative and collisional transitions were included in the analysis and the laser gain product was derived from the computed population densities and the plasma length. The results of these calculations indicate significant gain products for $3p \rightarrow 3s$ ionic transitions in an amplified spontaneous emission (ASE) mode, i.e., without a resonant cavity, and for a quasi-cw equilibrium plasma model. With enhanced temperatures typical of a transient plasma heating phase, gains approaching saturation levels are predicted. The aspect ratio has been fixed throughout at $L/d = 10$; tandem operation³³ could conceivably increase this to 20 with a corresponding increase of a factor-of-three in the peak gain product,

with net equilibrium-mode gains ≥ 100 . Therefore, vacuum-UV lasing at wavelengths between 500 and 1000 Å using existing high-density discharge devices appears promising for a near term proof of feasibility of ASE in plasmas at short wavelengths.

Shorter wavelengths may subsequently evolve using smaller volumes heated by such high-power lasers as currently under development for compressed pellet fusion; here helium-like ion transitions might also become useful at very high densities.

V. REFERENCES

1. R. W. Waynant and R. C. Elton, *Proc. IEEE* **64**, 1059 (1976).
2. P. K. Cheo and H. G. Cooper, *J. Appl. Phys.* **36**, 1862 (1965).
3. W. B. Bridges and A. N. Chester, in *Handbook of Lasers*, ed. R. J. Pressley (Cleveland: Chemical Rubber Co., 1971), Chapter 7.
4. C. K. Rhodes, *IEEE J. Quant. Electron.* **QE-10**, 153 (1974).
5. Y. Hashino, Y. Katsuyama, and K. Fukuda, *Jap. J. Appl. Phys.* **11**, 907 (1972); **12**, 470 (1973).
6. R. C. Elton, R. W. Waynant, R. A. Andrews, M. H. Reilly, Naval Research Laboratory Report No. 7412, May 1972.
7. R. C. Elton, *Appl. Opt.* **14**, 97 (1975). The present numerical results are consistent with the analytical results in this paper when adjustments for density and improved rates are made.
8. R. C. Elton, in *Progress in Lasers and Laser Fusion*, eds. B. Kursunoglu, A. Perlmutter, and S. M. Widmayer (New York: Plenum Press, 1975).
9. R. C. Elton, *Appl. Opt.* **14**, 2243 (1975).
10. An alternate possibility of pumping by collisional ionization directly into excited states from the next lower ionization species is not considered here; a justification is agreement of the present model with existing experiments⁵.
11. T. N. Lee, Proceedings International Conference on the Physics of X-Ray Spectra, National Bureau of Standards, August 1976 (to be published).
12. R. C. Elton, in *Methods of Experimental Physics*, Volume 9A, *Plasma Physics*, eds. H. R. Griem and R. H. Lovberg (New York: Academic Press, 1970) Chapter 4.
13. J. C. Weisheit, *J. Phys. B* **8**, 2556 (1975).
14. A. L. Merts, R. D. Cowan, N. H. Magee, Jr., Los Alamos Scientific Laboratory Report LA-6220-MS (March 1976).
15. For $n=3$, $\Delta n=0$ transitions an electron collisional rate⁷ derived from line broadening calculations yields results similar to the effective Gaunt factor formulation within the factor-of-two accuracy expected.
16. M. J. Seaton, in *Atomic and Molecular Processes*, D. R. Bates, ed. (New York: Academic Press, 1962) Chapter 11.

17. H. Van Regemorter, *Astrophys. J.* **136**, 906 (1962).
18. W. L. Wiese, M. W. Smith, and B. M. Glennon, Atomic Transition Probabilities - Volume I: Hydrogen through Neon, NSRDS-NBS-4 (Washington, D.C.: U.S. Government Printing Office, 1969).
19. C. E. Moore, Atomic Energy Levels - Volume I, NSRDS-NBS-35 (Washington, D.C.: U.S. Government Printing Office, 1971).
20. R. L. Kelly with L. J. Palumbo, Atomic and Ionic Emission Lines below 2000 Angstroms - Hydrogen through Krypton, Naval Research Laboratory Report 7599 (Washington, D.C.: U.S. Government Printing Office, 1973).
21. W. L. Wiese, *Nucl. Instr. and Methods* **90**, 25 (1970); W. L. Wiese and J. R. Fuhr, *J. Phys. Chem. Ref. Data* **4**, 263 (1975).
22. O. Bely, *Proc. Phys. Soc.* **88**, 587 (1966); M. Blaha, *Astrophys. J.* **157**, 473 (1969); H. -J. Kunze and W. D. Johnston, III, *Phys. Rev. A* **3**, 1384 (1971), **4**, 962 (1971); J. Davis and S. Morin, *J. Quant. Spectros. and Radiative Transfer* **11**, 463 (1971); L. A. Vainshtein, I. I. Sobelman, and E. A. Yukov, Cross Sections for Electron Excitation of Atoms and Ions (Moscow: Nauka, 1973); J. Davis, P. C. Kepple, and M. Blaha, Naval Research Laboratory Memorandum Reports 2939 and 3171, 1974 and 1975 (unpublished); J. Davis and K. G. Whitney, *J. Appl. Phys.* **47**, 1426 (1976); R. U. Datla, M. Blaha, and H. -J. Kunze, *Phys. Rev. A* **12**, 1076 (1975); R. K. Landshoff and J. D. Perez, *Phys. Rev. A* **13**, 1619 (1976).
23. R. W. P. McWhirter, in Plasma Diagnostic Techniques, eds. R. H. Huddles and S. L. Leonard (New York: Academic Press, 1965) Chapter 5.
24. L. M. Biberman, *Zh. Exp. Theor. Fiz.* **17**, 416 (1947) [English transl. *Phys. Rev. A* **17**, 584 (1949)].
25. T. Holstein, *Phys. Rev.* **72**, 1212 (1947); **83**, 1159 (1951).
26. Stark broadening is negligible for the present conditions, as computed from Eq. (526) of H. R. Griem, Spectral Line Broadening by Plasmas, (New York: Academic Press, 1974).
27. H. -J. Kunze, *Phys. Rev. A* **3**, 937 (1971).
28. W. Lotz, *Astrophys. J. Suppl.* **14**, 207 (1967); *Z. Physik* **216**, 241 (1968).
29. R. U. Datla, L. J. Nugent, and H. R. Griem, *Phys. Rev. A* **14**, 979 (1976).
30. H. R. Griem, Plasma Spectroscopy (New York: McGraw-Hill, 1964).
31. G. R. Fowles, Introduction to Modern Optics (New York: Holt, Rinehart, and Winston, Inc., 1968).

32. J. W. Mather, in Methods of Experimental Physics, Volume 9B, Plasma Physics, eds. H. R. Griem and R. H. Lovberg (New York: Academic Press, 1970), Chapter 15.
33. J. H. Lee, D. R. McFarland, and F. Hohl, "Dense Plasma Focus Production in a Hypocycloidal Pinch," NASA Report TN-D-8116, December 1975 (unpublished).
34. T. P. Hughes, Plasmas and Laser Light (London: Halsted, and New York: John Wiley, 1975).
35. K. G. Whitney and J. Davis, J. Appl. Phys. 45, 5294 (1974).

Table 1. Atomic Data Used in Calculations

Carbon-Like Ions, $z = Z$				
lower term, j	upper term, k	ΔE_{jk}	f_{jk}	$\langle \bar{g} \rangle_{jk}$
$2p^2 \ ^3P$	$2p3s \ ^3P^o$	$2.35 \ z^2$	0.05	(c)
$2p^2 \ ^3P$	$2p3p \ ^3D$	(a)	0.3 (f)	(c)
$2p^2 \ ^3P$	$2p3d \ ^3D^o$	(a)	0.65	(c)
$2p3s \ ^3P^o$	$2p3p \ ^3D$	$1.10 \ z$	$2.9/z$	(d)
$2p3s \ ^3P^o$	$2p3d \ ^3D^o$	(a)	0.0 (b)	(d)
$2p3p \ ^3D$	$2p3d \ ^3D^o$	$1.38 \ z$	$0.75/z$	(d)
$2p^2 \ ^3P$	$2p \ ^2P^o + e$	$3.75 \ z^2$ (I.P.)	---	---
Helium-Like Ions, $z = Z-1$				
lower term, j	upper term, k	ΔE_{jk}	f_{jk}	$\langle \bar{g} \rangle_{jk}$
$1s^2 \ ^1S$	$1s2p \ ^1P^o$	$10.9 \ z^2$	$0.83 - 1.1/z$	(d)
$1s^2 \ ^1S$	$1s3s \ ^1S$	(a)	$.032 - .022/z$ (e)	(d)
$1s^2 \ ^1S$	$1s3p \ ^1P^o$	$12.7 \ z^2$	$0.16 - 0.11/z$	(d)
$1s2p \ ^1P^o$	$1s3s \ ^1S$	(a)	$0.014 + .053/z$	(c)
$1s2p \ ^1P^o$	$1s3p \ ^1P^o$	(a)	$.21 - .26/z$	(c)
$1s3s \ ^1S$	$1s3p \ ^1P^o$	$0.184 \ z$	$1.04/z$	(d)
$1s^2 \ ^1S$	$1s \ ^2S + e$	$14.1 \ z^2$ (I.P.)	---	---

- (a) Energy gap computed from other gaps listed using $\Delta E_{ln} = \Delta E_{lm} + \Delta E_{mn}$, where $l, m,$ and n are any three terms. Scaling used is both predicted⁷ and typical of measurements²¹.
- (b) This quadrupole mixing is believed to be small and is taken to be zero. It has little effect on the computed gain for most cases even if it is assumed to be as large as the $3s \rightarrow 3p$ dipole rate.
- (c) Gaunt factor fitted to $\langle \bar{g} \rangle_{jk} = 0.17 (\Delta E_{jk}/kT_e)^{-0.47}$ for $\Delta E_{jk}/kT_e \leq 1$ and $\langle \bar{g} \rangle_{jk} = 0.17$ for $\Delta E_{jk}/kT_e > 1$.
- (d) Gaunt factor fitted to $\langle \bar{g} \rangle_{jk} = 0.63 (\Delta E_{jk}/kT_e)^{-0.18}$.
- (e) Derived from collisional rates for helium-like ions calculated by Landshoff and Perez²².
- (f) Deduced from data of Vainshtein, et al., in Ref. 22.

FIGURE CAPTIONS

- Fig. 1 - Term diagram for 3p-3s lasing scheme in carbon-like ions showing important terms and transitions used in numerical modeling results described. Dashed arrows designate radiative transitions; solid arrows represent electron-collisional transitions. Numbers in parentheses correspond to subscripts in the text.
- Fig. 2 - Term diagram for 3s-2p lasing scheme in helium-like ions showing important terms and transitions used in numerical modeling results described. Dashed arrows designate radiative transitions; solid arrows represent electron-collisional transitions. Numbers in parentheses correspond to subscripts in the text.
- Fig. 3 - Computed gain products gL versus atomic number and wavelength for 6-electron carbon-like ions at temperatures T_e , T_i equal to one-third the ionization potential, I.P. (from Table 1). Curves a through d correspond respectively to electron densities of 10^{19} , 10^{20} , 10^{21} and 10^{22} cm^{-3} and to relevant respective plasma diameters of 3, 1, 0.1 and 0.01 mm. The required plasma energies in Joules are indicated for each curve at peak gain; lower values at higher densities reflect a volume decreasing as the third power of the diameter.
- Fig. 4 - Computed gain products gL versus atomic number and wavelength for 6-electron carbon-like ions at enhanced non-equilibrium temperatures T_e , T_i equal to the ionization potential, I.P. (from Table 1). As in Fig. 3, curves a through d correspond respectively to electron densities of 10^{19} , 10^{20} , 10^{21} and 10^{22} cm^{-3} and to relevant plasma diameters of 3, 1, 0.1 and 0.01 mm. The required plasma energies in Joules are indicated for each curve at peak gain; lower values at higher densities reflect a volume decreasing as the third power of the diameter.
- Fig. 5 - Computed gain products gL versus atomic number and wavelength for 2-electron helium-like ions at temperatures T_e , T_i equal to 0.7 times the ionization potential, I.P. (from Table 1). As in Figs. 3 and 4, curves a through d correspond respectively to electron densities of 10^{19} , 10^{20} , 10^{21} and 10^{22} cm^{-3} and to relevant plasma diameters of 3, 1, 0.1 and 0.01 mm. The required plasma energies in Joules are indicated for each curve at peak gain; lower values at higher densities reflect a volume decreasing as the third power of the diameter.

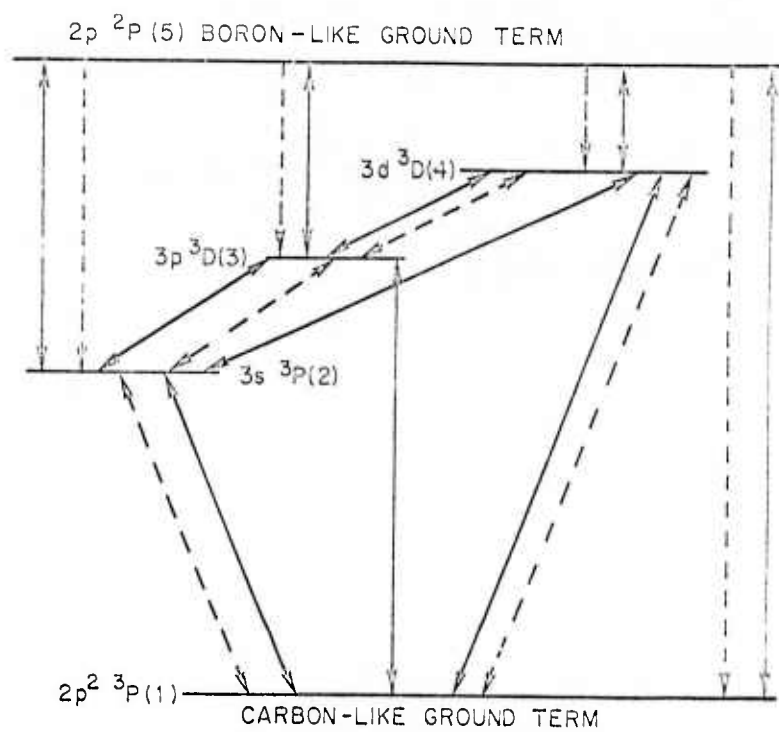


Figure 1

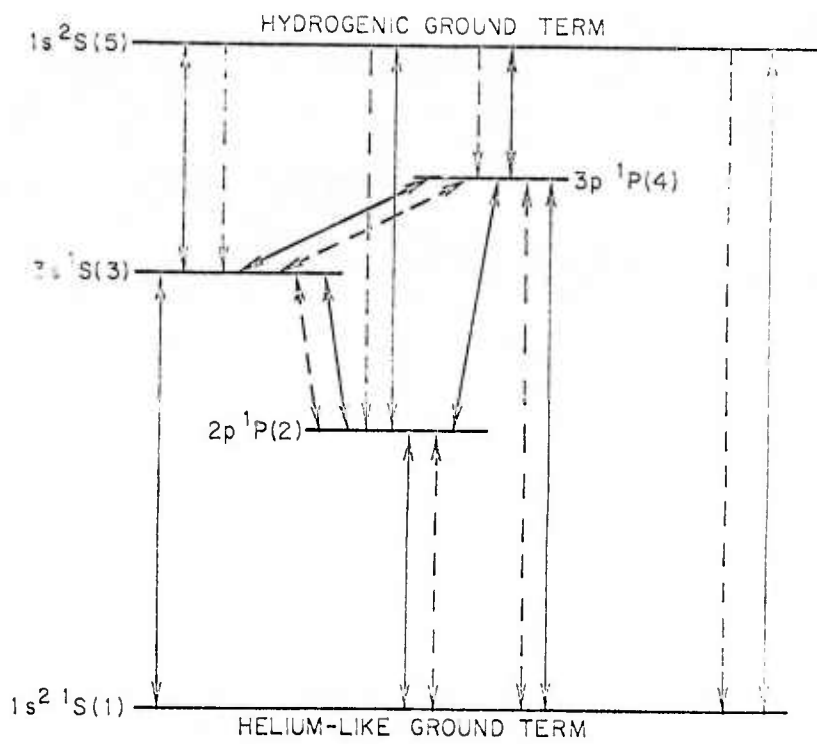


Figure 2

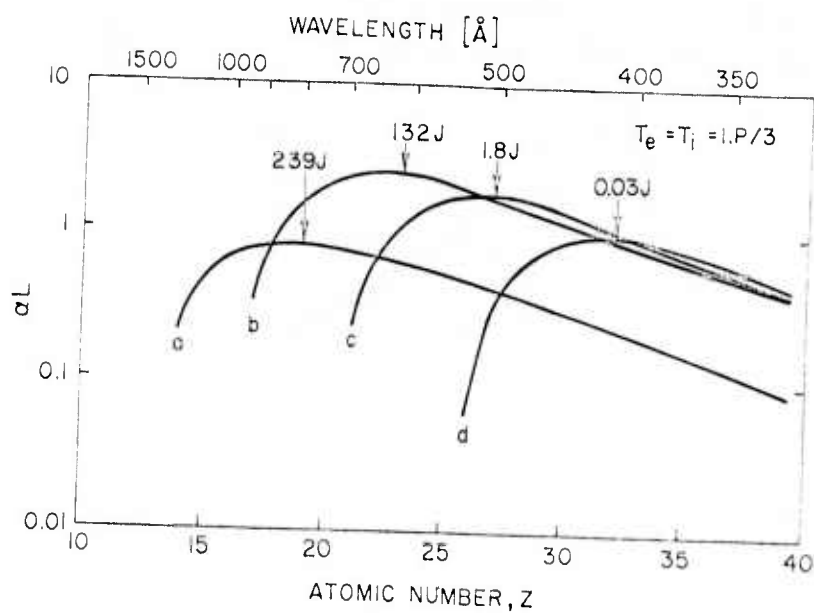


Figure 3

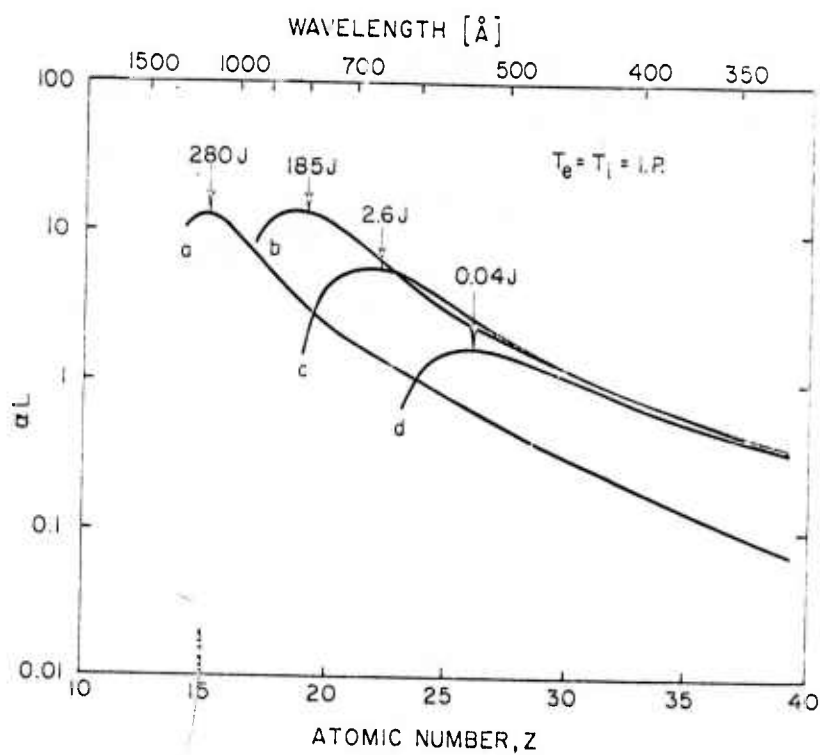


Figure 4

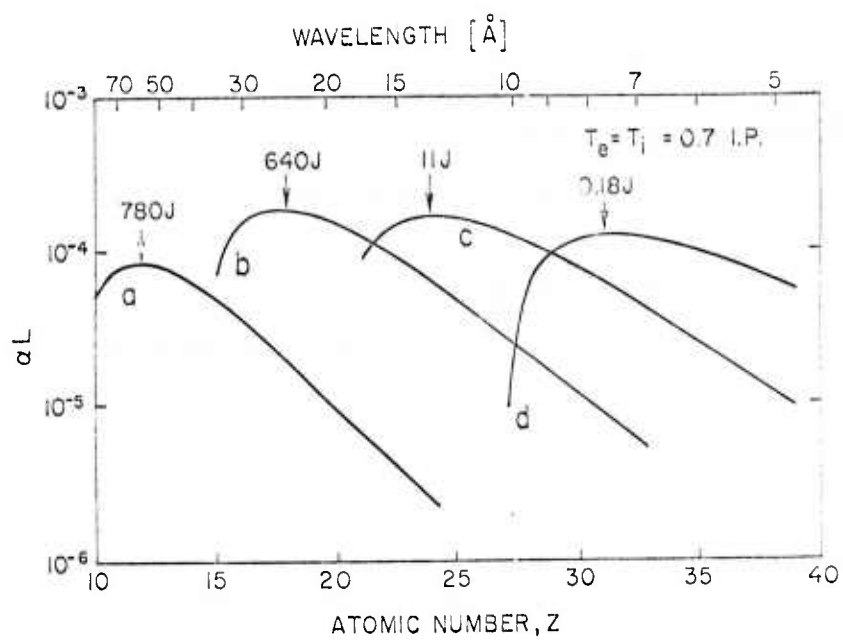


Figure 5

Phys. Rev. Lett. 37, 1540, (1976)

Generation of Coherent Radiation at 53.2 nm by
Fifth-Harmonic Conversion*

J. Reintjes, R. C. Eckardt, C. Y. She†
N. E. Karangelen, R. C. Elton and R. A. Andrews

Naval Research Laboratory
Washington, D.C. 20375

The generation of coherent radiation at 53.2 nm by fifth harmonic conversion of laser pulses at 266.1 nm in both Ne and He is reported.

Generation of Coherent Radiation at 53.2 nm by
Fifth-Harmonic Conversion*

J. Reintjes, R. C. Eckardt, C. Y. Sheu
N. E. Karangelen, R. C. Elton, and R. A. Andrews

Frequency upconversion using third-harmonic generation and four-wave mixing has received attention in recent years for the generation of coherent radiation in the vacuum ultraviolet (VUV) region of the spectrum^{1,2,3}. Such processes have been used to produce coherent radiation at wavelengths as short as 57.0 nm⁴. The generation of coherent light in the extreme ultraviolet region by third-order processes becomes increasingly difficult because of the scarcity of intense coherent sources at the required pumping wavelengths. The development of frequency conversion techniques utilizing higher order nonlinearities offers an attractive alternative to this approach, since it would allow larger steps along the frequency scale to be made in a single conversion process.

Several of these processes have been suggested in the literature^{5,6}. Although reasonable conversion efficiencies have been predicted for some of these interactions, the only published experimental evidence of such processes has been the fifth-harmonic conversion of Nd:glass radiation (1.06 μ m) in calcite⁷. No experimental evidence has been published for the generation of fifth or higher harmonics in vapors or in the VUV⁸.

In this letter we report the generation of coherent radiation at 53.2 nm. To our knowledge this is the shortest wavelength coherent radiation reported to date⁹. It was achieved through fifth-harmonic conversion of laser pulses at 266.1 nm (the fourth harmonic of a Nd:YAG laser). This process was observed

in both He gas and Ne gas. The present work represents the first application of higher order nonlinearities in the generation of coherent radiation in the extreme ultraviolet and indicates the feasibility of use of such processes for the generation of still shorter wavelengths.

Energy level diagrams for Ne and He are shown in Fig. 1. The fifth order susceptibility in Ne at 266.1 nm is dominated by a near four-photon resonance ($\Delta\tilde{\nu} = 12 \text{ cm}^{-1}$) between the ground state and the $3p [1\frac{1}{2}] J=2$ level. The wavelength of the generated radiation lies in the ionizing continuum. Efficient fifth-harmonic conversion is therefore limited to tight focusing arrangements in which the focal depth is shorter than the absorption length. The four-photon resonance is not nearly as exact in He ($\Delta\tilde{\nu} \approx 16000 \text{ cm}^{-1}$). However, the generated radiation lies below the continuum, at a level 1760 cm^{-1} above the $3p$ state. Calculations of the refractive index which include the effects of the continuum indicate that He is negatively dispersive for this process. Thus optimization by tight focusing in He should be possible¹⁰.

The pump pulses at 266.1 nm were derived from a mode-locked Nd:YAG laser followed by two successive stages of second-harmonic generation with about 70% conversion in each stage¹¹. Quartz prisms were used to separate the fourth-harmonic pulses from the fundamental and second-harmonic pulses. The pump pulses entered a sample cell through a MgF_2 window. The cell was attached to a 1-m normal incidence vacuum spectrometer. A CaF_2 lens was used to focus the radiation at the center of a 500 μm diameter aperture which replaced the entrance slit of the spectrometer. The gas used for nonlinear mixing was flowed into the cell and was differentially pumped behind the entrance aperture. The energy in the pump pulses was measured with a calibrated joule meter after the focusing lens, indicating a peak power of 330 MW. The infrared and second-

harmonic pulses were observed with a 5 psec resolution streak camera which showed pulse durations of about 30 psec with no amplitude substructure. The experiments were performed using lenses of both 5 and 10 cm focal lengths. The characteristics of the beam in the focus of both lenses were measured with a Si photodiode array. A Gaussian profile was observed in each case, with spot sizes ($1/e$ field radius) of 10 μm and 5 μm and confocal parameters of 2 mm and 0.5 mm for the 10 cm and 5 cm lenses, respectively.

The radiation at 53.2 nm was observed both photographically and photoelectrically. A microdensitometer tracing of the spectrum of fifth-harmonic light generated in Ne at a pressure of 40 torr is shown in Fig. 2. The spectrum was recorded on Kodak 101-01 film through a 1200 \AA thick Al filter. A single spectral line is seen in the range covered. Its width of 0.02 nm is limited by the size of the beam at the focus. A comparison tracing of a spectrum from a He arc source in the same spectral region is also shown, with three of the He emission lines evident.

Photoelectric signals were observed through two 1200 \AA Al filters with an EMI 9750QA photomultiplier tube and a sodium salicylate scintillator. For wavelength measurements, the spectrometer dial was calibrated against the He discharge spectrum to an accuracy of ± 0.05 nm. Using a 200 μm exit slit, the center wavelength of the fifth-harmonic signal was determined by tuning the monochromator dial to be 53.2 ± 0.1 nm for both gases. This measured value is in excellent agreement with expected value of 53.225 which was determined from calibration of the laser second-harmonic wavelength with a Ne discharge spectrum.

The variation of the fifth-harmonic signal with pump intensity was measured in neon at a pressure of 40 torr using the 10 cm focusing lens. Data are shown

in Fig. 3 for 24 laser shots. The pump intensity in the focus at the highest level shown is approximately $3 \times 10^{14} \text{ W/cm}^2$. A least square fit to the data points (solid line) gave a power law dependence with a slope of 4.7 on a log-log scale in excellent agreement with the expected value of 5. The proper power law dependence of signal strength with pump intensity, along with the exact agreement of the wavelength measurement, was taken as confirmation that fifth-harmonic generation had been observed.

Relative signal levels were compared for the two gases at various pressures using both the 5 and 10 cm focal length lenses. When the 10 cm lens was used, the signal level in neon was about twice as strong as that in helium at the same pressure. For these conditions the highest signal levels were observed in neon at a pressure of 40 torr. The conversion efficiency was estimated from the photomultiplier response to be of the order of 10^{-6} to 10^{-7} for an intensity at 266.1 nm of $3 \times 10^{14} \text{ W/cm}^2$. Higher conversion was obtained when the 5 cm focal length lens was used with a pump intensity in the focus of 10^{15} W/cm^2 . Under these conditions the fifth-harmonic signal in helium was greater than that in neon, and an estimated conversion level of 10^{-5} to 10^{-6} was observed at a helium pressure of 160 torr. This conversion level is already greater than that reported for some third-order conversion processes³

Conversion in neon appears to be limited by breakdown which was observed to occur at a pressure of 60 torr for the weaker focusing arrangement (10 cm lens) and at lower pressures for the tighter focus. Abrupt cut-off of the 53.2 nm signal on the strongest laser pulses was taken as preliminary evidence of breakdown, with confirmation of the process being provided by the observation of Ne III emission lines at 37.93 nm and 48.95 nm. No signals at all were observed at 53.2 nm for either focusing arrangement for neon pressures greater

than 80 torr. Breakdown in He as evidenced by either of these two effects has not yet been seen at pressures up to 160 torr.

The fifth-harmonic processes reported here have not yet been optimized for either gas. In neon the absorption length at 40 torr is 0.7 mm, shorter than the depth of focus of the 10 cm lens and comparable to that of the 5 cm lens. Increased conversion may be possible by further reduction of the focal depth, although breakdown may become important in limiting conversion at the higher intensities. Still higher conversions should be possible in helium, since the negative dispersion allows conversion to be optimized in a tight focus region. Calculations show that optimum conversion should occur at a pressure of 640 torr when the 5 cm lens is used. Pressures this high could not be reached with the existing pumping system. Increased conversion is thus expected in helium when the system is operated at the optimum pressure.

In summary, we have used fifth-harmonic generation in He and Ne to extend the range of coherent wavelengths to 53.2 nm. Conversion is in the range of 10^{-5} to 10^{-6} with further optimization believed to be possible. This work represents the first application of frequency upconversion to the extreme ultraviolet using optical nonlinearities of higher order than third, and indicates the feasibility of using such processes to extend the range of available coherent wavelengths ever closer to the soft x-ray range.

The authors would like to thank T. N. Lee for advice and assistance with the VUV photography, W. Hunter for advice on VUV equipment, M. Fink for preparation of the Al filters, and E. Tiedemann for laboratory assistance.

REFERENCES

*Work partially supported by the Defense Advanced Research Projects Agency, ARPA Order 2694.

-On sabbatical leave from Colorado State University, Ft. Collins, Colorado 80523.

1. A. H. Kung, J. F. Young, G. C. Bjorklund and S. E. Harris, Phys. Rev. Lett. 29, 985 (1972).
2. R. T. Hodgson, P. P. Sorokin and J. J. Wynne, Phys. Rev. Lett. 32, 343 (1974).
3. A. H. Kung, Appl. Phys. Lett. 25, 653 (1974).
4. M. H. R. Hutchinson, C. C. Ling and D. J. Bradley, Postdeadline Paper S.1, IXth International Quantum Electronics Conference, Amsterdam, The Netherlands, 1976.
5. S. E. Harris, Phys. Rev. Lett. 31, 341 (1973).
6. I. V. Tomov and M. C. Richardson, IEEE J. Quant. Elect. QE-12, 521 (1976).
7. S. A. Akhmanov, V. A. Martynov, S. M. Saltiel and V. G. Tunkin, Pisma Zh. Eksp. Theor. Fiz. 22, 143 (1975) [Sov. Phys. JETP Lett. 22, 65 (1975)].
8. A. H. Kung, Private Communication. Although a preliminary observation of the process $5 \times 532.0 \text{ nm} = 106.4 \text{ nm}$ was noted in ref. 5, no record of this observation has been published.
9. Preliminary results of this work were presented as a postdeadline paper at the International Conference on the Physics of X-Ray Spectra, National Bureau of Standards, Gaithersburg, Md., August 1976.
10. G. C. Bjorklund, IEEE J. Quant. Elect. QE11, 287 (1975).
11. J. Reintjes and R. C. Eckardt, to be published in Appl. Phys. Lett.

FIGURE CAPTIONS

1. Partial energy level diagrams of Ne and He showing states involved in fifth-harmonic conversion of 266.1 nm to 53.2 nm.
2. Microdensitometer traces of a fifth-harmonic spectrum in Ne (top) and a He discharge comparison spectrum (bottom).
3. Variation of fifth-harmonic signal with pump intensity in neon at a pressure of 40 torr. The highest pump intensity shown is approximately $3 \times 10^{14} \text{ W/cm}^2$. The solid line is a least square fit to the data points.

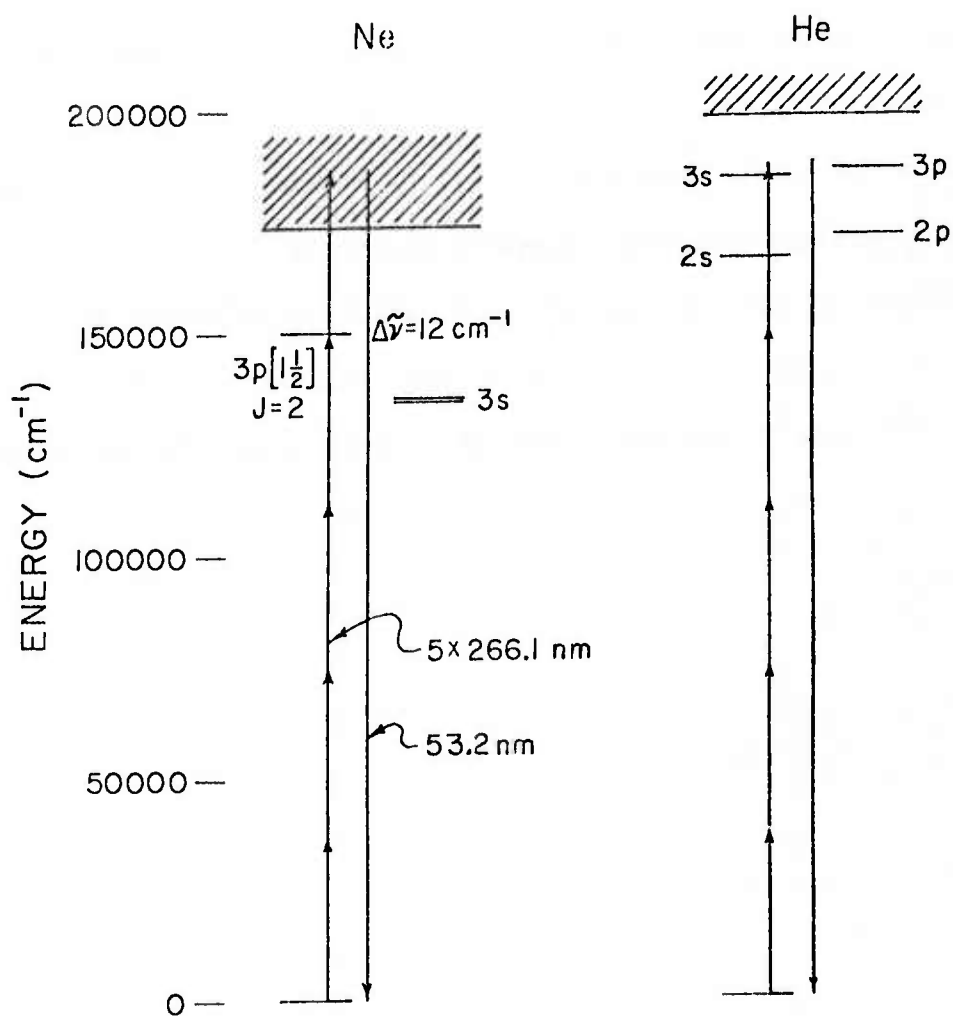


Figure 1

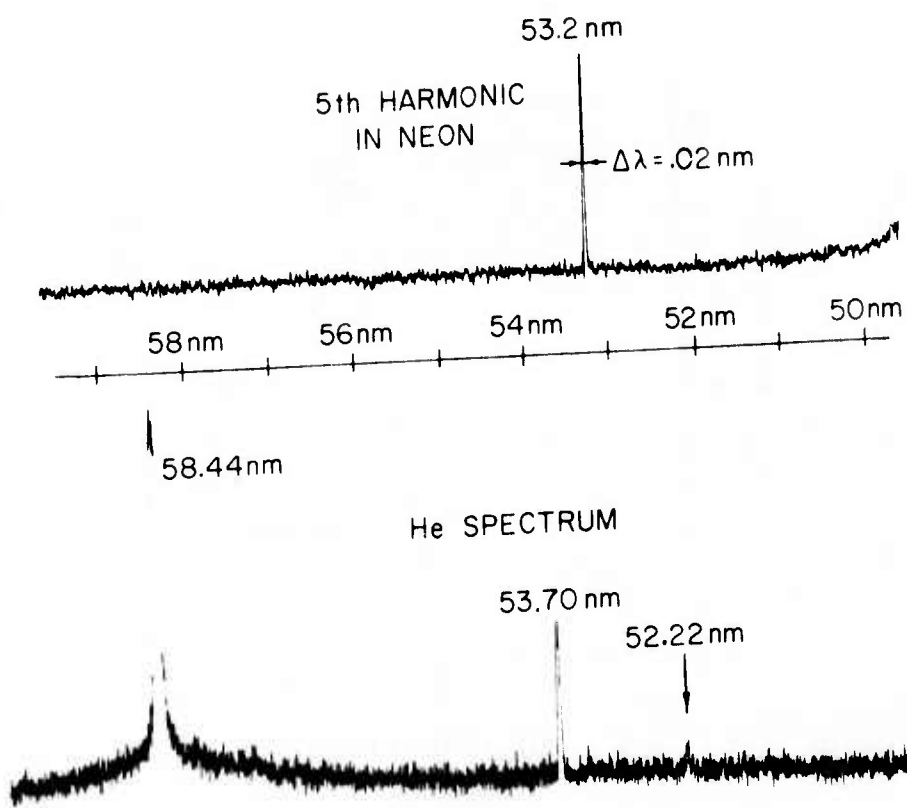


Figure 2

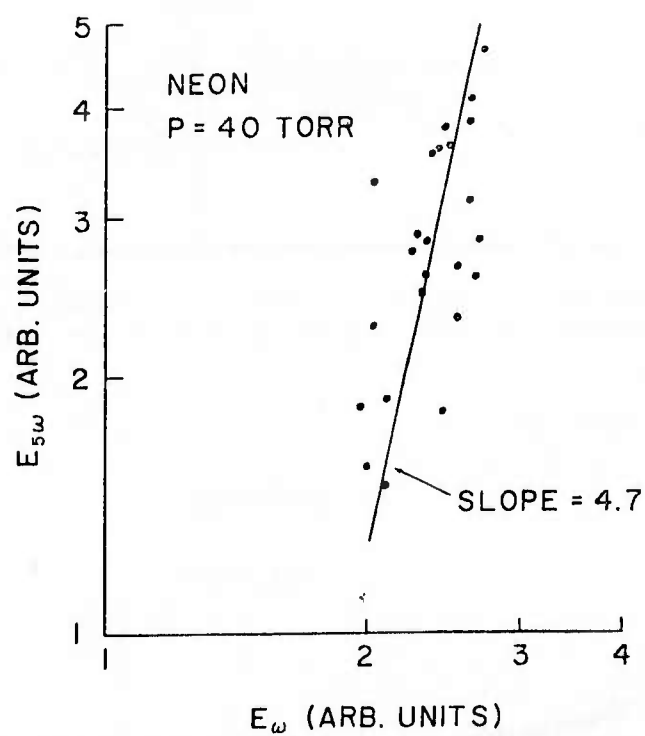


Figure 3

Complete Compensation of Self-Phase Modulation
in Cesium Vapor at $1.06 \mu^*$

R. H. Lehmborg, J. Reintjes and R. C. Eckardt

Naval Research Laboratory
Washington, D.C. 20375

We have observed a complete cancellation of self-phase modulation in 1.06μ pulses propagating through cesium vapor. The negative nonlinear refractive index responsible for this is measured as $n_2/N = - (2.5 \pm .5) \times 10^{-30}$ esu, in good agreement with theory.

Complete Compensation of Self-Phase Modulation
in Cesium Vapor at $1.06 \mu^*$

R. H. Lehmberg, J. Reintjes and R. C. Eckardt

Recently, we reported the observation of self-defocusing of mode-locked pulses at 1.06μ in cesium vapor, and attributed the effect primarily to a nearby two-photon resonance with the $6s \ ^2S_{1/2} - 7s \ ^2S_{1/2}$ levels [1,2]. From these measurements, we inferred a negative nonlinear refractive index $n_2 \simeq -1.5 \times 10^{-30}$ N esu, in reasonable agreement with the theoretical value -2.62×10^{-30} N esu [2]. Thus, the magnitude of n_2 at cesium vapor densities of approximately 10^{17} cm^{-3} will be comparable to that of typical laser glass [3,4], giving rise to the possibility of compensation for the whole beam self-focusing and self-phase modulation in the amplifier chains of large glass lasers. The recent use of spatial filters to suppress small-scale self focusing has allowed operation of lasers at peak nonlinear phase retardations up to 3π [5], where these effects are appreciable.

In this paper we report initial studies of the compensation process. We have observed complete compensation of the self-phase modulation (and therefore whole beam self focusing) induced by YAG amplifiers and CS_2 on mode-locked pulses from a Nd:YAG laser by propagating the pulses through a cesium vapor cell. From the variation of nonlinear phase compensation with Cs number density we have determined a value of $n_2/N = -(2.5 \pm .5) \times 10^{-30}$ esu, which is in excellent agreement with the theoretical value. Finally, the degree of compensation that we have been able to achieve indicates that the nonlinear refraction in Cs is instantaneous (i.e., $\delta n(t) \sim n_2 I(t)$); therefore, this process should be useful for compensating the self-phase

modulation introduced by other rapidly responding media.

A pulse propagating through such a medium develops an intensity dependent phase shift:

$$B(t) = \frac{8\pi^2}{n_o \lambda_o c} \int_0^L n_2 I(z,t) dz. \quad (1)$$

where $I(z,t)$ is the intensity, and L is the path length. The instantaneous frequency shift of the pulse $\delta\omega(t) = -B(t)$ results in spectral broadening with a Bessel function modulation that is characteristic of self-phase modulation (SPM). Typical calculated spectra are shown in Fig. 1 for temporally Gaussian pulses with various values of peak nonlinear phase shift B . The FWHM spectral width $\Delta\lambda$ and spacing $\Delta\lambda_{pp}$ between the outermost peaks (normalized to the unchirped FWHM width $\Delta\lambda_o$) are shown as a function of B in Fig. 2. It is evident from this figure that $\Delta\lambda$ is approximately equal to the maximum instantaneous wavelength excursion due to the chirp $\delta\lambda_{\max} - \delta\lambda_{\min} = (\lambda_o^2/\pi c) B(\max) = 1.03B\Delta\lambda_o$ for $B \gg 1$.

If a pulse with this type of phase structure is subsequently propagated through a second medium with n_2 of opposite sign to that of the first, the nonlinear phase structure can be cancelled. This cancellation should occur at all times during the pulse and at all positions across the beam profile if the spatial changes due to self focusing and defocusing are negligible within or between the two media; i.e., if the nonlinear refraction affects only the phase of the pulse [7].

In order to investigate these concepts, we performed the experiment indicated schematically in Fig. 3. Single mode-locked pulses from a Nd:YAG

laser were self phase modulated in a positive sense by propagation through the YAG amplifiers and 2 mm of CS₂. The pulses incident on the CS₂ cells contained nominally 40 mJ of energy with a 35 ps pulse width, as determined by a 5 psec resolution streak camera. The spatial profile, as determined by a silicon diode array, was an Airy pattern with a 4.0 mm 1/e diameter, which was truncated at its first minimum by aperture A₁. After a 2.1:1 expansion by a Galilean telescope to minimize the spatial effects of self defocusing, the pulses were propagated through a 1 m long, two-temperature cesium cell, which has been described elsewhere [2]. The pulse energy was monitored before and after the cell with a calibrated photo diode. The peak on-axis intensity at the entrance was approximately 1 GW/cm², and the insertion loss (due to cesium dimers [2,8]) was less than 20% under optimum compensation conditions.

Time-integrated spectra of the on-axis portion of the pulse were recorded both before and after the cell by a 1 m normal incidence grating monochromator and a streak camera. The streak camera was operated with a time resolution of 350 psec, thereby providing time-integrated spectra of each pulse, while allowing the incident and transmitted pulses to be separated in time. The spectral resolution was 0.18 Å.

Densitometer traces of typical spectra are shown in Fig. 4. The incident spectra (lower traces) were broadened to widths of 2-4 Å, with approximately equal contributions from the CS₂ cells and the YAG laser amplifiers. They have the double-peaked appearance characteristic of their phase modulation depths B_{in} between 1.5π and 1.7π. The spectral asymmetry is due to a temporal asymmetry of the laser pulse that arises from gain

saturation in the final YAG amplifier. For an empty cell (Fig. 4a), the output spectrum is actually broadened slightly due to additional positive self-phase modulation in the lenses and cell windows. At intermediate cesium densities (4b), partial compensation is evident, with the spectrum narrowing and becoming single-peaked. At a density $N \approx .76 \times 10^{17} \text{ cm}^{-3}$ (4c), compensation is complete, and the spectrum of the initially phase-modulated pulse narrows to its time-bandwidth limit. Higher densities (4d) result in overcompensation; i.e., the pulse becomes self phase modulated in a negative sense, with its spectrum broadened and the spectral asymmetry reversed. Further studies showed that optimal compensation could be achieved for the largest values of B_{in} that we were able to produce without beam breakup ($\sim 3 \pi$).

The numerical value of n_2/N was obtained from Eq. (1) with $B \equiv B_{\text{out}} - B_{\text{in}}$, using nine shots of known peak intensities and cesium pressures. B_{in} , which ranged from 1.5π to 2.5π , was estimated by measuring the peak-to-peak spacing, of the input spectra, calculating $\Delta\lambda_{\text{pp}}/\Delta\lambda_0$, and using Fig. 2 [9]. For a pulsewidth $\Delta t = 35 \text{ psec}$, $\Delta\lambda_0 = (2\ln 2) \lambda_0^2 / \pi c \Delta t = 0.48 \text{ \AA}$. At the output, where B_{out} ranged from $.55 \pi$ to 1.0π , the spectra were single-peaked in most of the cases chosen. B_{out} was estimated by measuring the FWHM spectral widths relative to those of time-limited pulses of similar intensity and film exposure. No shots in which $|B_{\text{out}}| < .5 \pi$ or $1.0 \pi < B_{\text{in}} < 1.5 \pi$ were used, because of the difficulty of estimating accurate B values from spectra in these ranges. (See Fig. 2.) In all of the shots that were used, the calculated B values matched closely with values inferred from theoretical spectra of similar qualitative appearance. (See Fig. 1.)

The result of our n_2/N measurement is compared with the theory and our earlier measurement [2] in Table 1. Although the value of n_2/N determined in the present work is in good agreement with the theory, the precision is somewhat poorer than in our earlier measurement because of the difficulty in evaluating accurate B values of the input and output pulses from the spectra. The inaccuracy of our earlier value of n_2/N probably arose from inaccuracy in measuring N. In the present experiment, we allowed a significantly longer time for the two-temperature cesium oven to reach thermal equilibrium at each new density, and this appears to have remedied the problem.

In summary, we have demonstrated that the negative nonlinear refractive index of Cs vapor at 1.06μ can be used to compensate for the self-phase modulation introduced on laser pulses by propagation through media with positive n_2 values. The value of n_2/N determined in these measurements is in excellent agreement with that obtained from ab-initio calculations. Although the major thrust of the current work was to observe compensation of self-phase modulation artificially introduced in CS_2 , some of the phase modulation that was compensated arose in the amplifier stages of the laser. In addition, virtually complete compensation was observed for our maximum modulated pulses up to 3π which is comparable to the phase modulation found in some lasers currently being built for fusion research [5]. Our work therefore indicates the feasibility of using cesium to compensate self-phase modulation, and hence whole beam self focusing, in large Nd:Glass laser systems.

The authors wish to thank J. M. McMahon and O. C. Barr for stimulating and useful discussions.

REFERENCES

*Work supported jointly by the U.S. Energy Research & Development Administration and Defense Advanced Research Projects Agency ARPA Order 2694.

1. R. H. Lehmberg, J. Reintjes and R. C. Eckardt, Appl. Phys. Lett. 25, 374 (1974).
2. R. H. Lehmberg, J. Reintjes and R. C. Eckardt, Phys. Rev. A 13, 1095 (1976).
3. M. J. Moran, C. Y. She and R. L. Carman, IEEE J. Quantum Electron. QE-11, 259 (1975).
4. D. Milam and M. J. Weber, J. Appl. Phys. 47, 2497 (1976); Opt. Comm. 18, 172 (1976).
5. A. Bettinger, C. Charles, J. Osmalin and J. G. Girand, Opt. Comm. 18, 176 (1976).
6. E. S. Bliss, J. T. Hunt, P. A. Renard, G. E. Sommargren and H. J. Weaver, IEEE J. Quantum Electron. QE-12, 402 (1976).
7. R. H. Lehmberg, J. Reintjes and R. C. Eckardt, Naval Research Laboratory Memorandum Report 3130 (September 1975) p. 25-30.
8. P. P. Sorokin and J. R. Lankard, IEEE J. Quantum Electron. QE-8, 813 (1972).
9. For the cases here, where the pulse is only mildly distorted, the largest effect of the distortion is to shift the spectrum slightly and change the distribution of energy in the peaks. The peak-to-peak spacings remain approximately unchanged.

FIGURE CAPTIONS

Fig. 1 - Calculated spectra of self phase modulated Gaussian pulses with peak nonlinear phase shifts $B = 0, 0.5 \pi, 1.0 \pi, 1.5 \pi$ and 2.0π .

Fig. 2 - Calculated FWHM spectral width $\Delta\lambda$ and outer peak spacing $\Delta\lambda_{pp}$ (normalized to the time-bandwidth limited width $\Delta\lambda_0$) of self phase modulated Gaussian pulses of peak nonlinear phase shift B . The dashed line is the normalized maximum instantaneous wavelength excursion due to the chirp.

Fig. 3 - Schematic illustration of the Cs compensation experiment, showing the use of a slow streak camera to separate the time-integrated input and output spectra.

Fig. 4 - Densitometer traces of the incident spectra (lower) and transmitted spectra (upper) for cesium densities of (a) $N=0$, (b) $4.6 \times 10^{16} \text{ cm}^{-3}$, (c) $7.6 \times 10^{16} \text{ cm}^{-3}$, and (d) $1.13 \times 10^{17} \text{ cm}^{-3}$.

$$\frac{n_2}{N} \times 10^{30} \text{ (esu)}$$

EXPERIMENTAL		THEORETICAL
(A)	(B)	(C)
-1.5 ± .2	-2.5 ± .5	-2.62
(A) Self defocusing experiment (Ref. 2)		
(B) Frequency compensation experiment		
(C) Ab-initio calculation (Ref. 2)		

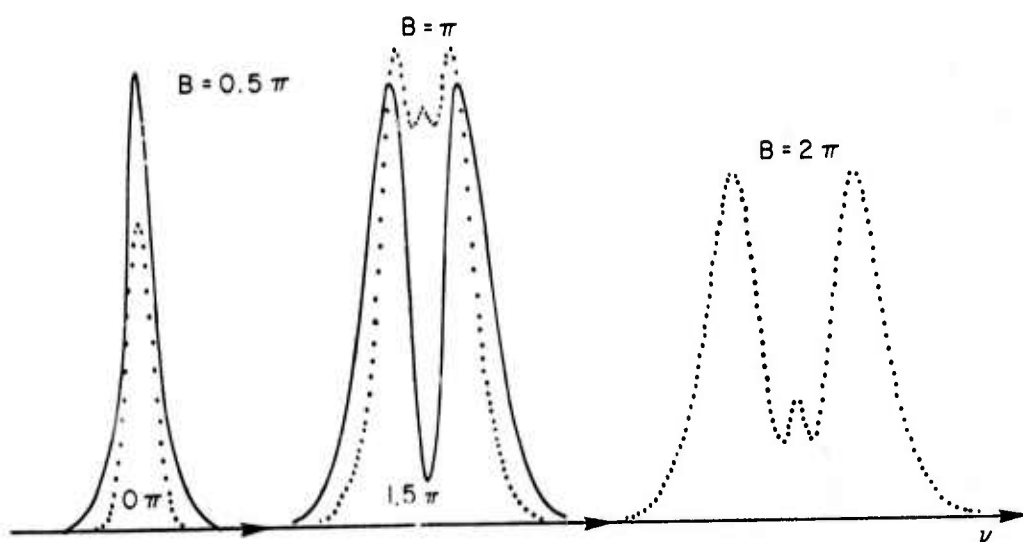


Figure 1

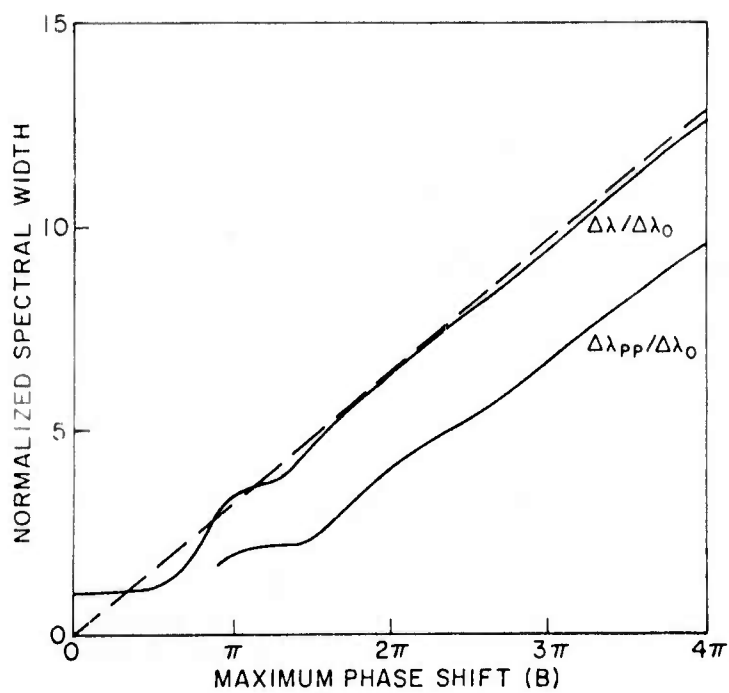


Figure 2

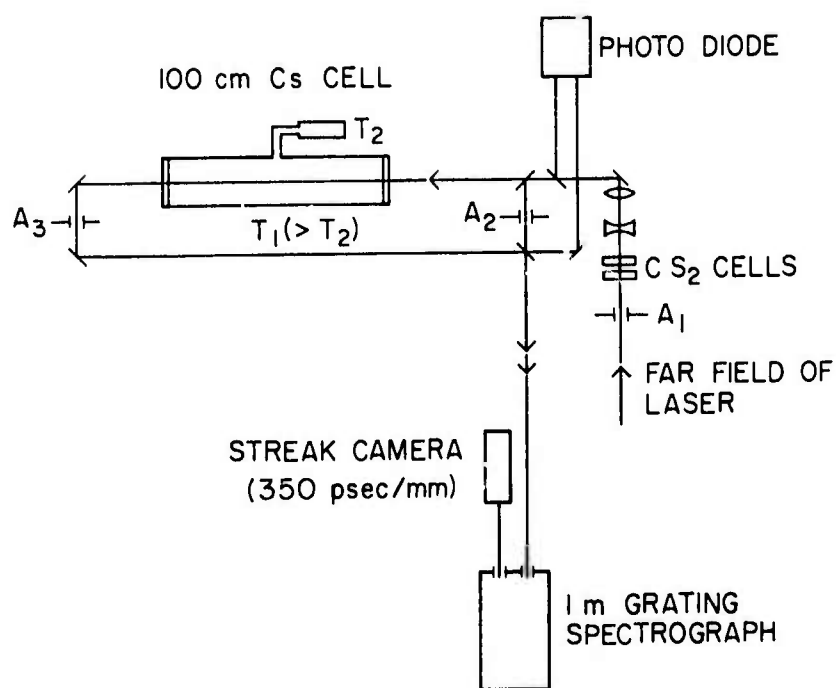


Figure 3

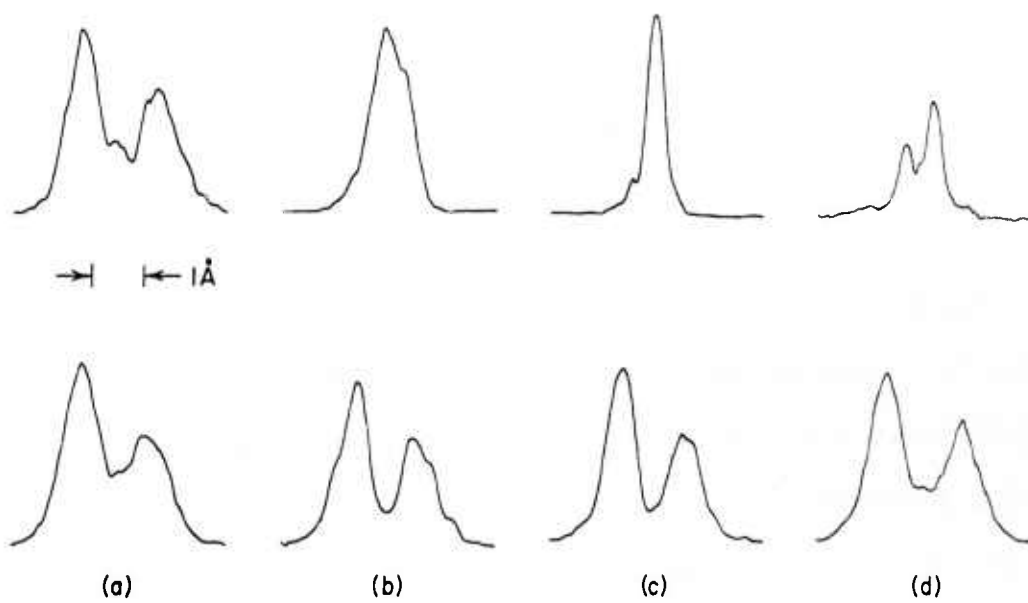


Figure 4

A Discharge-Pumped ArCl Superfluorescent Laser at 175.0 nm

Ronald W. Waynant

Naval Research Laboratory
Washington, D.C. 20375

Initial observations have been made of laser action in ArCl excimers pumped by a high-voltage, fast-risetime Blumlein discharge circuit.

The new laser emits at 175.0 nm and operates at atmospheric pressure.

The gas from which the molecules are formed consists of 1% Cl₂, 15% Ar and 84% He. A gain coefficient of 0.012 cm⁻¹ has been determined for ArCl.

PACS numbers: 82.50 Et, 78.76 Fi, 42.60 Cz, 52.80 Pi

A Discharge-Pumped ArCl Superfluorescent Laser at 175.0 nm

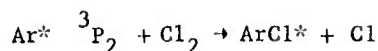
Ronald W. Waynant

Naval Research Laboratory
Washington, D.C. 20375

Observations of numerous rare gas halide lasers (XeF, XeCl, XeBr, KrF, ArF, and KrCl) have been made using electron beam excitation¹⁻¹⁰. Some of these molecules have also exhibited stimulated emission in discharge-pumped systems¹¹⁻¹⁵. This paper reports the first observations of superfluorescent emission from ArCl at 175.0 nm. This wavelength is the shortest yet obtained from rare gas halide excimers. It was produced with a fast (2.5 ns current risetime) Blumlein discharge circuit, which also was capable of exciting XeF, KrF, ArF, and KrCl with no difficulty. (This is also the first report of discharge pumping of KrCl.)

While the basic operating principles of the traveling-wave Blumlein discharge system have been described previously¹⁶ for use in generating vacuum ultraviolet emission from H₂ and CO, the system used for this work was extensively modified to produce a uniform discharge at higher pressures. These modifications included the creation of a gas chamber capable of handling several atmospheres of pressure and new electrodes raised from the polyethylene Blumlein dielectric. The electrodes, constructed from stainless steel, were 160 cm long, 2.5 cm high, and could be varied in separation from 1 to 7 cm. Electrically the Blumlein circuit was triggered by the sequential firing of nine mylar switches timed to produce a traveling wave of excitation in the direction of proposed pulse propagation (this has also been called the "swept gain" mode of operation). The resulting voltages across the electrodes could be varied from about 80 to 110 kV. Several electrode shapes were tried before settling on a nearly flat pair which gave a uniform discharge free from arcing with pressures in the one-half to one atmosphere range.

The emission spectra of the rare gas halides were first studied by Golde and Thrush¹⁷ and Velazco and Setser¹⁸. The emission spectrum of ArCl formed by the reaction



is given by Golde and Thrush and shows a rather broadband (~ 8.0 nm) spectrum with a maximum at 175.0 nm and a secondary peak at about 169.0 nm. Ewing and Brau also observed the emission spectra of the rare gas monohalides and realized the possibility of uv and vacuum uv lasers¹⁹. They were able to estimate the features of a number of these lasers, and some of these lasers have now been realized. Because of an interest in short wavelengths the work reported here is an initial attempt at investigating those rare gas halides which are predicted to lase in the vacuum ultraviolet.

Initial experiments with this device were carried out in XeF, and the spectrum at 355 nm showed the discrete lines characteristic of transitions between stable molecular levels. The gas mixture used was 1.5% NF₃, 5% Xe and then filled with He to make total pressures of up to 500 Torr. Attempts to generate emission from KrF produced poor results with NF₃, and attempts to generate ArF with NF₃ produced only a weak spontaneous spectrum accompanied by numerous lines attributable to the excitation of NF₃ or its decomposed fragments. Substitution of pure F₂ eliminated all difficulties in producing stimulated emission in KrF and ArF as shown in Fig. 1. Gas mixtures consisted of about 1% F₂, 10% Ar or Kr, and the rest He to make pressures of about one atmosphere. It is possible that pressures above one atmosphere may produce higher powers, but this was not investigated because of our interest in obtaining shorter wavelengths. Therefore, Cl₂ was substituted for F₂, and the laser emission spectra shown in Fig. 1 were obtained from KrCl and ArCl. Using similar gas mixtures and pressures with Cl₂ as used with F₂, lasing was easily obtained.

All of the excimers lased in the superfluorescent (or amplified spontaneous emission) mode of operation. No resonant cavity was needed to obtain lasing, although as Burnham¹¹ has indicated, considerable improvement could be expected in the output when resonant cavities are employed. The emission was extracted through a LiF window and traversed a vacuum path of about one meter length before entering a McPherson Model 225 one-meter vacuum spectrograph. The dispersed radiation was recorded on Kodak 101-01 vacuum uv film. A Hg lamp was used to calibrate the wavelengths.

Evidence of amplification was obtained by numerous methods. The most straightforward method consists of measuring the output as a function of length of excited gas. For lengths below saturation intensity an exponential dependency would occur when amplification takes place. By placing an absorbing material (a glass plate) across the discharge channel to keep emission from one end of the discharge from reaching the remaining excited gas, the effective length can be varied without changing the discharge parameters anywhere along the length of the electrodes. Observations were made of exponential behavior when the amplifying length was cut from 160 cm to 80 cm. These indicate unsaturated amplification for the excimers investigated and allow measurement of the small signal gain coefficients of 0.012 cm^{-1} for ArCl, 0.017 cm^{-1} for ArF, 0.018 cm^{-1} for KrCl, and 0.019 cm^{-1} for KrF.

The temporal history of the amplified output was monitored both by a photomultiplier-spectrograph system and by the use of bandpass filters manufactured by Acton Research which were placed over an ITT 4018 photodiode with a sapphire window. Typical pulses for ArCl and ArF are shown in Fig. 2. The output pulse widths of KrF and ArF were longer (FWHM $\sim 20 \text{ ns}$) than the pulse widths of KrCl and ArCl (FWHM $\sim 10 \text{ ns}$). Similar observations can be found in the comparison of KrF and KrCl by Murray and Powell⁹.

There is likely to be a considerable improvement in the output power of ArCl and the other rare gas halides by optimizing electrode structure, gas mixture, and resonator configuration. Present energy estimates made with a Molelectron calorimeter (J3-02) indicate about 0.2 mJ for ArCl, 1 mJ for ArF, 1.3 mJ for KrCl and 1.7 mJ for KrF from this system. Therefore, the peak power generated in these gases ranges from 20 to 90 kW.

Numerous applications of ArCl might be expected as performance improves. One application is that of pumping doped crystals to produce lasing over wavelengths tunable from 175 nm to 260 nm²⁰. Such tunable wavelengths would likely have numerous applications in photochemistry and isotope separation. As Ewing and Brau predict¹⁹ it is likely that other rare gas halides can be made to lase at even shorter vacuum ultraviolet wavelengths. Several candidates which remain to be tried are KrBr which should lase at 203 nm, KrI at 185 nm, ArBr at 161 nm and NeF at 107 nm.

The author gratefully acknowledges numerous discussions, encouragement, and initial supply of NF₃ by R. Burnham and the technical assistance of L. J. Verna.

REFERENCES

1. S. K. Searles and G. A. Hart, Appl. Phys. Lett. 27, 243 (15 August 1975).
2. J. J. Ewing and C. A. Brau, Appl. Phys. Lett. 27, 350 (15 September 1975).
3. E. R. Ault, R. S. Bradford, Jr., and M. L. Bhaumik, Appl. Phys. Lett. 27, 413 (1 October 1975).
4. G. C. Tisone, A. K. Hays, and J. M. Hoffman, Opt. Comm. 15, 188 (October 1975).
5. M. L. Bhaumik, R. S. Bradford, Jr., and E. R. Ault, Appl. Phys. Lett. 28, 23 (1 January 1976).
6. J. M. Hoffman, A. K. Hays, and G. C. Tisone, Appl. Phys. Lett. 28, 538 (1 May 1976).
7. S. K. Searles, Appl. Phys. Lett. 28, 602 (15 May 1976).
8. G. A. Hart and S. K. Searles, J. Appl. Phys. 47, 2033 (May 1976).
9. J. R. Murray and H. T. Powell, Appl. Phys. Lett. 29, 252 (15 August 1976).
10. J. G. Eden and S. K. Searles, Appl. Phys. Lett. 29, 356 (15 September 1976).
11. R. Burnham, N. W. Harris, and N. Djeu, Appl. Phys. Lett. 28, 86 (15 January 1976).
12. C. P. Wang, H. Mirels, D. G. Sutton, and S. N. Suchard, Appl. Phys. Lett. 28, 326 (15 March 1976).
13. J. H. Jacob and J. A. Mangano, Appl. Phys. Lett. 28, 724 (15 June 1976).
14. C. P. Wang, Appl. Phys. Lett. 29, 103 (15 July 1976).
15. J. A. Mangano, J. H. Jacob, and J. B. Dodge, Appl. Phys. Lett. 29, 426 (1 October 1976).
16. R. W. Waynant, J. D. Chipman, Jr., R. C. Elton, and A. W. Ali, Appl. Phys. Lett. 17, 383 (1 November 1970).
17. M. F. Golde and B. A. Thrush, Chem. Phys. Lett. 29, 486 (15 December 1974).
18. J. E. Velazco and D. W. Setser, J. Chem. Phys. 62, 1990 (1 March 1975).

19. J. J. Ewing and C. A. Brau, Phys. Rev. A 12, 129 (July 1975).
20. K. H. Yang and J. A. DeLuca, Appl. Phys. Lett. 29, 499 (15 October 1976).

FIGURE CAPTIONS

Fig. 1 - Spectra of discharge-pumped superfluorescent laser emission from four rare gas halides. Each laser line was recorded in vacuum on the same piece of Kodak 101-01 film by placing the appropriate gases in the discharge chamber. Hg lines were used for calibration.

Fig. 2 - Traces of typical time resolved emission waveforms from a) ArF and b) ArCl. 20 ns/division.

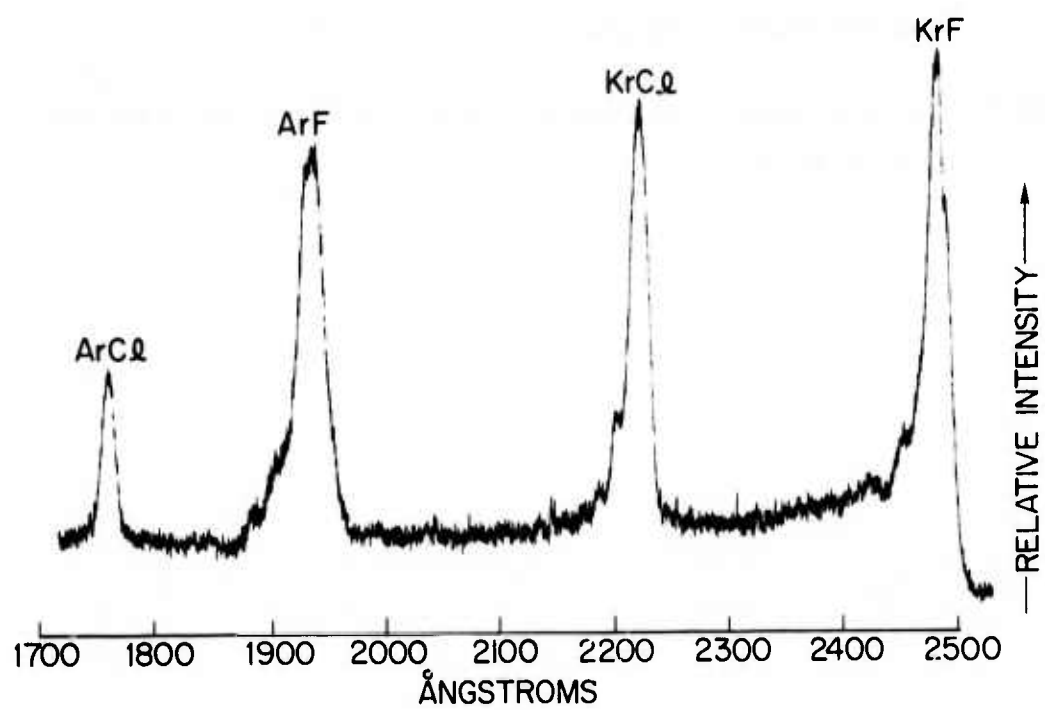


Figure 1

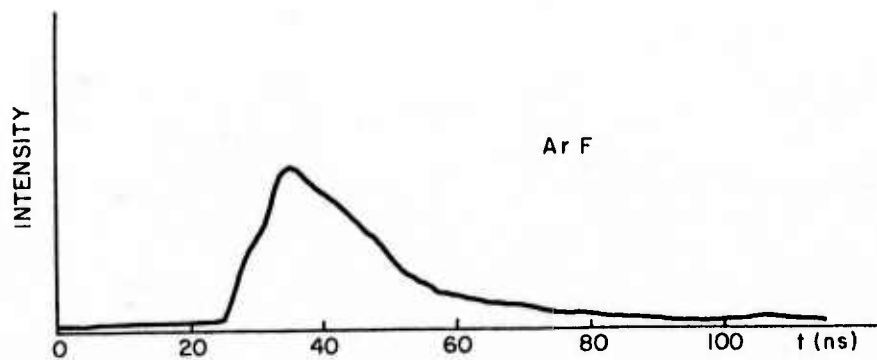
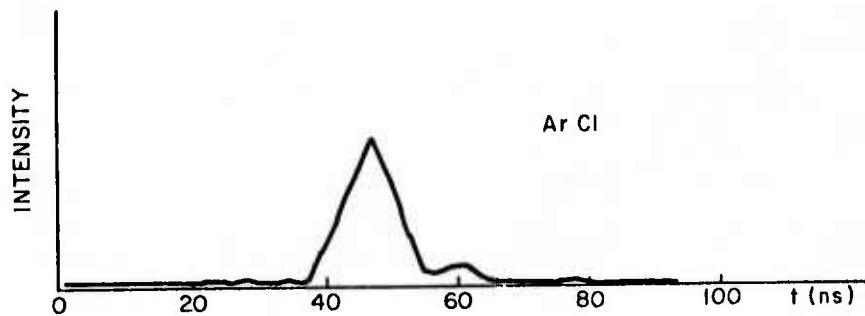


Figure 2

END
6-77